

©Copyright 2020

Jesse Stryker

Compiling Quantum Gauge Theories for Quantum Computation

Jesse Stryker

A dissertation
submitted in partial fulfillment of the
requirements for the degree of

Doctor of Philosophy

University of Washington

2020

Reading Committee:

David B. Kaplan, Chair

Martin J. Savage

Stephen R. Sharpe

Program Authorized to Offer Degree:
Physics

University of Washington

Abstract

Compiling Quantum Gauge Theories for Quantum Computation

Jesse Stryker

Chair of the Supervisory Committee:
Professor David B. Kaplan
Department of Physics

This dissertation gives a survey of formal issues of Hamiltonian lattice gauge theories in the context of simulation by quantum computers. The basic properties of gauge field theories and their lattice regularizations are first reviewed, especially as they pertain to the local constraint that arises in canonical quantization: Gauss’s law, the satisfaction of which is synonymous with gauge invariance and charge conservation. Digital quantum algorithms are developed for the basic task of checking Gauss’s law in $U(1)$ and $Z(N)$ Abelian gauge theories, as they are conventionally formulated. We then analyze $U(1)$ gauge theories by reconstructing them in terms of dual variables that make Gauss’s law manifest. The task of quantum simulation is then studied for the non-Abelian gauge group $SU(2)$. The first quantum simulation of $SU(2)$ gauge bosons using existing IBM quantum hardware is presented, made possible by partially solving the Gauss law constraints in a small system. The quest for the “right” variables to use for quantum algorithms begun with $U(1)$ is then taken up for $SU(2)$. Building on the prepotential formulation of lattice gauge theories, a complete ‘loop-string-hadron’ (LSH) framework is developed for one fermion flavor interacting with $SU(2)$ gauge bosons, in terms of strictly $SU(2)$ -invariant variables. The LSH Hamiltonian is unpacked at a low level, making it transparent what would have to be implemented on a quantum computer. This LSH framework is then applied to provide the first quantum circuits for validating wave functions in $SU(2)$ gauge theories and the associated resource requirements are discussed.

TABLE OF CONTENTS

	Page
List of Figures	iii
List of Tables	vii
Glossary	ix
Chapter 1: Introduction	1
1.1 Classical gauge fields in the continuum	5
1.2 Quantization	10
1.3 Gauge fields on the lattice	12
1.4 Quantized Hamiltonian formulation	15
1.5 Schwinger boson formulation	24
Chapter 2: Gauss law circuits for Abelian gauge theories	28
2.1 Mapping of $Z(N)$ and $U(1)$	28
2.2 Oracles for constraints	31
2.3 Examples and remarks	34
2.4 Discussion	40
Chapter 3: Gauss's Law, duality, and the Hamiltonian formulation of $U(1)$ lattice gauge theory	44
3.1 $U(1)$ Hamiltonian and Hilbert space	45
3.2 $U(1)$ dual formulation	48
3.3 Conclusions	53
Chapter 4: Digital quantum simulation of an $SU(2)$ gauge theory in one dimension	55
Chapter 5: Loop-string-hadron formulation	68

5.1	Loop-string-hadron formulation: One dimension	73
5.2	Loop-string-hadron formulation: Multiple dimensions	97
5.3	3D lattice with matter	110
5.4	Comparison of loop-string-hadron and Kogut-Susskind	117
5.5	Conclusion	118
Chapter 6:	Solving Gauss's Law on digital quantum computers with loop-string-hadron digitization	121
6.1	LSH digitization	122
6.2	Implementing gauge invariance	126
6.3	Discussion	132
6.4	Conclusion	136
Chapter 7:	Conclusion	138
Bibliography	141
Appendix A:	Trotter approximation errors in the Schwinger model	158
Appendix B:	Two plaquette SU(2) Hamiltonian and data tables	160
B.1	Plaquette operator for $\Lambda_j = 1/2$ lattices of arbitrary plaquette number in one dimension	161
B.2	Alternate plaquette gauge variant completion	165
Appendix C:	Simple harmonic oscillator	167
Appendix D:	Gluonic site state normalization	169

LIST OF FIGURES

Figure Number	Page	
1.1	A link (x, i) from a Cartesian lattice starting at x and terminating at $x+e_i$. We denote the starting side “left” (L) and the terminal side “right” (R). Link ends each host a bosonic oscillator doublet, here indicated by $a(L) = (a_1(L), a_2(L))$ at L and $a(R) = (a_1(R), a_2(R))$ at R . The arrow indicates the link orientation, pointing from L to R	26
2.1	A multi-qubit subroutine \oplus for comparing two n -bit integers x and y by adding all their corresponding bits modulo two: A (non)zero result for $y \oplus x$ means x is (not) equal to y	33
2.2	A generic adder A for adding two n -bit integers “in place.” A is assumed to take an incoming carry bit $c_0(=0,1)$, whose value can be added to $y + x$ at no additional cost. The overflow bit $h = 0$ is needed to express the $(n + 1)$ -bit sum.	34
2.3	A query to the oracle for $U(1)$ or $Z(2^n)$ gauge theory in 1D.	35
2.4	A query to the oracle for $U(1)$ gauge theory in 2D. This example accommodates one flavor of Dirac fermion via the occupation numbers ν and p . To modify this for $G = Z(2^n)$, the overflow bits $h^{\text{OUT,IN}}$ would be removed.	37
2.5	A query to the oracle for $U(1)$ gauge theory in 3D. This example accommodates one flavor of Dirac fermion via the occupation numbers $\nu^{1,2}$ and $p^{1,2}$. To modify this for $G = Z(2^n)$, the four overflow bits $h^{\{\text{OUT,IN}\},\{1,2\}}$ would be removed.	39
3.1	An $n = 16$ site lattice with periodic boundary conditions in $d = 2$ with $nd = 32$ links. The $(n - 1) = 15$ links on a maximal tree (dashed blue) are eliminated via Gauss’s Law. The $d = 2$ links in dashed red are eliminated by constraining the net electric flux through the dotted green lines to equal the topological quantum numbers $\nu_{x,y}$. The remaining $(n - 1)(d - 1) = 15$ black links represent the physical variables of the theory. This procedure generalizes to arbitrary d, n	48

4.1	(top) Diagram of the lattice distribution of $\lceil \log_2(2\Lambda_j + 1) \rceil$ -qubit registers and the action of $\hat{\square}$ on SU(2) plaquettes in one dimension. $\hat{\square}$ operates on the four qubit registers in the plaquette and is controlled by the four neighboring qubit registers to enforce the Gauss's law constraint. (bottom) The plaquette operator with labeled angular momentum registers. [image credit: Natalie Klco]	60
4.2	Digital circuit implementation of the plaquette operator centered on j_a for a truncated lattice with $\Lambda_j = 1/2$, two plaquettes, and PBCs as depicted at the right. The angles $\tilde{\beta}$ defining this circuit are given in Eq. (B.4) to be $\tilde{\beta} = (3/8, 5/8)$. [image credit: Natalie Klco]	60
4.3	(top) Expectation value of the electric energy contribution of the first plaquette in the two-plaquette lattice with PBCs and coupling $g^2 = 0.2$ computed on IBM's Tokyo. The dashed(purple) and dot-dashed(blue) lines are the $N_{\text{Trot}} = 1, 2$ Trotterized expectation values, while the thick gray line is the exact time evolution. (bottom) Measured survival probability to remain in the physical subspace for one and two trotter steps, N_{Trot} , and one and two r values indicating stochastically inserted $2r - 1$ CNOTs per CNOT in the digital implementation. Uncertainties represent statistical variation, as well as a systematic uncertainty estimated from reproducibility measurements. The icons (defined in Ref. [1]) denote computations performed on quantum devices. [image credit: Natalie Klco]	64
5.1	Depiction of a basis state in the loop-string-hadron framework. It represents a quark and gauge flux configuration on a 2D spatial lattice. The red flux portions are unterminated and indicated sites where Abelian flux conservation fails.	68
5.2	Pictorial representation of a 1D lattice with matter. Every site on the 1D lattice is associated with a fermionic doublet $\psi = (\psi_1, \psi_2)$. Bosonic doublets $a(L) = (a_1(L), a_2(L))$ and $a(R) = (a_1(R), a_2(R))$ are associated with link ends attached to any site along directions o and i , respectively.	76
5.3	Depiction of SU(2)-invariant configurations at a quark site. The on-site state is characterized by a loop quantum number n_l (the solid lines) and two quark quantum numbers n_i and n_o (the blobs).	84
5.4	Pictorial representation of changes in quantum numbers between initial and final states, which represent (a) flux creation and annihilation, (b) quark creation and annihilation, and (b') hadron creation and annihilation (a composite action).	94

5.5	Virtual point splitting of a 2D lattice site x into gluonic sites x', \bar{x}' , with matter living on the central quark site x	98
5.6	Connectivity of a point-split plaquette in two dimensions. Arrows indicated flow from the “left” end of a link to its “right” end.	104
5.7	Depiction of SU(2)-invariant configurations at a gluonic site. The on-site state is characterized by three loop quantum numbers ℓ_{pq}, ℓ_{qr} , and ℓ_{rp} , with ℓ_{ij} counting the flux lines flowing into i and out of j	106
5.8	Virtual point splitting of a 3D lattice site into gluonic sites $x, x', \bar{x}', x'', \bar{x}''$ connected by internal links, with matter again at the central quark site x	110
5.9	Connectivity of a xy -plaquette in three dimensions.	113
5.10	Connectivity of a yz -plaquette in three dimensions.	114
5.11	Connectivity of a zx -plaquette in three dimensions.	116
6.1	A routine for checking the Abelian Gauss law along a link joining two quark sites. The registers here are specific to a 1D link, with the constraint $[n_\ell + n_o(1 - n_i)]_x = [n_\ell + n_i(1 - n_o)]_{x+1}$	127
6.2	Top: A reduced adder A' for adding one bit to an M -bit integer (shown for $M = 3$). Here c_0 is added to the M -bit integer y , with the $(M + 1)$ -bit result $s = y + c_0$. This uses M ancillae, M Toffoli gates, and M CNOTs. Bottom: A generic adder circuit A for in-place addition of two M -bit integers, $(y, z) \rightarrow (y, z + y)$. One ancilla is introduced to express the $(M + 1)$ -bit output.	129
6.3	A routine for checking the Abelian Gauss law along a link joining a quark site and a gluonic site. The registers here are specific to a $3-i$ (virtual) link in two dimensions, with the constraint $\ell_{23} + \ell_{31} = n_\ell + n_i(1 - n_o)$. The adders A and string of CNOTs are detailed in Fig. 6.2 and in the text, respectively.	129
6.4	A routine for checking the Abelian Gauss law along a link joining two gluonic sites. The registers here are specific to a $1-\bar{1}$ (physical direction) link in 2D space, with the constraint $\ell_{23}(x) + \ell_{31}(x) = \ell_{\bar{2}\bar{3}}(x + e_1) + \ell_{\bar{3}\bar{1}}(x + e_1)$. The adder circuits A are detailed in Fig. 6.2, and the CNOTstring is detailed in the text.	130
6.5	The qubit costs per (unsplit) 2D lattice site as a function of the Casimir cutoff \bar{j} . The bases considered are the conventional Kogut-Susskind (K-S, thin solid line), loop-string-hadron (LSH), and modifications of these as described in the text.	133
6.6	The qubit costs per (unsplit) 3D lattice site as a function of \bar{j} . The bases considered are the conventional Kogut-Susskind (K-S, thick solid line), loop-string-hadron (LSH), and modifications of these as described in the text.	134

B.1 Digital circuit implementation of the plaquette operator centered on j_a for a truncated lattice with $\Lambda_j = 1/2$. The circuit elements appearing in this circuit are the Hadamard, CNOT, and Z-axis single-qubit rotation implementing a Z-to-X basis change, a controlled bit flip, and a relative phase, respectively. 165

LIST OF TABLES

Table Number	Page
2.1	T-counts associated with the arithmetic routines in the oracles for $U(1)$ or $Z(2^n)$ gauge theories, coupled to one Dirac fermion, using the RCA method [2]. 40
4.1	Matrix elements of the $\Lambda_j = 1/2$, Hermitian plaquette operator $\hat{\square}^{(1/2)}$, as calculated in Eq. (4.6) with $j_{\ell,a,r}^t = j_{\ell,a,r}^b$. All other matrix elements between physical states are zero. 61
5.1	Commutator algebra for the loop, string, and hadron operators at a matter site. 79
5.2	Anticommutator algebra for incoming and outgoing string operators at a matter site. 79
5.3	Commutator algebra for the loop operators at a gluonic (pure gauge) vertex. ($d \geq 2$) 80
5.4	Factorization of all $SU(2)$ invariant operators into canonically normalized fermionic modes times a loop ladder operator times a function of number operators. The operator exponentials are conditional ladder operators defined in (5.34). 90
5.5	Graphical representation of the (1D) LSH operators. Left column: Pictorial representations of the operators. Right column: The operators' actions on local LSH states $ n_l, n_i, n_o\rangle_x$, in terms of the graphical rules in Sec. 5.1.3. 96
5.6	Factorization of all $SU(2)$ singlet operators at a gluonic site. 108
6.1	Resource counts for implementing the oracles using simple subroutines from the literature. $N \geq 3$ refers to the gluonic loop number register size; the quark site loop number register size is $N + 1$. The counted resources are numbers of ancillary qubits (Anc.), CNOTgates, and Toffoli-congruent [$C^2(X)$ cong.] or exact Toffoli [$C^2(X)$] gates. 131
6.2	CNOTcounts for the circuits assuming $N \geq 3$, the use of Toffoli-congruent gates, and Corollary 6.2 of [3]. 132

B.1	Convergence of the ground state energy density and the energy gap to the first excited state, ΔE , of a two-plaquette SU(2) lattice with periodic boundary conditions as the truncation in the maximum excitation on any single link, Λ_j , is increased. Columns two and three show the number of states included in the basis of physical states below truncation and the number of non-zero matrix elements in the single plaquette operator.	162
B.2	Numerical values of the expectation value of the single electric plaquette energy contribution for time evolutions implemented with 1,2 Trotter steps as measured on IBM's quantum device Tokyo shown in the top panel of Fig. 4.3. Uncertainties represent statistical variation, as well as a systematic uncertainty estimated from reproducibility measurements.	163
B.3	Survival probabilities in the physical subspace as measured on IBM's quantum device Tokyo shown in the bottom panel of Fig. 4.3. The label indicates (N_{Trot}, r) values. The linear extrapolation is determined by extrapolation of computational basis state probabilities in r for $N_{\text{Trot}} = 1$. Uncertainties represent statistical variation, as well as a systematic uncertainty estimated from reproducibility measurements.	164

GLOSSARY

AGL: Abelian Gauss law, the constraint of Abelian flux conservation along a lattice link.

ALGEBRA: LIE: i) The linear vector space spanned by generators of a Lie group. ii) The particular commutation relations of the generators of a given Lie group.

BITWISE SUM: The bitwise sum of two integers a and b is the integer c such that the n^{th} bit of c is the sum of the n^{th} bit of a and n^{th} bit of b modulo 2.

INDICES: GROUP OR COLOR: indices running over the components of a group representation. Usually indicated by early or mid-alphabet Roman letters.

INDICES: ADJOINT OR GENERATOR: indices labeling the generators of a group, e.g., $1, \dots, N^2 - 1$ for $SU(N)$. Usually indicated by early alphabet Greek letters.

INDICES: LORENTZ OR SPACETIME: indices running over $0, 1, \dots, d$, where d is the spatial dimensionality. Usually indicated by mid-alphabet Greek letters μ, ν , etc.

METRIC: MINKOWSKI: the rank-two metric tensor for flat spacetime, with the “mostly plus” convention, e.g., $\eta_{\mu\nu} = \text{diag}(-, +, +, +)$ in 3+1 dimensions

ACKNOWLEDGMENTS

I am indebted to the individuals that have surrounded me throughout my years becoming a physicist.

Needless to say, I would not be where I am today without the guidance of my advisor, David Kaplan. This guidance truly started before I was his Ph.D. student, during a general relativity summer reading course. Fielding his questions at the board on how I approached solving the problems started off intimidating, but it built up an indispensable skill. Our meetings foreshadowed how David would later advise me – our discussions primarily took place dynamically, in real time, with me at the blackboard. Over the years, David consistently encouraged me and supported me in carving out my path in physics, from sponsoring my trips to workshops and summer schools around the globe, to urging me to write up my first single-author paper the moment I articulated a concise research problem I could solve myself. At lower points, David would deliver the candid feedback needed to accelerate me through the pertinent learning processes. The only complaint I have (or am willing to state publicly) is that he can never keep up with me on a hiking trail... just kidding—it's the opposite that is true.

Martin Savage's informal advising was also an unexpected gift to my training as a scientist. Martin will not budge an inch when it comes to his ethical code, whether that is in producing research results, navigating academic bureaucracy, or anything in between. Witnessing him be so adamant about doing what is right or necessary helped to affirm tendencies I naturally lean towards, but for which I see few examples; knowing what is right is one thing, but it is another to actually have an example of what it looks like to stick to your guns. What I need now is to develop a Martin-like ability to detect bullshit and shady intentions

in others.

A crucial element of my overall well-being in every chapter of my life has always been my friends – physicists and normies alike. Dylan Abbott, Erika Hammer, the Ward family, and Henry Panait continue to be there for me year after year, even as our daily lives continue to diverge, and I love them for that. The closer physics colleagues I’ve had—Ramya Bhaskar, Jon Craig, Dorota Grabowska, Julieta Gruszko, Natalie Klco, John Lombard, Kerkira Stockton, Michael Wagman, and Michael Wilensky—all enriched my journey through the Physics Ph.D. program in their own way. I must thank my other Seattle-derived friends—Aakash, Ari, Beggers, Dathan, David B., Ell, Helen, Ian, Ingber, Karl, Kelly, Natalie S., Nick D., Noah, plus any remaining Physics House alumni—for providing me with vital social stimulation that work cannot provide, such as trips outdoors or evenings spent dancing at shows.

There are also those who’ve had a lasting impact on my trajectory but through briefer encounters. Silas Beane, Ann Nelson, and Michael Wagman each expressed belief in my long-term prospects before I truly believed in them myself. Gerald Miller provided invaluable support to me as a first-year – especially in helping me assemble a strong application for the NSF Graduate Research Fellowship. Lee Brown and her husband, Mike, were the benefactors for my ARCS Fellowship in my early graduate school career; Lee is no longer with us, but I will never forget her enthusiastic support for me as a junior scientist.

The project collaborators I’ve had thus far—David Kaplan, Natalie Klco, Pavel Lougovski, Gerald Miller, Indrakshi Raychowdhury, Martin Savage, Alex Shaw, and Nathan Wiebe—should all be recognized for their tacit patience, as I am not always the easiest person to work with, but the complementarity of skills brought to each project considerably shaped the quality of the papers I was a part of.

Before graduate school, Ricardo Alarcón, David Blyth, Cecilia Lunardini, Robert Nemanich, and Tianyin Sun supported the start of my physics journey at Arizona State University. My secondary education teachers, Mr. Trigg (math), Mrs. Govert (chemistry) and

Mrs. Gibson (calculus), also must be credited with having first made their STEM classrooms a sanctuary for me.

Finally, I thank my patient mother for entertaining all the questions I badgered her with as a kid. On one occasion, she listened to me count out loud all the way up to 550, before finally teaching me what “infinity” was and having me grapple with that. My mom, my brothers, and the rest of my family have always supported me in honing my talents.

DEDICATION

To my lifelong friends.

Chapter 1

INTRODUCTION

The development of the Standard Model profoundly transformed humanity's theoretical understanding of the fundamental properties of matter and energy over the latter half of the twentieth century. The Standard Model is a quantum field theory, which characterizes particles as excitations of underlying fields that permeate spacetime and generalize the more familiar electric and magnetic fields from classical physics. All the familiar particles are associated with their own field; there is a photon field, charged lepton fields that include the electron field, quark fields for all the different flavors, gluon fields, neutral lepton fields for neutrinos, and finally fields for the W , Z , and Higgs bosons. The dynamics of these fields are intertwined, giving rise to the rich variety of particle reactions and decays confirmed by experiments.

Among the most salient features of the Standard Model are its local gauge group symmetries. These symmetries are a convenient redundancy in how the quantum fields are represented. The notion of gauge redundancy is one that is familiar from classical electrodynamics, wherein an electric potential field $\Phi(x)$ and vector potential field $\vec{A}(x)$ can be used to represent both the electric field $\vec{E}(x)$ and magnetic field $\vec{B}(x)$. In this so-called gauge theory, there are whole classes of numerically different Φ and \vec{A} fields that encode the same measurable \vec{E} and \vec{B} fields; the observationally equivalent choices of Φ and \vec{A} are related by spacetime-dependent gauge transformations, and the gauge transformations form what is known as a group. A mathematically concise way of expressing this redundancy is to note that the observable electromagnetic fields $\vec{E}(x)$ and $\vec{B}(x)$, which are derived from $\Phi(x)$ and $\vec{A}(x)$, are invariant under local “gauge transformations” of Φ and \vec{A} .

The Lagrange density of the Standard Model has the internal symmetry gauge group

$U(1) \times SU(2) \times SU(3)$, where each of the factors is a distinct symmetry group unto its own. For example, the simplest of these, $U(1)$ or the group of complex phase factors, tells us that the overall phase of the underlying fermion fields, at any point in space, is arbitrary; one can locally adjust or ‘rotate’ the fields’ overall phases (in a certain correlated way) such that the Lagrange density derived from the deformed fields remains the same.

The $SU(3)$ sector, referred to as quantum chromodynamics (QCD), is at the heart of the physics of hadrons and nuclei. Unlike the situation in the electroweak sector, the $SU(3)$ color symmetry is a symmetry of both the Lagrangian and the vacuum (it is not spontaneously broken). Each flavor of quark field is really itself a triplet of quark fields, each carrying its own color charge, but these colors are all on an equal footing; in this case, the redundancy is such that one can mix the quarks by apply a rotation matrix to their fields from the non-Abelian group $SU(3)$. What is physically meaningful is the fact that there are three types, along with their antiparticles, and that quarks are always observed in combinations having zero net color charge. A nucleon, which has three valence quarks, is thought of as the colorless combination resulting from having all three quark colors present. A pion, on the other hand, is a colorless combination arising from having internal color charge balanced by equal amounts of anticolor.

At low energies it becomes considerably harder or altogether impossible to harness the predictive power of the Standard Model with analytic calculations. Non-Abelian gauge theories such as QCD are known for admitting asymptotic freedom and becoming strongly coupled at low energies. Lattice quantum field theory, namely lattice QCD [4], has proven to be a successful approach to studying gauge theories in the nonperturbative regime numerically. In the lattice approach, the continuum of spacetime is ‘discretized’ by a lattice of points and quantum fields are defined only on the sites or along the links joining them. In addition, time is usually analytically continued to ‘imaginary’ time or Euclidean spacetime. The lattice is further reduced to a box of finite size, at which point the number of degrees of freedom is finite and simulatable by computers. One then computes observables by sampling the path integral formulation of the quantum field theory and taking the continuum limit of

small lattice spacing.

Lattice QCD has enabled novel *ab initio* calculations in a variety of applications, such as heavy quark physics [5], low-lying hadron masses [6], QCD thermodynamics [7, 8], baryon number fluctuations [9], and weak matrix elements [10, 11]. These computational feats have predominantly characterized static or equilibrium properties at zero chemical potential [12]. However, lattice QCD calculations with non-zero baryon chemical potential, with a topological θ -term, or in real (Minkowskian) time are generally hampered by exponentially hard sign problems. The difficulty can be traced to how these scenarios are formulated for simulation on classical machines, i.e., the path integral and the breakdown of Monte Carlo methods when applied to it. A class of problems that especially stands to benefit from new methods is real-time dynamics; the Hamiltonian formulation of gauge theories, which requires singling out a direction for time, may be more natural for describing intrinsically real-time processes that do not lend themselves well to Wick rotation.

In the 1980s, it was proposed that computers based on quantum mechanical degrees of freedom ought to be better suited for simulating quantum many-body systems [13], such as a gauge theory. The idea is that degrees of freedom of the system under study be mapped onto those of the quantum computer, and unitary operations are done on it to mimic time evolution. In this scenario, it seems far more natural to express theories with Hamiltonians and Hilbert spaces rather than functional integrals and classical field configurations.

The arrival of functional quantum devices [14] thus creates an urgent need for a thorough grasp of Hamiltonian lattice gauge theory and how its structure can be related to that of quantum architectures. Several proposals or steps toward proposals for quantum-simulating lattice gauge theories have been made in recent years [15–17]. So far, most of them have been for simpler models like $Z(2)$ gauge theories [17–19] or $U(1)$ gauge theories in $1 + 1$ dimensions [20–23], including the first digital quantum simulation of the Schwinger model on a small lattice [24]. Such simulations are instructive, but generalizing to non-Abelian gauge groups and multidimensional space is necessary to address the important problems where classical computers fall short. Work on these generalizations is underway [25–34] (see

also Refs. [16,17] and references therein), but the state of these studies is even less mature due to the significant practical complications involved with non-Abelian interactions.

Designing a protocol for a quantum simulation at the theoretical level involves planning out at least three major steps: i) Creating an initial state. ii) Simulating the intended process, e.g., time evolution in the Schrödinger picture. iii) Extracting the observables of interest. Detailing any one of these, however, necessitates a choice of basis. The basis choice can have far-reaching consequences for the complexity of any one of the procedures, and it may well be tied in to their planning.

This dissertation is chiefly concerned with the formulation of [U(1) and SU(2)] Hamiltonian lattice gauge theories. Special attention is given to the fact that gauge theory Hilbert spaces are accompanied by local Gauss law constraints, which will have to be addressed by any simulation, and to the relationship between gauge constraints and the choice of basis. In some cases, the constraints and conventional bases are taken as a given and the practical issues they imply are examined. In others, work is done to improve the prospects for designing simulations whose dynamics will respect gauge constraints.

In chapter 2, we take a first look at what would be needed to implement gauge invariance for a Kogut-Susskind-like simulation in Abelian gauge theories. Characterizing legitimate wave functions should a basic task for theories with constrained dynamics, so we look at quantum algorithms that would enable one to validate wave functions as they are conventionally formulated. This work was published in *Physical Review A* 99, 042301 (2019).

In chapter 3, we examine what happens in trying to eliminate gauge redundancy in U(1) gauge theories (without matter). By using choosing to represent only those gauge invariant excitations the Hamiltonian can generate, we are naturally led a magnetic dual theory, which has different constraints. This work, done in collaboration with D.B. Kaplan, is drawn from arXiv:1806.08797.

In chapter 4, we take up the simulation problem for the non-Abelian gauge group SU(2), where a conventional (Kogut-Susskind-like) starting point is especially impractical for quantum simulation at this point in time. We study a system with enough room for dynamics to

happen, but small enough that we are also still able to partially solve the non-Abelian Gauss law, simulate it on existing hardware, and post-select on the leftover gauge constraints. This work, done in collaboration with N. Klco and M.J. Savage, was published in *Physical Review D* 101, 074512 (2020).

Then, in chapter 5, we follow an approach that goes much farther in solving non-Abelian constraints, using what we call a loop-string-hadron (LSH) formulation. This amounts to deconstructing the theory entirely and reassembling it in a language where charge conservation is made intrinsic. There are still constraints leftover in the LSH formulation, so in chapter 6, we give the quantum circuits analogous to those developed for $U(1)$, except these routines check flux conservation along links instead of at sites. These works were both done in collaboration with I. Raychowdhury and are published in *Physical Review D* 101, 114502 (2020) and *Physical Review Research* 2, 033039 (2020).

The remainder of the present chapter is dedicated to reviewing the fundamental properties of the gauge field theories that we are most interested in simulating. The emphasis is particularly on fundamentals of Hamiltonian gauge theory, its lattice formulation, and the implications of gauge constraints. The concepts from quantum computation that are used are standard textbook material; see, for example, Ref. [35].

1.1 Classical gauge fields in the continuum

Here we summarize the key features of continuum theories, especially as they pertain to the features lattice formulations must reproduce. This section also serves to set conventions. The development follows Ref. [36] and Ref. [37].

The theories of interest, such as QED or QCD, are special in that they have notions of conserved charges. In QED, conservation of charge dictates that the charge of the Universe is conserved. Particles can be created or destroyed but they must do so in such a way that equal parts of positive and negative charges are created or destroyed. In QCD, we say “color” is conserved—quarks can be “red,” “green,” or “blue,” and antiquarks can carry the corresponding anticolors. The combination of r, g, and b quarks would give a colorless

combination (no net color). A proton can be thought of as such a state. In any reaction of particles, no net color can be created or destroyed.

Not only is charge universally conserved, but where there is charge, its fingerprint is evident in the configuration of the gauge fields. In electrodynamics, this is expressed by Gauss's law,

$$\vec{\nabla} \cdot \vec{E} = \rho . \quad (1.1)$$

The requirements of Lorentz invariance and charge conservation constrain how the involved quantum fields may interact.

The most direct path to constructing continuum gauge field theories is to start with the principle of local gauge invariance. A Lagrangian for matter fields is first observed to have a conservation law (total number of particles minus antiparticles, say) associated with a continuous and global transformation on the fields; the symmetry transformation is then “promoted” to a local symmetry by insisting that the transformation can be done locally while still leaving the Lagrangian invariant.

Concretely, the classical Lagrange density is formed from fields $\psi_l(x)$ that can be transformed by symmetry transformations belonging to a Lie group. Local, Lie group gauge transformations on matter fields ψ_l take the form

$$\psi_l(x) \rightarrow [e^{i\epsilon^\alpha(x)T_\alpha}]_l^m \psi_m(x) \quad (1.2)$$

$$\equiv \Omega(\epsilon(x))_l^m \psi_m(x) , \quad (1.3)$$

$$\text{or in matrix/vector notation, } \psi(x) \rightarrow \Omega(\epsilon(x)) \psi(x) . \quad (1.4)$$

Here, l and m are generalized indices for fields that transform under the symmetry.¹ Ω_l^m is a square matrix-valued function of x defining how the fields are locally mixed, with $\epsilon(x)$ being real parameters for the gauge transformation function Ω . The matrices T_α are matrices in some representation of the Lie algebra. They are generators of the group and each T_α labels

¹For example, $\psi_{\sigma l} = (q_{\sigma 1}, q_{\sigma 2}, q_{\sigma 3})$ for the theory of a single quark flavor, but with the Dirac index σ suppressed since eq. (1.3) does not mix Dirac components. A two-flavor theory of up and down quarks could have $\psi_l = (u_1, u_2, u_3, d_1, d_2, d_3)$, in which case the T_α would be block diagonal.

a distinct transformation. The generators form a Lie algebra under commutation:

$$[T_\alpha, T_\beta] = i C^\gamma_{\alpha\beta} T_\gamma \quad (\text{real } C^\gamma_{\alpha\beta}). \quad (1.5)$$

The $C^\gamma_{\alpha\beta}$ are known as structure constants. We assume the Lie algebra is a direct sum of commuting compact simple and U(1) subalgebras (cf. §15.2 of [36]).

The principle of local gauge invariance is the requirement that the Lagrange density constructed from the fields is unchanged by all such transformations in eq. (1.3). A locally gauge invariant Lagrange density will involve derivatives of the fields, but the issue arises that spatial derivatives $\partial_\mu \psi_l$ do not transform simply like ψ_l ; ∂ is not a gauge covariant operator. For example,

$$\partial_\mu \psi \rightarrow \partial_\mu (\Omega \psi) = \Omega (\partial_\mu \psi) + (\partial_\mu \Omega) \psi. \quad (1.6)$$

The first term matches the form of eq. (1.3), but we would like to avoid the second term (which does vanish for global gauge transformations, i.e., constant Ω). A covariant derivative is formed by introducing ‘gauge fields’ A_μ^α (one four-vector field per generator α) as follows:

$$D_\mu \psi_l = \partial_\mu \psi_l - i A_\mu^\alpha (T_\alpha)_l^m \psi_m. \quad (1.7)$$

This is expressed more compactly by collecting the gauge fields into a matrix-valued field,

$$A_\mu(x) \equiv A_\mu^\alpha(x) T_\alpha, \quad (1.8)$$

$$D_\mu \psi_l = \partial_\mu \psi_l - i (A_\mu)_l^m \psi_m \quad (1.9)$$

$$\text{or just } D_\mu \psi = (\partial_\mu - i A_\mu) \psi. \quad (1.10)$$

The covariant derivative $D_\mu \psi_l$ is made to transform like ψ_l by having the gauge fields A_μ^α undergo simultaneous transformations:

$$A_\mu \rightarrow \Omega A_\mu \Omega^{-1} + i \Omega (\partial_\mu \Omega^{-1}) \quad (1.11)$$

$$\Rightarrow D_\mu \psi_l \rightarrow \Omega_l^m (D_\mu \psi)_m \quad (1.12)$$

$$\text{or just } D_\mu \psi \rightarrow \Omega D_\mu \psi. \quad (1.13)$$

To make A_μ a dynamical field too, we will need to couple derivatives of A_μ , but we again need to avoid the same problem of how spatial derivatives transform. The solution is to form the field strength tensor using covariant derivatives of A :

$$F_{\mu\nu} = i[D_\mu, D_\nu] \quad (1.14)$$

$$= \partial_\mu A_\nu - \partial_\nu A_\mu - i[A_\mu, A_\nu] \quad (1.15)$$

$$= \partial_\mu A_\nu - \partial_\nu A_\mu + C^\gamma_{\alpha\beta} A_\mu^\alpha A_\nu^\beta T_\gamma \quad (1.16)$$

$$F_{\mu\nu}^\alpha \equiv \partial_\mu A_\nu^\alpha - \partial_\nu A_\mu^\alpha + C^\alpha_{\beta\gamma} A_\mu^\beta A_\nu^\gamma \quad (1.17)$$

Gauge transformations on the field strength are indeed homogeneous:

$$F_{\mu\nu} \rightarrow \Omega F_{\mu\nu} \Omega^{-1} \quad (1.18)$$

$$\text{or equivalently, } F_{\mu\nu}^\alpha \rightarrow (\Omega^A)^\alpha_\beta F_{\mu\nu}^\beta \quad \text{with } (\Omega^A)^\alpha_\beta = r \text{tr}(T_\alpha \Omega T_\beta \Omega^{-1}) \quad (1.19)$$

The latter shows how the field strength transforms like a matter field in the adjoint representation. To summarize the gauge transformations thus far,

$$\psi \rightarrow \Omega \psi \quad (1.20)$$

$$A_\mu \rightarrow \Omega A_\mu \Omega^{-1} + i \Omega (\partial_\mu \Omega^{-1}) \quad (= i \Omega (\partial_\mu - i A_\mu) \Omega^{-1}) \quad (1.21)$$

$$\Rightarrow F_{\mu\nu} \rightarrow \Omega F_{\mu\nu} \Omega^{-1} \quad (1.22)$$

ψ , D_μ , $F_{\mu\nu}$ all transform homogeneously, so as long as we only couple fields via these objects, it will be trivial to construct locally gauge invariant Lagrangians:

$$\mathcal{L} = \mathcal{L}(\psi, D_\mu, F_{\mu\nu}, \dots) \quad (1.23)$$

The simplest gauge invariant and Lorentz invariant kinetic Lagrangian for the gauge fields is known as the Yang-Mills Lagrangian, with

$$\mathcal{L}_{YM} \propto \text{tr}(F_{\mu\nu} F^{\mu\nu}) \quad (1.24)$$

$$= g_{\alpha\beta} F_{\mu\nu}^\alpha F^{\beta\mu\nu} \quad (1.25)$$

$$g_{\alpha\beta} = \text{tr}(T_\alpha T_\beta) \quad (1.26)$$

(where $g_{\alpha\beta}$ should not be confused with the Minkowski metric tensor η). The quadratic form also has the lowest possible mass dimension (D_μ being of mass dimension 1 and $F_{\mu\nu}$ being of mass dimension 2). For the groups we consider, we can take

$$g_{\alpha\beta} = \frac{1}{2g^2} \delta_{\alpha\beta} . \quad (1.27)$$

The conventionally normalized continuum Lagrangian is then

$$\mathcal{L}_{YM} = -\frac{1}{4g^2} \delta_{\alpha\beta} F^{\alpha\mu\nu} F_{\mu\nu}^\beta = -\frac{1}{2g^2} \text{tr}(\delta_{\alpha\beta} F_{\mu\nu} F^{\mu\nu}) . \quad (1.28)$$

From this point forward, we will have little to say about the continuum Lagrangians.

Going over to Hamiltonian dynamics, we need conjugate momenta to the gauge fields:

$$\frac{\partial}{\partial(\partial_\rho A_\sigma^\beta)} (F_{\mu\nu}^\alpha F_{\alpha}^{\mu\nu}) = 4F_\beta^{\rho\sigma} \quad (1.29)$$

$$\Rightarrow \frac{\partial \mathcal{L}_{YM}}{\partial(\partial_0 A_j^\alpha)} = \Pi_\alpha^j = -F_\alpha^{0j}/g^2 = F^{j0}/g^2 = F_{0j}/g^2 . \quad (1.30)$$

Note the correspondence of the momenta with the Maxwell electric fields $\vec{E} = (-\partial_t \vec{A} - \vec{\nabla}\Phi)/g$:

$$\text{(Maxwell)} \quad A^\mu = (\Phi, \vec{A}) \quad (1.31)$$

$$\text{(Maxwell)} \quad \Pi_i = \frac{1}{g^2} (\partial_0 A_i - \partial_i A_0) \quad (1.32)$$

$$\Rightarrow E_i^\alpha = -g \Pi_i^\alpha . \quad (1.33)$$

We can also identify the generalization of the Maxwell magnetic field $\vec{B} = \vec{\nabla} \times \vec{A}/g$,

$$\text{(Maxwell)} \quad B_i = \epsilon_{ijk} (\partial^j A^k - \partial^k A^j)/g \quad (1.34)$$

$$\Rightarrow B_i^\alpha = \epsilon_{ijk} F^{\alpha jk}/g . \quad (1.35)$$

The conjugate momentum Π_α^0 evidently vanishes, so A_0 is not actually dynamical. In the canonical formalism, it can therefore be convenient to fix the potential to Weyl gauge,

$$A_0 \equiv 0 \quad (1.36)$$

$$\Rightarrow \Pi_\alpha^j = g^{-2} \dot{A}_\alpha^j . \quad (1.37)$$

Spatial gauge transformations $\Omega(x) = \Omega(\vec{x})$ are still a symmetry since these preserve the gauge fixing condition. The Hamiltonian density resulting from Legendre transformation is then

$$\mathcal{H} = \frac{g^2}{2} \Pi_a^j \Pi_{aj} + \frac{1}{2g^2} \text{tr}(F_{ij} F^{ij}) . \quad (1.38)$$

1.2 Quantization

The gauge fields are quantized by stipulating the equal-time commutation relations:

$$[\hat{A}_i^\alpha(\vec{x}), \hat{\Pi}_\beta^j(\vec{y})] = i \delta_\beta^\alpha \delta_i^j \delta(\vec{x} - \vec{y}) \quad (1.39)$$

Gauge transformations must now be realized in operator form—we need symmetry operators to effect the matrix multiplications. Infinitesimally, the requirement on the operator gauge fields is (for $\Omega = 1 + i \epsilon^\alpha T_\alpha + \dots$)

$$\delta \hat{A}_\mu^\alpha = \partial_\mu \epsilon^\alpha - i (\hat{A}_\mu^A)^\alpha{}_\beta \epsilon^\beta \quad (1.40)$$

$$= (\hat{D}_\mu^A \epsilon)^\alpha \quad (1.41)$$

The covariant divergences $D_i \Pi_\alpha^i$ generate the infinitesimal gauge transformations on the gauge fields:

$$\hat{\mathcal{T}}_\alpha \equiv (\hat{D}_i \hat{\Pi}^i)_\alpha \quad (1.42)$$

$$= -(\hat{D}_i \hat{E}^i)_\alpha / g \quad (1.43)$$

$$\left[(-i) \int d^d x \epsilon^\alpha(\vec{x}) (\hat{D}_i \hat{\Pi}^i)_\alpha(\vec{x}), \hat{A}_j^\beta(\vec{y}) \right] = \left[(-i) \int d^d x \epsilon^\alpha(\vec{x}) \hat{\mathcal{T}}_\alpha(\vec{x}), \hat{A}_j^\beta(\vec{y}) \right] \quad (1.44)$$

$$= \partial_j \epsilon^\beta(\vec{y}) - i \hat{A}_j^A(\vec{y})^\beta{}_\gamma \epsilon^\gamma(\vec{y}) \quad (1.45)$$

$$= (\hat{D}_j^A \epsilon(\vec{y}))^\beta \quad (1.46)$$

(with a discarded boundary term). The $D_i \Pi_\alpha^i$ are themselves a representation of the Lie group, satisfying the exact same algebra of the generators in a distributional sense:

$$\int d^d x \epsilon^\alpha(x) \left[(\hat{D}_i \hat{\Pi}^i)_\alpha(x), (\hat{D}_j \hat{\Pi}^j)_\beta(y) \right] = \epsilon^\alpha(y) i C^\gamma{}_{\alpha\beta} (\hat{D}_i \hat{\Pi}^i)_\gamma(y) \quad (1.47)$$

$$\text{or just } \left[(\hat{D}_i \hat{\Pi}^i)_\alpha(x), (\hat{D}_j \hat{\Pi}^j)_\beta(y) \right] = i C^\gamma{}_{\alpha\beta} (\hat{D}_i \hat{\Pi}^i)_\gamma(y) \delta(\vec{x} - \vec{y}) \quad (1.48)$$

So the unitary operator to effect the matrix transformation $\Omega_\epsilon(\vec{x}) = \exp[i\epsilon^\alpha(\vec{x})T_\alpha]$ on \hat{A} would be the quantum (Hilbert space) operator $\exp[-i \int d^d x \epsilon^\alpha(\vec{x})\hat{\mathcal{T}}_\alpha(\vec{x})]$:

$$\hat{\Omega}(\epsilon) \equiv e^{i \int d^d x \epsilon^\alpha(x)\hat{\mathcal{T}}_\alpha(x)} \quad (1.49)$$

$$\Rightarrow \hat{\Omega}^\dagger(\epsilon)\hat{A}_j(\vec{y})\hat{\Omega}(\epsilon) = \Omega_\epsilon(\vec{y})\hat{A}_j\Omega_\epsilon^\dagger(\vec{y}) + i\Omega_\epsilon(\vec{y})\partial_j\Omega_\epsilon^\dagger(\vec{y}) \quad (1.50)$$

where \hat{A}_j is in any representation and the dagger placement is not accidental. In particular, note that $\hat{\Omega}(\epsilon)$ is a functional of the spatial gauge transformation function $\epsilon(x)$ —it is not a field, it is a single quantum operator fixed by ϵ , and it lacks “group indices”—while the classical matrix $\Omega_\epsilon(\vec{x})$ does carry group indices, is still a function of space, and acts like a c-number as far as quantum operations are concerned.

Later we will consider fermionic matter. Here we have

$$\delta\hat{\psi}_l = i\epsilon^\alpha(T_\alpha)_l^m\hat{\psi}_m \quad (1.51)$$

$$J_\alpha^0 = \psi^\dagger T_\alpha \psi \quad (1.52)$$

$$[\hat{J}_\alpha^0(t, \vec{x}), \hat{J}_\beta^0(t, \vec{y})] = iC^\gamma_{\alpha\beta}\hat{J}_\gamma^0(t, \vec{x})\delta(\vec{x} - \vec{y}) \quad (1.53)$$

$$[(-i)\hat{J}_\alpha^0(t, \vec{x}), \hat{\psi}_l(t, \vec{y})] = i(T_\alpha)_l^m\hat{\psi}_m(t, \vec{x})\delta(\vec{x} - \vec{y}) \quad (1.54)$$

Combining the above, we have the Gauss law operators that generate gauge transformations and satisfy the same Lie algebra:

$$\hat{\mathcal{G}}_\alpha(x) = (\hat{D}_i\hat{\Pi}^i(x))_\alpha + \hat{\psi}^\dagger(x)T_\alpha\hat{\psi}(x) = -\frac{1}{g}(\hat{D}_i\hat{E}^i(x))_\alpha + \hat{J}_\alpha^0(x) \quad (1.55)$$

$$\Rightarrow \int d^d x \epsilon^\alpha(x) [\hat{\mathcal{G}}_\alpha(x), \hat{\mathcal{G}}_\beta(y)] = \epsilon^\alpha(y) iC^\gamma_{\alpha\beta}\hat{\mathcal{G}}(y)_\gamma \quad (1.56)$$

$$\text{or just} \quad [\hat{\mathcal{G}}_\alpha(x), \hat{\mathcal{G}}_\beta(y)] = iC^\gamma_{\alpha\beta}\hat{\mathcal{G}}(y)_\gamma \delta(\vec{x} - \vec{y}) \quad (1.57)$$

To summarize, using the Gauss law operators $\hat{\mathcal{G}}_\alpha(x)$ we can construct the symmetry operators

$\hat{\Theta}$ that effect the gauge transformations introduced in the classical theory as follows:

$$\hat{\Theta}(\epsilon) \equiv e^{i \int d^d x \epsilon^\alpha(x) \hat{\mathcal{G}}_\alpha(x)} \quad (1.58)$$

$$\hat{\Theta}^\dagger(\epsilon) \hat{A}_j(\vec{x}) \hat{\Theta}(\epsilon) = \Omega_\epsilon(\vec{x}) \hat{A}_j(\vec{x}) \Omega_\epsilon^\dagger(\vec{x}) + i \Omega_\epsilon(\vec{x}) \partial_j \Omega_\epsilon^\dagger(\vec{x}) \quad (1.59)$$

$$\hat{\Theta}^\dagger(\epsilon) \hat{F}_{\mu\nu}(\vec{x}) \hat{\Theta}(\epsilon) = \Omega_\epsilon(\vec{x}) \hat{F}_{\mu\nu}(\vec{x}) \Omega_\epsilon^\dagger(\vec{x}) \quad (1.60)$$

$$\hat{\Theta}^\dagger(\epsilon) \hat{F}_\alpha^{\mu\nu}(\vec{x}) \hat{\Theta}(\epsilon) = [\Omega_\epsilon^A(\vec{x})]_\alpha^\beta \hat{F}_\beta^{\mu\nu}(\vec{x}) \quad (1.61)$$

$$\hat{\Theta}^\dagger(\epsilon) \hat{\psi}_l(\vec{x}) \hat{\Theta}(\epsilon) = [\Omega_\epsilon(\vec{x})]_l^m \hat{\psi}_m(\vec{x}) \quad (1.62)$$

1.3 Gauge fields on the lattice

For any numerical simulation, the continuum of degrees of freedom of a field theory must be truncated. This is traditionally done by defining the fields only on a discrete $(d+1)$ -dimensional lattice of points in Euclidean spacetime. It is standard to use a Cartesian geometry with lattice spacing a , as it preserves the largest possible symmetry subgroup of the $(d+1)$ -dimensional rotation group. A volume truncation is also necessary; it is common to use a $(d+1)$ -dimensional box, with length L_x along d “spatial” directions and L_t along the “time” direction. For Euclidean simulations, singling out a direction to call “time” is due to the fact that the $(d+1)$ -dimensional Euclidean path integral is identified with the partition function of the same system in d spatial dimensions, in thermal equilibrium at temperature $1/L_t$. Ground state properties are thus extracted by taking the limit of large Euclidean time extent.

The lattice is itself a regularization scheme for the continuum quantum field theory. The nonzero lattice spacing a means that particles can only be resolved with momenta below the scale π/a —an ultraviolet cutoff—and the finite volume also implies a cutoff on wavelength at the scale of the box size L_x —an infrared cutoff. These two limits are important considerations for what physics will be accessible, e.g., L_x must be larger than 1 femtometer to study the proton, while a must be much smaller than 1 femtometer.

At a more practical level, latticization renders the domain of the functional integral finite-dimensional so that the functional integral is itself well-defined and amenable to Monte Carlo

integration. In addition, while the continuum limit is formally taken by sending $a \rightarrow 0$, in practice the continuum limit is approached by instead tuning parameters in the lattice action to ‘critical values’ at which correlation lengths diverge (in lattice units) [38]. In this way, the effects of lattice discretization are made small or negligible relative to the probed physics.

In the subsequent chapters, we will be primarily concerned with the UV structure of the theory, meaning the local lattice degrees of freedom themselves. These depart from traditional lattice field theory because we are most interested in Hamiltonian mechanics, in which time remains continuous and only space is discretized, with a lattice spacing a_s . Of course, we also work with Hilbert spaces rather than classical field configurations. For gauge theories, we take the Weyl gauge $A_0 = 0$ so that gauge fields have only spatial components. The details of extrapolating to the continuum and ameliorating lattice “artifacts” will not be taken up because Hamiltonian simulation problems are still in such a nascent stage of development. It is not even known how different these processes will be when working with spatially-discretized Hamiltonians in real time, as opposed to spatiotemporally-discretized actions in imaginary time.

On the lattice, matter field transformations take the form they did in the continuum,

$$\psi(x) \rightarrow \Omega(x)\psi(x) \tag{1.63}$$

at all sites x . For derivative fields, we have to choose what we mean by ‘derivative’ on the lattice. A simple choice is the forward derivative $\partial_\mu^+ f(x) = (f(x+1) - f(x))/a_s$. The discrete operator ∂_μ^+ suffers a problem like that encountered in the continuum,

$$\partial_\mu^+(\Omega(x)\psi_l(x)) = \Omega(x)\partial_\mu^+\psi_l(x) + (\partial_\mu^+\Omega(x))\psi_l(x + e_\mu) \tag{1.64}$$

[cf. discussion around (1.6)], but the second term is arguably worse now, due to the dependence on the translated value $\psi_l(x + e_\mu)$. A covariant derivative is formed this time by introducing group matrices $U(x, x + e_\mu)$:

$$D_\mu\psi(x) = a_s^{-1}[U(x, x + e_\mu)\psi(x + e_\mu) - \psi(x)] \tag{1.65}$$

These matrices are prescribed the simultaneous transformations

$$U(x, x + e_\mu) \rightarrow \Omega(x)U(x, x + e_\mu)\Omega^{-1}(x + e_\mu) . \quad (1.66)$$

The $U(x, x + e_\mu)$ are referred to as link variables. For brevity, we can also take $U_\mu(x) \equiv U(x, x + e_\mu)$ and $U_\mu(x)^{-1} = U(x + e_\mu, x)$. The link variables are most closely related to the continuum A_μ by path-ordered products in the continuum, which have the same transformation rules:

$$\mathcal{P} \exp \left[-i \int_z^x dy^\mu A_\mu(y) \right] \rightarrow \Omega(x) \mathcal{P} \exp \left[-i \int_z^x dy^\mu A_\mu(y) \right] \Omega^{-1}(z) \quad (1.67)$$

$$\Rightarrow U_\mu(x, x + e_\mu) \sim \mathcal{P} \exp \left[-i \int_{x+e_\mu}^x dy^\mu A_\mu(y) \right] . \quad (1.68)$$

Also by analogy with the continuum, the transformation rules of the path ordered product imply that gauge invariant Wilson loops from the continuum have lattice counterparts formed by multiplying together U_μ 's along links to form closed contours. The smallest such loop is called a plaquette, given by

$$U_{\mu\nu}(x) = U_\mu(x)U_\nu(x + e_\mu)U(x + e_\nu)_\mu^{-1}U(x)_\nu^{-1} \quad (1.69)$$

$$U_{\mu\nu}(x) \rightarrow \Omega(x)U_{\mu\nu}(x)\Omega^{-1}(x) \quad (1.70)$$

$$\Rightarrow \text{tr}(U_{\mu\nu}) \rightarrow \text{tr}(U_{\mu\nu}) . \quad (1.71)$$

Using the plaquettes and lattice covariant derivative, the Wilson gauge action with naïve fermions is

$$S = - \sum_{x\mu\nu} \frac{1}{2g^2 r a_s^4} \text{tr}(1 - U_{\mu\nu}) - \sum_{x\mu} \frac{1}{2a_s} \left[\bar{\psi}(x)\gamma^\mu U_\mu(x, x + e_\mu)\psi(x + e_\mu) - \bar{\psi}(x + e_\mu)\gamma^\mu U_\mu^\dagger(x, x + e_\mu)\psi(x) \right] . \quad (1.72)$$

The continuum limit of the Wilson action reproduces the classical action. The naïve lattice action is so named because it is known to suffer from so-called fermion ‘‘doublers’’, but addressing them is outside the scope of this dissertation and a variety of improvements are already known and regularly employed (for example, staggered [39], clover [40], domain wall [41–44], overlap [45], Ginsparg-Wilson [46], and fixed point [47, 48] fermions).

1.4 Quantized Hamiltonian formulation

In this section we review the basic setup of Hamiltonian lattice gauge theory. This largely follows Chapter 4 of Ref. [37] on lattice gauge fields. Ref. [49] is also an instructive contemporary resource.

In Hamiltonian lattice gauge theory, we work with Hilbert spaces corresponding to elements of the gauge group G , one such space for each link. In a path integral formulation, we integrate over all classical matrices U^ρ in some irrep ρ of the gauge group. Where necessary, we take ρ to be a unitary representation. We can think of these classical matrices as positions on the group manifold G in the particular representation ρ . The local link Hilbert space $\mathcal{H}_{\text{link}}$ can then be constructed from the eigenstates of a position operator \hat{U}^ρ . The operator-matrix eigenvalue relation is

$$\hat{U}^\rho |g\rangle = |g\rangle D^\rho(g) , \quad \text{i.e.,} \quad \hat{U}^\rho_{m'm} |g\rangle = |g\rangle D^\rho(g)_{m'm} \quad (1.73)$$

where $D^\rho(g)$ is a Wigner matrix for g , in the representation ρ . With respect to Hilbert space operations, the eigenvalue matrix behaves as a c-number. Note that even if we had started from a path integral for a particular irrep, we can freely choose ρ in (1.73) to be any irrep we like, with the action of \hat{U}^ρ defined as given.

In the path integral formulation, the Lagrangian is defined to be invariant under local gauge transformations. The generators are of course the matrices T_α introduced at the start. What are needed now are the quantum generators that will induce the right transformations on link variables.

The effect of a lattice gauge transformation $\Omega(x)$ is to rotate the link operators just like the classical transformation:

$$\hat{U}^\rho(x, i) \xrightarrow{\Omega} \hat{U}^\rho(x, i)' = \Omega^\rho(x) \hat{U}^\rho(x, i) \Omega^\rho(x + e_i)^{-1} . \quad (1.74)$$

We will often use L (R) to refer to the “left” (“right”) end of the link, namely x ($x + e_i$) for link $U_i(x)$.

We will denote the Hilbert space symmetry transformations that perform these local gauge transformations for us by $\hat{\Theta}_L$ and $\hat{\Theta}_R$. $\hat{\Theta}_L(g)$ will be defined to shift the eigenvalue of \hat{U}^ρ by left-multiplication with g :

$$\hat{U}^\rho \hat{\Theta}_L(g) |h\rangle \equiv D^\rho(g h) \hat{\Theta}_L(g) |h\rangle \quad (1.75)$$

$$\Rightarrow \hat{\Theta}_L(g)^{-1} \hat{U}^\rho \hat{\Theta}_L(g) = D^\rho(g) \hat{U}^\rho . \quad (1.76)$$

Similarly, $\hat{\Theta}_R(g)$ is defined so that the eigenvalue of \hat{U}^ρ is right-multiplied by g^{-1} :

$$\hat{U}^\rho \hat{\Theta}_R(g) |h\rangle \equiv D^\rho(h g^{-1}) |h\rangle \quad (1.77)$$

$$\Rightarrow \hat{\Theta}_R(g)^{-1} \hat{U}^\rho \hat{\Theta}_R(g) = \hat{U}^\rho D^\rho(g^{-1}) . \quad (1.78)$$

Defined this way, the left and right transformations each provide representations of the group, namely

$$\hat{\Theta}_L(g_1) \hat{\Theta}_L(g_2) = \hat{\Theta}_L(g_1 g_2) , \quad (1.79)$$

$$\hat{\Theta}_R(g_1) \hat{\Theta}_R(g_2) = \hat{\Theta}_R(g_1 g_2) . \quad (1.80)$$

The generators of left and right rotations are those operators \hat{L}_α and \hat{R}_α such that

$$\hat{\Theta}_L(g) = \exp(i \omega^\alpha \hat{L}_\alpha) , \quad (1.81)$$

$$\hat{\Theta}_R(g) = \exp(i \omega^\alpha \hat{R}_\alpha) . \quad (1.82)$$

Since the $\hat{\Theta}_{L/R}$ have the same multiplication table as the elements of G , the generators must obey the same Lie algebra as the generators T_α :

$$[\hat{L}_\alpha, \hat{L}_\beta] = i C^\gamma_{\alpha\beta} \hat{L}_\gamma , \quad (1.83)$$

$$[\hat{R}_\alpha, \hat{R}_\beta] = i C^\gamma_{\alpha\beta} \hat{R}_\gamma . \quad (1.84)$$

The $\hat{\Theta}_{L/R}$ operators effectively translate the link operator through the group manifold. The operators \hat{L}_α and \hat{R}_α are then infinitesimal generators of translations along that manifold. This makes it natural to ask what the commutation relations are for \hat{U}^ρ with \hat{L}_α and \hat{R}_α . The properties given above are all we need to infer the commutation relations.

First, by acting $[\hat{\Theta}_L(g), \hat{U}^\rho]$ on an arbitrary state $|h\rangle$ and factoring out \hat{U}^ρ , we obtain the operator identity

$$[\hat{\Theta}_L(g), \hat{U}^\rho] = \hat{\Theta}_L(g)(I^\rho - D^\rho(g))\hat{U}^\rho . \quad (1.85)$$

Now taking $g = \exp(i\omega^\alpha T_\alpha)$ with $\omega^\alpha \ll 1$, the left-hand side is $i\omega^\alpha[\hat{L}_\alpha, \hat{U}^\rho] + O(\omega)^2$. On the right-hand side, we have $D^\rho(g) = \exp(i\omega^\alpha T_\alpha^\rho)$, and since the factor $(I^\rho - D^\rho(g))$ is already $O(\omega)$, the leading order behavior is obtained by dropping $O(\omega)$ corrections to $\hat{\Theta}_L(g)$. Thus,

$$i\omega^\alpha[\hat{L}_\alpha, \hat{U}^\rho] + O(\omega)^2 = -i\omega^\alpha T_\alpha^\rho \hat{U}^\rho + O(\omega^2) \quad (1.86)$$

From here we can read off the canonical commutation relation $[\hat{L}_\alpha, \hat{U}^\rho] = -T_\alpha^\rho \hat{U}^\rho$.

We can then do an analogous exercise using $\hat{\Theta}_R(g)$. This time we find

$$[\hat{\Theta}_R(g), \hat{U}^\rho] = \hat{U}^\rho(D^\rho(g) - I^\rho)\hat{\Theta}_R(g) \quad (1.87)$$

Using infinitesimals as was done with $\hat{\Theta}_L$, we find $[\hat{R}_\alpha, \hat{U}^\rho] = \hat{U}^\rho T_\alpha^\rho$. The results of both calculations are summarized as

$$[\hat{L}_\alpha, \hat{U}^\rho] = -T_\alpha^\rho \hat{U}^\rho , \quad (1.88a)$$

$$[\hat{R}_\alpha, \hat{U}^\rho] = +\hat{U}^\rho T_\alpha^\rho . \quad (1.88b)$$

To be sure, T_α^ρ are matrices in group space, while \hat{U}^ρ have both group space and Hilbert space structure.

So far left and right generators have been discussed as separate objects. However, they are related by parallel transport, which will be important for characterizing states later.

A right rotation $\hat{\Theta}_R(h)$ on a state can be expressed in terms of a left rotation in a trivial way by noting

$$\hat{\Theta}_R(h) |g\rangle = |gh^{-1}\rangle = \hat{\Theta}_L(gh^{-1}g^{-1}) |g\rangle . \quad (1.89)$$

To relate right and left generators, however, we are after an operator relation and not just a ket-dependent equivalence. To proceed we will concentrate on infinitesimal transformations since that is enough to tell us about the generators.

We start by taking $h = e^{i\eta^\alpha T_\alpha}$ for small η . Then the left-hand side of 1.89 expands out to

$$\hat{\Theta}_R(h) |g\rangle = (\hat{1} + i\eta^\alpha \hat{R}_\alpha + \dots) |g\rangle . \quad (1.90)$$

As for the right-hand side, we first need to expand the argument of $\hat{\Theta}_L$ as

$$gh^{-1}g^{-1} = 1 - i\eta^\alpha g T_\alpha g^{-1} + \dots . \quad (1.91)$$

We know that if the linear term of this group element is put into the form $i\omega^\alpha T_\alpha$, then the linear term of the left rotation $\hat{\Theta}_L$ will simply be $i\hat{L}_\alpha \omega^\alpha$. Here we will need the automorphism property relating the adjoint representation to any other representation (Appendix A of Ref. [37])

$$(\Omega^\rho)^{-1} T_\alpha^\rho \Omega^\rho = (\Omega^A)_\alpha{}^\beta T_\beta^\rho \quad (1.92)$$

or equivalently $\Omega^\rho T_\alpha^\rho (\Omega^\rho)^{-1} = T_\beta^\rho (\Omega^A)^\beta{}_\alpha$. The linear term of the argument to $\hat{\Theta}_L$ is therefore $-i T_\alpha D^A(g)^\alpha{}_\beta \eta^\beta$, from which we see that $\omega^\alpha = -D^A(g)^\alpha{}_\beta \eta^\beta$. Thus, the right-hand side of eq. (1.89) is given by

$$\hat{\Theta}_L(gh^{-1}g^{-1}) |g\rangle = [\hat{1} + i\hat{L}_\alpha (-D^A(g)^\alpha{}_\beta \eta^\beta) + \dots] |g\rangle \quad (1.93)$$

$$= (\hat{1} - i\eta^\alpha \hat{L}_\beta (\hat{U}^A)^\beta{}_\alpha + \dots) |g\rangle . \quad (1.94)$$

Comparing this with eq. (1.90), we finally see the parallel transport relation of left and right generators:

$$\hat{R}_\alpha = -\hat{L}_\beta (\hat{U}^A)^\beta{}_\alpha . \quad (1.95)$$

We have motivated a parallel transport relationship between \hat{L} and \hat{R} , but the real test is if \hat{R} as defined has all the properties we expect. A natural starting point would be the canonical commutation relations. To show that (1.88) works out, we will need the automorphism property again as well as the fact that elements of \hat{U} from any representations

commute with each other. Proceeding,

$$\begin{aligned}
[\hat{R}_\alpha, \hat{U}^\rho{}_\beta{}^\gamma] &= -[\hat{L}_\delta(\hat{U}^A)^\delta{}_\alpha, \hat{U}^\rho{}_\beta{}^\gamma] \\
&= -[\hat{L}_\delta, \hat{U}^\rho{}_\beta{}^\gamma](\hat{U}^A)^\delta{}_\alpha - \hat{L}_\delta[(\hat{U}^A)^\delta{}_\alpha, \hat{U}^\rho{}_\beta{}^\gamma] \\
&= (T_\delta^\rho)_{\beta}{}^\epsilon \hat{U}^\rho{}_\epsilon{}^\gamma (\hat{U}^A)^\delta{}_\alpha - 0 \\
&= (T_\delta^\rho (\hat{U}^A)^\delta{}_\alpha)_{\beta}{}^\epsilon \hat{U}^\rho{}_\epsilon{}^\gamma \\
&= (\hat{U}^\rho T_\alpha^\rho (\hat{U}^\rho)^{-1})_{\beta}{}^\epsilon \hat{U}^\rho{}_\epsilon{}^\gamma \\
&= (\hat{U}^\rho T_\alpha^\rho)_{\beta}{}^\gamma
\end{aligned} \tag{1.96}$$

$$\Rightarrow [\hat{R}_\alpha, \hat{U}^\rho] = \hat{U}^\rho T_\alpha^\rho, \tag{1.97}$$

as required.

Another check is that left and right generators commute:

$$\begin{aligned}
-[\hat{R}_\alpha, \hat{L}_\beta] &= [\hat{L}_\gamma(\hat{U}^A)^\gamma{}_\alpha, \hat{L}_\beta] \\
&= [\hat{L}_\gamma, \hat{L}_\beta](\hat{U}^A)^\gamma{}_\alpha + \hat{L}_\delta[(\hat{U}^A)^\delta{}_\alpha, \hat{L}_\beta] \\
&= i C^\delta{}_{\gamma\beta} \hat{L}_\delta(\hat{U}^A)^\gamma{}_\alpha + \hat{L}_\delta(T_\beta^A)^\delta{}_\gamma (\hat{U}^A)^\gamma{}_\alpha \\
&= i C^\delta{}_{\gamma\beta} \hat{L}_\delta(\hat{U}^A)^\gamma{}_\alpha + \hat{L}_\delta(-i C^\delta{}_{\gamma\beta})(\hat{U}^A)^\gamma{}_\alpha \\
&= 0.
\end{aligned} \tag{1.98}$$

Yet another important test is reproducing the Lie algebra. Using a couple applications of a product rule for commutators, one finds

$$\begin{aligned}
[\hat{R}_\alpha, \hat{R}_\beta] &= [\hat{R}_\alpha, -\hat{L}_\delta(\hat{U}^A)^\delta{}_\beta] \\
&= -\hat{L}_\delta[\hat{R}_\alpha, (\hat{U}^A)^\delta{}_\beta] - [\hat{R}_\alpha, \hat{L}_\delta](\hat{U}^A)^\delta{}_\beta \\
&= \hat{L}_\delta[\hat{L}_\gamma(\hat{U}^A)^\gamma{}_\alpha, (\hat{U}^A)^\delta{}_\beta] - 0 \\
&= \hat{L}_\delta \left([\hat{L}_\gamma, (\hat{U}^A)^\delta{}_\beta](\hat{U}^A)^\gamma{}_\alpha + \hat{L}_\gamma[(\hat{U}^A)^\gamma{}_\alpha, (\hat{U}^A)^\delta{}_\beta] \right) \\
&= \hat{L}_\delta[\hat{L}_\gamma, (\hat{U}^A)^\delta{}_\beta](\hat{U}^A)^\gamma{}_\alpha + 0.
\end{aligned} \tag{1.99}$$

The last expression is easily shown to equal $i \hat{L}_\delta C^\delta{}_{\epsilon\gamma} (\hat{U}^A)^\epsilon{}_\beta (\hat{U}^A)^\gamma{}_\alpha$. Here we note that the

invariance of the structure constants under any rotation Ω^A is expressed by

$$C^{\delta}_{\varepsilon\gamma}(\Omega^A)^{\varepsilon}_{\beta}(\Omega^A)^{\gamma}_{\alpha} = C^{\gamma}_{\beta\alpha}(\Omega^A)^{\delta}_{\gamma} , \quad (1.100)$$

giving

$$\begin{aligned} \hat{L}_{\delta}[\hat{L}_{\gamma}, (\hat{U}^A)^{\delta}_{\beta}](\hat{U}^A)^{\gamma}_{\alpha} &= i \hat{L}_{\delta} C^{\gamma}_{\beta\alpha} (\hat{U}^A)^{\delta}_{\gamma} \\ &= i C^{\gamma}_{\alpha\beta} (-\hat{L}_{\delta} (\hat{U}^A)^{\delta}_{\gamma}) \\ &= i C^{\gamma}_{\alpha\beta} \hat{R}_{\gamma} . \end{aligned} \quad (1.101)$$

We have therefore seen that $[\hat{R}_{\alpha}, \hat{R}_{\beta}] = i C^{\gamma}_{\alpha\beta} \hat{R}_{\gamma}$, as required.

Finally, the parallel transport relationship can be used to show that the quadratic Casimirs at either end of a link are equal. This follows by noting that the parallel transport relation is equivalently expressed by

$$\hat{R}^{\alpha} = -(\hat{U}^A)^{-1\alpha}_{\beta} \hat{L}^{\beta} . \quad (1.102)$$

Therefore,

$$\hat{R}_{\alpha} \hat{R}^{\alpha} = \hat{L}_{\beta} (\hat{U}^A)^{\beta}_{\alpha} (\hat{U}^A)^{-1\alpha}_{\gamma} \hat{L}^{\gamma} \quad (1.103)$$

$$= \hat{L}_{\beta} \hat{L}^{\beta} . \quad (1.104)$$

Considering a particular link $(x, x+e_i)$ within a Cartesian lattice, the operators associated with it are $\hat{U}_i^{\rho}(x) = \hat{U}^{\rho}(x, x+e_i)$, $\hat{L}_{\alpha}^i(x)$, and $\hat{R}_{\alpha}^i(x+e_i)$. We have fixed Weyl gauge, so $\hat{U}^{\rho}(x, x+e_0) = 1$ and only the spatial links are dynamical and affected by the residual gauge symmetry. Both the \hat{L}_{α} and \hat{R}_{α} from a given link obey the Lie algebra of the group. Summing all of them around a site then gives generators for all links joined to the site simultaneously,

$$\hat{\mathcal{T}}_{\alpha}(x) = a_s^{-d} \sum_i (\hat{L}_{\alpha}^i(x) + \hat{R}_{\alpha}^i(x)) \quad (1.105)$$

The factors a_s^{-d} are inserted to get the same mass dimension as the covariant divergences $(\hat{D}_i \hat{\Pi}^i)_{\alpha}$ from the continuum, which the above operators must correspond to given how they

generate gauge transformations on all links emanating from a site. These operators satisfy lattice analogues of the continuum commutation relations:

$$[\hat{\mathcal{T}}_\alpha(\vec{x}), \hat{\mathcal{T}}_\beta(\vec{y})] = i C^\gamma_{\alpha\beta} \hat{\mathcal{T}}_\gamma(\vec{x}) a_s^{-d} \delta_{\vec{x}, \vec{y}} . \quad (1.106)$$

To explicitly see the correspondence with the covariant divergences $(\hat{D}_i \hat{\Pi}^i)_\alpha$ from the continuum, let us identify gauge fields $A^\rho(x, x + e_i)$ with link operators by $\hat{U}^\rho(x, x + e_i) \equiv \exp(-i a_s \hat{A}^\rho(x, x + e_i))$. Then we have

$$\begin{aligned} (\hat{L}_\alpha^i(x) + \hat{R}_\alpha^i(x)) &= \left(\hat{L}_\alpha^i(x) - (\hat{U}^A)^\beta{}_\alpha(x - e_i, x) \hat{L}_\beta(x - e_i) \right) \\ &= \left(\hat{L}_\alpha^i(x) - \left(\delta_\alpha^\beta - i a_s \hat{A}^\gamma(x - e_i, x) (T_\gamma^A)^\beta{}_\alpha + O(a_s^2) \right) \hat{L}_\beta(x - e_i) \right) \\ &= \left(a_s \partial_i^- \hat{L}_\alpha^i(x) + i a_s \hat{A}^A(x - e_i, x)^\beta{}_\alpha \hat{L}_\beta(x - e_i) + O(a_s^2) \right) \\ &= a_s \partial_i^- \hat{L}_\alpha^i(x) + a_s C^\beta{}_{\alpha\gamma} \hat{A}^\gamma(x - e_i, x) \hat{L}_\beta(x - e_i) + O(a_s^2) . \end{aligned} \quad (1.107)$$

Or, alternatively,

$$(\hat{L}_\alpha^i(x) + \hat{R}_\alpha^i(x)) = -a_s \partial_i^+ \hat{R}_\alpha^i(x) - C^\beta{}_{\alpha\gamma} A^\gamma(x, x + e_i) \hat{R}_\beta^i(x + e_i) + O(a_s^2) . \quad (1.108)$$

The above two results show that the lattice generators $\hat{\mathcal{T}}_\alpha$ can be identified with $\hat{D}_i \hat{\Pi}_\alpha^i$ in the continuum limit if we identify $\hat{\Pi}_\alpha^i$ with $a_s^{1-d} \hat{L}_\alpha^i$ or with $-a_s^{1-d} \hat{R}_\alpha^i$.

Summarizing these observations, \hat{L}_α^i and \hat{R}_α^i can essentially be thought of as being $\hat{\Pi}_\alpha^i$ evaluated at infinitesimal distances to either side of the site,

$$\begin{aligned} \hat{\Pi}_\alpha^i(\vec{x} + \delta e_i) &= a_s^{1-d} \hat{L}_\alpha^i(\vec{x}) , \\ \hat{\Pi}_\alpha^i(\vec{x} - \delta e_i) &= -a_s^{1-d} \hat{R}_\alpha^i(\vec{x}) , \\ 0 &< \delta \ll 1 . \end{aligned}$$

Note, however, that at nonzero a_s the conjugate momenta identified as such do not commute.

Instead, we have only that

$$\left[a_s^{1-d} \hat{L}_\alpha^i(\vec{x}), a_s^{1-d} \hat{L}_\beta^j(\vec{y}) \right] = a_s i C^\gamma_{\alpha\beta} (a_s^{1-d} \hat{L}_\gamma^i(\vec{x})) (a_s^{-d} \delta_{\vec{x},\vec{y}}) \delta^{ij} \quad (1.109)$$

$$\sim a_s i C^\gamma_{\alpha\beta} (a_s^{1-d} \hat{L}_\gamma^i(\vec{x})) \delta(\vec{x} - \vec{y}) \delta^{ij} , \quad (1.110)$$

$$\left[-a_s^{1-d} \hat{R}_\alpha^i(\vec{x}), -a_s^{1-d} \hat{R}_\beta^j(\vec{y}) \right] = a_s i C^\gamma_{\alpha\beta} (a_s^{1-d} \hat{R}_\gamma^i(\vec{x})) (a_s^{-d} \delta_{\vec{x},\vec{y}}) \delta^{ij} \quad (1.111)$$

$$\sim a_s i C^\gamma_{\alpha\beta} (a_s^{1-d} \hat{R}_\gamma^i(\vec{x})) \delta(\vec{x} - \vec{y}) \delta^{ij} . \quad (1.112)$$

These commutators are suppressed by a factor of a_s , so the requirement that $[\hat{\Pi}_\alpha(\vec{x}), \hat{\Pi}_\beta(\vec{y})] = 0$ is recovered in the continuum limit.

For matter fields, gauge transformations at a site should take the form

$$\hat{\Theta}^{-1}(g) \hat{\psi}_l \hat{\Theta}(g) = D^\rho(g) l^m \hat{\psi}_m \quad (1.113)$$

$$\hat{\Theta}^{-1}(g) \hat{\psi} \hat{\Theta}(g) = D^\rho(g) \hat{\psi} . \quad (1.114)$$

If $\hat{J}_\alpha^0(x)$ are Noether charge densities such that

$$[\hat{J}_\alpha^0(x), \hat{\psi}_l(y)] = -(T_\alpha^\rho) l^m \hat{\psi}_m(x) \delta_{\vec{x},\vec{y}} / a_s^d , \quad (1.115)$$

$$[\hat{J}_\alpha^0(\vec{x}), \hat{J}_\beta^0(\vec{y})] = i C^\gamma_{\alpha\beta} \hat{J}_\gamma^0(\vec{x}) \delta_{\vec{x},\vec{y}} / a_s^d , \quad (1.116)$$

then complete generators of local gauge transformations are given by the lattice Gauss law operators $\hat{\mathcal{G}}_\alpha$:

$$\hat{\mathcal{G}}_\alpha(x) = a_s^{-d} \sum_{i=1}^d (\hat{L}_{\alpha,i}(x) + \hat{R}_{\alpha,i}(x)) + \hat{J}_\alpha^0(x) . \quad (1.117)$$

Like in the continuum, examples of such a charge density would be $\psi^\dagger(x) T_\alpha^\rho \psi(x)$ for fermionic fields. Then the symmetry operator associated to an aggregate gauge transformation parametrized by $\epsilon^\alpha(\vec{x})$ would be

$$\hat{\Theta}[\epsilon] = \exp \left[i \sum_{\vec{x}} a_s^d \epsilon^\alpha(\vec{x}) \hat{\mathcal{G}}_\alpha(\vec{x}) \right] = \prod_{\vec{x}} \exp \left[i a_s^d \epsilon^\alpha(\vec{x}) \hat{\mathcal{G}}_\alpha(\vec{x}) \right] . \quad (1.118)$$

When we speak of a theory being gauge invariant, we mean foremost that its Hamiltonian commutes with the Gauss law operators. The Gauss law operators then give a collection of

constants of motion, and we will always consider “allowed” or “physical” lattice states to be those that are invariant under gauge transformations, with

$$\hat{\mathcal{G}}_\alpha(x) |\text{phys}\rangle = 0 \quad (1.119)$$

being the lattice realization of $\hat{D}_i \hat{E}_\alpha^i |\text{phys}\rangle = g \hat{J}_\alpha^0 |\text{phys}\rangle$ from the continuum.² However, one can in principle change these constants of motion to describe static charge sources, giving rise to charge superselection sectors that are dynamically isolated from each other.

For calculations, one must eventually choose a basis, and in Hamiltonian lattice gauge theory it is common to use one that diagonalizes electric fields rather than their conjugate gauge fields. This is because the Gauss law constraints given above are expressed in terms of electric fields, so characterizing and working in the subspace of allowed states is easier. The quantum numbers characterizing a link state correspond to some complete set of commuting operators (CSCO) for the generators.

For $SU(2)$, the familiar CSCO is $\{\vec{J} \cdot \vec{J}, J_3\}$; $\vec{J} \cdot \vec{J}$ has angular momentum eigenvalues $j(j+1)$ for half-integers j and completely characterizes any irreducible representation of $SU(2)$, while J_3 can have eigenvalues $m = j, j-1, \dots, -j$. Recalling that a link comes with mutually commuting left and right electric fields,

$$\{\hat{L}_\alpha \hat{L}^\alpha, \hat{L}_3, \hat{R}_\alpha \hat{R}^\alpha, \hat{R}_3\} \quad (1.120)$$

are all mutually commuting, but we also have that the quadratic Casimir is a link invariant, $\hat{L}_\alpha \hat{L}^\alpha = \hat{R}_\alpha \hat{R}^\alpha$. Putting this all together, a basis of $SU(2)$ irreducible representation or “irrep” states can be labeled as

$$|j, m_L, m_R\rangle . \quad (1.121)$$

For $SU(3)$, an additional Casimir invariant would be available, $d^{\alpha\beta\gamma} T_\alpha T_\beta T_\gamma$. A CSCO is then given by the two Casimir operators, along with isospin $t_1^2 + t_2^2 + t_3^2$, isospin projection t_3 ,

²A proper physical Hilbert space should generally respect more symmetries than just gauge constraints, such as translational invariance, parity, etc., but this dissertation is primarily concerned with the gauge constraints.

and hypercharge t_8 . The latter three, not being invariants, have distinct quantum numbers on each side of a link, so that states would be of the form

$$|p, q, I_L, I_{3,L}, Y_L, I_R, I_{3,R}, Y_R\rangle \quad (1.122)$$

[with p and q labeling the irreducible representation of $SU(3)$.] We will not have much to say about $SU(3)$ in this dissertation, but details of the formalism have been discussed and worked out, e.g., in Refs. [25, 50, 51].

1.5 Schwinger boson formulation

The Hamiltonian generates dynamics among states that satisfy Gauss's law, i.e.,

$$\hat{\mathcal{G}}_\alpha(x) |\text{phys}\rangle = 0 \quad \text{for all } x, \alpha. \quad (1.123)$$

Dynamics of this sort is usually described using redundant but local degrees of freedom. Alternatively, these states can be described in terms of arbitrary gauge-invariant Wilson loop and Wilson line operators acting on some reference state. Characterizing states this way, however, leads to a highly overcomplete basis; mutually dependent loops satisfy Mandelstam constraints [52–54], which are nonlocal and notoriously hard to solve. A central aim of the remainder of this work is to encode dynamics using local degrees of freedom that both satisfy Gauss's law and are orthogonal, starting from multiplets of harmonic oscillators [55].

The method of Schwinger bosons [56] is a way of providing an explicit realization of the algebraic structure in terms of simple harmonic oscillators, satisfying the familiar commutation relations

$$[\hat{a}_i, \hat{a}_j^\dagger] = \delta_{ij} , \quad (1.124)$$

$$[\hat{a}_i, \hat{a}_j] = [\hat{a}_i^\dagger, \hat{a}_j^\dagger] = 0 . \quad (1.125)$$

This follows from the fact that, given generators T_α , the same Lie algebra is obeyed by

contracting the generators with the oscillators,

$$\hat{\tau}_\alpha = \hat{a}^\dagger T_\alpha \hat{a} = \hat{a}^{\dagger b} (T_\alpha)_b^c \hat{a}_c \quad (1.126)$$

$$\Rightarrow [\hat{\tau}_\alpha, \hat{\tau}_\beta] = i C^\gamma{}_{\alpha\beta} \hat{\tau}_\gamma . \quad (1.127)$$

The beauty of this trick is the simplicity of working in terms of simple harmonic oscillators.

Working with the new degrees of freedom can introduce redundancy. It is apparent by inspection that the generators $\hat{\tau}_\alpha$ are linear combinations of total-number-conserving operators – they all commute with $\hat{a}^\dagger \hat{a}$. If all operators in the theory are like this, then the dynamics started in one eigenspace of $\hat{a}^\dagger \hat{a}$ will never explore any other sector of the Hilbert space.

This occupation number conservation corresponds to a continuous U(1) symmetry:

$$\hat{a}_i \rightarrow e^{i\theta} \hat{a}_i . \quad (1.128)$$

This transformation preserves the oscillator commutation relations and consequently the algebra of $\hat{\tau}_\alpha$. The symmetry transformation is generated by the total number operator,

$$[\hat{N}, \hat{a}_i] = -\hat{a}_i , \quad (1.129)$$

$$e^{-i\theta\hat{N}} \hat{a}_i e^{i\theta\hat{N}} = e^{i\theta} \hat{a}_i . \quad (1.130)$$

The “prepotential” formulation of lattice gauge theory [51, 55, 57–59] is an application of this method that provides an alternative, equivalent framework to the formalism of Kogut and Susskind. This formulation replaces \hat{E} and \hat{U} with bilinears of harmonic oscillator doublets $\hat{a}_a(L/R)$ (the Schwinger bosons or prepotentials) at the left (L) and right (R) ends of each link $(x, x + e_i)$, as shown in Fig. 1.1.

The electric fields on a link are realized by introducing multiplets for each side of the link,

$$\hat{L}_\alpha \equiv \hat{a}^\dagger(L) T_\alpha \hat{a}(L) , \quad (1.131a)$$

$$\hat{R}_\alpha \equiv \hat{a}^\dagger(R) T_\alpha \hat{a}(R) . \quad (1.131b)$$

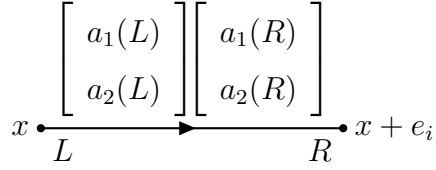


Figure 1.1: A link (x, i) from a Cartesian lattice starting at x and terminating at $x + e_i$. We denote the starting side “left” (L) and the terminal side “right” (R). Link ends each host a bosonic oscillator doublet, here indicated by $a(L) = (a_1(L), a_2(L))$ at L and $a(R) = (a_1(R), a_2(R))$ at R . The arrow indicates the link orientation, pointing from L to R .

It is always possible to form $U(1)$ generators on each side,

$$\hat{N}_{L/R} = \hat{a}^\dagger(L/R) \cdot \hat{a}(L/R) . \quad (1.132)$$

The requirement that left and right Casimirs be equal leads to an Abelian Gauss law (AGL) relating these $U(1)$ generators along each link:

$$\hat{N}_L(x, i) |\text{phys}\rangle = \hat{N}_R(x + e_i, i) |\text{phys}\rangle . \quad (1.133)$$

It is useful to define Hermitian projectors for the AGL-satisfying subspace within the tensor product space of all Schwinger boson modes:

$$\hat{\mathcal{P}}_A(x, i) = \int_{-\pi}^{\pi} \frac{d\phi}{2\pi} e^{i\phi(\hat{N}_R(x+e_i, i) - \hat{N}_L(x, i))} . \quad (1.134)$$

In later chapters we will be most concerned with $SU(2)$ gauge theories. An explicit decomposition of a link operator in this case is

$$\hat{U} \equiv \hat{U}_L \hat{U}_R , \quad (1.135)$$

$$\hat{U}_L \equiv \frac{1}{\sqrt{\hat{N}_L + 1}} \begin{pmatrix} \hat{a}_2^\dagger(L) & \hat{a}_1(L) \\ -\hat{a}_1^\dagger(L) & \hat{a}_2(L) \end{pmatrix} , \quad (1.136a)$$

$$\hat{U}_R \equiv \begin{pmatrix} \hat{a}_1^\dagger(R) & \hat{a}_2^\dagger(R) \\ -\hat{a}_2(R) & \hat{a}_1(R) \end{pmatrix} \frac{1}{\sqrt{\hat{N}_R + 1}} . \quad (1.136b)$$

With the above definitions, the relations (1.88) follow. One can also show that the Schwinger boson construction of \hat{U} is indeed a ‘special unitary’ matrix on the AGL-satisfying Hilbert space:

$$\begin{aligned}\hat{\mathcal{P}}_A \hat{U}^\dagger \hat{U} \hat{\mathcal{P}}_A &= \hat{\mathcal{P}}_A \hat{U} \hat{U}^\dagger \hat{\mathcal{P}}_A \\ &= \hat{\mathcal{P}}_A \begin{pmatrix} 1 & 0 \\ 0 & 1 \end{pmatrix} \hat{\mathcal{P}}_A ,\end{aligned}\tag{1.137}$$

$$\begin{aligned}\hat{\mathcal{P}}_A \det(\hat{U}) \hat{\mathcal{P}}_A &= \hat{\mathcal{P}}_A (\hat{U}_{11} \hat{U}_{22} - \hat{U}_{12} \hat{U}_{21}) \hat{\mathcal{P}}_A \\ &= \hat{\mathcal{P}}_A (1) \hat{\mathcal{P}}_A = \hat{\mathcal{P}}_A .\end{aligned}\tag{1.138}$$

That this link operator can really be thought of as an $SU(2)$ matrix is exemplified by the relation

$$\hat{\mathcal{P}}_A (\hat{U}_{22} - \hat{U}_{11}^\dagger) \hat{\mathcal{P}}_A = \hat{\mathcal{P}}_A (\hat{U}_{21} + \hat{U}_{12}^\dagger) \hat{\mathcal{P}}_A = 0 .\tag{1.139}$$

And finally, the link operator elements commute as they should within the allowed Hilbert space,

$$\hat{\mathcal{P}}_A [\hat{U}_{\alpha\beta}, \hat{U}_{\gamma\delta}] \hat{\mathcal{P}}_A = \hat{\mathcal{P}}_A [\hat{U}_{\alpha\beta}, \hat{U}_{\gamma\delta}^\dagger] \hat{\mathcal{P}}_A = 0 .\tag{1.140}$$

$$(1.141)$$

Schwinger bosons are an expedient device for doing explicit calculations involving electric and link operators in non-Abelian gauge theories. In Abelian theories, however, it is not so cumbersome to work in the Hilbert spaces as they are conventionally formulated. In the next two chapters, we will simply take Abelian gauge theories and immediately begin analyzing their structure, without any detour through Hilbert spaces of harmonic oscillator multiplets.

Chapter 2

GAUSS LAW CIRCUITS FOR ABELIAN GAUGE THEORIES

In this chapter,¹ algorithms are developed to projectively measure physicality, i.e. consistency of Gauss’s law, on states in Abelian lattice gauge theories by using constraint-checking oracles: a state $|\Psi\rangle = \cos(\theta) |\Psi_{\text{phys}}\rangle + \sin(\theta) |\Psi_{\text{unphys}}\rangle$ will collapse to either $|\Psi_{\text{phys}}\rangle$ or $|\Psi_{\text{unphys}}\rangle$. This could be useful as a method of filtering out non-gauge invariant errors – e.g., an accept-reject step in a simulation (see also [60, 61]), or a subroutine for curing states afflicted with unphysical errors – without the need for all the qubits of fault-tolerant computation. Rejecting unphysical states would be useful when working with small lattices, although large lattices presumably require a more sophisticated solution. A generalization of the approach to a non-Abelian gauge theory is the subject of chapter 6.

In §2.1, the needed gauge theory background is summarized. Then, in §2.2, a procedure is given for constructing oracles that projectively distinguish physical states from unphysical ones. In §2.3, constructions are shown in example theories. Additional remarks on implementation follow since the examples omit details about the exact gates that would be programmed to a device. Section 2.4 then expands on the significance of constraint-checking circuits and their potential applications.

2.1 Mapping of $Z(N)$ and $U(1)$

This section summarizes the Abelian lattice gauge theory structure to be mapped onto a quantum computer. The gauge groups considered are $G = Z(N)$ and $G = U(1)$. Space is discretized using a cubic lattice L with sites s . For simplicity, L is given periodic boundary conditions. The lattice links $\ell \in L$ are associated with independent gauge field Hilbert spaces

¹This chapter is based on *Physical Review A* 99, 042301 (2019).

\mathcal{H}_ℓ , each having an identical discrete basis:

$$\langle m' | m \rangle = \delta_{m'm} , \quad (2.1)$$

$$\hat{1} = \sum_m |m\rangle \langle m| , \quad (2.2)$$

where

$$m', m \in \begin{cases} \mathbb{Z}(N) , & \text{if } G = \mathbb{Z}(N) , \\ \mathbb{Z} , & \text{if } G = \text{U}(1) . \end{cases} \quad (2.3)$$

(The same symbol $\mathbb{Z}(N)$ will be used for the integers modulo N and for the N^{th} roots of unity.) The Hamiltonian is a function of link operators \hat{U}_ℓ associated with the links ℓ and their (dimensionless) conjugate electric fields \hat{E}_ℓ ,

$$\hat{U}_\ell = \sum_{m_\ell} |m_\ell + 1\rangle \langle m_\ell| , \quad (2.4)$$

$$\hat{E}_\ell = \sum_{m_\ell} |m_\ell\rangle m_\ell \langle m_\ell| . \quad (2.5)$$

For $G = \mathbb{Z}(N)$, the Hermitian electric field is periodic and the Hamiltonian really depends on its exponentiated form \hat{Q}_ℓ ,

$$|m_\ell\rangle \equiv |m_\ell \pmod{N}\rangle , \quad (2.6)$$

$$\hat{Q}_\ell \equiv e^{2\pi i \hat{E}_\ell / N} = \sum_{m_\ell=0}^{N-1} |m_\ell\rangle e^{2\pi i m_\ell / N} \langle m_\ell| . \quad (2.7)$$

Operators associated with different links commute, and the same-link commutation relations are

$$\hat{Q}_\ell \hat{U}_\ell \hat{Q}_\ell^\dagger = \hat{U}_\ell e^{2\pi i / N} , \quad \text{if } G = \mathbb{Z}(N) , \quad (2.8)$$

$$[\hat{E}_\ell, \hat{U}_\ell] = \hat{U}_\ell , \quad \text{if } G = \text{U}(1) . \quad (2.9)$$

For the remainder of this chapter, link labels ℓ will only be shown when necessary.

For adding in matter there are many possibilities; to keep things simple yet illustrative, I consider matter fields with anticommuting statistics and carrying unit charge. Each matter

species is labeled with a collective index σ , which could include flavor or Dirac indices, and has possible occupation numbers $0 \leq n_\sigma \leq 1$. The results of this chapter are easily extended to other possibilities.

A lattice “configuration” or “basis state” will be used to refer to any state $|\mathbf{E}, \rho\rangle$ with definite electric fields on the links and occupation numbers on the sites. Usually only one site $s \in L$ is under consideration, so the quantum numbers associated with other sites or links not attached to s are suppressed,

$$|\mathbf{E}, \rho\rangle \rightarrow \otimes_{i=1}^d |E_i(s)\rangle \otimes_{i=1}^d |E_i(s - e_i)\rangle \otimes_\sigma |n_\sigma(s)\rangle .$$

Physicality of a state means the Gauss law constraint is satisfied at each site s . It is convenient to express this by using Gauss law and physicality operators $\hat{\mathcal{G}}_s$ and \hat{F}_s ,

$$\hat{\mathcal{G}}_s \equiv (\nabla \cdot \hat{\mathbf{E}})(s) - \hat{\rho}(s) , \quad (2.10)$$

$$= \sum_{i=1}^d (\hat{E}_i(s) - \hat{E}_i(s - e_i)) - \sum_\sigma e_\sigma \hat{n}_\sigma(s) \quad (2.11)$$

$$\hat{F}_s \equiv \int_0^{2\pi} \frac{d\phi}{2\pi} \begin{cases} \sum_{k=-\infty}^{\infty} e^{-i\phi(\hat{\mathcal{G}}_s - kN)} , & \text{if } G = \text{Z}(N), \\ e^{-i\phi\hat{\mathcal{G}}_s} , & \text{if } G = \text{U}(1). \end{cases} \quad (2.12)$$

Above, $\nabla \cdot$ is a discrete divergence operator and $e_\sigma = \pm 1$ are charges. The physicality operator \hat{F}_s is synonymous with the projector onto the subspace of configurations with Gauss’s law satisfied at s ,

$$\hat{F}_s |\text{phys}\rangle = |\text{phys}\rangle , \quad (2.13)$$

$$\hat{F}_s |\text{unphys}\rangle = 0 . \quad (2.14)$$

The notation $F_s(\mathbf{E}, \rho)$ will be used for the eigenvalue of $|\mathbf{E}, \rho\rangle$ with respect to \hat{F}_s . The operators \hat{F}_s are spatially local, but a full lattice configuration is only physical if $F_s(\mathbf{E}, \rho) = 1$ for all $s \in L$. Oracle operators \hat{O}_s can now be introduced that are related simply to the physicality operators,

$$\hat{O}_s = \hat{1} - 2\hat{F}_s . \quad (2.15)$$

The oracle “flags” states that satisfy Gauss’s law at s ,

$$\hat{O}_s |\mathbf{E}, \rho\rangle = |\mathbf{E}, \rho\rangle (-)^{F_s(\mathbf{E}, \rho)} . \quad (2.16)$$

Operators with such behavior are closely related to Grover’s quantum search algorithm [35, 62]. Understanding \hat{O}_s as a quantum circuit that computes or checks constraints is a central task in the remaining sections.

Quantum simulation requires a Hilbert space of finite dimensionality. For $G = \mathbb{Z}(N)$, the finite lattice volume automatically renders the gauge Hilbert space finite-dimensional. For $G = \text{U}(1)$, the links’ electric fields are uniformly truncated as well. Anticipating the use of qubits (rather than more general qudits or some mixture thereof), the local link dimension for either G is fixed to

$$\dim \mathcal{H}_\ell = 2^n , \quad (2.17)$$

and the states are labeled by non-negative integers $0 \leq \epsilon \leq 2^n - 1$. These correspond to some range of uniformly-spaced electric field values E , the linear relationship being

$$\epsilon = E - E_{\min} , \quad E_{\max} = E_{\min} + 2^n - 1 . \quad (2.18)$$

The truncation when $G = \text{U}(1)$ renders the link operators \hat{U}, \hat{U}^\dagger non-unitary since they can destroy states at the ends of the ladder. Crucially, the commutation relation $[\hat{E}, \hat{U}] = \hat{U}$ survives truncation, and all of the formalism introduced above carries over straightforwardly.

2.2 Oracles for constraints

In this section, the oracle \hat{O}_s is given as a quantum algorithm that internally checks the constraint (2.10) for computational basis states and applies a conditional phase flip. A basic familiarity with quantum computation and notation of the quantum circuit model is assumed. To state an algorithm for constructing \hat{O}_s , the formalism of the previous section will be tailored to a quantum computer.

A binary representation for electric fields $|\epsilon\rangle$ is used. The number of qubits per link is n , so the local link Hilbert space takes the form

$$\mathcal{H}_\ell = \{|0\rangle, |1\rangle\}^{\otimes n}, \quad \dim \mathcal{H}_\ell = 2^n. \quad (2.19)$$

The bit strings represented by the computational basis states are regarded as binary expressions for the electric field labels $0 \leq \epsilon \leq (2^n - 1)$. $\epsilon_i(s)$ and $\epsilon_i(s - e_i)$ are referred to as ϵ_i^{OUT} and ϵ_i^{IN} . And, for simplicity, the occupation numbers $n_\sigma = 0, 1$ will be identified with the computational labels 0 and 1.

The constraint function (2.10) at s can be rewritten as

$$\nabla \cdot \mathbf{E} - \rho = \left(\sum_{i=1}^d \epsilon_i^{\text{OUT}} + \sum_{\sigma: e_\sigma < 0} n_\sigma \right) - \left(\sum_{i=1}^d \epsilon_i^{\text{IN}} + \sum_{\sigma: e_\sigma > 0} n_\sigma \right). \quad (2.20)$$

Writing it this way suggests the negative and positive charges be separately absorbed into the internal computation of the out-flux and in-flux. One can easily imagine a variety of ways to arrange the internal arithmetic to compute the constraint, but with the procedure outlined below it turns out there are cheap ways to include small numbers of fermions if the addition subroutines use incoming “carry” qubits.

The main ideas of the algorithm can be illustrated by constructing the oracle and entangling it with an auxiliary “query bit” $|q\rangle$ that gets flipped if Gauss’s law holds at site s for a given wave function. (“Bit” will frequently be used in place of “qubit.”) This query bit is the probe for the oracle’s action, since a global phase change alone is not observable. The procedure is as follows:

1. Initialize needed work bits. This includes the query bit $|q\rangle$ in a \hat{Z} basis state $|0\rangle$ or $|1\rangle$.
2. Apply a Hadamard gate to the query bit.
3. Compute both sums on the right-hand side of (2.20).
4. Compute the difference of (or compare) these sums.

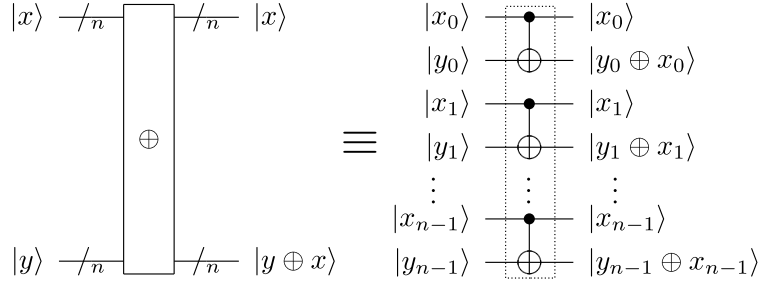


Figure 2.1: A multi-qubit subroutine \oplus for comparing two n -bit integers x and y by adding all their corresponding bits modulo two: A (non)zero result for $y \oplus x$ means x is (not) equal to y .

5. Apply a phase flip if and only if the constraint vanishes and the query bit is set to $|1\rangle$.
6. Undo (uncompute) the arithmetic of steps 4 and 3, restoring the state's original quantum numbers.
7. Apply another Hadamard gate to the query bit.
8. Measure the query bit in the \hat{Z} basis.

A flip of the query bit $|q\rangle \rightarrow |q \oplus 1\rangle$ is found if and only if Gauss's law is satisfied at the site. In practice, it is usually cheaper to forego evaluating \mathcal{G}_s proper (step 4) in favor of a more direct comparison of two integers. This is accomplished with a string of CNOTs, as shown in Fig. 2.1. These CNOTs are denoted by a multi-qubit gate, \oplus .

Calls to the oracle will generally be described in terms of their action on computational basis states. When the input lattice wave function is any superposition of physical ($F_s = 1$) and unphysical ($F_s = 0$) components, measuring the query bit afterward will probabilistically project the wave function onto one eigenspace of \hat{F}_s or the other.

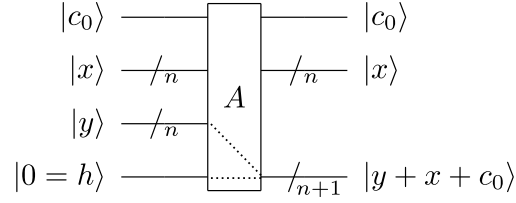


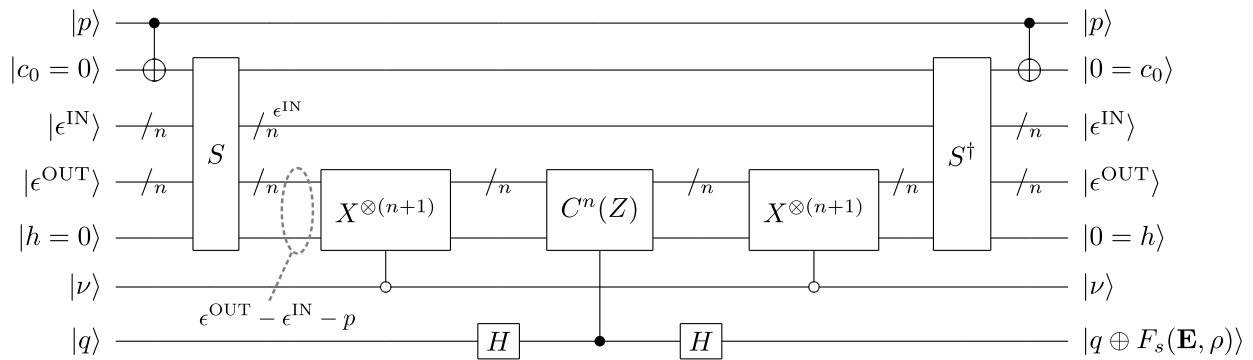
Figure 2.2: A generic adder A for adding two n -bit integers “in place.” A is assumed to take an incoming carry bit $c_0(=0,1)$, whose value can be added to $y + x$ at no additional cost. The overflow bit $h = 0$ is needed to express the $(n + 1)$ -bit sum.

2.3 Examples and remarks

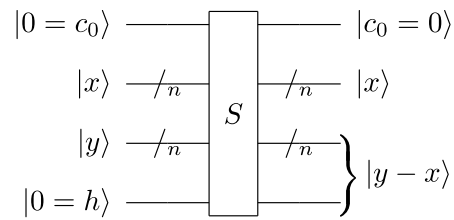
This section expands on how the oracles work by showing circuits for example theories. Truncated $U(1)$ shares more features with the simulation of non-Abelian groups than does $Z(2^n)$, so figures are shown for the former case and the small modifications needed for the latter are explained in the text. The adders needed for checking a constraint are indicated by multi-qubit gates A , defined in Fig. 2.2. It is common for addition algorithms to take an incoming carry bit c_0 initialized to zero, which can be exploited to account for fermions. For now, the adders’ inner workings will be neglected because the exact choice of algorithm they use is mostly irrelevant to the oracle. The simplest interesting matter scenarios will be seen to cost essentially the same as their pure gauge counterparts (except in 1D), but more general matter content requires introducing more adder subroutines—thereby increasing the number of required gates. Thereafter, remarks are made about the adders, and T gate counts are given for the examples.

2.3.1 1D $U(1)$ and $Z(N)$

Figure 2.3a depicts an oracle for 1D $U(1)$ gauge theory coupled to one Dirac fermion. The physical inputs from a lattice site are two n -bit electric field states $|\epsilon^{\text{OUT,IN}}\rangle$ and occupation numbers $|\nu\rangle, |p\rangle$. The incoming carry bit $|c_0\rangle$ is set equal to $|p\rangle$. (One could simply use $|p\rangle$



(a) A quantum circuit for checking Gauss's law. This circuit accommodates one Dirac fermion and uses the subtractor routine S as defined to the right.



(b) A subtractor routine S , which may be thought of as a modified version of A .

Figure 2.3: A query to the oracle for $U(1)$ or $Z(2^n)$ gauge theory in 1D.

as the carry bit.) An overflow bit $|h\rangle$ is used for storing the result of the subtraction routine S , which is defined in Fig. 2.3b. This is the only example in which actually performing the subtraction in (2.20) does not cost more gates than a simple comparison. Additional work bits could be needed by the subtraction subroutine S , or by the controlled- Z .

In more detail: The subtractor S , regarded as a modified version of A , first computes the difference of two n -bit electric fields, $\epsilon^{\text{OUT}} - \epsilon^{\text{IN}}$, using the relation

$$a - b = \overline{\bar{a} + b} , \quad (2.21)$$

$$|\bar{a}\rangle = X^{\otimes n} |a\rangle . \quad (2.22)$$

The bar notation defined in (2.22) defines the “ones’ complement” of a . However, this notation is abused in (2.21); the precise meaning is

$$\underbrace{|a\rangle}_{n \text{ bits}} - \underbrace{|b\rangle}_{n \text{ bits}} \equiv 1 \otimes \underbrace{X \otimes \cdots \otimes X}_{X^{\otimes n}} \underbrace{|\bar{a} + b\rangle}_{n+1 \text{ bits}} , \quad (2.23)$$

meaning the overflow bit supplied to the internal A is not flipped after addition. When $b > a$, (2.21) yields $a - b$ modulo 2^{n+1} . Setting $|c_0\rangle = |p\rangle$ manipulates the subtraction to yield $|\epsilon^{\text{OUT}} - \epsilon^{\text{IN}} - p\rangle$, which is flipped when $|\nu\rangle = |0\rangle$. Inversion operators at the end uncompute the constraint, restoring the original configuration. The net result of the circuit is that q is flipped if and only if $\mathcal{G}_s(\mathbf{E}, \rho)$ vanishes.

This is all made clearer by considering some simple inputs (taking $q = 1$):

- (i) $\epsilon^{\text{OUT}} = \epsilon^{\text{IN}} = p = \nu = 0$: The output of S is $|0\rangle^{\otimes(n+1)}$. Because $\nu = 0$, this gets flipped to $|1\rangle^{\otimes(n+1)}$. The $C^n(Z)$ gate is therefore triggered by the physical configuration.
- (ii) $\epsilon^{\text{OUT}} = \epsilon^{\text{IN}} = 0, \nu = p = 1$: The output of S will be $|1\rangle^{\otimes(n+1)}$. Because $\nu = 1$, this output is not flipped. The $C^n(Z)$ gate is therefore triggered by the physical configuration.
- (iii) $\epsilon^{\text{OUT}} = 1, \epsilon^{\text{IN}} = p = \nu = 0$: The output of S will be $|0 \cdots 01\rangle$, which gets flipped to $|1 \cdots 10\rangle$. The $C^n(Z)$ gate is consequently not triggered by the unphysical configuration.

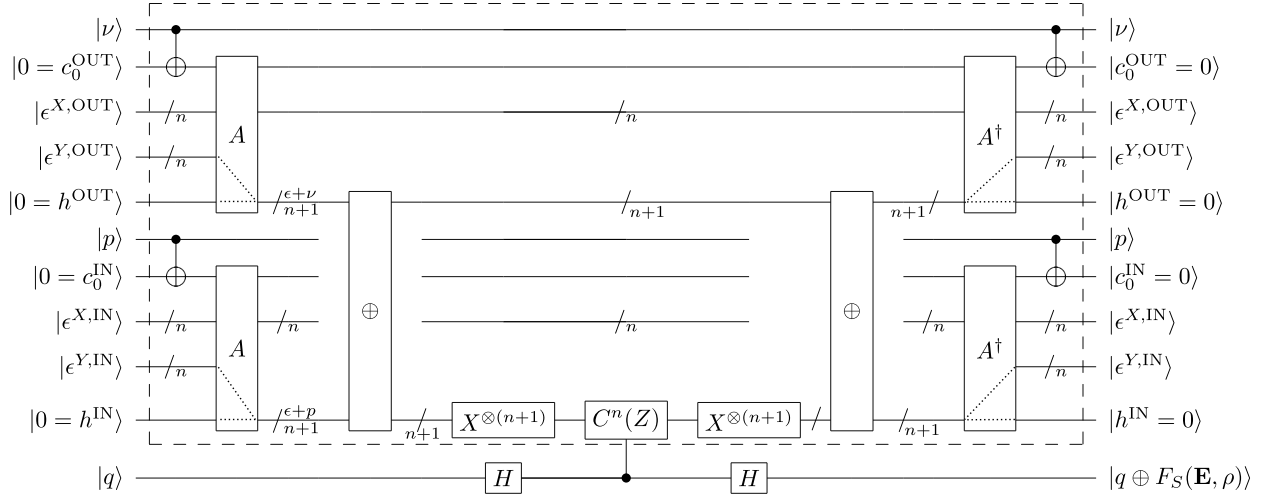


Figure 2.4: A query to the oracle for $U(1)$ gauge theory in 2D. This example accommodates one flavor of Dirac fermion via the occupation numbers ν and p . To modify this for $G = Z(2^n)$, the overflow bits $h^{\text{OUT,IN}}$ would be removed.

More generally, the circuit does not always compute \mathcal{G}_s proper, but the $C^n(Z)$ gate is nevertheless triggered exactly when \mathcal{G}_s vanishes.

The modification needed for $Z(2^n)$ is to omit the overflow bit h and only work with an n -bit difference (instead of the $n + 1$ bits from (2.23)). The modification for 1D pure gauge theory is more significant: For either $G = U(1)$ or $G = Z(2^n)$, physicality is equivalent to saying E^{OUT} are E^{IN} identical. The oracle is therefore simply constructed using the \oplus gates introduced earlier, bit flips, and a controlled- Z .

2.3.2 2D $U(1)$: Pure gauge or one Dirac fermion

In Fig. 2.4, an oracle for 2D $U(1)$ gauge theory with one Dirac fermion is illustrated. The inputs to the oracle from the lattice are four n -bit electric field states $|\epsilon^{\{x,y\},\{\text{OUT,IN}\}}\rangle$ and occupation numbers $|\nu\rangle, |p\rangle$. Carry bits $|c_0^{\text{OUT,IN}}\rangle$ and overflow bits $|h^{\text{OUT,IN}}\rangle$ are provided for the adders. Some lines break over multi-qubit gates, emphasizing that they do not participate

in those gates. Additional work bits could be required by the subtraction subroutine S or by the controlled- Z . The result of the circuit is that q is flipped if and only if $\mathcal{G}_s(\mathbf{E}, \rho) = 0$.

In more detail: The first stage of this circuit involves summing the total out-flux and total in-flux in parallel. When ϵ_y^{OUT} is added to ϵ_x^{OUT} , a CNOT controlled by $|\nu\rangle$ on the incoming carry can have the effect of counting one unit of negative charge in the sense of (2.20); this observation also applies to the in-flux computation with $|p\rangle$ as the control. The second stage “adds” these two results bit-wise. Third, a phase flip is applied if and only if the bit-wise sum was $0 \cdots 00$: this is accomplished by flipping the bits, acting with a $C^{n+1}(Z)$ gate, and then flipping them back.

For this matter scenario, checking (2.20) costs essentially the same as its pure gauge analogue. The point is that an adder/subtractor for the “ $-\rho$ ” term in \mathcal{G}_s has been avoided; more flavors would require more adder subroutines, i.e., many more gates than the four explicit CNOTs in Fig. 2.4. The pure gauge version is obtained by omitting $|\nu\rangle$, $|p\rangle$, and the four CNOT gates attached to them. To modify the 2D oracle for $G = Z(2^n)$, the overflow bits $h^{\text{OUT,IN}}$ are omitted from the circuit because they do not need to be calculated.

2.3.3 3D $U(1)$: Pure gauge or one Dirac fermion

In Fig. 2.5, an oracle for 3D $U(1)$ gauge theory is illustrated. It is very similar to the 2D oracle. Dirac fermions in 3D have four components, here denoted $|\nu^{1,2}\rangle$ and $|p^{1,2}\rangle$. Like the previous examples, including one flavor costs marginally more gates than the pure gauge analogue—no more than 12 additional CNOTs. Some of these explicit CNOTs serve to reset and reuse the carry bits $c_0^{\text{OUT,IN}}$ a few times throughout the 3D oracle, saving qubits. Similar comments apply to modifying the algorithm for $G = Z(2^n)$ as in 2D: overflow bits are simply omitted from the computation.

2.3.4 Remarks on implementation

While the details of the adder subroutines have thus far been neglected, their implementation generally dominates the oracle gate requirements. There are several known quantum adder

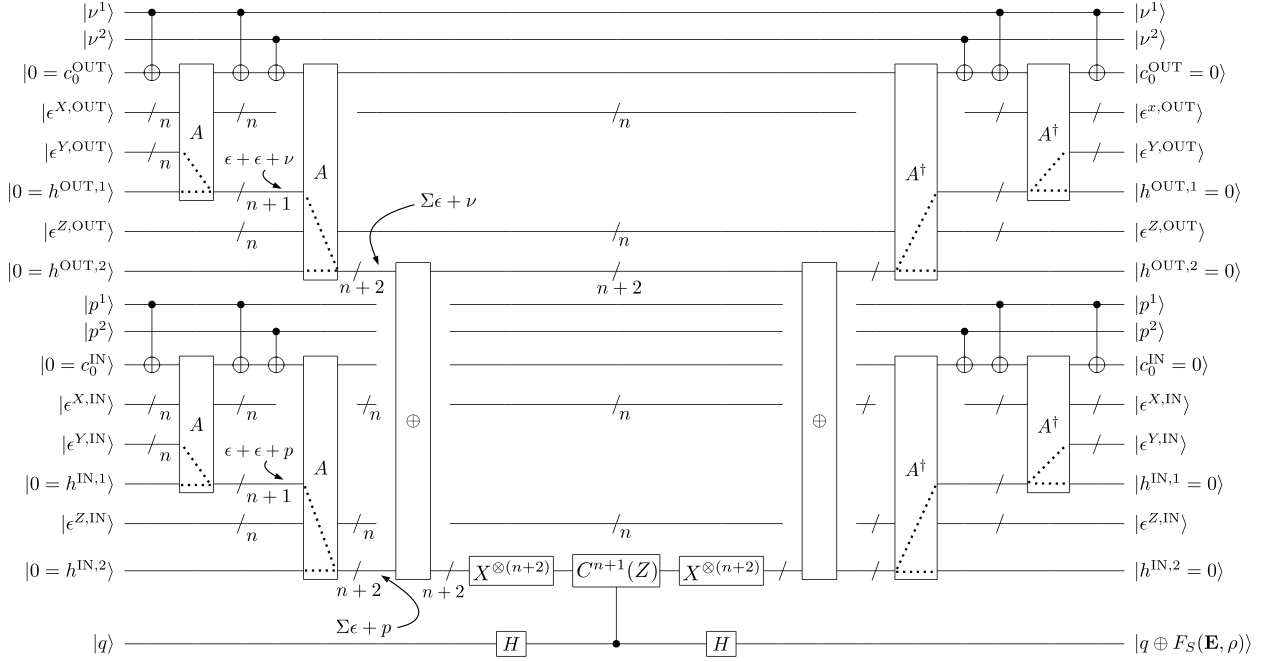


Figure 2.5: A query to the oracle for U(1) gauge theory in 3D. This example accommodates one flavor of Dirac fermion via the occupation numbers $\nu^{1,2}$ and $p^{1,2}$. To modify this for $G = Z(2^n)$, the four overflow bits $h^{\{\text{OUT,IN}\},\{1,2\}}$ would be removed.

Table 2.1: T-counts associated with the arithmetic routines in the oracles for $U(1)$ or $Z(2^n)$ gauge theories, coupled to one Dirac fermion, using the RCA method [2].

Dimension	T-count using RCA (controlled- Z 's excluded)
1D (Fig. 2.3)	$2(8n + O(1))$
2D (Fig. 2.4)	$4(8n + O(1))$
3D (Fig. 2.5)	$4(16n + 8 + O(1))$

algorithms with varying complexities and resource requirements: these include ripple-carry [2, 63], quantum Fourier transformation [64], carry-lookahead [65], carry-save [66], and later developments of these [67–70]. When simulating something as complicated as a lattice gauge theory, an $O(1)$ number of ancillary or scratch bits seems reasonable to ask for, in which case the ripple-carry adder [2] would be suitable. The ripple-carry adder (RCA) costs $8n + O(1)$ T gates, and in Table 2.1 the T-counts are given for the examples of the previous section. Note that a variant of ripple-carry using temporary logical-ANDs [70] could be useful if one can further supply $O(n)$ work qubits, because it can halve the T count associated with the oracle’s arithmetic.

Finally, the examples only explicitly considered one flavor of Dirac matter. It is unlikely that several charged species on sites could be accommodated without introducing more adder subroutines to sum E ’s and ρ ’s, which would appreciably increase the number of gates in the oracle per the remarks above. This is already exemplified by the fact that 1D pure gauge oracles require no adder circuits, but one charged species does require an adder.

2.4 Discussion

The previous sections have introduced routines for testing physicality of wave functions in Abelian lattice gauge theory simulations by essentially calculating the Gauss law operator. The simplest interesting examples involving anticommuting matter in $d = 1, 2, 3$, have been

worked out explicitly. It has been shown that the matter content of those theories requires only a small number of gates (independent of n) more than the pure-gauge computation, but generally more adders are needed somewhere (increasing the T gate count by $O(n)$). The remainder of this work revisits the relevance of these routines to a quantum lattice gauge theory simulation, addressing a couple concerns raised in the Introduction and highlighting the potential applications to error detection.

The first issue is there is a very real possibility (also pointed out by [31, 71]) that Trotter evolution can generate unphysical components in a state vector due to algorithmic approximation errors. The first-order Trotter approximation involves replacing time evolution by the full Hamiltonian $H = \sum_j H_j$ with a sequence of small time steps by each H_j , and taking the limit of small time steps:

$$e^{-it \sum_j H_j} = \lim_{N_t \rightarrow \infty} \left(\prod_j e^{-i \Delta t H_j} \right)^{N_t}, \quad \Delta t = t/N_t. \quad (2.24)$$

In general the individual steps $\exp(-i \Delta t H_j)$ do not commute, so $\prod_j \exp(-i \Delta t H_j) \neq \exp(-i \Delta t \sum_j H_j)$ and the state vector suffers $O(\Delta t^2)$ errors dictated by the Baker-Campbell-Hausdorff (BCH) formula. In a lattice gauge theory, the usual H_j are all gauge invariant operators, so deviations from the BCH formula do not affect Gauss's law. But to simulate using qubits, each H_j would itself need Trotterization down to the level of qubit operations, which is commonly done by decomposing H_j into multi-qubit Pauli operators. It is well-known how to implement the Trotter steps once they are in the form $\exp(-i t \sigma_{\mu_1} \otimes \sigma_{\mu_2} \otimes \dots)$. It is the errors from this second level of decomposition that generally do not commute with Gauss's law. Hence, at any finite Trotter step size, even a physical initial state and evolution via noiseless gates generically creates unphysical components in the state. A more explicit discussion of the problems with first-order Trotterization is given for the Schwinger model in Appendix A. These theoretical errors (as opposed to stochastic) can in principle be quantified, and it may be possible to apply methods from oblivious amplitude amplification [72, 73] to help rotate wave functions closer to the physical subspace. An algorithm to help "fix" a state that has acquired overlap onto the unphysical subspace by rotating it would be extremely useful, and

if one exists it will almost certainly require constraint-checking oracles.

The second issue has to do with finite quantum noise—even in the optimistic case of gauge invariant time evolution. Most of the basis states available to the quantum computer violate Gauss’s law, which means there is ample unphysical Hilbert space for a state vector to wander into [71, 74]. Error-correcting codes can help to protect against the bit flips that would induce such wandering, but for the foreseeable future it is crucial to save qubits wherever possible. Therefore routines for verifying gauge invariance would be valuable to filtering out this class of errors. Such tests could be accept-reject steps either during time evolution or on the final state.

Indeed, a promising application of the oracles is as collective detection mechanisms for bit flip errors in the vicinity of a site; the gauge invariance condition probes many qubits at once for an error. To better appreciate this, consider a lattice wave function prepared by acting on a physical initial state with some series of gates. If bit flip errors are relatively rare throughout the execution, those that do occur are likely to appear as localized Gauss law violations. This is because a constraint \mathcal{G}_s involves quantum numbers from the site s and its $2D$ links, and any single-qubit X (or Y) error on them will necessarily change \mathcal{G}_s . For multiple X errors on different qubits to look gauge invariant would require they conspire to change the constraint function by compensating amounts. That is, bit flips can only be overlooked if the error itself corresponds to a gauge invariant operator. (Note that any function of qubit Z s is gauge invariant, so phase errors are invisible to the oracle.) On small lattices it might be acceptable to simply reject unphysical states, however the probability of all constraints being preserved in the presence of noise becomes exponentially small with increasing lattice volume. The benefit is that when all the constraints are found to be satisfied, any unphysical components will have been removed from the wave function. Alternatively, knowing where or if a lattice wave function has suffered a bit flip error could serve as input for a correction scheme.

Lastly, it should be noted that this chapter has focused on the digitization of Abelian lattice gauge theories using conventional electric variables, but that is not the only option for

quantum simulating lattice gauge theories. In particular, lattice gauge theories with finite-dimensional link Hilbert spaces have been introduced [75–78] and proposed for quantum simulation [27, 79, 80]. Among these are the Quantum Link Models (QLMs). QLMs have the same local gauge symmetries as the Kogut-Susskind Hamiltonian, but their operator algebra is not identical [30]. Chandrasekharan and Wiese argue in Ref. [77] that 4D Yang-Mills theory can be obtained from a QLM in the limit of infinite extent of a fifth dimension. In taking this limit, they relax the Gauss law constraint, which could have some practical advantages; on the other hand, simulating an extra dimension will present its own challenges. Another approach to lattice gauge theory is the prepotential formalism [51, 58, 81]; a non-Abelian generalization of the oracles in this chapter based on prepotentials is the subject of chapter 6. Many more references for different lattice gauge theory simulation schemes can be found in the review Ref. [82].

Chapter acknowledgments

I thank David B. Kaplan, Natalie Klco, Indrakshi Raychowdhury, Alessandro Roggero, and Martin J. Savage for helpful discussions and feedback during the preparation of this work. I also thank Natalie Klco and Alessandro Roggero for directing me to important references. The work in this chapter was supported by DOE Grant No. DE-FG02-00ER41132 and by the National Science Foundation Graduate Research Fellowship under Grant No. DGE-1256082.

Chapter 3

GAUSS'S LAW, DUALITY, AND THE HAMILTONIAN FORMULATION OF U(1) LATTICE GAUGE THEORY

Quantum computers offer hope for surmounting some of the obstacles encountered in classical lattice simulations, and a number of papers have proposed using the Kogut-Susskind [39] lattice Hamiltonian H_{KS} as a starting point for the study of gauge theories, introducing a cutoff on the electric field (in addition to the finite lattice spacing) in order to render the Hilbert space \mathcal{H} finite-dimensional [25, 30, 83] (for discussions of Hamiltonian lattice gauge theory, see [37, 84]). The vast majority of states in that \mathcal{H} are unphysical; the physical space is limited to those obeying Gauss's Law, which we will call $\mathcal{H}_{\text{phys}} \subset \mathcal{H}$.

There are a couple of drawbacks to this approach which we address in this chapter¹: (i) It appears preferable to work entirely in $\mathcal{H}_{\text{phys}}$ if possible, in order to require fewer qubits and to avoid computational errors causing states initially in $\mathcal{H}_{\text{phys}}$ to evolve into the much larger space of unphysical states; (ii) A cutoff on electric fields is appropriate for strong coupling, for which electric fluctuations are suppressed, but is not ideal for weak coupling, such as one would encounter in the continuum limit for any gauge theory in $d < 3$, or asymptotically-free theories in $d = 3$, where d is the spatial dimension. Instead, a cutoff on magnetic fluctuations would likely be a more efficient regulator, allowing one to approach the continuum limit with a smaller Hilbert space. In this chapter we examine these issues in two of the simplest gauge theories – U(1) theories without matter in $d = 2$ and $d = 3$ – and find that both concerns lead directly to a formulation of the electromagnetic dual theory. While these theories are not of direct physical interest, they are simple enough to clearly illustrate some of the issues that must be faced when simulating U(1) gauge theories with matter, or non-Abelian gauge

¹This chapter is drawn from arXiv:1806.08797, done in collaboration with D.B. Kaplan.

theories.

3.1 $U(1)$ Hamiltonian and Hilbert space

The Hamiltonian for a $U(1)$ gauge theory in the continuum is $\hat{H} = (1/2) \int d^d x (\hat{E}^2 + \hat{B}^2)$, where the electric field operator \hat{E}_i is the conjugate momentum for the vector potential \hat{A}_i . Here we consider compact $U(1)$ gauge theory formulated on a spatial lattice L with lattice spacing a_s , periodic boundary conditions, and coordinates $\{\mathbf{n}, \boldsymbol{\ell}, \mathbf{p}, \mathbf{c}\}$ for sites, links, plaquettes, and cubes, respectively. Compact $U(1)$ theory is interacting at finite a_s ; because time and space are treated asymmetrically, there are two coupling constants $g_{t,s}$ which must be independently renormalized, with dimensionless couplings defined as $\tilde{g}_{t,s}^2 = a_s^{3-d} g_{t,s}^2$. The continuum limit is equivalent to $\tilde{g}_{t,s}^2 \rightarrow 0$ for $d < 3$ (as well as for asymptotically-free non-Abelian gauge theories in $d = 3$). We fix $A_0 = 0$ gauge, and replace the vector potential $\mathbf{A}(x)$ by a unitary operator $\hat{U}_{\boldsymbol{\ell}} = \exp(-i a_s \hat{A}_{\boldsymbol{\ell}})$ on every link; $\hat{U}_{\boldsymbol{\ell}}$ can be thought of as the coordinate operator for a particle moving on the group manifold. The space \mathcal{H} can be represented in the coordinate basis of product states $\otimes_{\boldsymbol{\ell}} |U_{\boldsymbol{\ell}}\rangle$, where $|U_{\boldsymbol{\ell}}\rangle$ at each link $\boldsymbol{\ell}$ is an eigenstate of $\hat{U}_{\boldsymbol{\ell}}$ with eigenvalue $U_{\boldsymbol{\ell}}$, which is a phase. Alternatively, one can work in the momentum basis, which diagonalizes the electric field $E_{\boldsymbol{\ell}}$ also residing on the links. The rescaled electric field

$$\hat{\mathcal{E}}_{\boldsymbol{\ell}} \equiv \frac{a_s^{\frac{d+1}{2}}}{\tilde{g}_s} \hat{E}_{\boldsymbol{\ell}} \quad (3.1)$$

satisfies the commutation relation

$$\left[\hat{\mathcal{E}}_{\boldsymbol{\ell}}, \hat{U}_{\boldsymbol{\ell}'} \right] = \delta_{\boldsymbol{\ell}, \boldsymbol{\ell}'} \hat{U}_{\boldsymbol{\ell}}, \quad (3.2)$$

and has integer eigenvalues $\varepsilon_{\boldsymbol{\ell}}$, analogous to the angular momentum of a particle on a circle. \mathcal{H} can then be represented in the electric field basis of product states $\otimes_{\boldsymbol{\ell}} |\varepsilon_{\boldsymbol{\ell}}\rangle$ and regulated in a gauge-invariant way by restricting fluctuations of the electric field, $|\varepsilon_{\boldsymbol{\ell}}| \leq \Lambda$ for some cutoff Λ [25].

Our starting point for the lattice Hamiltonian is $\hat{H} = \hat{H}_E + \hat{H}_B$, with

$$\hat{H}_B = \frac{1}{2a_s} \left[\frac{1}{\tilde{g}_s^2} \sum_{\mathbf{p}} \left(2 - \hat{P}_{\mathbf{p}} - \hat{P}_{\mathbf{p}}^\dagger \right) \right],$$

$$\hat{H}_E = \frac{1}{2a_s} \left[\frac{\tilde{g}_t^2}{\xi^2} \sum_{\ell} \left(2 - \hat{Q}_{\ell} - \hat{Q}_{\ell}^{\dagger} \right) \right], \quad (3.3)$$

where we define

$$\hat{Q}_{\ell} \equiv e^{i\xi\hat{\mathcal{E}}_{\ell}}, \quad \hat{P}_{\mathbf{n},ij} \equiv \hat{U}_{\mathbf{n},i} \hat{U}_{\mathbf{n}+\mathbf{e}_i,j} \hat{U}_{\mathbf{n}+\mathbf{e}_j,i}^{\dagger} \hat{U}_{\mathbf{n},j}^{\dagger}. \quad (3.4)$$

Here \hat{H}_B is conventional with \hat{P}_p being the usual plaquette operator, but in \hat{H}_E we have introduced the dimensionless parameter ξ for convenience, where eq. (3.3) yields the Kogut-Susskind Hamiltonian H_{KS} in the limit $\xi \rightarrow 0$. This is similar to the Hamiltonian for $Z(N)$ gauge theory in [85]. The parameter $a_t \equiv \xi a_s$ can be thought of as a “temporal lattice spacing,” and additional irrelevant terms subleading in a_t could be added, but the above symmetric form suits our purposes best. Eq. (3.2) implies that \hat{U} acts as a raising operator for the electric quantum number, and can be expressed in the electric field basis as $\hat{U} = \sum_{\varepsilon} |\varepsilon + 1\rangle \langle \varepsilon|$. The action of \hat{P} , therefore, is to create an oriented loop of unit electric flux around the edge of the plaquette, while \hat{P}^{\dagger} creates a unit loop in the opposite direction. At the same time, \hat{P} measures magnetic field, the phase of its eigenvalue being the magnetic flux through the plaquette to leading order in a_s . The above form for \hat{H} is bounded and written as a sum of unitary operators, which may be convenient for simulation by quantum walks [86].

Note that fluctuations in the magnetic field are large at strong coupling, while electric fluctuations are large at weak coupling. This is similar to the case of a harmonic oscillator with mass m and spring constant k , where $\langle \hat{x}^2 \rangle \propto 1/\sqrt{km}$, while $\langle \hat{p}^2 \rangle \propto \sqrt{km}$, the operators \hat{x} , \hat{p} being analogues of \hat{B} , \hat{E} respectively, while $m \sim 1/\tilde{g}_t^2$ and $k \sim 1/\tilde{g}_s^2$. Thus regulating the theory with a cutoff on electric field values is a poor choice for gauge theories in $d < 3$, as the continuum limit occurs in the weak coupling limit.

The physical subspace $\mathcal{H}_{\text{phys}} \subset \mathcal{H}$ consists of those states obeying the Gauss law constraint $\vec{\nabla} \cdot \vec{E} = 0$, i.e., those states invariant under spatial gauge transformations. On the lattice, the analogue constraint is that at each lattice site the product of the \hat{Q} on each

outgoing link and \hat{Q}_ℓ^\dagger on each incoming link must equal the unit operator:

$$\left(\prod_{\ell \text{ into } \mathbf{n}} \hat{Q}_\ell \prod_{\ell \text{ out of } \mathbf{n}} \hat{Q}_\ell^\dagger - \hat{\mathbf{1}} \right) |\text{phys}\rangle = 0 . \quad (3.5)$$

Most states in \mathcal{H} violate eq. (3.5) and are unphysical, and therefore on a quantum computer more qubits than necessary will be needed to simulate this Hamiltonian. Most states in \mathcal{H} violate eq. (3.5) and are unphysical, and therefore simulating Hamiltonian evolution in \mathcal{H} will use more qubits on a quantum computer than physically necessary. To better understand this constraint, consider the lattice L with periodic boundary conditions in $d = 2, 3$ dimensions with n sites, and therefore $\ell = nd$ links, $p = nd(d-1)/2$ plaquettes, and $c = nd(d-1)(d-2)/6$ cubes. The Hilbert space \mathcal{H} is characterized by the eigenvalues of the ℓ electric field variables, \hat{Q}_ℓ . States fall into topological sectors labeled by an integer-valued d -tuple, $\boldsymbol{\nu} = (\nu_1, \dots, \nu_d)$ designating ν_i units of electric flux wrapping around the \mathbf{e}_i direction of the lattice. For a given topological sector we have $(n+d-1)$ constraints on the $\ell = nd$ electric field variables: $(n-1)$ constraints from Gauss's law and d from fixing the topology. Therefore there are $[nd - (n+d-1)] = (n-1)(d-1)$ variables to describe physical states in a particular topological sector. If we place a cutoff on electric field values to regulate the theory, and assume $n \gg 1$, then the minimum number of qubits required to describe $\mathcal{H}_{\text{phys}}$ will scale as $(d-1)/d$ times the minimum number required for \mathcal{H} ; this ratio is expected to be significantly smaller for non-Abelian theories.

The benefit of restricting a computation to $\mathcal{H}_{\text{phys}}$ is not only in reduction of qubits, but also in ensuring that computational errors do not propagate states into the unphysical part of \mathcal{H} , a process that would look like violation of charge conservation. A brute-force approach for restricting $\mathcal{H} \rightarrow \mathcal{H}_{\text{phys}}$ is to eliminate the constrained variables in the quantum theory by the procedure illustrated in Fig. 3.1: (i) Define a maximal tree on the lattice, with $(n-1)$ links; (ii) eliminate the $|\varepsilon_\ell\rangle$ states from \mathcal{H} for each link in the tree; (iii) set $\hat{U}_\ell \equiv 1$ in \hat{H} for each eliminated link; (iv) recursively solve for the \hat{Q}_ℓ in \hat{H} at each eliminated link, in terms of the \hat{Q} 's on the free links; (v) remove the final d links by enforcing a fixed topology $\boldsymbol{\nu}$. The fourth step involves defining \hat{Q} operators on each of the tree links as the appropriate product

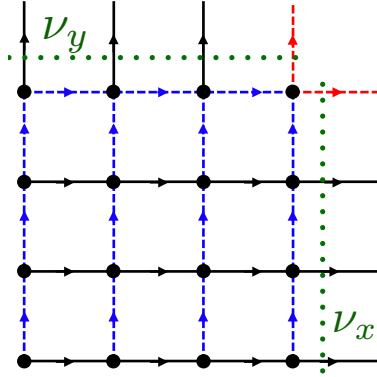


Figure 3.1: An $n = 16$ site lattice with periodic boundary conditions in $d = 2$ with $nd = 32$ links. The $(n - 1) = 15$ links on a maximal tree (dashed blue) are eliminated via Gauss's Law. The $d = 2$ links in dashed red are eliminated by constraining the net electric flux through the dotted green lines to equal the topological quantum numbers $\nu_{x,y}$. The remaining $(n - 1)(d - 1) = 15$ black links represent the physical variables of the theory. This procedure generalizes to arbitrary d, n .

of the other \hat{Q}, \hat{Q}^\dagger operators meeting at the same vertex, beginning at the ends of the tree branches; fixing the topology (step five) can be easily done at the border of the maximal tree, as indicated in Fig. 3.1. The resulting $\mathcal{H}_{\text{phys}}$ on a given sector ν is written using products of the $|\varepsilon_\ell\rangle$ states over each of the $(n - 1)(d - 1)$ free links; a heavy price is paid, however, in the loss of locality and discrete translational invariance of the resulting Hamiltonian. We next describe an alternative procedure, which leads directly to a duality transformation.

3.2 $U(1)$ dual formulation

Physical states can be defined in terms of gauge-invariant operators acting on the trivial state $|0\rangle$ with zero electric field everywhere [39]; those operators can be constructed out of Wilson loops – products of \hat{U}_ℓ along closed paths. We first define the Polyakov loop operators $\hat{W}(C_i)$ to be the product of oriented \hat{U} link operators along a closed loop C_i that wraps around the

lattice in the \mathbf{e}_i compact direction. We then define the state

$$|\boldsymbol{\nu}\rangle \equiv \prod_{i=1}^d \left(\hat{W}(C_i) \right)^{\nu_i} |0\rangle, \quad \nu_i \in \mathbb{Z}. \quad (3.6)$$

All the physical states within a topological class are then created by acting on $|\boldsymbol{\nu}\rangle$ with powers of plaquette operators:

$$|\mathcal{A}\rangle_{\boldsymbol{\nu}} = \prod_{\mathbf{p}} \left(\hat{P}_{\mathbf{p}} \right)^{\mathcal{A}_{\mathbf{p}}} |\boldsymbol{\nu}\rangle, \quad \mathcal{A}_{\mathbf{p}} \in \mathbb{Z}, \quad (3.7)$$

where \mathbf{p} runs over all p plaquette coordinates. It is evident that $|\mathcal{A}\rangle_{\boldsymbol{\nu}} \in \mathcal{H}_{\text{phys}}$ for all \mathcal{A} and $\boldsymbol{\nu}$ since both the \hat{W} and \hat{P} operators are gauge-invariant, each producing only closed loops of electric flux. It is also easy to see that any of the $\otimes_{\ell} |\varepsilon_{\ell}\rangle$ basis states obeying Gauss's law can be written in this form. The particular choice of the C_i paths is unimportant, since two such paths can be deformed into each other by the application of plaquette operators. The problem now, however, is that the $|\mathcal{A}\rangle_{\boldsymbol{\nu}}$ states are an over-complete basis for $\mathcal{H}_{\text{phys}}$, since a state in a particular topological sector depends on $p = nd(d-1)/2$ variables instead of the required $(n-1)(d-1)$. The number of redundant \mathcal{A} variables is therefore $R = (d-1)[1 + (d-2)n/2]$. For $d = 2$, the redundancy is $R = 1$, independent of the number of sites n ; for $d = 3$, $R = 2 + n$, scaling with the volume of the lattice. These redundancies arise because the product of plaquette operators around any closed surface is an identity operation, expressing the discretized integral form of $\vec{\nabla} \cdot \vec{B} = 0$; R simply counts the number of independent closed surfaces. We will deal with the redundancy by treating all of the $|\mathcal{A}\rangle_{\boldsymbol{\nu}}$ states as independent, then subsequently imposing the magnetic Gauss law constraint.

The action of the Hamiltonian eq. (3.3) on the $|\mathcal{A}\rangle_{\boldsymbol{\nu}}$ states is simple to characterize: \hat{H}_B applies plaquette operators to the state, and therefore either raises or lowers $\mathcal{A}_{\mathbf{p}}$ by one. \hat{H}_E measures the electric field, which at each link is determined by differences between the $\mathcal{A}_{\mathbf{p}}$ for the plaquettes the link borders — with a possible additional contribution from the Polyakov loop in eq. (3.6) if the link lies along one of the C_i curves. \hat{H}_E therefore looks like a finite difference operator acting on $\mathcal{A}_{\mathbf{p}}$. The behavior of H_B and H_E can be most naturally described in terms of operators on the dual lattice. We first discuss the simpler case of

$d = 2$, where the duality transformation maps the $\{\mathbf{n}, \boldsymbol{\ell}, \mathbf{p}\}$ coordinates of L to $\{\mathbf{p}^*, \boldsymbol{\ell}^*, \mathbf{n}^*\}$, respectively, on the dual lattice L^* . \mathbf{n} sits at the center of plaquette \mathbf{p}^* and \mathbf{n}^* sits at the center of \mathbf{p} , while $\boldsymbol{\ell}^*$ and $\boldsymbol{\ell}$ intersect each other; we adopt a convention where the x -links of the two lattices are oriented anti-parallel to each other, while the y -links are parallel. By ignoring the redundancy in our definition of $|\mathcal{A}\rangle_{\boldsymbol{\nu}}$ in eq. (3.7), we can treat $\mathcal{A}_{\mathbf{n}^*}$ as an independent integer-valued variable on each site and use product states $\otimes_{\mathbf{n}^*} |\mathcal{A}_{\mathbf{n}^*}\rangle$ as a basis for a Hilbert space \mathcal{H}^* . In terms of these states, we can define the two local coordinate and shift operators, $\hat{\mathcal{U}}_{\mathbf{n}^*}$ and $\hat{\mathcal{Q}}_{\mathbf{n}^*}$, living on sites of the dual lattice as

$$\begin{aligned}\hat{\mathcal{U}}_{\mathbf{n}^*} &= \sum_{\mathcal{A}_{\mathbf{n}^*}} |\mathcal{A}_{\mathbf{n}^*}\rangle e^{i\xi\mathcal{A}_{\mathbf{n}^*}} \langle\mathcal{A}_{\mathbf{n}^*}|, \\ \hat{\mathcal{Q}}_{\mathbf{n}^*} &= \sum_{\mathcal{A}_{\mathbf{n}^*}} |\mathcal{A}_{\mathbf{n}^*} + 1\rangle \langle\mathcal{A}_{\mathbf{n}^*}|.\end{aligned}\quad (3.8)$$

For a given topological sector $\boldsymbol{\nu}$, the matrix elements of the Hamiltonian \hat{H} of eq. (3.3) between the $|\mathcal{A}\rangle_{\boldsymbol{\nu}}$ states are reproduced then by the dual Hamiltonian $\hat{\mathcal{H}}_{\boldsymbol{\nu}}$ on L^* ,

$$\begin{aligned}\hat{\mathcal{H}}_{\boldsymbol{\nu}} &= \frac{1}{2a_s} \sum_{\mathbf{n}^*} \left[\frac{1}{\tilde{g}_s^2} \left(2 - \hat{\mathcal{Q}}_{\mathbf{n}^*} - \hat{\mathcal{Q}}_{\mathbf{n}^*}^\dagger \right) \right. \\ &\quad \left. - \frac{\tilde{g}_t^2}{\xi^2} a_s^2 \hat{\mathcal{U}}_{\mathbf{n}^*}^\dagger \Delta \hat{\mathcal{U}}_{\mathbf{n}^*} \right] \quad (d = 2).\end{aligned}\quad (3.9)$$

In this expression, Δ is a discrete covariant Laplacian $\Delta = D_i^+ D_i^-$, where D_i^\pm are the difference operators

$$\begin{aligned}D_1^+ F_{\mathbf{n}^*} &= (\mathcal{W}_{\{\mathbf{n}^*, \mathbf{n}^* - \mathbf{e}_1\}} F_{\mathbf{n}^* - \mathbf{e}_1} - F_{\mathbf{n}^*}) / a_s, \\ D_2^+ F_{\mathbf{n}^*} &= (\mathcal{W}_{\{\mathbf{n}^*, \mathbf{n}^* + \mathbf{e}_2\}} F_{\mathbf{n}^* + \mathbf{e}_2} - F_{\mathbf{n}^*}) / a_s,\end{aligned}\quad (3.10)$$

$D_i^- \equiv -(D_i^+)^\dagger$, and the discrete vector gauge field \mathcal{W} accounts for the topological charges $\boldsymbol{\nu}$:

$$\mathcal{W}_{\boldsymbol{\ell}^*} = \begin{cases} e^{i\xi\nu_i}, & \text{if } \boldsymbol{\ell} \in C_i; \\ 1, & \text{otherwise;} \end{cases}\quad (3.11)$$

$\boldsymbol{\ell}^*$ being the link dual to $\boldsymbol{\ell}$. Note that D_1^+ is a derivative in the $-\mathbf{e}_1$ direction because on L^* we have oriented the x -links anti-parallel to those on L , unlike the y -links, which are parallel.

The gauge symmetry associated with \mathscr{W} reflects the equivalence of constructions based on different C_i paths for the Polyakov loops in eq. (3.6).

The first term in eq. (3.9) arises from \hat{H}_B , while the second from \hat{H}_E , and we see that the roles of the two have been reversed: \hat{H}_B becomes an operator that translates the value of the dual field \mathscr{A} , while \hat{H}_E measures gradients in \mathscr{A} . The discrete gauge field \mathscr{W} corresponding to the topological electric fields of the original theory seems to have no analogue in the original theory, but that is simply because we did not build in topological magnetic field loops; to do so would require a field analogous to \mathscr{W} added to the original Hamiltonian \hat{H} .

As mentioned above, in $d = 2$ there is one redundant variable arising from the fact that $\prod_p \hat{P}_p = \hat{\mathbf{1}}$. Thus the restriction to $\mathcal{H}_{\text{phys}} \subset \mathcal{H}^*$ requires applying the single constraint on physical states

$$\left(\hat{\mathcal{Q}}_{L^*} - \hat{\mathbf{1}} \right) |\mathscr{A}\rangle_{\nu} = 0, \quad \hat{\mathcal{Q}}_{L^*} \equiv \prod_{\mathbf{n}^*} \hat{\mathcal{Q}}_{\mathbf{n}^*}. \quad (3.12)$$

This constraint can be solved by setting $\mathscr{A} = 0$ at a single site \mathbf{n}^* and equating $\hat{\mathcal{Q}}$ at that site to the product of $\hat{\mathcal{Q}}^\dagger$ over all the other sites — again at the cost of sacrificing locality and discrete translational invariance. A more attractive alternative is to work directly in \mathcal{H}^* and simply use an initial wave function that satisfies eq. (3.12). Unlike in the conventional formulation, where the number of constraints scales with the number of lattice sites, here with only a single unphysical variable, the problems of constructing the initial state obeying the constraint — or of subsequently becoming “lost in space” due to computational error — should be vastly diminished compared to simulations in the original space \mathcal{H} subject to eq. (3.5). Because there is one $\hat{\mathcal{Q}}_{\mathbf{n}^*}, \hat{\mathcal{U}}_{\mathbf{n}^*}$ variable pair per site on L^* , as compared with two $\hat{Q}_\ell, \hat{U}_\ell$ variable pairs per site on L , we see the expected $(d-1)/d = 1/2$ reduction in degrees of freedom, which should correspond to a similar reduction in the number of qubits required to characterize the system. However, for this statement to be meaningful, we first have to discuss regulating \mathcal{H}^* to make it finite-dimensional.

To regulate the dual theory in $d = 2$ one cannot simply limit $\mathscr{A}_{\mathbf{n}^*}$ to lie in the finite range $-\Lambda \leq \mathscr{A}_{\mathbf{n}^*} \leq \Lambda$, taking $\Lambda \rightarrow \infty$ in the continuum limit: the operator $\hat{\mathcal{Q}}_{L^*}$ shifts

the $\hat{\mathcal{A}}_{\mathbf{n}^*}$ field uniformly so that the constraint eq. (3.12) cannot hold in a space spanned by eigenstates of the $\hat{\mathcal{A}}_{\mathbf{n}^*}$ with finite eigenvalues. Instead, one can regulate the eigenvalues of the unitary $\mathcal{Q}_{\mathbf{n}^*}$ operators, equivalent to placing a cutoff on magnetic field fluctuations in the original theory. The regulated Hamiltonian will then commute with the constraint, and an initial wave function chosen to satisfy the constraint eq. (3.12) will continue to do so as it evolves. Therefore, in $d = 2$, there are several advantages to simulating $\hat{\mathcal{H}}_{\nu}$ on a quantum computer instead of \hat{H} : (i) the variables are scalars, rather than vectors, reducing the number of degrees of freedom by half; (ii) there is a single redundant variable, rather than the $(n - 1)$ unphysical variables in the conventional formulation; (iii) it is natural to regulate magnetic fluctuations rather than electric, which is likely to converge more efficiently to the continuum limit.

We now turn to the problem of constructing the $d = 3$ Hamiltonian for the $|\mathcal{A}\rangle_{\nu}$ states of eq. (3.7). As for $d = 2$, this naturally leads to a duality transformation, interchanging the coordinates for sites, links, plaquettes and cubes from L to L^* as $\{\mathbf{n}, \boldsymbol{\ell}, \mathbf{p}, \mathbf{c}\} \leftrightarrow \{\mathbf{c}^*, \mathbf{p}^*, \boldsymbol{\ell}^*, \mathbf{n}^*\}$. In particular, the plaquettes \mathbf{p} on L get mapped to the links $\boldsymbol{\ell}^*$ on L^* piercing them in the direction opposite to their normal vectors, so that L^* is parity inverted relative to L . Therefore the plaquette variable $\mathcal{A}_{\mathbf{p}}$ on L gets mapped to a dual vector field $\mathcal{A}_{\boldsymbol{\ell}^*}$ living on the links of L^* , unlike in $d = 2$ where a scalar $\mathcal{A}_{\mathbf{n}^*}$ lives on sites. We can then define link operators $\mathcal{U}_{\boldsymbol{\ell}^*}$ and $\mathcal{Q}_{\boldsymbol{\ell}^*}$ operators exactly as in eq. (3.8), and the dual Hamiltonian is computed to be

$$\begin{aligned} \hat{\mathcal{H}}_{\nu} = \frac{1}{2a_s} & \left[\sum_{\mathbf{n}^*} \frac{1}{\tilde{g}_s^2} \left(2 - \hat{\mathcal{Q}}_{\boldsymbol{\ell}^*} - \hat{\mathcal{Q}}_{\boldsymbol{\ell}^*}^{\dagger} \right) \right. \\ & \left. + \frac{\tilde{g}_t^2}{\xi^2} \sum_{\mathbf{p}^*} \left(2 - \left(\mathcal{W}_{\mathbf{p}^*} \hat{\mathcal{P}}_{\mathbf{p}^*} + \text{h.c.} \right) \right) \right] \quad (d = 3). \end{aligned} \quad (3.13)$$

In this expression, $\hat{\mathcal{P}}_{\mathbf{p}^*}$ is the plaquette operator on L^* constructed out of $\mathcal{U}_{\boldsymbol{\ell}^*}$'s in the same way $P_{\mathbf{p}}$ is constructed from $U_{\boldsymbol{\ell}}$'s in eq. (3.4), while $\mathcal{W}_{\mathbf{p}^*}$ is a phase that is nontrivial whenever the topological electric field loops C_i on L pierce the \mathbf{p}^* plaquette on L^* ,

$$\mathcal{W}_{\mathbf{p}^*} = \begin{cases} e^{i\xi\nu_i}, & \text{if } \boldsymbol{\ell} \in C_i; \\ 1, & \text{otherwise;} \end{cases} \quad (3.14)$$

ℓ being the link dual to \mathbf{p}^* .

In $d = 3$ the $|\mathcal{A}\rangle_{\nu}$ states in eq. (3.7) are again over-complete, but the problem is more severe than in $d = 2$ as the product of plaquette operators on the surface of any cube \mathbf{c} in L should be an identity transformation, the number of cubes scaling with n . The constraint on the dual lattice to remove this degeneracy is (unsurprisingly) the dual of the electric Gauss law constraint eq. (3.5): the same equation with the substitution $\hat{Q}_{\ell} \rightarrow \hat{\mathcal{Q}}_{\ell^*}$. Thus, we see a “conservation of difficulty” between the original and dual theories for $d = 3$, each form of the theory having a Gauss law constraint of identical form. The one advantage of the dual formulation common with the $d = 2$ example is that regulating the eigenvalues of the $\hat{\mathcal{Q}}$ operators controls magnetic fluctuations, which we expect to be more efficient at weak coupling than a cutoff on the electric field.

3.3 Conclusions

We have focused here entirely on U(1) gauge theories without matter and have shown the consequences of defining these theories on the space of gauge-invariant states. In particular, we found that this leads to a dual formulation subject to a magnetic Gauss law constraint. This result can lead to a substantial reduction of variables in $d = 2$, but not in $d = 3$; in both cases though it offers the opportunity to regulate the theory by limiting magnetic fluctuations rather than electric, which is expected to be advantageous in approaching the continuum limit in $d = 2$, or studying the weak field limit in $d = 3$. One can hope for a similar approach to regulating asymptotically-free gauge theories in $d = 3$, for which the continuum limit is also at weak coupling. Extending the analysis to include charged matter fields and non-Abelian gauge symmetries is complicated by the fact that not all gauge-invariant states in the theory can be written in the form eq. (3.7); much previous work on related issues for non-Abelian gauge theories exists [57, 58, 87, 88] and could serve as a basis for quantum computations. Understanding such theories better, and developing the tools to efficiently represent these theories on a quantum computer and extrapolate to the continuum theory, remain as fascinating theoretical challenges to be tackled before one can contemplate solving

outstanding computational problems in QCD.

* * *

Following the preparation of the work presented in this chapter, Ref. [89] appeared, investigating the impact of different truncation schemes in Abelian lattice gauge theories as a function of the bare coupling. That work analyzes in great detail (2+1)-dimensional U(1) theories, including fermionic matter, in both electric and magnetic representations. They find that recovering the weak-coupling ground state wave function of a 2×2 periodic lattice with high overlap requires a truncation level scaling like $\tilde{g}_s^{8/5}$ in a magnetic representation, as compared to \tilde{g}_s^{-2} in an electric representation. The former is clearly much more efficient on qubit resources at weak coupling, quantitatively confirming the qualitative arguments given above. Their obtained magnetic basis results rely on approximating the U(1) gauge group by its $Z(N)$ subgroups, however, and so there is no direct way to extend their analysis to non-Abelian gauge groups.

Chapter acknowledgments

DBK and JRS thank N. Klco, J. Lombard, M. Savage, and L. Yaffe for insightful conversations during the preparation of the work presented in this chapter. This work was supported in part by DOE Grant No. DE-FG02-00ER41132 and by the Thomas L. and Margo G. Wyckoff Endowed Faculty Fellowship; JRS was also supported in part by the National Science Foundation Graduate Research Fellowship under Grant No. DGE-1256082 and by the Seattle Chapter of the Achievement Rewards for College Scientists Foundation.

Chapter 4

DIGITAL QUANTUM SIMULATION OF AN SU(2) GAUGE THEORY IN ONE DIMENSION

Great success has been achieved in computing the properties and low-energy dynamics of hadronic systems using the numerical technique of lattice QCD [90,91] on the world’s largest supercomputers. Current lattice QCD calculations at the physical quark masses have resulted from a sustained co-development effort over the last ~ 50 years. Those developments began with calculations on small lattices, with unphysical quark masses, and with large lattice spacings using computers available during the 1970’s [91]. While good progress is being made in designing Hilbert spaces for [92–110], creating detailed hardware-specific proposals for [111–126], and implementing [1,127–131] quantum field theories on quantum devices, non-Abelian gauge theories have not yet been simulated on today’s limited and noisy hardware. It is in the spirit of the early days of lattice gauge theory that we develop an improved algorithm to evolve a string of SU(2) plaquettes, and use it to simulate a non-Abelian gauge field theory on IBM’s digital quantum hardware.¹,

The Hamiltonian formulation of lattice gauge theories [132] includes exponentially-large sectors of unphysical ² Hilbert space in order to maintain spatially-local interactions while satisfying gauge constraints. The hardware error rates and gate fidelities of current NISQ-era [133] quantum devices, and the lack of error correction capabilities, allow quantum states to disperse into these unphysical sectors. To avoid such dispersion, previous quantum simulations of lattice gauge theories have employed various procedures to remove the unphysical

¹This chapter is drawn from *Physical Review D* 101, 074512 (2020), done in collaboration with N. Klco and M.J. Savage.

²The space referred to as unphysical can be naturally interpreted as isolated Hilbert spaces with non-zero external sources.

Hilbert space from the embedding onto quantum devices [127–129, 131, 134]. However, these techniques do not scale efficiently, and a generic description for multi-dimensional lattices with non-trivial gauge groups in terms of only local, physical degrees of freedom is not currently known. A variety of approaches for quantumly simulating gauge theories are being pursued—reformulating the interactions, lattice structure, and degrees of freedom by designing Hilbert space bases of group elements, Schwinger bosons, duality transformations, loop variables, tensor networks, and more [49, 105, 107, 108, 112, 118, 121, 132, 135–157]—often with the explicit goal of mitigating unphysical degrees of freedom. Reductions have been obtained by solving Gauss’s law, which is related to loop formulations where the fundamental degrees of freedom are gauge invariant [138, 144, 158–168]. Proposed for both analog and digital quantum implementation, progress is being made toward using renormalization group methods to connect quantum link models [95, 114, 117, 169–173] to continuum theories of importance [172, 174–176]. Classical numerical explorations of truncation errors arising from gauge field digitization in lattice QCD calculations [107], and exploring the use of the crystal groups associated with $SU(3)$ to discretize the gluon fields for quantum simulations have begun [110]. Here marks the introduction of an explicit quantum algorithm for digital implementation of dynamics with generalizable operator structures.

In this work, the angular momentum basis [132, 135, 136] is utilized, which is made computationally feasible on quantum devices by exploiting the local gauge symmetry to remove the angular momentum alignment variables. A similar reduction in degrees of freedom has been suggested to be an advantageous mapping for quantum simulations [100], and has been employed in calculations using matrix product states. The associated qubit mapping, along with the flexibility of the introduced *gauge variant completion* (GVC), has made possible the exploration of operator structures necessary for generalization to larger lattices and higher dimensions on current hardware. As an explicit example, time evolution of a one-dimensional string of two $SU(2)$ plaquettes is implemented on IBM’s Tokyo [177] quantum device with employed error mitigation techniques. The new mappings and techniques that we introduce here generalize to quantum simulations of gauge field theories in higher numbers of spatial

dimensions.

The Hamiltonian of spatially-discretized Yang-Mills gauge theory is [132] (in lattice units)

$$\hat{H} = \frac{g^2}{2} \sum_{\text{links}} \hat{E}^2 - \frac{1}{2g^2} \sum_{\square} (\hat{\square} + \hat{\square}^\dagger) \quad (4.1)$$

where \hat{E}^2 is the local gauge-invariant Casimir operator, $\hat{\square}$ is the gauge-invariant plaquette operator contracting closed loops of link operators, and $\hat{\square} = \hat{\square}^\dagger$ for SU(2). On a square lattice, the single plaquette operator is

$$\hat{\square} = \sum_{\alpha, \beta, \gamma, \delta = -\frac{1}{2}}^{\frac{1}{2}} \hat{U}_{\alpha\beta} \hat{U}_{\beta\gamma} \hat{U}_{\gamma\delta} \hat{U}_{\delta\alpha} \quad (4.2)$$

where $\hat{U}_{\alpha\beta}$ is a $j = 1/2$ link operator with definite starting and ending points oriented around a plaquette. In the limit of strong coupling, $g^2 \rightarrow \infty$, this Hamiltonian is dominated by the electric contributions and fluctuations between configurations of definite link angular momentum vanish. In weak coupling, the magnetic contributions dominate and a theory of dynamical loops emerges.

The angular momentum basis describes the quantum state of a generic link by its irreducible representation, j , and associated third-component projections at the left and right end of the link in the $\mathbf{2}$ and $\bar{\mathbf{2}}$ representations, $|j, m, m'\rangle \equiv |j, m\rangle \otimes |j, m'\rangle$, respectively. In one dimension, SU(2) lattice gauge theory can be spatially discretized onto a string of plaquettes (see Fig. 4.1). With periodic boundary conditions (PBCs), only three-point vertices contribute to such a plaquette chain. To form gauge singlets, components of the three links at each vertex are contracted with an SU(2) Clebsch-Gordan coefficient. While these coefficients are conventionally incorporated into the state space allowing plaquette operators to be localized to four active links, the qubit Hilbert space is more naturally structured as an unconstrained grid. Thus the Clebsch-Gordan coefficient at each vertex will be here included in the plaquette operator itself. This decision delocalizes the plaquette operator at the scale of immediately neighboring links as shown in Fig. 4.1, where the green, circular parts of the operator denote the dependence of the operator on the quantum state of qubits on neighboring links.

To calculate the plaquette operator, the state is first structured with Clebsch-Gordans at each vertex such that the wavefunction has the form

$$V \sim \sum_{b,c,e} \langle j_1, b, j_2, e | q, c \rangle |j_1, a, b\rangle \otimes |q, c, d\rangle \otimes |j_2, e, f\rangle, \quad (4.3)$$

where indices b, c , and e are located at the vertex. By focusing on a system with an even number of plaquettes, matrix elements of the arbitrary plaquette operator may be determined. The wavefunction of a lattice with an even number of plaquettes in one dimension with PBCs in the link angular momenta basis is

$$|\chi\rangle = \mathcal{N} \sum_{\{m\}} \prod_{i=1}^L \langle j_i^t, m_{i,R}^t, j_{i+1}^t, m_{i+1,L}^t | q_i, m_{q_i}^t \rangle \\ \langle j_i^b, m_{i,R}^b, j_{i+1}^b, m_{i+1,L}^b | q_i, m_{q_i}^b \rangle \\ |j_i^t, m_{i,L}^t, m_{i,R}^t\rangle \otimes |j_i^b, m_{i,L}^b, m_{i,R}^b\rangle \otimes |q_i, m_{q_i}^t, m_{q_i}^b\rangle \quad (4.4)$$

with $j_{L+1} = j_1$, $m_{L+1} = m_1$, and normalization $\mathcal{N} = \prod_i (\dim(q_i))^{-1}$ with $\dim(q) = 2q + 1$. Referring to the plaquette string's ladder structure, on links located as rungs of the ladder, angular momentum values are labeled by q . Thus, a plaquette string is created by two strings of j -type registers connected periodically by rungs of q -type registers. The contraction with Clebsch-Gordan coefficients at each vertex ensures the local gauge singlet structure required by Gauss's law. The link operator acts on the degrees of freedom at each end of a link and is a source of $j = 1/2$ angular momentum,

$$\hat{U}_{AB} |j, a, b\rangle = \sum_{\oplus J} \sqrt{\frac{\dim(j)}{\dim(J)}} |J, a + A, b + B\rangle \langle j, a; \frac{1}{2}, A | J, a + A\rangle \langle j, b; \frac{1}{2}, B | J, b + B\rangle, \quad (4.5)$$

which contains non-vanishing contributions only for $J = j \pm \frac{1}{2}$ [49]. By acting this operator on the above wavefunction of Eq. (4.4) and summing over alignment variables, that matrix elements of the plaquette operator in one dimension and in the tensor product basis of

magnetic quantum numbers, j , are calculated to be

$$\begin{aligned}
& \langle \chi_{\dots, j_\ell^{t,b}, q_{\ell f}, j_{af}^{t,b}, q_{rf}, j_r^{t,b}, \dots} | \hat{\square} | \chi_{\dots, j_\ell^{t,b}, q_{\ell i}, j_{ai}^{t,b}, q_{ri}, j_r^{t,b}, \dots} \rangle \\
&= \sqrt{\dim(j_{ai}^t) \dim(j_{af}^t) \dim(j_{ai}^b) \dim(j_{af}^b)} \sqrt{\dim(q_{\ell i}) \dim(q_{\ell f}) \dim(q_{ri}) \dim(q_{rf})} \\
&\quad \times (-1)^{j_\ell^t + j_\ell^b + j_r^t + j_r^b + 2(j_{af}^t + j_{af}^b - q_{\ell i} - q_{ri})} \left\{ \begin{matrix} j_\ell^t & j_{ai}^t & q_{\ell i} \\ \frac{1}{2} & q_{\ell f} & j_{af}^t \end{matrix} \right\} \left\{ \begin{matrix} j_\ell^b & j_{ai}^b & q_{\ell i} \\ \frac{1}{2} & q_{\ell f} & j_{af}^b \end{matrix} \right\} \left\{ \begin{matrix} j_r^t & j_{ai}^t & q_{ri} \\ \frac{1}{2} & q_{rf} & j_{af}^t \end{matrix} \right\} \left\{ \begin{matrix} j_r^b & j_{ai}^b & q_{ri} \\ \frac{1}{2} & q_{rf} & j_{af}^b \end{matrix} \right\} \\
& \tag{4.6}
\end{aligned}$$

where the indices $j_\ell^{t,b}$, $q_{\ell i}$, $q_{\ell f}$, $j_{ai}^{t,b}$, q_{ri} , q_{rf} , and $j_r^{t,b}$ are used to indicate the j -values relevant for the single plaquette operator (as depicted in Fig. 4.1) and the brackets indicate Wigner's 6- j symbols. The four registers $j_{\ell,r}^{t,b}$ outside the plaquette are not modified by the action of the plaquette operator. However, their inclusion as control registers is necessary to maintain Gauss's law. The sums over alignment in each gauge-invariant space yield a dramatically reduced Hilbert space to be mapped onto a quantum device, characterized entirely by the $|j\rangle$'s (rather than the $|j, m, m'\rangle$'s [100]) incrementing naturally by half-integers. As a result, the Hilbert space dimension scales with the number of links, L , as $(2\Lambda_j + 1)^L$ —a small asymptotic savings in terms of qubit number, but an important savings for noisy devices where survival probabilities in the physical subspace are imperfect. This concept is here exemplified by embedding a four dimensional physical subspace into a sixteen dimensional computational space rather than into what would be a $\geq 5^4$ -dimensional Hilbert space in the $|j, m, m'\rangle$ basis. The qubit representation of the periodic plaquette string is shown on the top panel of Fig. 4.1, where each link contains a $\lceil \log_2(2\Lambda_j + 1) \rceil$ -qubit register with Λ_j the angular momentum truncation per link.

Quantum circuits were devised for the plaquette operator with angular momentum truncation $\Lambda_j = 1/2$. For time evolution beginning in the strong-coupling (empty) vacuum, the top and bottom j values are equivalent with this cutoff and the plaquette operator reduces to a five-qubit operator.

While the value of plaquette operator matrix elements connected to the physical Hilbert space are important for implementation of accurate time evolution, those within the unphysi-

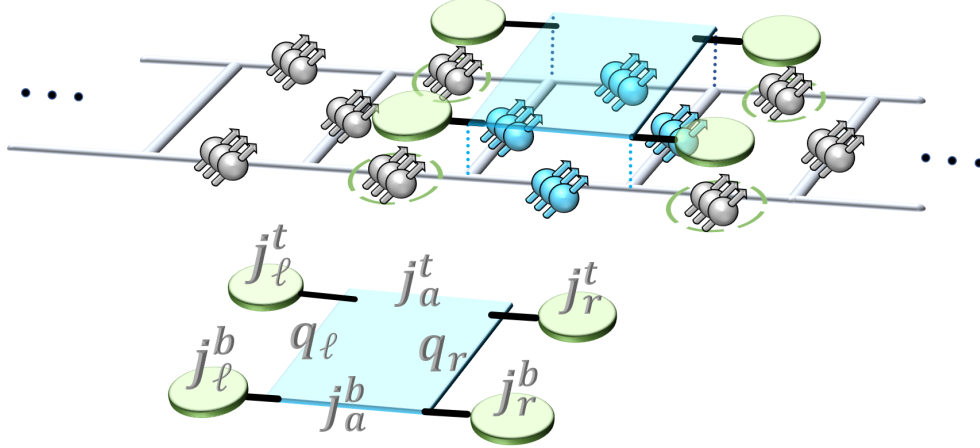


Figure 4.1: (top) Diagram of the lattice distribution of $\lceil \log_2(2\Lambda_j + 1) \rceil$ -qubit registers and the action of $\hat{\square}$ on $SU(2)$ plaquettes in one dimension. $\hat{\square}$ operates on the four qubit registers in the plaquette and is controlled by the four neighboring qubit registers to enforce the Gauss's law constraint. (bottom) The plaquette operator with labeled angular momentum registers. [image credit: Natalie Klco]

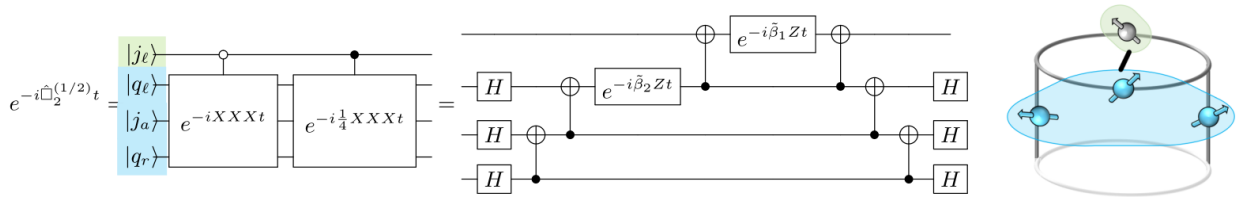


Figure 4.2: Digital circuit implementation of the plaquette operator centered on j_a for a truncated lattice with $\Lambda_j = 1/2$, two plaquettes, and PBCs as depicted at the right. The angles $\tilde{\beta}$ defining this circuit are given in Eq. (B.4) to be $\tilde{\beta} = (3/8, 5/8)$. [image credit: Natalie Klco]

$\langle j_{\ell f} q_{\ell f} j_{af} q_{rf} j_{rf} \hat{\square}^{(1/2)} j_{\ell i} q_{\ell i} j_{ai} q_{ri} j_{ri} \rangle$	
$\langle 00000 \hat{\square}^{(1/2)} 0 \frac{1}{2} \frac{1}{2} \frac{1}{2} 0 \rangle$	1
$\langle 000 \frac{1}{2} \frac{1}{2} \hat{\square}^{(1/2)} 0 \frac{1}{2} \frac{1}{2} 0 \frac{1}{2} \rangle$	$\frac{1}{2}$
$\langle \frac{1}{2} \frac{1}{2} 000 \hat{\square}^{(1/2)} \frac{1}{2} 0 \frac{1}{2} \frac{1}{2} 0 \rangle$	$\frac{1}{2}$
$\langle \frac{1}{2} 0 \frac{1}{2} 0 \frac{1}{2} \hat{\square}^{(1/2)} \frac{1}{2} \frac{1}{2} 0 \frac{1}{2} \frac{1}{2} \rangle$	$\frac{1}{4}$

Table 4.1: Matrix elements of the $\Lambda_j = 1/2$, Hermitian plaquette operator $\hat{\square}^{(1/2)}$, as calculated in Eq. (4.6) with $j_{\ell,a,r}^t = j_{\ell,a,r}^b$. All other matrix elements between physical states are zero.

cal space are not. Thus, significant freedom exists in designing the operator in the unphysical space to hardware-specifically optimize quantum computation. Operators with equivalent physical matrix elements but differing in their unphysical operation will be described as different gauge variant completions (GVCs) of the same physical operator. For example, here it is convenient to use a GVC within the set of Pauli operators to minimize the quantum gate resource requirements. Observing the plaquette operator matrix elements in Table 4.1, states are connected when q_ℓ, j_a , and q_r experience a qubit inversion with a matrix element dependent on the j_ℓ, j_r -sector. Such a controlled operator is depicted schematically at the bottom of Figure 4.1 (with top and bottom j 's identified) and may be written as

$$\hat{\square}^{(1/2)} = \mathcal{P}_0 X X X \mathcal{P}_0 + \frac{1}{2} \mathcal{P}_0 X X X \mathcal{P}_1 + \frac{1}{2} \mathcal{P}_1 X X X \mathcal{P}_0 + \frac{1}{4} \mathcal{P}_1 X X X \mathcal{P}_1 \quad (4.7)$$

with $\mathcal{P}_0 = \frac{1}{2}(\mathbb{I} + Z)$ and $\mathcal{P}_1 = \frac{1}{2}(\mathbb{I} - Z)$, the $j = 0(\frac{1}{2})$ state mapped to quantum state $|0\rangle(|1\rangle)$, and the Hilbert spaces ordered as in the heading of Table 4.1. With this GVC, the plaquette Hamiltonian has 24 non-zero couplings between unphysical states that would otherwise vanish in the evaluation of Eq. (4.6)³. One possible digital qubit implementation of the associated time evolution operator with the GVC above is shown explicitly in Fig. B.1

³Equation (B.1) shows explicitly the Hamiltonian structure with the chosen GVC. If the GVC of Eq. (4.6) was used without modification, a factor of four in quantum gates is expected as shown in Appendix B.2.

of Appendix B.1. As written, this operator acts equivalently throughout the one-dimensional string of plaquettes to implement time evolution of the lattice. We anticipate that the concept of GVC will play an important role in quantum simulations of quantum field theories in higher dimensions, and other physical systems with conserved quantities or constraints.

Specializing to the two-plaquette system with PBCs, only the matrix elements in the first and last rows of Table 4.1 remain. The second plaquette operator in the two-plaquette system reduces to the following four-qubit operator,

$$\hat{\square}_2^{(1/2)} = \mathcal{P}_0 XXX + \frac{1}{4} \mathcal{P}_1 XXX \quad . \quad (4.8)$$

Digital implementation of this operator is shown in Fig. 4.2. The reduced linear combination structure defined by the first and fourth rows and columns of the matrix shown in Eq. (B.4) produces the vector $\tilde{\beta}$ appearing in Fig. 4.2. A natural qubit representation of the electric operator is

$$\hat{H}_E^{(1/2)} = \frac{g^2}{2} \sum_{\text{links}} \frac{3}{4} \left(\frac{\mathbb{I} - Z}{2} \right) \quad , \quad (4.9)$$

including 12 non-zero elements in the unphysical Hilbert space.

Real-time evolution of two plaquettes with PBCs (see the right panel of Fig. 4.2) and truncation $\Lambda_j = 1/2$ has been here implemented on IBM’s quantum device **Tokyo**, selected for its available connectivity of a four-qubit loop. The top panel of Fig. 4.3 shows time-evolved expectation values of the energy contributions from the first electric plaquette calculated with one and two Trotter steps⁴. The electric contributions, being localized in their measurement to the four-dimensional physical subspace, are well determined after a small number of samples. In contrast, measuring the energy contributions from the magnetic Hamiltonian requires increased sampling due to the operator’s natural representation in the Pauli- X basis of the q_ℓ, j_a , and q_r qubit registers—distributing the wavefunction’s amplitude throughout the Hilbert space. Results have been corrected for measurement error by the constrained inversion of a 16-dimensional calibration matrix informed by preparation of each of the

⁴The Trotter step in this calculation has been ordered in application as the first plaquette, the second plaquette as written in Eq. (4.8), and lastly the electric time evolution operator.

16 computational basis states prior to calculation. The resulting probabilities are linearly extrapolated in the presence of CNOT gates, post-selected within the gauge-invariant space, and renormalized. The linear extrapolation is informed by $r = 1, 2$, where $r = 1$ is the circuit in Fig. 4.2 and $r = 2$ stochastically inserts a pair of CNOTs accompanying each of the three CNOTs either in the first or second half of the plaquette operator. The combined noise and gate fidelity of the device were found to limit the ability to extrapolate further in CNOT noise, even with a single Trotter step. These error mitigation techniques have allowed calculation of the electric energy associated with the $SU(2)$ gauge field to the precision obtained after a single Trotter step.

It is important to determine the feasibility of retaining gauge-invariant Hilbert spaces with near-term quantum hardware. For our calculations on IBM's Tokyo quantum device, before CNOT extrapolation, the $(N_{\text{Trot}}, r) = (1, 1)$ measurements were found to remain in the gauge invariant space with a survival population of $\sim 45\%$, as shown in the bottom panel of Fig. 4.3. After linear extrapolation in the probabilities, this was increased to $\sim 65\%$, with survival population decreasing as evolution time increases. The survival population for $N_{\text{Trot}} = 2$ was found to be $\sim 25\%$, consistent with loss of quantum coherence of a four-dimensional physical space embedded onto four qubits, precluding CNOT extrapolation. This observable is a diagnostic of the calculation. As it approaches the decorrelated limit (25%), CNOT extrapolations become less reliable, leading to the underestimate of systematic uncertainties in Fig. 4.3. Because neither the proposed qubit representation nor the subsequent Trotterization produce gauge-variant error contributions, the observed decay of population in the physical subspace is a measure of the device's ability to robustly isolate Hilbert subspaces. This is likely to be an essential capability for evolving lattice gauge theories and other systems with conserved quantities, as well as for quantum error correction.

When increasing Λ_j , the plaquette operator must be calculated and designed over 8 registers of qubits, each containing $\lceil \log_2(2\Lambda_j + 1) \rceil$ qubits. The classical computational resources required to define this operator with Eq. (4.6) scales with the number of unique non-zero matrix elements, which is polynomial in Λ_j . When constructing the time evolution

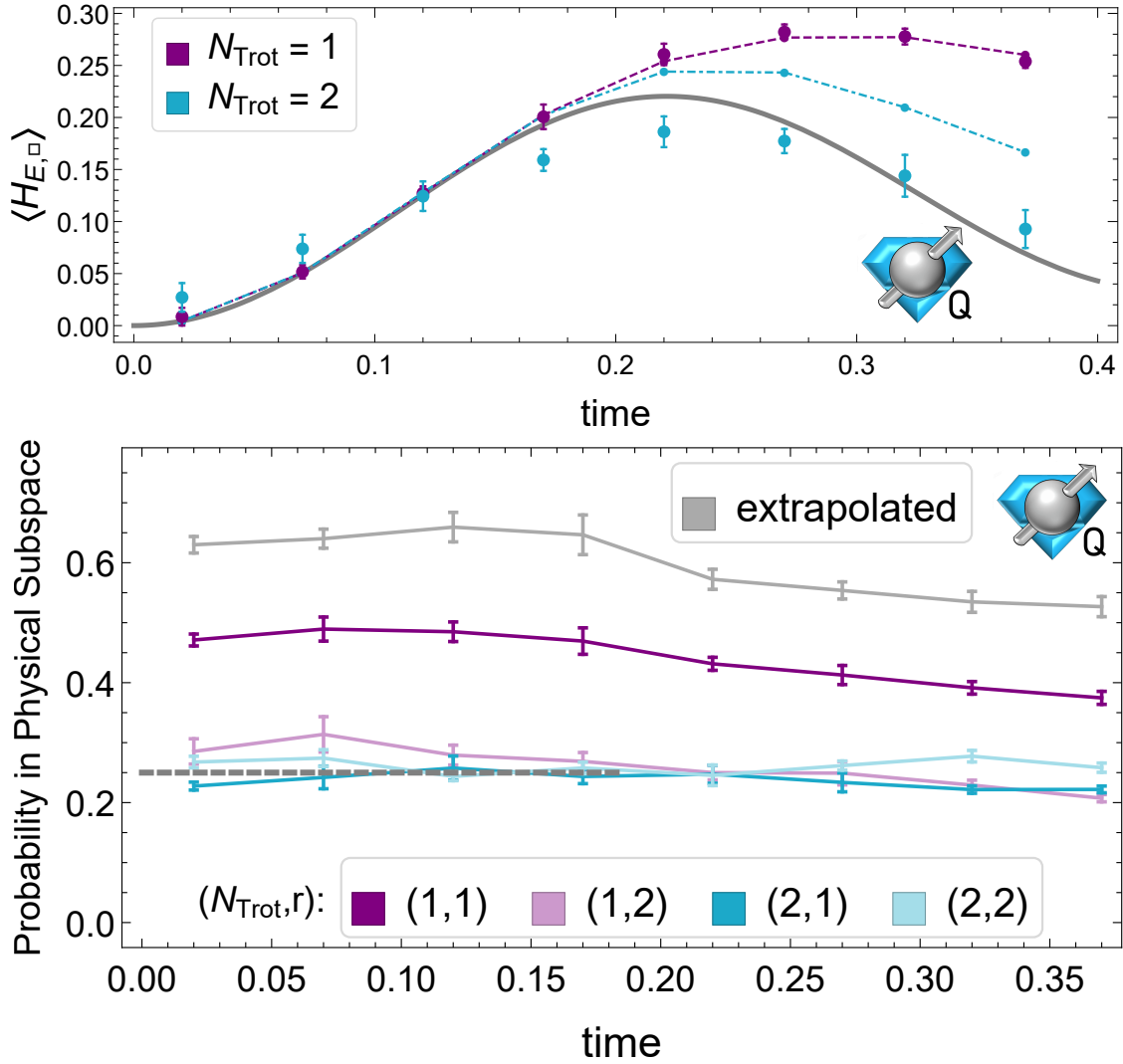


Figure 4.3: (top) Expectation value of the electric energy contribution of the first plaquette in the two-plaquette lattice with PBCs and coupling $g^2 = 0.2$ computed on IBM's Tokyo. The dashed(purple) and dot-dashed(blue) lines are the $N_{\text{Trot}} = 1, 2$ Trotterized expectation values, while the thick gray line is the exact time evolution. (bottom) Measured survival probability to remain in the physical subspace for one and two trotter steps, N_{Trot} , and one and two r values indicating stochastically inserted $2r - 1$ CNOTs per CNOT in the digital implementation. Uncertainties represent statistical variation, as well as a systematic uncertainty estimated from reproducibility measurements. The icons (defined in Ref. [1]) denote computations performed on quantum devices. [image credit: Natalie Klco]

operator for $\Lambda_j > 1/2$, the combination of Trotterization and Pauli decomposition of the 4-register operators in $j_{\ell,r}$ -controlled sectors generically generates interactions breaking gauge invariance [142,153,178]. While a unitary operator preserving gauge invariance exists, it will generically require an exponential amount of quantum resources to implement and classical resources to define. The breaking of gauge invariance will be important to control if this decomposition is used in future calculations.

For the simulated system, the SU(2) Hilbert space associated with each link and the spatial lattice are significantly truncated. This work represents an early step along the long road ahead for quantum simulations of gauge field theories. As Hamiltonian operators are local in such field theories, thoughtful design and optimization of quantum operators in small, classically manageable systems will impact the design and execution of future quantum simulations of larger dimensionality. The impact of the truncation on the continuous-field system of two plaquettes (for the value of g^2 used in this work) is presented in Table B.1 of Appendix B. We find that the employed truncation of $\Lambda_j = 1/2$ leads to a $\sim 56\%$ change to the ground state energy and a much larger change to the “glueball” mass. A larger value of g^2 would lead to smaller deviations in both quantities, as the system becomes more amenable to perturbative methods. At the selected value of g^2 , where the system is nonperturbative, enlarging the simulation to include three qubits per link (a cutoff of $\Lambda_j = 7/2$), rather than one qubit per link ($\Lambda_j = 1/2$), causes these low-energy observables to become calculable with an accuracy exceeding 2% using the basis discussed in this paper. The fidelity of the ground state in the enlarged simulation is $\sim 90\%$ with respect to the untruncated ground state. The convergence properties of this formulation of gauge theories, and others intended for quantum simulation, are important topics of future research.

Developing quantum computation capabilities for non-Abelian gauge field theories is a major objective of nuclear physics and high-energy physics research. We have presented the first quantum simulation of a non-Abelian gauge field theory on a digital quantum computer, which required the development of a number of new techniques. One of the challenges facing such calculations is that the mapping of the gauge theory onto the register of a digital

quantum computer involves a digitization of the gauge fields. We have presented calculations of the dynamics of a one-dimensional $SU(2)$ plaquette string with implementation on IBM's Q Experience superconducting hardware. This was made feasible by an improved mapping of the angular momentum basis states describing link variables and recognizing the utility of gauge-variant completions. Our design of the plaquette operator for digital quantum devices requires local control from qubit registers beyond the active plaquette. This key feature is expected to persist in future developments of quantum computing for gauge theories. Extension of this analytic reduction beyond one dimension is naturally suited to lattices with three-point vertices, but generalizes to n -point vertices and thus to quantum simulations in higher dimensions. Comparisons, at the level of explicit digital implementation, of this mapping with proposed alternatives will be of importance for realizing physically-relevant quantum computations of non-Abelian gauge theories.

Chapter acknowledgments

We (NK, MJS, and JRS) thank David Kaplan, Indrakshi Raychowdhury and Erez Zohar for important discussions. We also thank Donny Greenberg, the IBM quantum computing research group, and the ORNL Q Hub for informative discussions and facilitating access to the IBM quantum devices. We acknowledge use of the IBM Q for this work. The views expressed are those of the authors (NK, MJS, and JRS) and do not reflect the official policy or position of IBM or the IBM Q team. This work is supported in part by the U.S. Department of Energy, Office of Science, Office of Advanced Scientific Computing Research (ASCR) quantum algorithm teams program, under field work proposal number ERKJ333. We thank Raphael Pooser and ORNL collaborators with the U.S. Department of Energy, Office of Science, Office of Advanced Scientific Computing Research (ASCR) quantum Testbed Pathfinder program, under field work proposal number ERKJ335. This work was performed, in part, at the Aspen Center for Physics, which is supported by National Science Foundation Grant No. PHY-1607611. NK, MJS, and JRS were supported by the Institute for Nuclear Theory with DOE Grant No. DE-FG02-00ER41132 and Fermi National Accelerator Labo-

ratory PO No. 652197. NK was supported in part by a Microsoft Research PhD Fellowship, and JRS was supported in part by the National Science Foundation Graduate Research Fellowship Program under Grant No. DGE-1256082.

Chapter 5

LOOP-STRING-HADRON FORMULATION

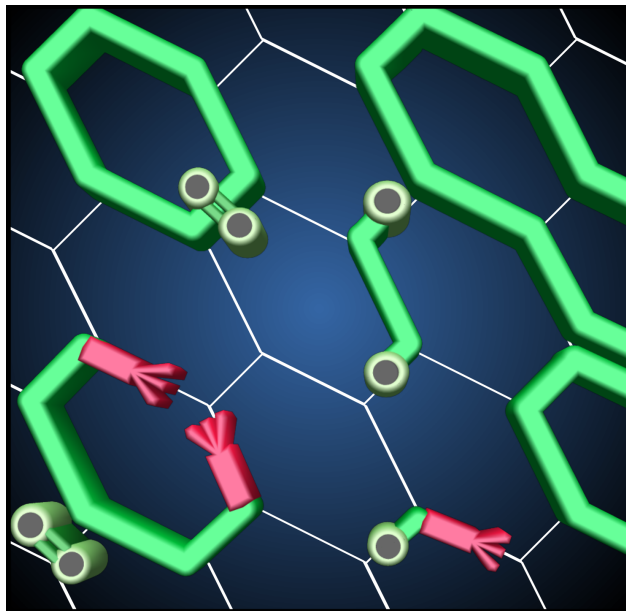


Figure 5.1: Depiction of a basis state in the loop-string-hadron framework. It represents a quark and gauge flux configuration on a 2D spatial lattice. The red flux portions are unterminated and indicated sites where Abelian flux conservation fails.

In this chapter,¹ we revisit and reformulate a non-Abelian lattice gauge theory—SU(2) gauge theory in $d + 1$ dimensions with one flavor of staggered quarks—ultimately putting it into an explicit form to which (classical or) quantum algorithms can be readily applied. The main theoretical contributions of this work include a thorough introduction to a loop-string-

¹This chapter is drawn from *Physical Review D* 101, 114502 (2020), done in collaboration with I. Raychowdhury.

hadron (LSH) formulation of $SU(2)$ lattice gauge theory, which uses local loops, strings, and hadrons as dynamical variables. The derivations provide the detail needed to adapt the framework to similar $SU(2)$ theories. Furthermore, the exposition on the Hamiltonian contains the details required to develop comprehensive simulation algorithms. In a companion work [179], we provide a mapping of the LSH formalism to qubits along with quantum circuit solutions to all the constraints, representing a major advance toward implementing verifiably-gauge-invariant states and quantum error mitigation. Generalizing the present LSH formalism for $SU(3)$ would be a key step toward future quantum simulations of lattice QCD.

This LSH formulation is the result of working with strictly $SU(2)$ -invariant operators and is an extension of the Schwinger boson (prepotential) formulation of lattice gauge theory [51, 55–59, 180–182]. The non-Abelian Gauss law that usually appears as a constraint is made intrinsic, meaning the local excitations are physical and even intuitive. The price paid is the introduction of an Abelian Gauss law that must be enforced instead, and the introduction of additional lattice links. These are not fundamental hurdles because i) the Abelian constraints are simpler to work with and, ii) if the Abelian constraints are also solved, then the gauge-invariant Hilbert space is covered much more efficiently than it would be in a Kogut-Susskind formulation. (Addressing the latter point is the subject of ongoing work.) Importantly, by making the operator structure so explicit, algorithms can start being applied to simulating dynamics and compared against any other proposals made for non-Abelian simulations.

The organization of this chapter is as follows: Section 1.4 reviews key points of the Kogut-Susskind Hamiltonian formulation. In Sec. 1.5, we briefly review how that framework is expressed using Schwinger bosons. In Sec. 5.1, we describe the LSH formulation in one spatial dimension in detail. This includes the LSH operators and their algebra, the Hamiltonian and Gauss’s law, definition of an orthonormal LSH basis, and complete specification of LSH matrix elements in that basis. In Secs. 5.2 and 5.3, we generalize to $2+1$ and $3+1$ dimensions respectively. Finally, Sec. 5.4 compares the LSH formalism against a conventional framework.

A lattice Hamiltonian for $SU(2)$ gauge bosons coupled to one flavor of staggered fermionic

matter, in units of the lattice spacing, may now be formulated as [39]

$$\hat{H} = \hat{H}_E + \hat{H}_B + \hat{H}_M + \hat{H}_I , \quad (5.1)$$

with

$$\hat{H}_E = \frac{g^2}{2} \sum_{(x,i)} \hat{E}^2(x,i) , \quad (5.2a)$$

$$\hat{H}_B = \frac{1}{g^2} \sum_x \sum_{i < j} \text{tr} \left[2 - \hat{U}_{\square}^{(ij)}(x) - \hat{U}_{\square}^{(ij)}(x)^\dagger \right] , \quad (5.2b)$$

$$\hat{H}_M = m \sum_x (-)^x \hat{\psi}^\dagger(x) \hat{\psi}(x) , \quad (5.2c)$$

$$\hat{H}_I = \sum_{(x,i)} \hat{\psi}^\dagger(x) \hat{U}(x,i) \hat{\psi}(x + e_i) + \text{H.c.} \quad (5.2d)$$

Above, g and m are the bare coupling and bare mass; the magnetic energy \hat{H}_B is formed from gauge-invariant traces of plaquette operators,

$$\hat{U}_{\square}^{(ij)}(x) \equiv \hat{U}(x,i) \hat{U}(x + e_i, j) \hat{U}^\dagger(x + e_j, i) \hat{U}^\dagger(x, j) , \quad (5.3)$$

with $\text{tr}[\hat{U}_{\square}^\dagger] = \text{tr}[\hat{U}_{\square}]$ for SU(2); and the alternating sign $(-)^x \equiv (-1)^{\sum_i x_i}$ in the mass energy reflects the staggered fermion prescription.

5.0.1 Practical considerations

Compared to compact Abelian gauge groups, there are several aspects of the Kogut-Susskind formulation that make SU(N) groups especially formidable for simulation.

- *Noncommuting constraints.*—In U(1) lattice gauge theories, the constraints are simultaneously diagonalizable. This means it is possible to choose a basis where each basis ket is definitely in the allowed subspace or definitely in the unallowed subspace. But in SU(N) lattice gauge theory the Gauss law constraints form an algebra, $[\hat{\mathcal{G}}_\alpha(x), \hat{\mathcal{G}}_\beta(x)] = i C^\gamma_{\alpha\beta} \hat{\mathcal{G}}_\gamma(x)$, so simultaneously diagonalizing all constraints is impossible. Then the basis kets that would be represented by and measured on a quantum device would not be meaningful by themselves.

- *Asymmetric quantum numbers.*—For compact U(1) theories, the eigenstates of electric fields are characterized by a single integer quantum number. In that eigenbasis, link operators simply raise or lower the quantum number by one unit. In SU(2) theories one typically diagonalizes $\hat{E}^\alpha \hat{E}_\alpha$ and \hat{E}_3 at every side of every link, yielding local $|j, m\rangle$ structures on all link ends. Every irrep j has a different dimensionality, and these irreps are mixed by the action of link operators according to

$$\hat{U}_{MN} |j, m\rangle_L |j, n\rangle_R = \sum_{j', m', n'} |j', m'\rangle_L |j', n'\rangle_R \sqrt{\frac{\dim j}{\dim j'}} \langle \frac{1}{2}, M; j, m | j', m' \rangle \langle j', n' | \frac{1}{2}, N; j, n \rangle \quad (5.4)$$

[83]. [For SU(2), nonvanishing contributions on the right-hand side come from $j' = j \pm 1/2$.] Representing these mixings using qubit (or qudit) registers seems awfully forced and unnatural.

- *Group-specific coefficients.*—The action of link operators (5.4) more generally involves group-dependent Clebsch-Gordon coefficients. In principle, designing simulation protocols specific to SU(2) and to SU(3) is not unreasonable and should even be expected. But if SU(2) and SU(3) were first expressed in a common framework then one could expect optimizations found for the former to better translate to the latter.
- *Gauge redundancy in noisy simulations.*—Local gauge constraints mean basis states are largely wasted representing unallowed states. State vectors in non-error-corrected simulations will wander away from the exponentially small space of allowed states. Moreover, nontrivial gauge-invariant states are very specific linear combinations of conventional irrep basis states; if the computational basis represents the irrep basis, then any single-qubit error could potentially spoil gauge invariance.

All of these disadvantages provide the impetus for exploring alternative frameworks.

5.0.2 Hilbert space of states

Allowed states in the Schwinger boson framework are characterized similarly to the Kogut-Susskind formulation. Physically permissible wave functions must be annihilated by the Schwinger boson implementations of $\hat{\mathcal{G}}_\alpha(x)$, and the same reasons to diagonalize electric operators continue to apply.

Where the two diverge is in the local Hilbert space structure and choice of a complete set of commuting observables. Instead of having aggregate link Hilbert spaces, the gauge field Hilbert space is built from local harmonic oscillators: two modes at the left and right ends of every link. The natural choice of a CSCO for such Hilbert spaces is

$$\left\{ \hat{N}_1(L), \hat{N}_2(L), \hat{N}_1(R), \hat{N}_2(R) \right\} \quad (5.5)$$

for each link. This choice is equivalent to (1.120), but the spectrum of quantum numbers is different.

Truncating the Kogut-Susskind theory at some representation j_{\max} is equivalent to truncating all Schwinger boson occupation numbers to j_{\max} .

5.0.3 Practical considerations

The Schwinger boson formulation offers the following advantages:

- *Symmetric quantum numbers.*—All quantum numbers are on the same footing, being integer bosonic occupation numbers. Now it is obvious how one could represent these quantum numbers with binary registers. It is also obvious how to truncate the electric field [a uniform cutoff on all the occupation numbers in (5.5)].
- *Non-group-specific matrix elements.*—The link operator is expressed in terms of simple harmonic oscillator ladder operators, and Clebsch-Gordon coefficients are implicit in the various rescaling factors carried along by them. In this sense, the elementary degrees of freedom are group agnostic. [Of course, in going from SU(2) to SU(3), one needs SU(3) irreducible Schwinger bosons as described in [183].]

These features ought to be favorable for developing algorithms in this framework.

What remains to be addressed is the non-Abelian constraints, and redundancy of states. The former is addressed starting with the following observation: Local gauge transformations act site-locally, with Schwinger bosons and matter all transforming identically. This enables one to construct site-local intertwining operators automatically invariant under the action of the local generators; these can be identified as segments of all possible $SU(2)$ -invariant excitations hosted by a site (like a section of a Wilson loop). Using these, one can construct an $SU(2)$ -invariant Hilbert space locally at each site. For pure gauge theory, the resulting local “loop states” [57, 58, 88, 181] are characterized by integer-valued loop quantum numbers directly related to the angular momentum flux j . Truncating the Kogut-Susskind theory at some representation j_{\max} is equivalent to truncating all Schwinger boson occupation numbers to j_{\max} , and that is equivalent to truncating local loop numbers at $2j_{\max}/(2d - 1)$.

A drawback of the loop basis is that it is overcomplete. Finding the complete and orthogonal gauge-invariant Hilbert space requires solving the Mandelstam constraints, which becomes increasingly complicated in higher dimensions and with higher cutoff. These issues have been discussed in great detail in earlier works on the prepotential formulation of pure gauge theory. A central objective of the loop-string-hadron framework below will be to give a complete and local description of gauge-invariant dynamics with minimal redundancy, equipped with fundamental matter, and adaptable to any number of spatial dimensions.

5.1 Loop-string-hadron formulation: One dimension

The $SU(2)$ -invariant excitations at a site are parts of flux loops, parts of meson strings, or hadrons. We now derive a loop-string-hadron formulation starting from prepotentials that has non-Abelian gauge invariance built into it. We start in $1 + 1$ dimensions, where the essential features of coupling to matter—which was not previously a part of the prepotential framework—already appear.

In 1 + 1 dimensions, the Kogut-Susskind Hamiltonian (5.2) reduces to

$$\hat{H} = \hat{H}_E + \hat{H}_I + \hat{H}_M . \quad (5.6)$$

Each site x of this lattice is connected to one incoming link along direction i and one outgoing link along direction o , as in Fig. 5.2. Within the prepotential framework, Schwinger bosons $\hat{a}_a(L)$ ($\hat{a}_a(R)$) are attached to the link along the direction o (i). A staggered fermion field $\hat{\psi} = (\hat{\psi}_1, \hat{\psi}_2)$ lives on the sites themselves. We refer to 1D sites as ‘quark sites’ in anticipation of the need to distinguish their higher-dimensional counterparts from ‘gluonic sites.’

The site-local doublets shown in the box in Fig. 5.2 can contract in many possible ways to form SU(2) singlets. It follows that SU(2) invariance can be made manifest by passing from Schwinger boson and quark operators to using only their SU(2)-invariant combinations. The gauge theory will be expressed entirely in terms of the dynamics generated by all such operators.

5.1.1 SU(2) singlets: Loop, string, and hadron operators

The complete set of SU(2) invariants at a 1D site of a spatial lattice is obtained by constructing all possible singlet tensors out the available doublets and their conjugates. It is a special feature of SU(2) that fundamental doublets are unitarily equivalent to antifundamentals: if f transforms like a fundamental, then \tilde{f} given by

$$\epsilon \equiv i\sigma_y = \begin{pmatrix} 0 & 1 \\ -1 & 0 \end{pmatrix} , \quad (5.7)$$

$$\tilde{f}_a \equiv \epsilon_{ab} f_b , \quad (5.8)$$

transforms in the conjugate representation. This equivalence implies $\tilde{a}_a^\dagger(L/R) \equiv \epsilon_{ab} a_b^\dagger(L/R)$ gives another set of doublets to work with.

Using the available tensors, the complete set of nonvanishing singlets is listed below in (5.9)–(5.13):

- *Pure gauge loop operators.*— $\mathcal{L}^{\sigma,\sigma'}$:

$$\mathcal{L}^{++} = a(R)_a^\dagger a(L)_b^\dagger \epsilon_{ab} \quad (5.9a)$$

$$\mathcal{L}^{--} = a(R)_a a(L)_b \epsilon_{ab} = (\mathcal{L}^{++})^\dagger \quad (5.9b)$$

$$\mathcal{L}^{+-} = a(R)_a^\dagger a(L)_b \delta_{ab} \quad (5.9c)$$

$$\mathcal{L}^{-+} = a(R)_a a(L)_b^\dagger \delta_{ab} = (\mathcal{L}^{+-})^\dagger \quad (5.9d)$$

- *Incoming string operators.*— $\mathcal{S}_{\text{in}}^{\sigma,\sigma'}$:

$$\mathcal{S}_{\text{in}}^{++} = a(R)_a^\dagger \psi_b^\dagger \epsilon_{ab} \quad (5.10a)$$

$$\mathcal{S}_{\text{in}}^{--} = a(R)_a \psi_b \epsilon_{ab} = (\mathcal{S}_{\text{in}}^{++})^\dagger \quad (5.10b)$$

$$\mathcal{S}_{\text{in}}^{+-} = a(R)_a^\dagger \psi_b \delta_{ab} \quad (5.10c)$$

$$\mathcal{S}_{\text{in}}^{-+} = a(R)_a \psi_b^\dagger \delta_{ab} = (\mathcal{S}_{\text{in}}^{+-})^\dagger \quad (5.10d)$$

- *Outgoing string operators.*— $\mathcal{S}_{\text{out}}^{\sigma,\sigma'}$:

$$\mathcal{S}_{\text{out}}^{++} = \psi_a^\dagger a(L)_b^\dagger \epsilon_{ab} \quad (5.11a)$$

$$\mathcal{S}_{\text{out}}^{--} = \psi_a a(L)_b \epsilon_{ab} = (\mathcal{S}_{\text{out}}^{++})^\dagger \quad (5.11b)$$

$$\mathcal{S}_{\text{out}}^{+-} = \psi_a^\dagger a(L)_b \delta_{ab} \quad (5.11c)$$

$$\mathcal{S}_{\text{out}}^{-+} = \psi_a a(L)_b^\dagger \delta_{ab} = (\mathcal{S}_{\text{out}}^{+-})^\dagger \quad (5.11d)$$

- *Hadron operators.*— $\mathcal{H}^{\sigma,\sigma}$:

$$\mathcal{H}^{++} = -\frac{1}{2!} \psi_a^\dagger \psi_b^\dagger \epsilon_{ab} \quad (5.12a)$$

$$\mathcal{H}^{--} = \frac{1}{2!} \psi_a \psi_b \epsilon_{ab} = (\mathcal{H}^{++})^\dagger \quad (5.12b)$$

[Baryons and mesons are the same for SU(2).]

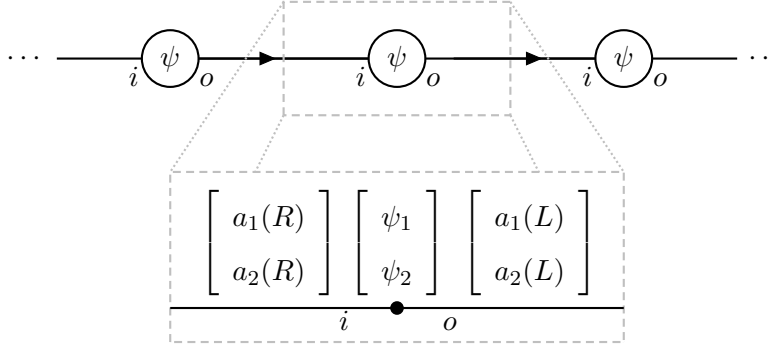


Figure 5.2: Pictorial representation of a 1D lattice with matter. Every site on the 1D lattice is associated with a fermionic doublet $\psi = (\psi_1, \psi_2)$. Bosonic doublets $a(L) = (a_1(L), a_2(L))$ and $a(R) = (a_1(R), a_2(R))$ are associated with link ends attached to any site along directions o and i , respectively.

- *Gauge flux, quark number operators.*— $\mathcal{N}_{L/R}, \mathcal{N}_\psi$:

$$\mathcal{N}_L = a(L)_a^\dagger a(L)_a \quad (5.13a)$$

$$\mathcal{N}_R = a(R)_a^\dagger a(R)_a \quad (5.13b)$$

$$\mathcal{N}_\psi = \psi_a^\dagger \psi_a \quad (5.13c)$$

These invariants exhaust all possible singlet bilinears and they are referred to as LSH operators. They obey a closed operator algebra, which will be necessary to establish since the original E , U , and ψ variables have been replaced.

Before giving the complete algebra, it is helpful to first build some intuition for these operators. One can visualize LSH operators in terms of creation and annihilation of the gauge and matter degrees of freedom appearing in their definitions. Below, this is done using line segments for gauge flux, circles for quarks, and solid (dotted) lines for creation

(annihilation) actions:

$$\begin{array}{ll}
 \widehat{\text{---}} \equiv \mathcal{L}^{++} & \widehat{\text{-----}} \equiv \mathcal{L}^{--} \\
 \widehat{\text{---}} \text{-----} \equiv \mathcal{L}^{+-} & \text{-----} \widehat{\text{---}} \equiv \mathcal{L}^{-+} \\
 \text{-----} \widehat{\circ} \equiv \mathcal{S}_{\text{in}}^{--} & \widehat{\circ} \text{-----} \equiv \mathcal{S}_{\text{out}}^{--} \\
 \text{---} \widehat{\circ} \equiv \mathcal{S}_{\text{in}}^{+-} & \widehat{\circ} \text{-----} \equiv \mathcal{S}_{\text{out}}^{+-} \\
 \text{-----} \widehat{\circ} \equiv \mathcal{S}_{\text{in}}^{-+} & \widehat{\circ} \text{---} \equiv \mathcal{S}_{\text{out}}^{-+} \\
 \text{---} \widehat{\circ} \equiv \mathcal{S}_{\text{in}}^{++} & \widehat{\circ} \text{---} \equiv \mathcal{S}_{\text{out}}^{++} \\
 \widehat{\circ} \text{---} \equiv \mathcal{H}^{++} & \widehat{\circ} \text{---} \equiv \mathcal{H}^{--}
 \end{array}$$

The placement of solid and dotted lines is in direct correspondence with the superscripts on the LSH operators.

The simplest examples from these are \mathcal{L}^{++} and \mathcal{L}^{--} , which create or destroy an $\text{SU}(2)$ -invariant flux line passing through the site. By contrast, the mixed-type operators $\mathcal{L}^{\pm\mp}$ deform a flux line flowing out one side to instead flow out the other; physically, this corresponds to changing the direction flux emanates from a single quark. The hadron operators \mathcal{H}^{++} and \mathcal{H}^{--} create or annihilate a hadron, consistent with the Pauli principle (at most two quarks present).

The actions of string operators are more subtle. For example, $\mathcal{S}_{\text{in}}^{++}$ will create the “right” end of a meson string, provided no quark is initially present. Alternatively, if a quark is already present in the form of an out-string, the strings ends actually join and leave behind independent hadron and loop flux excitations. The variety of actions $\mathcal{S}_{\text{in}}^{++}$ and other string operators can have will be summarized later on.

Further intuition for how LSH operators interact with each other is also gained from and made mathematically precise by now looking at their algebra. The algebra of LSH operators at any 1D lattice site (5.9)–(5.13) is tabulated in two parts. Table 5.1 lists commutators of operators where at most one operator from the pair has fermionic statistics. Table 5.2 lists anticommutators of operators that both have fermionic statistics. In addition to these, Table

5.3 contains the operators and algebra needed for $d > 1$ that will be discussed in Sec. 5.2.2; they are displayed now so they can be referred to alongside Tables 5.1 and 5.2. The 1D LSH algebra is sufficient to completely describe the dynamics of the theory, to be discussed below.

The commutation relations in Table 5.1 have a number of qualitative features:

- The $[\mathcal{N}, \cdot]$ rows and $[\cdot, \mathcal{N}]$ columns express simply how LSH operators change gauge flux or fermion density.
- The $[\mathcal{H}, \mathcal{L}]$ and $[\mathcal{L}, \mathcal{H}]$ sectors express the independence of exciting hadrons and exciting gauge flux.
- The $[\mathcal{S}, \mathcal{L}]$ sectors express how loop operators can deform outgoing (incoming) string operators into incoming (outgoing) string operators.
- The $[\mathcal{S}, \mathcal{H}]$ sectors express how hadron operators can change the behavior of \mathcal{S}_{in} and \mathcal{S}_{out} operators.

String operators inherit fermionic statistics and naturally obey anticommutation relations due to their linearity in fermionic fields. Qualitative patterns can also be found in Table 5.2:

- The $\{\mathcal{S}_{\text{in}}, \mathcal{S}_{\text{in}}\}$ and $\{\mathcal{S}_{\text{out}}, \mathcal{S}_{\text{out}}\}$ sectors express both the Pauli exclusion principle as well as the fact that certain combinations of string operators acting from the same side are equivalent to hadron creation or annihilation.
- The $\{\mathcal{S}_{\text{in}}, \mathcal{S}_{\text{out}}\}$ and $\{\mathcal{S}_{\text{out}}, \mathcal{S}_{\text{in}}\}$ sectors express how string operators acting on both sides without changing net quark number should be thought of as a loop action.

The closure of the operator algebra confirms the completeness that was asserted for the singlets in (5.9)-(5.13).

	$[\cdot, \mathcal{N}_R]$	$[\cdot, \mathcal{N}_L]$	$[\cdot, \mathcal{N}_\psi]$	$[\cdot, \mathcal{L}^{--}]$	$[\cdot, \mathcal{L}^{-+}]$	$[\cdot, \mathcal{L}^{+-}]$	$[\cdot, \mathcal{L}^{++}]$	$[\cdot, \mathcal{H}^{++}]$	$[\cdot, \mathcal{H}^{--}]$
$[\mathcal{N}_R, \cdot]$	0	0	0	$-\mathcal{L}^{--}$	$-\mathcal{L}^{-+}$	$+\mathcal{L}^{+-}$	$+\mathcal{L}^{++}$	0	0
$[\mathcal{N}_L, \cdot]$	0	0	0	$-\mathcal{L}^{--}$	$+\mathcal{L}^{-+}$	$-\mathcal{L}^{+-}$	$+\mathcal{L}^{++}$	0	0
$[\mathcal{N}_\psi, \cdot]$	0	0	0	0	0	0	0	$2\mathcal{H}^{++}$	$-2\mathcal{H}^{--}$
$[\mathcal{L}^{++}, \cdot]$	$-\mathcal{L}^{++}$	$-\mathcal{L}^{++}$	0	$-\mathcal{N}_L - \mathcal{N}_R - 2$	0	0	0	0	0
$[\mathcal{L}^{+-}, \cdot]$	$-\mathcal{L}^{+-}$	$+\mathcal{L}^{+-}$	0	0	$\mathcal{N}_R - \mathcal{N}_L$	0	0	0	0
$[\mathcal{L}^{-+}, \cdot]$	$+\mathcal{L}^{-+}$	$-\mathcal{L}^{-+}$	0	0	0	$\mathcal{N}_L - \mathcal{N}_R$	0	0	0
$[\mathcal{L}^{--}, \cdot]$	$+\mathcal{L}^{--}$	$+\mathcal{L}^{--}$	0	0	0	0	$\mathcal{N}_L + \mathcal{N}_R + 2$	0	0
$[\mathcal{S}_{\text{in}}^{++}, \cdot]$	$-\mathcal{S}_{\text{in}}^{++}$	0	$-\mathcal{S}_{\text{in}}^{++}$	$-\mathcal{S}_{\text{out}}^{+-}$	$+\mathcal{S}_{\text{out}}^{++}$	0	0	0	$-\mathcal{S}_{\text{in}}^{+-}$
$[\mathcal{S}_{\text{in}}^{+-}, \cdot]$	$-\mathcal{S}_{\text{in}}^{+-}$	0	$+\mathcal{S}_{\text{in}}^{+-}$	$-\mathcal{S}_{\text{out}}^{--}$	$-\mathcal{S}_{\text{out}}^{+-}$	0	0	$-\mathcal{S}_{\text{in}}^{++}$	0
$[\mathcal{S}_{\text{in}}^{-+}, \cdot]$	$+\mathcal{S}_{\text{in}}^{-+}$	0	$-\mathcal{S}_{\text{in}}^{-+}$	0	0	$+\mathcal{S}_{\text{out}}^{+-}$	$+\mathcal{S}_{\text{out}}^{++}$	0	$+\mathcal{S}_{\text{in}}^{--}$
$[\mathcal{S}_{\text{in}}^{--}, \cdot]$	$+\mathcal{S}_{\text{in}}^{--}$	0	$+\mathcal{S}_{\text{in}}^{--}$	0	0	$-\mathcal{S}_{\text{out}}^{--}$	$+\mathcal{S}_{\text{out}}^{+-}$	$+\mathcal{S}_{\text{in}}^{-+}$	0
$[\mathcal{S}_{\text{out}}^{++}, \cdot]$	0	$-\mathcal{S}_{\text{out}}^{++}$	$-\mathcal{S}_{\text{out}}^{++}$	$-\mathcal{S}_{\text{in}}^{-+}$	0	$+\mathcal{S}_{\text{in}}^{++}$	0	0	$+\mathcal{S}_{\text{out}}^{-+}$
$[\mathcal{S}_{\text{out}}^{-+}, \cdot]$	0	$-\mathcal{S}_{\text{out}}^{-+}$	$+\mathcal{S}_{\text{out}}^{-+}$	$-\mathcal{S}_{\text{in}}^{--}$	0	$-\mathcal{S}_{\text{in}}^{+-}$	0	$+\mathcal{S}_{\text{out}}^{++}$	0
$[\mathcal{S}_{\text{out}}^{+-}, \cdot]$	0	$+\mathcal{S}_{\text{out}}^{+-}$	$-\mathcal{S}_{\text{out}}^{+-}$	0	$+\mathcal{S}_{\text{in}}^{-+}$	0	$+\mathcal{S}_{\text{in}}^{++}$	0	$-\mathcal{S}_{\text{out}}^{--}$
$[\mathcal{S}_{\text{out}}^{--}, \cdot]$	0	$+\mathcal{S}_{\text{out}}^{--}$	$+\mathcal{S}_{\text{out}}^{--}$	0	$-\mathcal{S}_{\text{in}}^{--}$	0	$+\mathcal{S}_{\text{in}}^{+-}$	$-\mathcal{S}_{\text{out}}^{+-}$	0
$[\mathcal{H}^{--}, \cdot]$	0	0	$2\mathcal{H}^{--}$	0	0	0	0	$1 - \mathcal{N}_\psi$	0
$[\mathcal{H}^{++}, \cdot]$	0	0	$-2\mathcal{H}^{++}$	0	0	0	0	0	$\mathcal{N}_\psi - 1$

Table 5.1: Commutator algebra for the loop, string, and hadron operators at a matter site.

	$\{\cdot, \mathcal{S}_{\text{in}}^{++}\}$	$\{\cdot, \mathcal{S}_{\text{in}}^{+-}\}$	$\{\cdot, \mathcal{S}_{\text{in}}^{-+}\}$	$\{\cdot, \mathcal{S}_{\text{in}}^{--}\}$	$\{\cdot, \mathcal{S}_{\text{out}}^{++}\}$	$\{\cdot, \mathcal{S}_{\text{out}}^{+-}\}$	$\{\cdot, \mathcal{S}_{\text{out}}^{-+}\}$	$\{\cdot, \mathcal{S}_{\text{out}}^{--}\}$
$\{\mathcal{S}_{\text{in}}^{++}, \cdot\}$	0	0	$-2\mathcal{H}^{++}$	$2 + \mathcal{N}_R - \mathcal{N}_\psi$	0	0	$+\mathcal{L}^{++}$	$-\mathcal{L}^{+-}$
$\{\mathcal{S}_{\text{in}}^{+-}, \cdot\}$	0	0	$\mathcal{N}_R + \mathcal{N}_\psi$	$-2\mathcal{H}^{--}$	$+\mathcal{L}^{++}$	$+\mathcal{L}^{+-}$	0	0
$\{\mathcal{S}_{\text{in}}^{-+}, \cdot\}$	$-2\mathcal{H}^{++}$	$\mathcal{N}_R + \mathcal{N}_\psi$	0	0	0	0	$+\mathcal{L}^{-+}$	$+\mathcal{L}^{--}$
$\{\mathcal{S}_{\text{in}}^{--}, \cdot\}$	$2 + \mathcal{N}_R - \mathcal{N}_\psi$	$-2\mathcal{H}^{--}$	0	0	$-\mathcal{L}^{-+}$	$+\mathcal{L}^{--}$	0	0
$\{\mathcal{S}_{\text{out}}^{++}, \cdot\}$	0	$+\mathcal{L}^{++}$	0	$-\mathcal{L}^{-+}$	0	$2\mathcal{H}^{++}$	0	$2 + \mathcal{N}_L - \mathcal{N}_\psi$
$\{\mathcal{S}_{\text{out}}^{+-}, \cdot\}$	0	$+\mathcal{L}^{+-}$	0	$+\mathcal{L}^{--}$	$2\mathcal{H}^{++}$	0	$\mathcal{N}_L + \mathcal{N}_\psi$	0
$\{\mathcal{S}_{\text{out}}^{-+}, \cdot\}$	$+\mathcal{L}^{++}$	0	$+\mathcal{L}^{-+}$	0	0	$\mathcal{N}_L + \mathcal{N}_\psi$	0	$2\mathcal{H}^{--}$
$\{\mathcal{S}_{\text{out}}^{--}, \cdot\}$	$-\mathcal{L}^{+-}$	0	$+\mathcal{L}^{--}$	0	$2 + \mathcal{N}_L - \mathcal{N}_\psi$	0	$2\mathcal{H}^{--}$	0

Table 5.2: Anticommutator algebra for incoming and outgoing string operators at a matter site.

	$[\cdot, \mathcal{L}_{ij}^{++}]$	$[\cdot, \mathcal{L}_{ij}^{+-}]$	$[\cdot, \mathcal{L}_{ij}^{-+}]$	$[\cdot, \mathcal{L}_{ij}^{--}]$	$[\cdot, \mathcal{L}_{jk}^{++}]$	$[\cdot, \mathcal{L}_{jk}^{+-}]$	$[\cdot, \mathcal{L}_{jk}^{-+}]$	$[\cdot, \mathcal{L}_{jk}^{--}]$	$[\cdot, \mathcal{L}_{ki}^{++}]$	$[\cdot, \mathcal{L}_{ki}^{+-}]$	$[\cdot, \mathcal{L}_{ki}^{-+}]$	$[\cdot, \mathcal{L}_{ki}^{--}]$
$[\mathcal{L}_{ij}^{++}, \cdot]$	0	0	0	$-\mathcal{N}_i - \mathcal{N}_j - 2$	0	0	$+\mathcal{L}_{ki}^{++}$	$+\mathcal{L}_{ki}^{+-}$	0	$+\mathcal{L}_{jk}^{++}$	0	$+\mathcal{L}_{jk}^{+-}$
$[\mathcal{L}_{ij}^{+-}, \cdot]$	0	0	$\mathcal{N}_i - \mathcal{N}_j$	0	$-\mathcal{L}_{ki}^{++}$	$+\mathcal{L}_{ki}^{+-}$	0	0	0	$-\mathcal{L}_{jk}^{++}$	0	$+\mathcal{L}_{jk}^{--}$
$[\mathcal{L}_{ij}^{-+}, \cdot]$	0	$\mathcal{N}_j - \mathcal{N}_i$	0	0	0	0	$-\mathcal{L}_{ki}^{+-}$	$+\mathcal{L}_{ki}^{--}$	$-\mathcal{L}_{jk}^{++}$	0	$+\mathcal{L}_{jk}^{+-}$	0
$[\mathcal{L}_{ij}^{--}, \cdot]$	$\mathcal{N}_i + \mathcal{N}_j + 2$	0	0	0	$-\mathcal{L}_{ki}^{+-}$	$-\mathcal{L}_{ki}^{--}$	0	0	$-\mathcal{L}_{jk}^{++}$	0	$-\mathcal{L}_{jk}^{+-}$	0
$[\mathcal{L}_{jk}^{++}, \cdot]$	0	$+\mathcal{L}_{ki}^{++}$	0	$+\mathcal{L}_{ki}^{+-}$	0	0	0	$-\mathcal{N}_j - \mathcal{N}_k - 2$	0	0	$+\mathcal{L}_{ij}^{++}$	$+\mathcal{L}_{ij}^{+-}$
$[\mathcal{L}_{jk}^{+-}, \cdot]$	0	$-\mathcal{L}_{ki}^{++}$	0	$+\mathcal{L}_{ki}^{--}$	0	0	$\mathcal{N}_j - \mathcal{N}_k$	0	$-\mathcal{L}_{ij}^{++}$	$+\mathcal{L}_{ij}^{+-}$	0	0
$[\mathcal{L}_{jk}^{-+}, \cdot]$	$-\mathcal{L}_{ki}^{++}$	0	$+\mathcal{L}_{ki}^{+-}$	0	0	$\mathcal{N}_k - \mathcal{N}_j$	0	0	0	0	$-\mathcal{L}_{ij}^{+-}$	$+\mathcal{L}_{ij}^{--}$
$[\mathcal{L}_{jk}^{--}, \cdot]$	$-\mathcal{L}_{ki}^{++}$	0	$-\mathcal{L}_{ki}^{--}$	0	$\mathcal{N}_j + \mathcal{N}_k + 2$	0	0	0	$-\mathcal{L}_{ij}^{+-}$	$-\mathcal{L}_{ij}^{--}$	0	0
$[\mathcal{L}_{ki}^{++}, \cdot]$	0	0	$+\mathcal{L}_{jk}^{++}$	$+\mathcal{L}_{jk}^{+-}$	0	$+\mathcal{L}_{ij}^{++}$	0	$+\mathcal{L}_{ij}^{+-}$	0	0	0	$-\mathcal{N}_k - \mathcal{N}_i - 2$
$[\mathcal{L}_{ki}^{+-}, \cdot]$	$-\mathcal{L}_{jk}^{++}$	$+\mathcal{L}_{jk}^{+-}$	0	0	0	$-\mathcal{L}_{ij}^{++}$	0	$+\mathcal{L}_{ij}^{--}$	0	0	$\mathcal{N}_k - \mathcal{N}_i$	0
$[\mathcal{L}_{ki}^{-+}, \cdot]$	0	0	$-\mathcal{L}_{jk}^{+-}$	$+\mathcal{L}_{jk}^{--}$	$-\mathcal{L}_{ij}^{++}$	0	$+\mathcal{L}_{ij}^{+-}$	0	0	$\mathcal{N}_i - \mathcal{N}_k$	0	0
$[\mathcal{L}_{ki}^{--}, \cdot]$	$-\mathcal{L}_{jk}^{+-}$	$-\mathcal{L}_{jk}^{--}$	0	0	$-\mathcal{L}_{ij}^{+-}$	0	$-\mathcal{L}_{ij}^{--}$	0	$\mathcal{N}_k + \mathcal{N}_i + 2$	0	0	0

Table 5.3: Commutator algebra for the loop operators at a gluonic (pure gauge) vertex. ($d \geq 2$)

5.1.2 Gauss laws and translation of the Hamiltonian

The loop-string-hadron operators introduced above are sufficient to express the Hamiltonian for SU(2) gauge bosons coupled to one flavor of staggered fermions. This is all that is necessary to define dynamics, since the algebra of operators is known. In this section, all the pieces of the Hamiltonian are reconstructed from their LSH equivalents, leaving everything expressed in terms of SU(2)-invariant operators alone.

By working solely with SU(2) singlets, the only gauge constraints that will have to be enforced “by hand” are the Abelian Gauss laws (1.133):

$$(\mathcal{N}_R(x+1) - \mathcal{N}_L(x)) | \text{phys} \rangle = 0 . \quad (5.14)$$

This was always the case in the Schwinger boson formulation, but now the on-site non-Abelian Gauss law is solved at the operator level in the Hamiltonian. Importantly, the constraints all commute. Also note that these AGL constraints retain the same form they had in pure gauge loop formulations [51, 58, 59]. These constraints can be solved too, but for

now the map will be given just for passing to the SU(2)-invariant variables (5.9)–(5.13).²

The electric energy measures the gauge flux running along a link. The quadratic Casimirs are expressed in terms of LSH number operators as

$$\hat{L}^2 = \frac{1}{2}\mathcal{N}_L(x) \left(\frac{1}{2}\mathcal{N}_L(x) + 1 \right) \quad (5.15)$$

$$\hat{R}^2 = \frac{1}{2}\mathcal{N}_R(x) \left(\frac{1}{2}\mathcal{N}_R(x) + 1 \right) . \quad (5.16)$$

To form the system's electric energy, all link ends are put on the same footing by taking

$$\hat{H}_E \rightarrow \frac{g^2}{4} \sum_x \left[\frac{1}{2}\mathcal{N}_R(x) \left(\frac{1}{2}\mathcal{N}_R(x) + 1 \right) + \frac{1}{2}\mathcal{N}_L(x) \left(\frac{1}{2}\mathcal{N}_L(x) + 1 \right) \right] . \quad (5.17)$$

Note that $\mathcal{N}_R(x)$ and $\mathcal{N}_L(x)$ are on either side of some site x , rather than opposite ends of a link.

The staggered mass terms are given quite simply in terms of the quark number operators, $\mathcal{N}_\psi = \psi^\dagger \psi$, so the mass energy is just

$$\hat{H}_M \rightarrow m \sum_x (-)^x \mathcal{N}_\psi(x) . \quad (5.18)$$

The hopping terms from \hat{H}_I can create, destroy, break, or glue together meson strings, so their expressions naturally involve the local string operators. To translate a hopping term, the sites at each end of a link can be considered separately. Recall from (1.135) and (1.136) that link operators were given in terms of Schwinger bosons by

$$\begin{aligned} \hat{U}(x, i) &= \hat{U}_L(x) \hat{U}_R(x + e_i) , \\ \hat{U}_L(x, i) &= \frac{1}{\sqrt{\hat{N}_L + 1}} \left(\begin{array}{cc} \hat{a}_2^\dagger(L) & \hat{a}_1(L) \\ -\hat{a}_1^\dagger(L) & \hat{a}_2(L) \end{array} \right) \Big|_{x, i} , \\ \hat{U}_R(x, i) &= \left(\begin{array}{cc} \hat{a}_1^\dagger(R) & \hat{a}_2^\dagger(R) \\ -\hat{a}_2(R) & \hat{a}_1(R) \end{array} \right) \frac{1}{\sqrt{\hat{N}_R + 1}} \Big|_{x, i} . \end{aligned}$$

²It is well known that completely solving Gauss's law in 1D space is trivial. Doing so destroys locality and does not generalize to multidimensional space.

Using the separate $\hat{U}_{L/R}$ factors at quark sites, it follows that

$$\hat{\psi}^\dagger(x)\hat{U}_L(x) = \frac{1}{\sqrt{\mathcal{N}_L(x)+1}} \left(\mathcal{S}_{\text{out}}^{++}(x), \mathcal{S}_{\text{out}}^{+-}(x) \right), \quad (5.19a)$$

$$\hat{U}_R(x)\hat{\psi}(x) = \begin{pmatrix} \mathcal{S}_{\text{in}}^{+-}(x) \\ \mathcal{S}_{\text{in}}^{--}(x) \end{pmatrix} \frac{1}{\sqrt{\mathcal{N}_R(x)+1}}. \quad (5.19b)$$

Thus, the translation of the interaction into LSH operators is given by

$$\hat{H}_I \rightarrow \sum_x \frac{1}{\sqrt{\mathcal{N}_L(x)+1}} \left[\sum_{\sigma=\pm} \mathcal{S}_{\text{out}}^{+, \sigma}(x) \mathcal{S}_{\text{in}}^{\sigma, -}(x+1) \right] \frac{1}{\sqrt{\mathcal{N}_R(x+1)+1}} + \text{H.c.} \quad (5.20)$$

The entire Hamiltonian (5.17)-(5.20) is now expressed solely in terms of the SU(2) singlets from (5.9)-(5.13).

5.1.3 An orthonormal loop-string-hadron basis and operator factorization

To describe dynamics in a way useful for computational algorithms, it is helpful to set up a basis. It would seem natural to use as a CSCO the operators $\{\mathcal{N}_R, \mathcal{N}_L, \mathcal{N}_\psi\}$ since these naturally appeared in the algebra, and to then express the Hamiltonian in terms of their quantum numbers. However, these may not be the most desirable due to the fact that these are constrained by the possible excitations LSH operators can create. (For example, $\mathcal{N}_\psi = 1$ while $\mathcal{N}_R = \mathcal{N}_L = 0$ is not gauge invariant.) As will be shown below, one can instead enumerate states more directly in terms of SU(2)-invariant LSH excitations—leading to a loop-string-hadron basis. In this way, only allowed on-site states are ever represented.

A second practical issue to be addressed concerns operator factorization. The Hamiltonian was expressed in terms of LSH operators, but in an orthonormal basis these operators change state normalization in addition to changing quantum numbers. Factorizing these two behaviors has the benefits of making the matrix elements of any operator completely evident and also setting the stage for a Wigner-Jordan transformation. This factorization will be done for convenience with respect to a LSH basis (though the factorization itself is basis independent).

On-site Hilbert space construction

Until this point, the LSH constructions have been built on underlying harmonic oscillator operators, but there was no need to choose a basis. The formal tools introduced will now be used to construct a basis of SU(2)-invariant excitations in which to express the action of the Hamiltonian. This is done by first defining “on-site” bases and later stitching these together to construct lattice states.

An on-site Hilbert space for the 1D lattice has three apparent degrees of freedom corresponding to the original occupation numbers (5.13), i.e., n_L , n_R , and n_ψ . But as remarked above these are constrained by the possible excitations generated by LSH operators.

A more physical on-site basis consists of states $|n_l, n_i, n_o\rangle$ with a loop quantum number n_l and quark quantum numbers n_i, n_o that describe strictly SU(2)-invariant gauge and matter excitations. Such a “loop-string-hadron basis” of unnormalized kets, denoted by a double-bar ket $|| \ \rangle$, can be defined as follows.

$$||n_l, n_i = 0, n_o = 0\rangle \equiv (\mathcal{L}^{++})^{n_l} |0\rangle \ , \quad (5.21a)$$

$$||n_l, n_i = 0, n_o = 1\rangle \equiv (\mathcal{L}^{++})^{n_l} \mathcal{S}_{\text{out}}^{++} |0\rangle \ , \quad (5.21b)$$

$$||n_l, n_i = 1, n_o = 0\rangle \equiv (\mathcal{L}^{++})^{n_l} \mathcal{S}_{\text{in}}^{++} |0\rangle \ , \quad (5.21c)$$

$$||n_l, n_i = 1, n_o = 1\rangle \equiv (\mathcal{L}^{++})^{n_l} \mathcal{H}^{++} |0\rangle \ , \quad (5.21d)$$

where

$$n_i = 0, 1 \quad n_o = 0, 1 \quad n_l = 0, 1, 2, \dots \ , \quad (5.22)$$

$|0\rangle$ is the local vacant state annihilated by any LSH operator carrying at least one minus sign, and $\langle 0|0\rangle = 1$. Note that n_i and n_o indicate quark content, but not necessarily strings; exactly one of these equaling 1 implies the presence of a flux string, but both equaling 1 means they are paired up into a hadron. Furthermore, one must take care to remember that the quark numbers are properly handled as ordered fermionic occupation numbers. The states above uniquely enumerate all SU(2)-invariant excitations that can be hosted by a site.

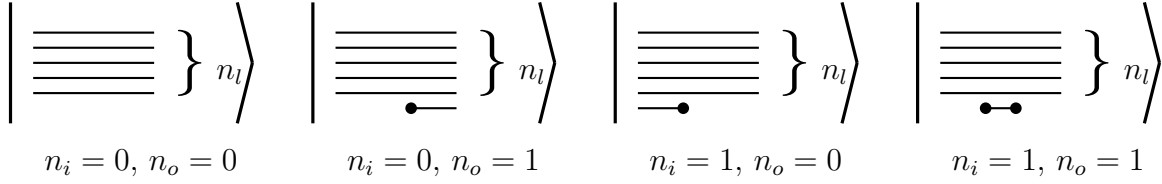


Figure 5.3: Depiction of $SU(2)$ -invariant configurations at a quark site. The on-site state is characterized by a loop quantum number n_l (the solid lines) and two quark quantum numbers n_i and n_o (the blobs).

3

The norms of $||n_l, n_i, n_o\rangle$ can be derived by repeated use of the operator algebra. These types of calculations are described in Appendix C. The result is that a normalized basis is given by

$$|n_l, n_i, n_o\rangle = \frac{||n_l, n_i, n_o\rangle}{\sqrt{n_l! (n_l + 1 + (n_i \oplus n_o))!}}, \quad (5.23)$$

where \oplus denotes addition modulo 2. Figure 5.3 depicts the various different basis states.

Before reexpressing the Hamiltonian, the $SU(2)$ -invariant LSH quantum numbers will have to be related to the prepotential quantum numbers. This relationship can be inferred from

$$\mathcal{N}_\psi |n_l, n_i, n_o\rangle = (n_i + n_o) |n_l, n_i, n_o\rangle, \quad (5.24a)$$

$$\mathcal{N}_L |n_l, n_i, n_o\rangle = (n_l + n_o(1 - n_i)) |n_l, n_i, n_o\rangle, \quad (5.24b)$$

$$\mathcal{N}_R |n_l, n_i, n_o\rangle = (n_l + n_i(1 - n_o)) |n_l, n_i, n_o\rangle. \quad (5.24c)$$

³Though its utility is limited, it is straightforward to give one unifying expression valid for all states: $||n_l, n_i, n_o\rangle = (\mathcal{L}^{++})^{n_l} [\mathcal{P}_{00} + \mathcal{P}_{01} + \mathcal{P}_{10} + (1/2)\mathcal{L}^{--}] (\mathcal{S}_{\text{in}}^{++})^{n_i} (\mathcal{S}_{\text{out}}^{++})^{n_o} |0\rangle$, where $\mathcal{P}_{00} = \mathcal{H}^- \mathcal{H}^{++}$, $\mathcal{P}_{01} = \mathcal{L}^{-+} \mathcal{L}^{+-}$, $\mathcal{P}_{10} = \mathcal{L}^{+-} \mathcal{L}^{-+}$, and $(1/2)\mathcal{L}^{--} (\mathcal{S}_{\text{in}}^{++})^{n_i} (\mathcal{S}_{\text{out}}^{++})^{n_o} |0\rangle = \delta_{n_i,1} \delta_{n_o,1} \mathcal{H}^{++} |0\rangle$.

These imply that the following act as number operators on the $|n_l, n_i, n_o\rangle$ states:

$$\mathcal{N}_i \equiv \frac{1}{2} [\mathcal{N}_\psi + \mathcal{N}_R - \mathcal{N}_L] , \quad (5.25a)$$

$$\mathcal{N}_o \equiv \frac{1}{2} [\mathcal{N}_\psi + \mathcal{N}_L - \mathcal{N}_R] , \quad (5.25b)$$

$$\mathcal{N}_l \equiv \frac{1}{2} [\mathcal{N}_L + \mathcal{N}_R - \mathcal{N}_\psi + \frac{1}{2} (\mathcal{N}_\psi^2 - (\mathcal{N}_L - \mathcal{N}_R)^2)] . \quad (5.25c)$$

(Note again that $\mathcal{N}_{R/L}$ belong to a common site, not opposite ends of a link.) The relations (5.24) can now be promoted to operator identities to be inserted in the Hamiltonian:

$$\mathcal{N}_\psi = \mathcal{N}_i + \mathcal{N}_o , \quad (5.26a)$$

$$\mathcal{N}_L = \mathcal{N}_l + \mathcal{N}_o(1 - \mathcal{N}_i) , \quad (5.26b)$$

$$\mathcal{N}_R = \mathcal{N}_l + \mathcal{N}_i(1 - \mathcal{N}_o) . \quad (5.26c)$$

To summarize, the LSH basis characterizes local states by counting units of loop flux passing through a site, and keeping track of quark species present. A lone “out quark” ($n_o = 1$) or a lone “in quark” ($n_i = 1$) is shorthand for indicating the type of string present, while completely full orbitals just signify a gauge-invariant hadron. The LSH quantum numbers $\{\mathcal{N}_l, \mathcal{N}_i, \mathcal{N}_o\}$ are equivalent to allowed combinations of the $\{\mathcal{N}_R, \mathcal{N}_L, \mathcal{N}_o\}$ quantum numbers, but have the benefit of being unconstrained over their ranges (5.22).

Global Hilbert space construction in one dimension

While the loop-string-hadron formulation largely focuses on characterizing site-local excitations, the dynamics ultimately couples sites and is expressed using states of the lattice as a whole. The global Hilbert space consists of the excitations coming from all sites: one bosonic loop mode and two fermionic quark modes each. However, the global space can only be viewed as a tensor product space of all the local modes to the extent that fermionic statistics are accounted for. One can account for fermionic statistics with binary occupation numbers if the associated basis states have a prescription for how the fermionic operators

are ordered. The ordered product of operators can then be applied to some fixed reference state that satisfies the Abelian Gauss law and any other desired symmetries.

In the loop-string-hadron framework, the lattice “vacant” state $|0\rangle$ (not to be confused with a qubit computational basis state) is characterized as a state devoid of any excitations,

$$\mathcal{N}_i(x) |0\rangle = \mathcal{N}_o(x) |0\rangle = \mathcal{N}_l(x) |0\rangle = 0 \quad \text{for all } x . \quad (5.27)$$

It is annihilated by any $\mathcal{L}^{\pm\pm}$, $\mathcal{S}^{\pm\pm}$, or $\mathcal{H}^{\pm\pm}$ carrying at least one minus sign:

$$\begin{aligned} \mathcal{L}^{+-}(x) |0\rangle &= \mathcal{L}^{-+}(x) |0\rangle = \mathcal{L}^{--}(x) |0\rangle = 0 , \\ \mathcal{S}_{\text{in}}^{+-}(x) |0\rangle &= \mathcal{S}_{\text{in}}^{-+}(x) |0\rangle = \mathcal{S}_{\text{in}}^{--}(x) |0\rangle = 0 , \\ \mathcal{S}_{\text{out}}^{+-}(x) |0\rangle &= \mathcal{S}_{\text{out}}^{-+}(x) |0\rangle = \mathcal{S}_{\text{out}}^{--}(x) |0\rangle = 0 , \\ \mathcal{H}^{--}(x) |0\rangle &= 0 . \end{aligned}$$

One can construct the entire Hilbert space by using $|0\rangle$ as a reference state.

Another reference state would be the staggered strong-coupling vacuum $|v\rangle$, which is the true vacuum at $g, m \rightarrow \infty$. The staggered strong-coupling vacuum is characterized by having vanishing electric fields and full fermion orbitals on odd sites; $|v\rangle$ can be related to $|0\rangle$ by applying to it \mathcal{H}^{++} from every even site.

For all the other lattice basis states, it is necessary to fix a convention for fermion ordering. A site-local ordering was already chosen earlier, so all that is necessary is to order sites. The convention we choose is that sites receive excitations from greatest x down to least; the associated expressions would then have $\mathcal{S}_{\text{in/out}}^{++}$ ’s written with x increasing from left to right. On a lattice with an even number of sites L_x , these states are denoted by

$$|n_l(0), n_i(0), n_o(0); n_l(1), n_i(1), n_o(1); \cdots ; n_l(L_x - 1), n_i(L_x - 1), n_o(L_x - 1)\rangle .$$

For example, the (normalized) staggered strong-coupling vacuum of a four site lattice is given

by

$$\begin{aligned}
|v\rangle &= |0, 0, 0; 0, 1, 1; 0, 0, 0; 0, 1, 1\rangle \\
&= \left[\frac{1}{2}\mathcal{L}^{--}(1)\mathcal{S}_{\text{in}}^{++}(1)\mathcal{S}_{\text{out}}^{++}(1)\right] \left[\frac{1}{2}\mathcal{L}^{--}(3)\mathcal{S}_{\text{in}}^{++}(3)\mathcal{S}_{\text{out}}^{++}(3)\right] |0\rangle \\
&= \mathcal{H}^{++}(1)\mathcal{H}^{++}(3) |0\rangle .
\end{aligned} \tag{5.28}$$

Of course, the ordering is especially important for states that actually have on-site net fermionic excitations. An example of this would be a basis state describing a meson string between sites $x = 0$ and $x = 1$, which is given by

$$\begin{aligned}
|\text{meson}\rangle &= |0, 0, 1; 0, 1, 0; 0, 0, 0; 0, 1, 1\rangle \\
&= \frac{1}{2}\mathcal{S}_{\text{out}}^{++}(0)\mathcal{S}_{\text{in}}^{++}(1)\mathcal{H}^{++}(3) |0\rangle ,
\end{aligned}$$

as opposed to $\frac{1}{2}\mathcal{S}_{\text{in}}^{++}(1)\mathcal{S}_{\text{in}}^{++}(0)\mathcal{H}^{++}(3) |0\rangle$ with the opposite ordering. This state appears after one application of \hat{H}_I to the staggered strong-coupling vacuum $|v\rangle$.

We can summarize the characterization of basis states with the following rule: Local quarks are created going from greatest x down to least, and with $\mathcal{S}_{\text{out}}^{++}(x)$ always acting before $\mathcal{S}_{\text{in}}^{++}(x)$.

Working with the full lattice, the Abelian Gauss law is imposed for physical states. In the $|n_l, n_i, n_o\rangle$ basis, this translates to

$$[n_l + n_o(1 - n_i)]_x = [n_l + n_i(1 - n_o)]_{x+1} . \tag{5.29}$$

Operator factorization

It was remarked at the beginning of this section that LSH operators in the Hamiltonian change quantum numbers as well as state normalization. The on-site operators can now be factored in order to isolate the two behaviors, at which point matrix elements with respect to the LSH basis can be read off trivially.

Pertaining to the loop quantum number n_l , we introduce *normalized ladder operators*,

Λ^+ and Λ^- :

$$\Lambda^\pm \equiv \mathcal{L}^{\pm\pm} \frac{1}{\sqrt{(\mathcal{N}_l + \frac{1}{2} \pm \frac{1}{2})(\mathcal{N}_l + \frac{3}{2} \pm \frac{1}{2} + (\mathcal{N}_i \oplus \mathcal{N}_o))}} \quad (5.30)$$

Here a “normalized operator” refers to any operator \mathcal{O} such that nonvanishing eigenvalues of $\mathcal{O}^\dagger \mathcal{O}$ are unity. The significance of Λ^\pm is that their nonvanishing matrix elements in the LSH basis are all unity:

$$\langle n'_l, n'_i, n'_o | \Lambda^\pm | n_l, n_i, n_o \rangle = \delta_{n'_l, n_l \pm 1} \delta_{n'_i, n_i} \delta_{n'_o, n_o} . \quad (5.31)$$

Hence, they move states up and down the ladder of n_l without changing normalization, except for the possibility of annihilation at the bottom. The ladder operators were constructed in (5.30) to make factoring \mathcal{L}^{++} and \mathcal{L}^{--} trivial.

As for the quark quantum numbers, these are affected by the string operators (and the mixed-type loop operators $\mathcal{L}^{\pm, \mp}$). The string operators were found to obey fermionlike anti-commutation relations, but they are not canonically normalized. This motivates introducing SU(2)-invariant fermionic modes χ_i, χ_o to describe them, with

$$\{\chi_{q'}, \chi_q\} = \{\chi_{q'}^\dagger, \chi_q^\dagger\} = 0 , \quad (q = i, o) \quad (5.32)$$

$$\{\chi_{q'}, \chi_q^\dagger\} = \delta_{q'q} . \quad (q = i, o) \quad (5.33)$$

These also qualify as normalized ladder operators. Because string operators can affect loop numbers, it will prove helpful to also introduce the following shorthand *conditional ladder operators*:

$$(\Lambda^\pm)^{\mathcal{N}_q} \equiv (1 - \mathcal{N}_q) + \Lambda^\pm \mathcal{N}_q , \quad (q = i, o) \quad (5.34a)$$

$$(\Lambda^\pm)^{1-\mathcal{N}_q} \equiv \Lambda^\pm (1 - \mathcal{N}_q) + \mathcal{N}_q . \quad (q = i, o) \quad (5.34b)$$

Each term in these operator exponentials projects on to one or the other eigenspace of \mathcal{N}_q and is followed by a corresponding loop ladder action or lack thereof.

The SU(2)-invariant quark modes χ_i and χ_o are also helpful for characterizing global basis states. One can express any of the LSH basis states by simply acting all the $\chi_{i/o}^\dagger$'s on

$|0\rangle$ with the same rule for ordering as before—there is no need for string and \mathcal{L}^{--} operators or factors of $1/2$ like those in (5.28).

Equipped with the normalized ladder operators, all loop and string operators can be factorized as shown in Table 5.4. It is straightforward to show that these operator factorizations completely reproduce the LSH algebra. The factorizations are all given in a canonical form, with diagonal scaling operators sitting on the right and normalized ladder operators following them. Acting an LSH operator on a ket $|n_l, n_i, n_o\rangle$, the numerical value of its matrix element can just be read off, and the resultant quantum numbers are easily deduced from the ladder operator content.

Wigner-Jordan transform for one dimension

Using fermionic operators can be convenient analytically, but computation models usually assume native operations that commute for different sites. In classical lattice QCD, Grassman variables are avoided because the quark fields can be integrated out of the functional integral analytically. Quantum simulation, however, frequently involves choosing a fermionic mapping onto commuting computational degrees of freedom.

Qubits are two-state systems with a “computational basis” often denoted with states $|0\rangle$ and $|1\rangle$, but most computation models do not regard these as having a fermionic character. For example, the “raising” operators $|1\rangle\langle 0|$ for distinct qubits commute with each other. The bottom line is that for applications the Hamiltonian will need to be converted to spin operators at some point. For one-dimensional systems with localized interactions, the Wigner-Jordan transformation maps fermionic modes into spin operators rather cleanly.

The fermionic modes $\chi_i(x)$, $\chi_o(x)$ for $x = 0, \dots, L_x - 1$ express physical (SU(2)-invariant) quark degrees of freedom that dynamically couple to each other through the hopping terms. However, it turns out that the χ_i ’s and χ_o ’s, in fact, decouple from each other. The operator-factorized Hamiltonian will be discussed below, but to see this decoupling one only needs the string operators from the hopping terms in (5.20). With the factorizations in (5.35), the

LOOP-STRING-HADRON OPERATOR FACTORIZATIONS

$$\mathcal{L}^{++} = \Lambda^+ \sqrt{(\mathcal{N}_l + 1)(\mathcal{N}_l + 2 + (\mathcal{N}_i \oplus \mathcal{N}_o))} \quad (5.35a)$$

$$\mathcal{L}^{--} = \Lambda^- \sqrt{\mathcal{N}_l(\mathcal{N}_l + 1 + (\mathcal{N}_i \oplus \mathcal{N}_o))} \quad (5.35b)$$

$$\mathcal{L}^{+-} = -\chi_i^\dagger \chi_o \quad (5.35c)$$

$$\mathcal{L}^{-+} = \chi_i \chi_o^\dagger \quad (5.35d)$$

$$\mathcal{S}_{\text{in}}^{++} = \chi_i^\dagger (\Lambda^+)^{\mathcal{N}_o} \sqrt{\mathcal{N}_l + 2 - \mathcal{N}_o} \quad (5.35e)$$

$$\mathcal{S}_{\text{in}}^{--} = \chi_i (\Lambda^-)^{\mathcal{N}_o} \sqrt{\mathcal{N}_l + 2(1 - \mathcal{N}_o)} \quad (5.35f)$$

$$\mathcal{S}_{\text{out}}^{++} = \chi_o^\dagger (\Lambda^+)^{\mathcal{N}_i} \sqrt{\mathcal{N}_l + 2 - \mathcal{N}_i} \quad (5.35g)$$

$$\mathcal{S}_{\text{out}}^{--} = \chi_o (\Lambda^-)^{\mathcal{N}_i} \sqrt{\mathcal{N}_l + 2(1 - \mathcal{N}_i)} \quad (5.35h)$$

$$\mathcal{S}_{\text{in}}^{-+} = \chi_o^\dagger (\Lambda^-)^{1-\mathcal{N}_i} \sqrt{\mathcal{N}_l + 2\mathcal{N}_i} \quad (5.35i)$$

$$\mathcal{S}_{\text{in}}^{+-} = \chi_o (\Lambda^+)^{1-\mathcal{N}_i} \sqrt{\mathcal{N}_l + 1 + \mathcal{N}_i} \quad (5.35j)$$

$$\mathcal{S}_{\text{out}}^{+-} = \chi_i^\dagger (\Lambda^-)^{1-\mathcal{N}_o} \sqrt{\mathcal{N}_l + 2\mathcal{N}_o} \quad (5.35k)$$

$$\mathcal{S}_{\text{out}}^{-+} = \chi_i (\Lambda^+)^{1-\mathcal{N}_o} \sqrt{\mathcal{N}_l + 1 + \mathcal{N}_o} \quad (5.35l)$$

$$\mathcal{H}^{++} = \chi_i^\dagger \chi_o^\dagger \quad (5.35m)$$

$$\mathcal{H}^{--} = -\chi_i \chi_o \quad (5.35n)$$

Table 5.4: Factorization of all SU(2) invariant operators into canonically normalized fermionic modes times a loop ladder operator times a function of number operators. The operator exponentials are conditional ladder operators defined in (5.34).

fermionic content of $\mathcal{S}_{\text{out}}^{+\sigma}(x)\mathcal{S}_{\text{in}}^{\sigma-}(x+1)$ terms takes the form

$$\begin{aligned}\mathcal{S}_{\text{out}}^{++}(x)\mathcal{S}_{\text{in}}^{+-}(x+1) &\sim \chi_o^\dagger(x)\chi_o(x+1)\cdots, \\ \mathcal{S}_{\text{out}}^{+-}(x)\mathcal{S}_{\text{in}}^{-}(x+1) &\sim \chi_i^\dagger(x)\chi_i(x+1)\cdots.\end{aligned}$$

The decoupling is now manifest.

Knowing this, we relabel the fermionic modes using Ψ_k for $k = 0, \dots, 2L_x - 1$, with the map

$$\Psi_k = \begin{cases} \chi_i(k), & 0 \leq k \leq L_x - 1 \\ \chi_o(k - L_x), & L_x \leq k \leq 2L_x - 1 \end{cases}.$$

The Wigner-Jordan transformation converts the Ψ_k into spin operators via

$$\Psi_k \equiv \sigma_k^+ \prod_{k'=0}^{k-1} Z_{k'} . \quad (5.36)$$

Assuming open boundary conditions, all fermionic couplings are then nearest-neighbor in the x coordinate as well as the k label, and as a result the Wigner-Jordan transformation has no leftover Pauli- Z strings. The couplings in the hopping terms will all take the form $\sigma_k^\pm \sigma_{k+1}^\mp$:

$$\chi_i^\dagger(x)\chi_i(x+1) \rightarrow \sigma_x^- \sigma_{x+1}^+ , \quad (5.37)$$

$$\chi_o^\dagger(x)\chi_o(x+1) \rightarrow \sigma_{L_x+x}^- \sigma_{L_x+x+1}^+ . \quad (5.38)$$

Hence, on the 1D open lattice only, it is possible to essentially replace anticommuting χ 's and χ^\dagger 's with commuting σ^- 's and σ^+ 's in the operator factorizations.

5.1.4 Dynamics of loop-string-hadron states

The terms of the Hamiltonian presented in Sec. 5.1.2 were expressed in terms of site-local loop-string-hadron operators. The Hamiltonian will now be reexpressed once more using the operator factorizations from above, with the final result expediting the process of calculating matrix elements in the LSH basis. Subsequently, a graphical method is given for determining how states are mixed by terms in the Hamiltonian.

Starting with the electric Hamiltonian, the Casimirs continue to be diagonal as they always were. Using the conversion (5.26) from prepotential to LSH number operators, we have

$$\hat{H}_E = \frac{g^2}{4} \sum_x \left\{ \left[\frac{1}{2} (\mathcal{N}_l + \mathcal{N}_o(1 - \mathcal{N}_i)) \right]_x \left[\frac{1}{2} (\mathcal{N}_l + \mathcal{N}_o(1 - \mathcal{N}_i)) + 1 \right]_x \right. \\ \left. + \left[\frac{1}{2} (\mathcal{N}_l + \mathcal{N}_i(1 - \mathcal{N}_o)) \right]_x \left[\frac{1}{2} (\mathcal{N}_l + \mathcal{N}_i(1 - \mathcal{N}_o)) + 1 \right]_x \right\} . \quad (5.39)$$

The mass Hamiltonian is also diagonal and given simply by

$$\hat{H}_M = m_0 \sum_x (-)^x (\mathcal{N}_i(x) + \mathcal{N}_o(x)) . \quad (5.40)$$

And lastly, the interaction \hat{H}_I in terms of SU(2) invariants was originally given as (5.20), with the off-diagonal part of a hopping term being $\sum_{\sigma=\pm} \sigma \mathcal{S}_{\text{out}}^{+, \sigma}(x) \mathcal{S}_{\text{in}}^{\sigma, -}(x+1)$. Using the operator factorizations (5.35), these hopping terms are given by

$$\mathcal{S}_{\text{out}}^{++}(x) \mathcal{S}_{\text{in}}^{+-}(x+1) = [\chi_o^\dagger]_x [\chi_o]_{x+1} \left[(1 - \mathcal{N}_i) + \Lambda^+ \mathcal{N}_i \right]_x \left[\mathcal{N}_i + \Lambda^+(1 - \mathcal{N}_i) \right]_{x+1} \times \\ \left[\sqrt{\mathcal{N}_l - \mathcal{N}_i + 2} \right]_x \left[\sqrt{\mathcal{N}_l - (1 - \mathcal{N}_i) + 2} \right]_{x+1} , \quad (5.41a)$$

$$\mathcal{S}_{\text{out}}^{--}(x) \mathcal{S}_{\text{in}}^{-+}(x+1) = [\chi_o]_x [\chi_o^\dagger]_{x+1} \left[(1 - \mathcal{N}_i) + \Lambda^- \mathcal{N}_i \right]_x \left[\mathcal{N}_i + \Lambda^-(1 - \mathcal{N}_i) \right]_{x+1} \times \\ \left[\sqrt{\mathcal{N}_l + 2(1 - \mathcal{N}_i)} \right]_x \left[\sqrt{\mathcal{N}_l + 2\mathcal{N}_i} \right]_{x+1} , \quad (5.41b)$$

$$\mathcal{S}_{\text{out}}^{+-}(x) \mathcal{S}_{\text{in}}^{--}(x+1) = [\chi_i^\dagger]_x [\chi_i]_{x+1} \left[\mathcal{N}_o + \Lambda^-(1 - \mathcal{N}_o) \right]_x \left[(1 - \mathcal{N}_o) + \Lambda^- \mathcal{N}_o \right]_{x+1} \times \\ \left[\sqrt{\mathcal{N}_l + 2\mathcal{N}_o} \right]_x \left[\sqrt{\mathcal{N}_l + 2(1 - \mathcal{N}_o)} \right]_{x+1} , \quad (5.41c)$$

$$\mathcal{S}_{\text{out}}^{-+}(x) \mathcal{S}_{\text{in}}^{++}(x+1) = [\chi_i]_x [\chi_i^\dagger]_{x+1} \left[\mathcal{N}_o + \Lambda^+(1 - \mathcal{N}_o) \right]_x \left[(1 - \mathcal{N}_o) + \Lambda^+ \mathcal{N}_o \right]_{x+1} \times \\ \left[\sqrt{\mathcal{N}_l + \mathcal{N}_o + 1} \right]_x \left[\sqrt{\mathcal{N}_l + (1 - \mathcal{N}_o) + 1} \right]_{x+1} . \quad (5.41d)$$

To complete \hat{H}_I , one also needs the diagonal “outer” factors that sandwich these. By (5.26),

$$\frac{1}{\sqrt{\mathcal{N}_{L/R} + 1}} = \frac{1}{\sqrt{\mathcal{N}_l + \mathcal{N}_{o/i} (1 - \mathcal{N}_{i/o}) + 1}} . \quad (5.42)$$

The above expressions in terms of diagonalized scaling operators and normalized ladder operators are everything one needs to immediately express the action of the Hamiltonian in the LSH basis.

The actions of the loop-string-hadron operators are easier to intuit given the fact they are 1-sparse in the LSH basis, i.e., any of the \mathcal{L} , \mathcal{S} , or \mathcal{H} operators acting on a basis state either turns it into another basis state or annihilates it. They do not expand into linear combinations like link operators do in irrep bases [cf. Eq.(5.4)]. To express all possible actions of the LSH operators in terms of quantum numbers, we introduce a pictorial mapping shown in Fig. 5.4 that associates pictures with changes in quantum numbers of the basis states.

A summary of these pictorial actions on quantum numbers is as follows:

- Solid (dashed) line: Increment (decrement) n_l by one unit.
- Solid (dashed) in-quark: Increment (decrement) n_i by one unit.
- Solid (dashed) out-quark: Increment (decrement) n_o by one unit.
- Solid (dashed) hadron: Increment (decrement) both n_i and n_o by one unit.

If the resulting quantum numbers are forbidden, this corresponds to annihilation of the basis state. Note also that these graphical rules use symbols that are related to, but distinct from, the basis-independent operator pictures introduced in Sec. 5.1.1.

As a simple example of their usage, the fact that $\mathcal{L}^{++} |n_l, n_i, n_o\rangle \propto |n_l + 1, n_i, n_o\rangle$ means the action of \mathcal{L}^{++} is represented by a single solid line:

$$\mathcal{L}^{++} |n_l, n_i, n_o\rangle \propto |n_l + 1, n_i, n_o\rangle$$

$$\Rightarrow \mathcal{L}^{++} = \text{---}^{\wedge} \sim \text{---}$$

In general, however, the operators may have composite actions, so the instructions are composed vertically along with an ordering to them. This is summarized as follows:

- Effect the changes indicated by each instruction, going from top to bottom.

GRAPHICAL QUANTUM NUMBER INSTRUCTIONS

$$\text{————} \equiv n_l \rightarrow n_l + 1$$

$$\text{- - - - -} \equiv n_l \rightarrow n_l - 1$$

(a)

$$\text{⊖} \equiv n_i \rightarrow n_i + 1$$

$$\text{⊘} \equiv n_i \rightarrow n_i - 1$$

$$\text{⊙} \equiv n_o \rightarrow n_o + 1$$

$$\text{⦶} \equiv n_o \rightarrow n_o - 1$$

(b)

$$\text{⊙⊙} \equiv \begin{pmatrix} n_i \\ n_o \end{pmatrix} \rightarrow \begin{pmatrix} n_i + 1 \\ n_o + 1 \end{pmatrix}$$

$$\text{⦶⦶} \equiv \begin{pmatrix} n_i \\ n_o \end{pmatrix} \rightarrow \begin{pmatrix} n_i - 1 \\ n_o - 1 \end{pmatrix}$$

(b')

Figure 5.4: Pictorial representation of changes in quantum numbers between initial and final states, which represent (a) flux creation and annihilation, (b) quark creation and annihilation, and (b') hadron creation and annihilation (a composite action).

- The state is annihilated if at any step the quantum numbers are forbidden.

Consider $\mathcal{S}_{\text{in}}^{++}$ for example. Using the factorization (5.35e) and conditional ladder operators (5.34), one can write $\mathcal{S}_{\text{in}}^{++} \sim \chi_i^\dagger(1 - \mathcal{N}_o) + \chi_i^\dagger \Lambda^+ \mathcal{N}_o$. Acting on a basis state, at most one of these terms can be nonzero. Each term tries to raise n_i , while only one can raise n_l . These behaviors are diagrammatically summarized by

$$\mathcal{S}_{\text{in}}^{++} = \text{---}\hat{\circ} \sim \begin{array}{c} \circ \\ \circ \\ \circ \end{array} + \text{---}\begin{array}{c} \circ \\ \circ \end{array},$$

where the first term creates an in-string on a quark-less site, while the second connects an in-string to an already-existing out-string to form a baryon and gauge flux line. We similarly represent and describe the actions of all loop-string-hadron operators pictorially in Table 5.5.

5.1.5 Summary of matter sites

To conclude this section, we summarize the results and what their significance is in 1 and higher dimensions.

Prepotentials were used to construct a closed algebra of manifestly SU(2)-invariant LSH operators, and it was shown how to translate the Hamiltonian into them. These operators were then used to construct a LSH basis in which every possible combination of quantum numbers (consistent with the Abelian Gauss law) describes a unique set of on-site excitations. For future applications, all LSH operators were then factored for convenience on that basis and the Hamiltonian was again reexpressed in a more explicit form.

For $d = 1$ and with open boundary conditions, one can essentially just forget about Fermi statistics and replace singlet-quark operators with spin operators. In higher dimensions this will no longer be the case. However, the local bases and operator factorizations will carry over to “matter sites” in $d > 1$, so the main feature that gets lost is really just simplicity of the Wigner-Jordan transformation.

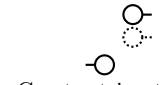
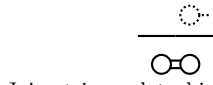
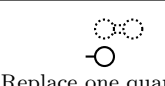
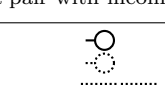
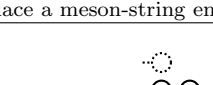
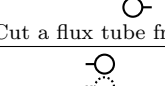
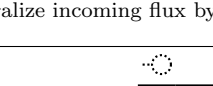
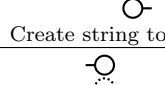
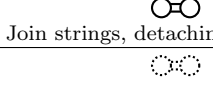
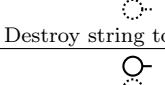
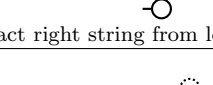
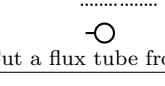
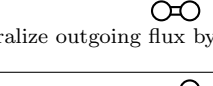
LSH operator	Physical description; Graphical action on state $ n_l, n_i, n_o\rangle_x$
$\mathcal{L}^{++}(x) \equiv \frac{\widehat{\quad}}{x}$	 Create unit of gauge flux.
$\mathcal{L}^{--}(x) \equiv \frac{\widehat{\cdots\cdots\cdots}}{x}$	 Destroy unit of gauge flux.
$\mathcal{L}^{+-}(x) \equiv \frac{\widehat{\cdots\cdots\cdots}}{x}$	 Change matter-sourced flux direction. ($d > 1$)
$\mathcal{L}^{-+}(x) \equiv \frac{\widehat{\cdots\cdots\cdots}}{x}$	 Change matter-sourced flux direction. ($d > 1$)
$\mathcal{S}_{\text{in}}^{++}(x) \equiv \frac{\widehat{\quad}}{x}$	 
$\mathcal{S}_{\text{in}}^{--}(x) \equiv \frac{\widehat{\cdots\cdots\cdots}}{x}$	 
$\mathcal{S}_{\text{in}}^{+-}(x) \equiv \frac{\widehat{\cdots\cdots\cdots}}{x}$	 
$\mathcal{S}_{\text{in}}^{-+}(x) \equiv \frac{\widehat{\cdots\cdots\cdots}}{x}$	 
$\mathcal{S}_{\text{out}}^{++}(x) \equiv \frac{\widehat{\quad}}{x}$	 
$\mathcal{S}_{\text{out}}^{--}(x) \equiv \frac{\widehat{\cdots\cdots\cdots}}{x}$	 
$\mathcal{S}_{\text{out}}^{+-}(x) \equiv \frac{\widehat{\cdots\cdots\cdots}}{x}$	 
$\mathcal{S}_{\text{out}}^{-+}(x) \equiv \frac{\widehat{\cdots\cdots\cdots}}{x}$	 
$\mathcal{H}^{++}(x) \equiv \frac{\widehat{\quad}}{x}$	 Create a hadron.
$\mathcal{H}^{--}(x) \equiv \frac{\widehat{\cdots\cdots\cdots}}{x}$	 Destroy a hadron.

Table 5.5: Graphical representation of the (1D) LSH operators. Left column: Pictorial representations of the operators. Right column: The operators' actions on local LSH states $|n_l, n_i, n_o\rangle_x$, in terms of the graphical rules in Sec. 5.1.3.

5.2 *Loop-string-hadron formulation: Multiple dimensions*

The prepotential formulation of pure SU(2) gauge theory on Cartesian lattices was studied in great detail in Refs. [51, 55, 57–59]. While it yields a local loop basis, on a Cartesian lattice that basis is overcomplete and consequently associated with a local form of Mandelstam constraints. Solving these constraints is involved and becomes increasingly difficult in higher dimensions.

More recently, a virtual “point splitting” of lattice sites on square lattices [88, 182] was found to be quite fruitful because it bypasses the Mandelstam constraints and casts all constraints of the theory into the Abelian form of (1.133). Below, the point splitting method is reviewed and how this development generalizes to higher dimensions is explained. We additionally describe how to couple to matter in higher dimensions, giving a complete suite for describing SU(2) lattice gauge theory coupled to one flavor of staggered quarks.

5.2.1 *Virtual point splitting: Two dimensions*

Virtual splitting of a site from a square lattice involves formally dividing each four-point vertex into a pair of three-point vertices with one shared virtual leg, as depicted in Fig. 5.5. It is notationally convenient to split the site by pairing the $+e_j$ ($-e_j$) directions together, to label the attached link ends 1 and 2 ($\bar{1}$ and $\bar{2}$), and to label their common vertex x' (\bar{x}'). As for the internal link, it is further broken into two links with an intermediate vertex that will accommodate matter. This extra division is not needed for pure gauge theory. Point splitting the two-dimensional (2D) square lattice results topologically in a hexagonal lattice. One can now formulate prepotentials on this virtual hexagonal lattice as in (1.131) and (1.135).

The virtual links can carry gauge flux, but the flux through them is not actually counted toward \hat{H}_E . The utility of the links really lies in the fact that a three point-vertex has no ambiguities in how nonintersecting SU(2) flux lines are routed through it. Four-point vertices do suffer from such an ambiguity, and this is responsible for redundant states on the square lattice that normally have to be removed via Mandelstam constraints. The formal

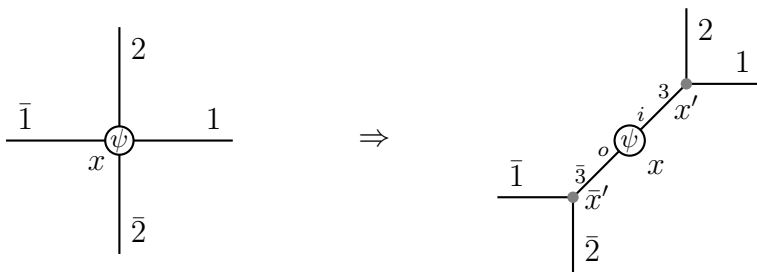


Figure 5.5: Virtual point splitting of a 2D lattice site x into gluonic sites x', \bar{x}' , with matter living on the central quark site x .

hexagonal lattice still harbors redundancy, but dealing with it is significantly easier: the relevant constraint is just another Abelian Gauss law for virtual links.

As for plaquettes, the elementary loops are indeed hexagonal plaquettes corresponding to six link operators in pure gauge theory.

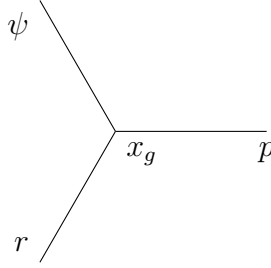
For more discussion on the original pure gauge version, see Ref. [88].

The matter field living at site x is now situated between two virtual links as shown in Fig. 5.5. The virtual matter vertex is locally identical to a 1D lattice site (cf. Fig. 5.2), so the on-site $SU(2)$ -invariant operators and local Hilbert space for x are handled as in one dimension. Because hosting matter divides each virtual link into two, the plaquette operators end up involving eight sites.

The other trivalent virtual sites x' and \bar{x}' are gluonic vertices on the same footing as in pure gauge theory [88], which we now review.

5.2.2 $SU(2)$ invariants: Loop operators at gluonic vertices

At any gluonic site x_g (x' and \bar{x}' vertices for the hexagonal lattice), links emerge in three directions and can be labeled with integers p, q, r such that $p < q < r$:



For the 2D lattice we only ever need $(p, q, r) = (1, 2, 3)$ ($(p, q, r) = (\bar{1}, \bar{2}, \bar{3})$) at the x' (\bar{x}') sites like in Fig. 5.5, but more (p, q, r) combinations will be used in three dimensions.

The attached link ends are associated with Schwinger bosons $\hat{a}^a(x_g, i)$ for $i = p, q, r$. From these doublets, one can form the complete set of $SU(2)$ invariants at x_g as given in (5.43)–(5.44).

- *Pure gauge loop operators.*— $\mathcal{L}_{ij}^{\sigma, \sigma'}$:

$$\mathcal{L}_{ij}^{++} \equiv \hat{a}_a^\dagger(i) \hat{a}_a^\dagger(j) \quad (5.43a)$$

$$\mathcal{L}_{ij}^{+-} \equiv \hat{a}_a^\dagger(i) \hat{a}_a(j) \quad (5.43b)$$

$$\mathcal{L}_{ij}^{-+} \equiv \hat{a}_a(i) \hat{a}_a^\dagger(j) = (\mathcal{L}_{ij}^{+-})^\dagger \quad (5.43c)$$

$$\mathcal{L}_{ij}^{--} \equiv \hat{a}_a(i) \hat{a}_a(j) = (\mathcal{L}_{ij}^{++})^\dagger \quad (5.43d)$$

- *Gauge flux number operators.*— \mathcal{N}_j :

$$\mathcal{N}_j = \hat{a}_a^\dagger(j) \hat{a}_a(j) . \quad (5.44)$$

Above, i and j are distinct direction indices from the set $\{p, q, r\}$. It is easily seen from (5.43) that the $\mathcal{L}_{ij}^{\sigma, \sigma'}$ are redundant in their link labels. For example, $\mathcal{L}_{12}^{++} = -\mathcal{L}_{21}^{++}$. More generally, this interdependence is summarized by

$$\mathcal{L}_{ij}^{\sigma, \sigma'} = -\sigma \sigma' \mathcal{L}_{ji}^{\sigma', \sigma} \quad (5.45)$$

To avoid this redundancy, we will usually deal only with the “cyclic” pairs $ij = (pq, qr, rs)$.

As with matter sites, the loop operators associated with gluonic vertices form a closed commutator algebra, displayed in Table 5.3.

5.2.3 Vertex factors and contractions

Completely migrating from the E , U , and ψ variables to LSH variables is greatly aided by furnishing a dictionary to translate spatially extended, composite operators. Since the LSH formalism isolates on-site degrees of freedom, such operators are formed by multiplying together LSH operators from the traversed vertices.

For example, when tracing out a plaquette operator ($d \geq 2$) or any other spatial Wilson line or loop, one would ordinarily encounter vertex contractions in four possible forms: $U_{ab}V_{b\gamma}$, $U_{ab}^\dagger V_{b\gamma}^\dagger$, $U_{ab}V_{b\gamma}^\dagger$, or $U_{ab}^\dagger V_{b\gamma}$ (with U and V being link operators attached to a given vertex). In the LSH framework, the four types of vertex contractions are naturally identified with *vertex factor* matrices. The four possible vertex contractions are expressed in (5.46)-(5.49), which show the appropriate factor to assign to a vertex depending on how the links are oriented relative to the “path” being traced by the Wilson line:

- *RL*-type traversal:

$$\begin{array}{c}
 \rightarrow \text{path of Wilson line} \rightarrow \\
 a = \begin{pmatrix} a_1 \\ a_2 \end{pmatrix} \quad b = \begin{pmatrix} b_1 \\ b_2 \end{pmatrix} \\
 \begin{array}{c} \xrightarrow{\hat{U}_R(a)} \bullet \xrightarrow{\hat{U}_L(b)} \\ \hat{U}_R(a) \quad \hat{U}_L(b) \end{array}
 \end{array}$$

$$\hat{U}_R(a)\hat{U}_L(b) = \frac{1}{\sqrt{\mathcal{N}_b + 1}} \begin{pmatrix} \mathcal{L}_{ab}^{++} & \mathcal{L}_{ab}^{+-} \\ -\mathcal{L}_{ab}^{-+} & \mathcal{L}_{ab}^{--} \end{pmatrix} \frac{1}{\sqrt{\mathcal{N}_a + 1}} \quad (5.46)$$

- *LR*-type traversal:

$$\begin{array}{c}
 \rightarrow \text{ path of Wilson line } \rightarrow \\
 \hline
 \hat{U}_L^\dagger(a) \quad \hat{U}_R^\dagger(b)
 \end{array}$$

$$\hat{U}_L^\dagger(a)\hat{U}_R^\dagger(b) = \frac{1}{\sqrt{\mathcal{N}_b + 1}} \begin{pmatrix} -\mathcal{L}_{ab}^{--} & -\mathcal{L}_{ab}^{-+} \\ \mathcal{L}_{ab}^{+-} & -\mathcal{L}_{ab}^{++} \end{pmatrix} \frac{1}{\sqrt{\mathcal{N}_a + 1}} \quad (5.47)$$

- *RR*-type traversal:

$$\begin{array}{c}
 \rightarrow \text{ path of Wilson line } \rightarrow \\
 \hline
 \hat{U}_R(a) \quad \hat{U}_R^\dagger(b)
 \end{array}$$

$$\hat{U}_R(a)\hat{U}_R^\dagger(b) = \frac{1}{\sqrt{\mathcal{N}_b + 1}} \begin{pmatrix} \mathcal{L}_{ab}^{+-} & -\mathcal{L}_{ab}^{++} \\ \mathcal{L}_{ab}^{--} & \mathcal{L}_{ab}^{-+} \end{pmatrix} \frac{1}{\sqrt{\mathcal{N}_a + 1}} \quad (5.48)$$

- *LL*-type traversal:

$$\begin{array}{c}
 \rightarrow \text{ path of Wilson line } \rightarrow \\
 \hline
 \hat{U}_L^\dagger(a) \quad \hat{U}_L(b)
 \end{array}$$

$$\hat{U}_L^\dagger(a)\hat{U}_L(b) = \frac{1}{\sqrt{\mathcal{N}_b + 1}} \begin{pmatrix} \mathcal{L}_{ab}^{-+} & -\mathcal{L}_{ab}^{--} \\ \mathcal{L}_{ab}^{++} & \mathcal{L}_{ab}^{+-} \end{pmatrix} \frac{1}{\sqrt{\mathcal{N}_a + 1}} \quad (5.49)$$

In the graphics, the symbols a and b are used to refer to the harmonic oscillator doublets encountered when “flowing in” to and “flowing out” of a vertex, respectively. Therefore, they make use of the following singlets:

$$\begin{aligned}
 \mathcal{L}_{ab}^{++} &= a^\dagger \cdot \epsilon \cdot b^\dagger & \mathcal{L}_{ab}^{--} &= a \cdot \epsilon \cdot b \\
 \mathcal{L}_{ab}^{+-} &= a^\dagger \cdot b & \mathcal{L}_{ab}^{-+} &= a \cdot b^\dagger \\
 \mathcal{N}_a &= a^\dagger \cdot a & \mathcal{N}_b &= b^\dagger \cdot b .
 \end{aligned}$$

The vertex factor matrices can be transformed into each other by using the ϵ matrix; schematically,

$$(LR) = (-\epsilon)(RL)(-\epsilon) ,$$

$$(RR) = (RL)(-\epsilon) ,$$

$$(LL) = (-\epsilon)(RL) ,$$

allowing all four types to be expressed in terms of one matrix and suitable contractions with ϵ .

To get a feel for how the vertex factors are used, consider an elementary plaquette in 2D pure gauge theory that follows the path $x \rightarrow x + e_2 \rightarrow x + e_1 + e_2 \rightarrow x + e_1 \rightarrow x$. [This corresponds to $U_{\square}^{(21)}(x)$ from (5.3).] By multiplying all vertex factors together going around the path and tracing over the leftover gauge indices, the associated loop takes the schematic form

$$\text{tr} \left([\mathcal{V}_{12}]_x [\mathcal{V}_{\bar{2}\bar{3}}\mathcal{V}_{31}]_{x+e_2} [\mathcal{V}_{\bar{1}\bar{2}}]_{x+e_1+e_2} [\mathcal{V}_{23}\mathcal{V}_{\bar{3}\bar{1}}]_{x+e_1} \right) ,$$

for appropriately chosen vertex factor matrices \mathcal{V} . Plaquette and Wilson loop operators will be constructed explicitly in Sec. 5.2.4 below.

To form hopping terms and general meson strings in the LSH framework, one additionally needs vertex factors at matter sites to form the string ends:

$$\hat{\psi}^\dagger(x)\hat{U}_L(x) = \frac{1}{\sqrt{\mathcal{N}_L(x)+1}} \left(\mathcal{S}_{\text{out}}^{++}(x), \mathcal{S}_{\text{out}}^{+-}(x) \right) \quad (5.50)$$

$$\hat{\psi}^\dagger(x)\hat{U}_R^\dagger(x) = \frac{1}{\sqrt{\mathcal{N}_R(x)+1}} \left(\mathcal{S}_{\text{in}}^{-+}(x), \mathcal{S}_{\text{in}}^{++}(x) \right) \quad (5.51)$$

$$\hat{U}_R(x)\hat{\psi}(x) = \begin{pmatrix} \mathcal{S}_{\text{in}}^{+-}(x) \\ \mathcal{S}_{\text{in}}^{--}(x) \end{pmatrix} \frac{1}{\sqrt{\mathcal{N}_R(x)+1}} \quad (5.52)$$

$$\hat{U}_L^\dagger(x)\hat{\psi}(x) = \begin{pmatrix} \mathcal{S}_{\text{out}}^{--}(x) \\ \mathcal{S}_{\text{out}}^{-+}(x) \end{pmatrix} \frac{1}{\sqrt{\mathcal{N}_L(x)+1}} \quad (5.53)$$

The full meson string operator is then a path-ordered product of pure-gluon vertex factors, sandwiched between two appropriate string ends. Elementary matrix multiplication of all

such factors leaves no uncontracted group indices.

5.2.4 The 2D Hamiltonian

The Hamiltonian for two dimensions will now be translated into loop-string-hadron operators. The essential difference from $d = 1$ will be the presence of magnetic energy \hat{H}_B .

The electric energy \hat{H}_E is the same as a square lattice, in the sense that contributions from all the 1- and 2-direction links constitute \hat{H}_E . That is,

$$\hat{H}_E = \frac{g^2}{4} \sum_x \sum_{j=1}^2 \left[\frac{1}{2} \mathcal{N}_j(x') \left(\frac{1}{2} \mathcal{N}_j(x') + 1 \right) + \frac{1}{2} \mathcal{N}_{\bar{j}}(\bar{x}') \left(\frac{1}{2} \mathcal{N}_{\bar{j}}(\bar{x}') + 1 \right) \right] . \quad (5.54)$$

Note that this $d > 1$ expression for \hat{H}_E only involves number operators from gluonic sites.

For one dimension, \hat{H}_M was translated in (5.40). The translation of \hat{H}_M carries over identically to $d > 1$:

$$\hat{H}_M = m \sum_x (-)^x (\mathcal{N}_i(x) + \mathcal{N}_o(x)) . \quad (5.55)$$

The hopping terms in \hat{H}_I were factored for one dimension in (5.41) and (5.42). The hopping terms for two dimensions are translated as follows: The links are naturally oriented such that a typical hopping term takes the schematic form $\psi^\dagger U^\dagger U U^\dagger \psi$, where the middle U comes from the original square lattice; these orientations can be seen from the cutout of a point-split plaquette shown in Fig. 5.6. In a 2D Schwinger boson framework, the hopping term in the j direction would be expanded as

$$\begin{aligned} \psi^\dagger(x) U(x, x + e_j) \psi(x + e_j) &\rightarrow \psi^\dagger(x) U_3^{R\dagger}(x) U_3^{L\dagger}(x') U_j^L(x') \times \\ &\times U_j^R(\overline{x + e_j}') U_3^{R\dagger}(\overline{x + e_j}') U_3^{L\dagger}(x + e_j) \psi(x + e_j) . \end{aligned}$$

This same object is realized in the LSH framework by stringing together the vertex factors

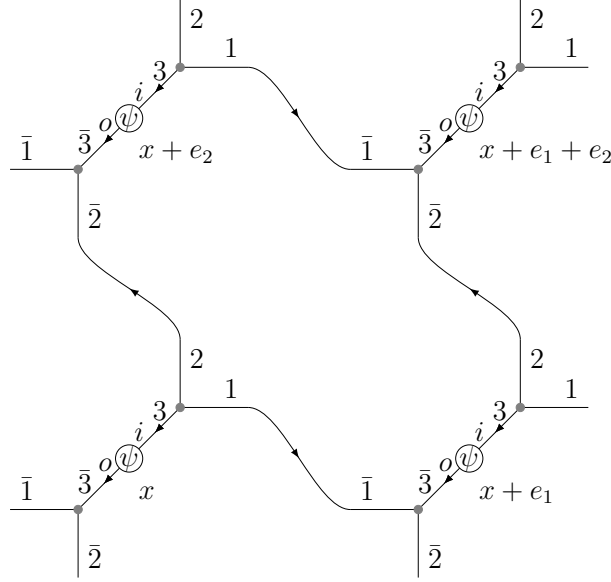


Figure 5.6: Connectivity of a point-split plaquette in two dimensions. Arrows indicated flow from the “left” end of a link to its “right” end.

from Sec. 5.2.3. The translation of the right-hand side into LSH operators is

$$\begin{aligned} & \left[\frac{1}{\sqrt{\mathcal{N}_R + 1}} \begin{pmatrix} \mathcal{S}_{\text{in}}^{-+} & \mathcal{S}_{\text{in}}^{++} \end{pmatrix} \right]_x \left[\frac{1}{\sqrt{\mathcal{N}_j + 1}} \begin{pmatrix} \mathcal{L}_{3j}^{-+} & -\mathcal{L}_{3j}^{--} \\ \mathcal{L}_{3j}^{++} & \mathcal{L}_{3j}^{+-} \end{pmatrix} \frac{1}{\sqrt{\mathcal{N}_3 + 1}} \right]_{x'} \times \\ & \times \left[\frac{1}{\sqrt{\mathcal{N}_3 + 1}} \begin{pmatrix} \mathcal{L}_{j\bar{3}}^{+-} & -\mathcal{L}_{j\bar{3}}^{++} \\ \mathcal{L}_{j\bar{3}}^{--} & \mathcal{L}_{j\bar{3}}^{-+} \end{pmatrix} \frac{1}{\sqrt{\mathcal{N}_j + 1}} \right]_{x+e_j}, \left[\begin{pmatrix} \mathcal{S}_{\text{out}}^{--} \\ \mathcal{S}_{\text{out}}^{-+} \end{pmatrix} \frac{1}{\sqrt{\mathcal{N}_L + 1}} \right]_{x+e_j}. \end{aligned}$$

To express the result of matrix multiplication, it is helpful to introduce a sign function $\eta_h^{(2D)}$ to carry overall signs:

$$\eta_h^{(2D)}(\vec{\sigma}) \equiv \eta_h^{(2D)}(\sigma_1, \sigma_2, \sigma_3) = (-1)^{\delta_{(\sigma_1, \sigma_2), (-, -)}} (-1)^{\delta_{(\sigma_2, \sigma_3), (+, +)}}. \quad (5.56)$$

Therefore, the translation into loop-string-hadron operators is

$$\begin{aligned}
\psi^\dagger(x)U(x, x + e_j)\psi(x + e_j) \rightarrow & \sum_{\sigma_1, \sigma_2, \sigma_3} \eta_h^{(2D)}(\vec{\sigma}) \left[\frac{1}{\sqrt{\mathcal{N}_R + 1}} \frac{1}{\sqrt{\mathcal{N}_j + 1}} \right]_x \left[\frac{1}{\sqrt{\mathcal{N}_3 + 1}} \right]_{x+e_j} \times \\
& \times \left[\mathcal{S}_{\text{in}}^{\sigma_1, +} \mathcal{L}_{3j}^{\sigma_1, \sigma_2} \right]_x \left[\mathcal{L}_{j3}^{\sigma_2, \sigma_3} \mathcal{S}_{\text{out}}^{-, \sigma_3} \right]_{x+e_j} \times \\
& \times \left[\frac{1}{\sqrt{\mathcal{N}_3 + 1}} \right]_x \left[\frac{1}{\sqrt{\mathcal{N}_j + 1}} \frac{1}{\sqrt{\mathcal{N}_L + 1}} \right]_{x+e_j}. \quad (5.57)
\end{aligned}$$

The final piece of the Hamiltonian is \hat{H}_B . The plaquette operators can be translated by following the gluonic-site vertex contractions around a plaquette as described in Sec. 5.2.3. A generic plaquette is depicted in Fig. 5.6. Similar to hopping terms, the result is given in terms of plaquette signs $\eta_p^{(2D)}$ stemming from the vertex contractions:

$$\begin{aligned}
\eta_p^{(2D)}(\vec{\sigma}) \equiv & \eta_p^{(2D)}(\sigma_1, \sigma_2, \dots, \sigma_8) \\
= & (-1)^{\delta(\sigma_1, \sigma_2), (+, -)} (-1)^{\delta(\sigma_2, \sigma_3), (-, -)} (-1)^{\delta(\sigma_3, \sigma_4), (+, +)} (-1)^{\delta(\sigma_4, \sigma_5), (-, -)} \times \\
& \times (-1)^{\delta(\sigma_5, \sigma_6), (-, +)} (-1)^{\delta(\sigma_6, \sigma_7), (+, +)} (-1)^{\delta(\sigma_7, \sigma_8), (-, -)} (-1)^{\delta(\sigma_8, \sigma_1), (+, +)} \quad (5.58)
\end{aligned}$$

$-\text{tr}(U_\square(x)) \rightarrow$

$$\begin{aligned}
& \sum_{\sigma_1, \dots, \sigma_8} \eta_p^{(2D)}(\vec{\sigma}) \left[\frac{1}{\sqrt{\mathcal{N}_2 + 1}} \mathcal{L}_{12}^{\sigma_7 \sigma_8} \frac{1}{\sqrt{\mathcal{N}_1 + 1}} \right]_x \times \\
& \times \left[\frac{1}{\sqrt{\mathcal{N}_3 + 1}} \frac{1}{\sqrt{\mathcal{N}_i + 1}} \frac{1}{\sqrt{\mathcal{N}_1 + 1}} \mathcal{L}_{23}^{\sigma_8 \sigma_1} \mathcal{L}_{oi}^{\sigma_1 \sigma_2} \mathcal{L}_{31}^{\sigma_2 \sigma_3} \frac{1}{\sqrt{\mathcal{N}_2 + 1}} \frac{1}{\sqrt{\mathcal{N}_o + 1}} \frac{1}{\sqrt{\mathcal{N}_3 + 1}} \right]_{x+e_2} \times \\
& \times \left[\frac{1}{\sqrt{\mathcal{N}_2 + 1}} \mathcal{L}_{12}^{\sigma_3 \sigma_4} \frac{1}{\sqrt{\mathcal{N}_1 + 1}} \right]_{x+e_1+e_2} \times \\
& \times \left[\frac{1}{\sqrt{\mathcal{N}_3 + 1}} \frac{1}{\sqrt{\mathcal{N}_o + 1}} \frac{1}{\sqrt{\mathcal{N}_1 + 1}} \mathcal{L}_{23}^{\sigma_4 \sigma_5} \mathcal{L}_{io}^{\sigma_5 \sigma_6} \mathcal{L}_{31}^{\sigma_6 \sigma_7} \frac{1}{\sqrt{\mathcal{N}_2 + 1}} \frac{1}{\sqrt{\mathcal{N}_i + 1}} \frac{1}{\sqrt{\mathcal{N}_3 + 1}} \right]_{x+e_1} \quad (5.59)
\end{aligned}$$

5.2.5 2D dynamics on an orthonormal basis

Following the development for one dimension, we have identified all SU(2)-invariant operators and used them to express the loop-string-hadron Hamiltonian. Now, we introduce a basis

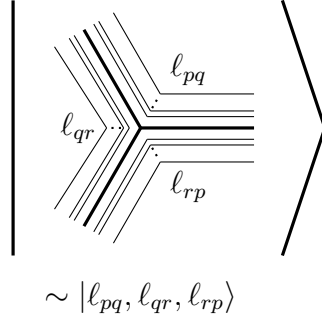


Figure 5.7: Depiction of $SU(2)$ -invariant configurations at a gluonic site. The on-site state is characterized by three loop quantum numbers l_{pq} , l_{qr} , and l_{rp} , with l_{ij} counting the flux lines flowing into i and out of j .

and factorize all loop-string-hadron operators for convenience in that basis. We then arrive at the Hamiltonian terms in their factorized form.

On-site gluonic Hilbert space

Here we summarize the local Hilbert space structure that has been studied in Ref. [88].

The local vacant state is again characterized as a normalized state $|0\rangle_{x_g}$ that is annihilated by any $\mathcal{L}_{ij}^{\sigma'\sigma}$ carrying at least one minus sign. Acting on $|0\rangle_{x_g}$, only the \mathcal{L}_{ij}^{++} are nonzero and will build up the local loop Hilbert space. A local loop state basis can be constructed following steps in analogy to the matter sites in Sec. 5.1.3. This local loop space is characterized by three independent linking numbers l_{ij} denoting the flux flowing along three (ij) directions $[(pq), (qr), \text{ and } (rp)]$. The orthonormal basis, depicted in is given by

$$|l_{pq}, l_{qr}, l_{rp}\rangle \equiv \frac{(\mathcal{L}_{pq}^{++})^{l_{pq}} (\mathcal{L}_{qr}^{++})^{l_{qr}} (\mathcal{L}_{rp}^{++})^{l_{rp}}}{\sqrt{l_{pq}! l_{qr}! l_{rp}! (l_{pq} + l_{qr} + l_{rp} + 1)!}} |0\rangle_{x_g} \quad (5.60)$$

The number operators analogous to (5.25) are

$$\mathcal{N}_{pq} \equiv \frac{1}{2}(\mathcal{N}_p + \mathcal{N}_q - \mathcal{N}_r) , \quad (5.61a)$$

$$\mathcal{N}_{qr} \equiv \frac{1}{2}(\mathcal{N}_q + \mathcal{N}_r - \mathcal{N}_p) , \quad (5.61b)$$

$$\mathcal{N}_{rp} \equiv \frac{1}{2}(\mathcal{N}_r + \mathcal{N}_p - \mathcal{N}_q) . \quad (5.61c)$$

It will also be convenient to introduce

$$\mathcal{N}_\Sigma \equiv \mathcal{N}_{pq} + \mathcal{N}_{qr} + \mathcal{N}_{rp} + 1 . \quad (5.62)$$

Operator factorization

Now we will factor operators at gluonic sites in such a way that their actions in the loop basis are transparent.

We have the following normalized ladder operators:

$$\hat{\Lambda}_{ij}^+ = \mathcal{L}_{ij}^{++} \frac{1}{\sqrt{(\mathcal{N}_{ij} + 1)(\mathcal{N}_\Sigma + 1)}} \quad (5.63a)$$

$$\hat{\Lambda}_{ij}^- = \frac{1}{\sqrt{(\mathcal{N}_{ij} + 1)(\mathcal{N}_\Sigma + 1)}} \mathcal{L}_{ij}^{--} \quad (5.63b)$$

The operator factorizations for gluonic sites are given in terms of these normalized shift operators in Table 5.6.

These simple local loop operators, contracted together along the links consistent with the AGL (1.133), reproduce the nonlocal loops and strings of the original theory. Moreover, these loop operators now act more like their U(1) counterparts; loop operators in U(1) theories shift E by unit increments along an infinite tower of states, but in U(1), the normalization factor is always trivial.

LOOP OPERATOR FACTORIZATIONS

$$\mathcal{L}_{ij}^{++} = \hat{\Lambda}_{ij}^+ \sqrt{(\mathcal{N}_{ij} + 1)(\mathcal{N}_\Sigma + 1)} \quad (5.64a)$$

$$\mathcal{L}_{ij}^{--} = \hat{\Lambda}_{ij}^- \sqrt{\mathcal{N}_{ij} \mathcal{N}_\Sigma} \quad (5.64b)$$

$$\mathcal{L}_{ij}^{+-} = -\hat{\Lambda}_{ki}^+ \hat{\Lambda}_{jk}^- \sqrt{(\mathcal{N}_{ki} + 1) \mathcal{N}_{jk}} \quad (5.64c)$$

$$\mathcal{L}_{ij}^{-+} = -\hat{\Lambda}_{ki}^- \hat{\Lambda}_{jk}^+ \sqrt{\mathcal{N}_{ki} (\mathcal{N}_{jk} + 1)} \quad (5.64d)$$

$$ijk = pqr, qrp, \text{ or } rpq$$

Table 5.6: Factorization of all SU(2) singlet operators at a gluonic site.

Global Hilbert space construction in two dimensions

As in one dimension, the 2D lattice vacant state is characterized as that state on which

$$\begin{aligned} \mathcal{N}_i(x) |0\rangle = \mathcal{N}_o(x) |0\rangle = \mathcal{N}_i(x) |0\rangle = 0 \quad \text{for all } x, \\ \mathcal{N}_{12}(x_g) |0\rangle = \mathcal{N}_{23}(x_g) |0\rangle = \mathcal{N}_{31}(x_g) |0\rangle = 0 \quad \text{for all } x_g. \end{aligned}$$

In two dimensions, we call a site x even (odd) if $x_1 + x_2$ is even (odd). The strong-coupling vacuum $|v\rangle$ is then defined analogously to one dimension:

$$\begin{aligned}
\mathcal{N}_l(x) |v\rangle &= 0 \\
(\mathcal{N}_i(x) + \mathcal{N}_o(x)) |v\rangle &= 0 \quad \text{for even } x \\
(\mathcal{N}_i(x) + \mathcal{N}_o(x)) |v\rangle &= 2|v\rangle \quad \text{for odd } x \\
\mathcal{S}_{\text{in}}^{\pm,-}(x) |v\rangle = \mathcal{S}_{\text{out}}^{-,\pm}(x) |v\rangle &= 0 \quad \text{for even } x \\
\mathcal{S}_{\text{in}}^{\pm,+}(x) |v\rangle = \mathcal{S}_{\text{out}}^{+,\pm}(x) |v\rangle &= 0 \quad \text{for odd } x \\
(\mathcal{N}_{12}(x_g) + \mathcal{N}_{23}(x_g) + \mathcal{N}_{31}(x_g)) |v\rangle &= 0 .
\end{aligned}$$

The 2D lattice Hilbert space structure is as follows:

1. The gluonic sites x', \bar{x}' have only loop states $|l_{12}, l_{23}, l_{31}\rangle_{x'/\bar{x}'}$, being treated identically as in pure gauge theory.
2. The matter sites x have loop and quark states $|n_l, n_i, n_o\rangle$, being structurally identical to sites with matter in one dimension. Physical quark degrees of freedom still require an ordering in order to treat lattice basis states as tensor products: We denote the physical quark modes associated with x by

$$\begin{aligned}
\chi_q^\dagger(x_1, x_2) \quad q = 0, 1 \\
0 \sim \text{in}, \quad 1 \sim \text{out}
\end{aligned}$$

and order fermions by the map

$$f(q, x_1, x_2) \rightarrow q + 2(x_1 + L_x x_2)$$

Generalizing the 1D convention, basis states are defined to have $\chi_q^\dagger(x)$'s being applied on $|0\rangle$ from greatest $f(q, x_1, x_2)$ to least.

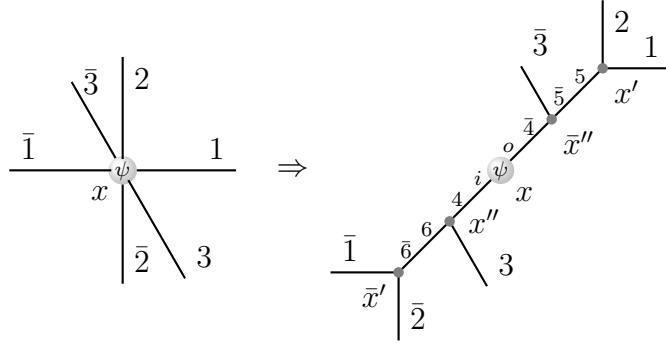


Figure 5.8: Virtual point splitting of a 3D lattice site into gluonic sites $x, x', \bar{x}, x'', \bar{x}''$ connected by internal links, with matter again at the central quark site x .

3. The Abelian Gauss laws along the three directions of the hexagonal lattice are

$$n_1(x') = n_{\bar{1}}(\overline{x + e_1}') , \quad (5.65a)$$

$$n_2(x') = n_{\bar{2}}(\overline{x + e_2}') , \quad (5.65b)$$

$$n_3(x') = n_l(x) + n_i(x)[1 - n_o(x)] \quad (5.65c)$$

$$n_{\bar{3}}(\bar{x}') = n_l(x) + n_o(x)[1 - n_i(x)] \quad (5.65d)$$

2D dynamics of loop-string-hadron states

Matrix elements of the Hamiltonian with respect to the global basis described above are straightforward to obtain by using the operator factorizations at gluonic sites (5.64) and at matter sites (5.35) in place of the LSH operators appearing in the various parts of the 2D Hamiltonian given in (5.54)–(5.59).

5.3 3D lattice with matter

The same scheme of point splitting used in two dimensions can be continued up to arbitrary spatial dimensionality d . As shown in Fig. 5.8, point splitting in three dimensions results in

four gluonic three-point vertices, while matter is accommodated by creating a fifth virtual site along one of the internal lines.

As in two dimensions, the local loop Hilbert space at gluonic vertices remains identical (three linking numbers) to the pure gauge theory. Matter is incorporated by dividing one virtual link (the $4 - \bar{4}$ in Fig. 5.8) into two; the Hilbert space at the virtual matter site has two string numbers and one loop number, again with the same structure used in one dimension. The modified Abelian Gauss laws on the three-dimensional (3D) lattice are

$$(\mathcal{N}_j(x_g) - \mathcal{N}_{\bar{j}}(x_g + e_j)) |\text{phys}\rangle = 0, \quad (j = 1, 2, 3) \quad (5.66a)$$

$$(\mathcal{N}_5(x') - \mathcal{N}_{\bar{5}}(\bar{x}'')) |\text{phys}\rangle = 0, \quad (5.66b)$$

$$(\mathcal{N}_6(x'') - \mathcal{N}_{\bar{6}}(\bar{x}')) |\text{phys}\rangle = 0, \quad (5.66c)$$

$$(\mathcal{N}_L(x) - \mathcal{N}_{\bar{4}}(\bar{x}'')) |\text{phys}\rangle = 0, \quad (5.66d)$$

$$(\mathcal{N}_R(x) - \mathcal{N}_4(x'')) |\text{phys}\rangle = 0. \quad (5.66e)$$

The Hamiltonian for three dimensions has no conceptually new objects—the terms present in two dimensions are just more numerous. The explicit decompositions in the LSH framework do, however, have more operator factors and there is less notational symmetry shared by all three spatial directions. Below, we provide a summary of the operators in the Hamiltonian of 3D SU(2) gauge theory with one staggered quark flavor.

For the interaction H_I , the hopping terms are given below, using sign factors $\eta_{h,j}^{(3D)}$ anal-

ogous to two dimensions:

$$\begin{aligned}\eta_{h,j}^{(3D)}(\vec{\sigma}) &\equiv \eta_{h,j}^{(3D)}(\sigma_1, \sigma_2, \dots, \sigma_5) & (j = 1, 2) \\ &= (-1)^{\delta(\sigma_1, \sigma_2), (+, +)} (-1)^{\delta(\sigma_2, \sigma_3), (-, -)} (-1)^{\delta(\sigma_3, \sigma_4), (+, +)} (-1)^{\delta(\sigma_4, \sigma_5), (-, -)}\end{aligned}\quad (5.67)$$

$$\begin{aligned}\eta_{h,3}^{(3D)}(\vec{\sigma}) &\equiv \eta_{h,3}^{(3D)}(\sigma_1, \sigma_2, \sigma_3) \\ &= (-1)^{\delta(\sigma_1, \sigma_2), (-, -)} (-1)^{\delta(\sigma_2, \sigma_3), (+, +)}\end{aligned}\quad (5.68)$$

$$\begin{aligned}\psi^\dagger(x)U(x, x + e_j)\psi(x + e_j) & & (j = 1, 2) \\ \rightarrow \sum_{\sigma_1, \dots, \sigma_5} \eta_{h,j}^{(3D)}(\sigma_1, \sigma_2, \sigma_3, \sigma_4, \sigma_5) \times \\ &\times \left[\frac{1}{\sqrt{\mathcal{N}_L + 1}} \frac{1}{\sqrt{\mathcal{N}_5 + 1}} \frac{1}{\sqrt{\mathcal{N}_j + 1}} \mathcal{S}_{\text{out}}^{+, \sigma_1} \mathcal{L}_{45}^{\sigma_1 \sigma_2} \mathcal{L}_{5j}^{\sigma_2 \sigma_3} \frac{1}{\sqrt{\mathcal{N}_4 + 1}} \frac{1}{\sqrt{\mathcal{N}_5 + 1}} \right]_x \times \\ &\times \left[\frac{1}{\sqrt{\mathcal{N}_6 + 1}} \frac{1}{\sqrt{\mathcal{N}_4 + 1}} \mathcal{L}_{j6}^{\sigma_3 \sigma_4} \mathcal{L}_{64}^{\sigma_4 \sigma_5} \mathcal{S}_{\text{in}}^{\sigma_5, -} \frac{1}{\sqrt{\mathcal{N}_j + 1}} \frac{1}{\sqrt{\mathcal{N}_6 + 1}} \frac{1}{\sqrt{\mathcal{N}_R + 1}} \right]_{x+e_j}\end{aligned}\quad (5.69)$$

$$\begin{aligned}\psi^\dagger(x)U(x, x + e_3)\psi(x + e_3) \\ \rightarrow \sum_{\sigma_1, \sigma_2, \sigma_3} \eta_{h,3}^{(3D)}(\sigma_1, \sigma_2, \sigma_3) \left[\frac{1}{\sqrt{\mathcal{N}_R + 1}} \frac{1}{\sqrt{\mathcal{N}_3 + 1}} \mathcal{S}_{\text{in}}^{\sigma_1, +} \mathcal{L}_{43}^{\sigma_1 \sigma_2} \frac{1}{\sqrt{\mathcal{N}_4 + 1}} \right]_x \times \\ \times \left[\frac{1}{\sqrt{\mathcal{N}_4 + 1}} \mathcal{L}_{34}^{\sigma_4 \sigma_5} \mathcal{S}_{\text{out}}^{-, \sigma_5} \frac{1}{\sqrt{\mathcal{N}_3 + 1}} \frac{1}{\sqrt{\mathcal{N}_L + 1}} \right]_{x+e_3}\end{aligned}\quad (5.70)$$

Turning to the magnetic energy \hat{H}_B , each plaquette trace is a contraction of LSH operators, with their three orientations being displayed in Figs. 5.9–5.11. As in two dimensions, there are sign factors to keep track of from the vertex contractions. All three plaquette operators can be expressed using a single sign function $\eta_p^{(3D)}(\vec{\sigma})$, as given in (5.71), and the

formulas for the \hat{H}_B contributions are given in (5.72) and (5.73):

$$\begin{aligned}
 \eta_p^{(3D)}(\vec{\sigma}) \equiv \eta_p^{(3D)}(\sigma_1, \sigma_2, \dots, \sigma_{12}) &= (-1)^{\delta(\sigma_1, \sigma_2), (-, +)} (-1)^{\delta(\sigma_2, \sigma_3), (+, +)} \\
 &\times (-1)^{\delta(\sigma_3, \sigma_4), (-, -)} (-1)^{\delta(\sigma_4, \sigma_5), (+, +)} \\
 &\times (-1)^{\delta(\sigma_5, \sigma_6), (-, -)} (-1)^{\delta(\sigma_6, \sigma_7), (+, +)} \\
 &\times (-1)^{\delta(\sigma_7, \sigma_8), (+, -)} (-1)^{\delta(\sigma_8, \sigma_9), (-, -)} \\
 &\times (-1)^{\delta(\sigma_9, \sigma_{10}), (+, +)} (-1)^{\delta(\sigma_{10}, \sigma_{11}), (-, -)} \\
 &\times (-1)^{\delta(\sigma_{11}, \sigma_{12}), (+, +)} (-1)^{\delta(\sigma_{12}, \sigma_1), (-, -)} \tag{5.71}
 \end{aligned}$$

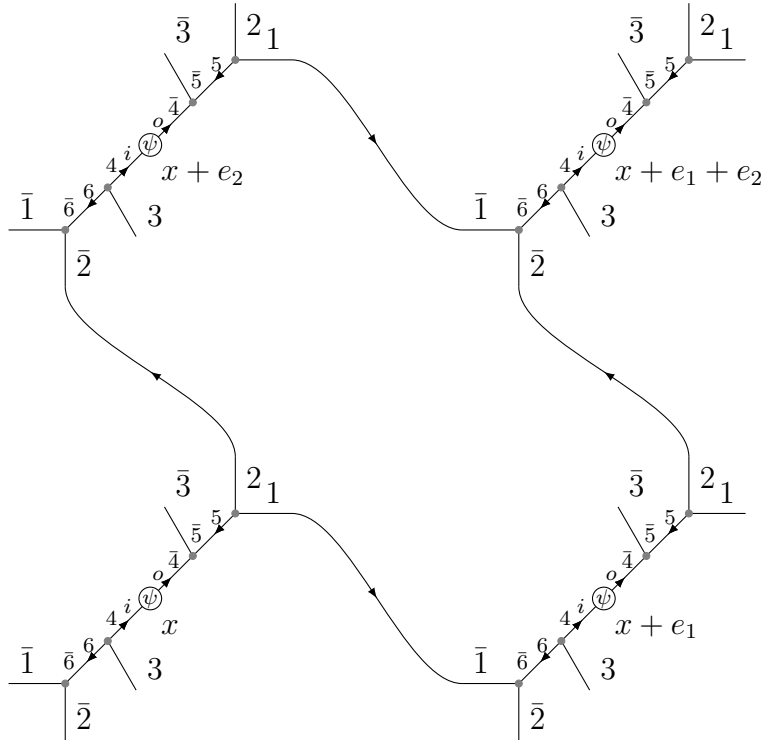


Figure 5.9: Connectivity of a xy -plaquette in three dimensions.

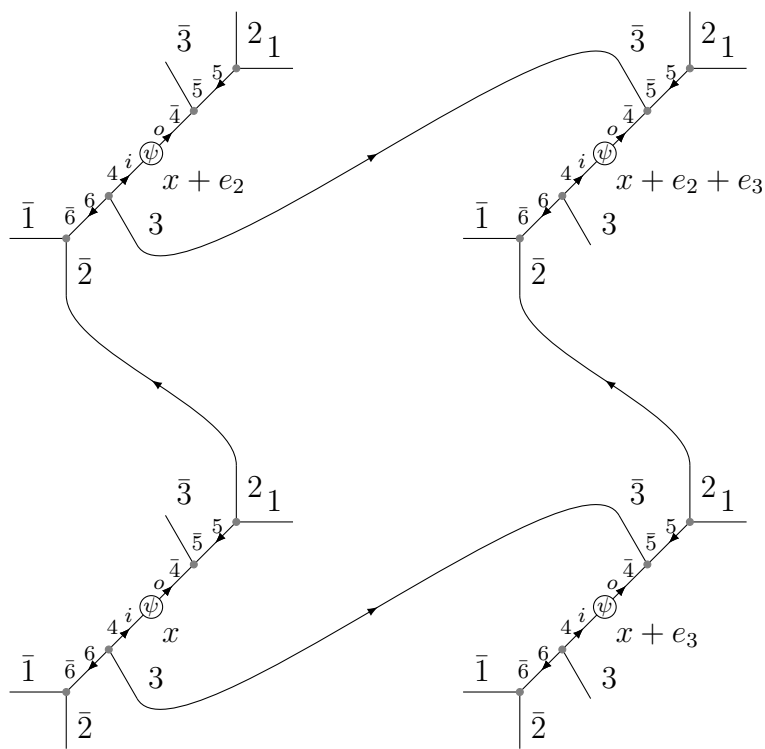


Figure 5.10: Connectivity of a yz -plaquette in three dimensions.

$$\begin{aligned}
-\text{tr} \left(U_{\square}^{(12)}(x) \right) &\rightarrow \sum_{\sigma_1, \dots, \sigma_{12}} \eta_p^{(3D)}(\vec{\sigma}) \left[\frac{1}{\sqrt{\mathcal{N}_2 + 1}} \frac{\mathcal{L}_{12}^{\sigma_{10}\sigma_{11}}}{\sqrt{\mathcal{N}_1 + 1}} \frac{1}{\sqrt{\mathcal{N}_1 + 1}} \right]_x \times \\
&\times \left[\frac{1}{\sqrt{\mathcal{N}_6 + 1}} \frac{1}{\sqrt{\mathcal{N}_4 + 1}} \frac{1}{\sqrt{\mathcal{N}_o + 1}} \frac{1}{\sqrt{\mathcal{N}_5 + 1}} \frac{1}{\sqrt{\mathcal{N}_1 + 1}} \frac{1}{\sqrt{\mathcal{N}_1 + 1}} \frac{\mathcal{L}_{26}^{\sigma_{11}\sigma_{12}}}{\mathcal{L}_{64}^{\sigma_{12}\sigma_1}} \frac{\mathcal{L}_{45}^{\sigma_2\sigma_3}}{\mathcal{L}_{51}^{\sigma_3\sigma_4}} \right]_{x+e_2} \times \\
&\times \left[\frac{1}{\sqrt{\mathcal{N}_2 + 1}} \frac{\mathcal{L}_{12}^{\sigma_4\sigma_5}}{\sqrt{\mathcal{N}_1 + 1}} \right]_{x+e_1+e_2} \times \\
&\times \left[\frac{1}{\sqrt{\mathcal{N}_5 + 1}} \frac{1}{\sqrt{\mathcal{N}_4 + 1}} \frac{1}{\sqrt{\mathcal{N}_i + 1}} \frac{1}{\sqrt{\mathcal{N}_6 + 1}} \frac{1}{\sqrt{\mathcal{N}_1 + 1}} \frac{\mathcal{L}_{25}^{\sigma_5\sigma_6}}{\mathcal{L}_{54}^{\sigma_6\sigma_7}} \frac{\mathcal{L}_{46}^{\sigma_7\sigma_8}}{\mathcal{L}_{61}^{\sigma_8\sigma_9}} \frac{\mathcal{L}_{61}^{\sigma_9\sigma_{10}}}{\mathcal{L}_{46}^{\sigma_{10}\sigma_1}} \right]_{x+e_1} \\
&\frac{1}{\sqrt{\mathcal{N}_2 + 1}} \frac{1}{\sqrt{\mathcal{N}_5 + 1}} \frac{1}{\sqrt{\mathcal{N}_o + 1}} \frac{1}{\sqrt{\mathcal{N}_4 + 1}} \frac{1}{\sqrt{\mathcal{N}_6 + 1}} \frac{1}{\sqrt{\mathcal{N}_6 + 1}} \Big]_{x+e_1} \\
&\quad (5.72) \\
-\text{tr} \left(U_{\square}^{(j3)}(x) \right) &\rightarrow \sum_{\sigma_1, \dots, \sigma_{12}} \eta_p^{(3D)}(\vec{\sigma}) \left[\frac{1}{\sqrt{\mathcal{N}_6 + 1}} \frac{1}{\sqrt{\mathcal{N}_3 + 1}} \frac{\mathcal{L}_{j6}^{\sigma_4\sigma_5}}{\mathcal{L}_{63}^{\sigma_5\sigma_6}} \frac{1}{\sqrt{\mathcal{N}_j + 1}} \frac{1}{\sqrt{\mathcal{N}_6 + 1}} \right]_{x+e_j} \times \\
&\times \left[\frac{1}{\sqrt{\mathcal{N}_4 + 1}} \frac{1}{\sqrt{\mathcal{N}_i + 1}} \frac{1}{\sqrt{\mathcal{N}_6 + 1}} \frac{1}{\sqrt{\mathcal{N}_j + 1}} \frac{\mathcal{L}_{34}^{\sigma_6\sigma_7}}{\mathcal{L}_{46}^{\sigma_7\sigma_8}} \frac{\mathcal{L}_{46}^{\sigma_8\sigma_9}}{\mathcal{L}_{6j}^{\sigma_9\sigma_{10}}} \frac{1}{\sqrt{\mathcal{N}_3 + 1}} \frac{1}{\sqrt{\mathcal{N}_o + 1}} \frac{1}{\sqrt{\mathcal{N}_4 + 1}} \frac{1}{\sqrt{\mathcal{N}_6 + 1}} \right]_{x+e_j+e_3} \times \\
&\times \left[\frac{1}{\sqrt{\mathcal{N}_5 + 1}} \frac{\mathcal{L}_{j5}^{\sigma_{10}\sigma_{11}}}{\mathcal{L}_{53}^{\sigma_{11}\sigma_{12}}} \frac{1}{\sqrt{\mathcal{N}_j + 1}} \frac{1}{\sqrt{\mathcal{N}_5 + 1}} \right]_{x+e_3} \times \\
&\times \left[\frac{1}{\sqrt{\mathcal{N}_4 + 1}} \frac{1}{\sqrt{\mathcal{N}_o + 1}} \frac{1}{\sqrt{\mathcal{N}_5 + 1}} \frac{1}{\sqrt{\mathcal{N}_j + 1}} \frac{\mathcal{L}_{34}^{\sigma_{12}\sigma_1}}{\mathcal{L}_{45}^{\sigma_2\sigma_3}} \frac{\mathcal{L}_{57}^{\sigma_3\sigma_4}}{\sqrt{\mathcal{N}_3 + 1}} \frac{1}{\sqrt{\mathcal{N}_i + 1}} \frac{1}{\sqrt{\mathcal{N}_4 + 1}} \frac{1}{\sqrt{\mathcal{N}_5 + 1}} \right]_x \\
&\quad (5.73)
\end{aligned}$$

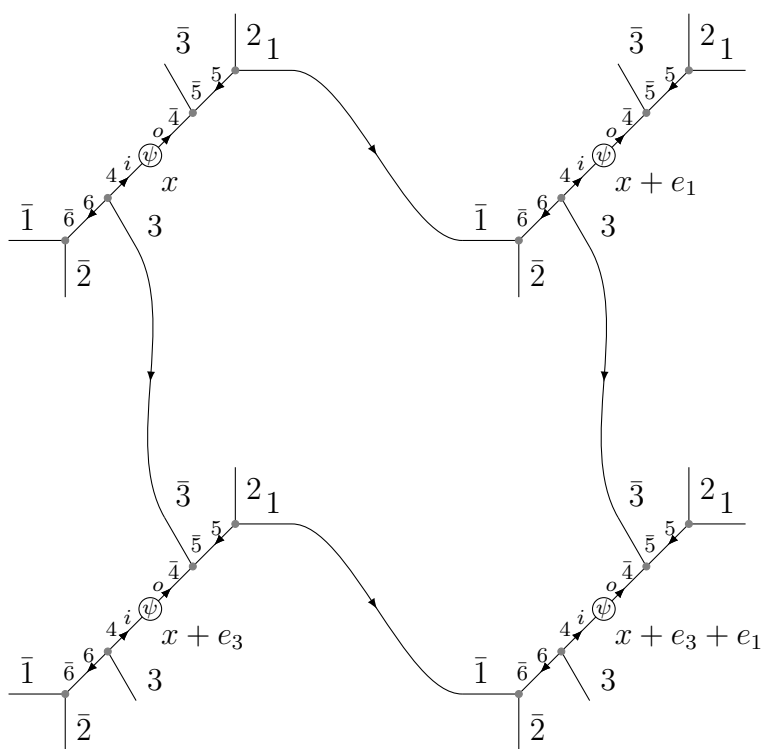


Figure 5.11: Connectivity of a zx -plaquette in three dimensions.

5.4 Comparison of loop-string-hadron and Kogut-Susskind

From the perspective of quantum computation and simulation, the LSH framework exhibits the following benefits:

- *Abelian constraints.*—The AGLs are the only remnant constraints in the LSH framework. A LSH basis naturally diagonalizes these constraints. Any basis state in the AGL-satisfying subspace is physically observable.
- *Simple quantum numbers.*—The LSH Hilbert space is naturally characterized by integers. Quark quantum numbers are bounded by the Pauli principle, while loop quantum numbers (n_l or ℓ_{ij}) can be any non-negative integer. Additionally, all elementary operators are 1-sparse in the LSH basis.
- *No Clebsch-Gordon coefficients.*—Like the prepotential formulation, the LSH treatment avoids the need for Clebsch-Gordon coefficients. What makes the theory describe SU(2) is the available set of operators and their algebra. Establishing the same for SU(3) is the subject of ongoing work.
- *Gauge redundancy in preliminary simulations.*—In $d = 1$, the LSH formulation gives a clear advantage over Kogut-Susskind in terms of qubit requirements—simulating the gauge degrees of freedom takes half the number of qubits. The qubit requirements are also less for pure gauge theory in $d = 2$. By bringing down the qubit costs in these cases, one can learn how to deal with the implementation of LSH structures sooner.

At the same time, there are some caveats:

- *Proliferation of Hamiltonian terms.*—Introducing virtual links causes the hopping and plaquette terms to grow in size and number. In $d = 3$, the number of terms is formidable. This would pose a problem for quantum simulation methods such as Trotter-Suzuki decompositions [184, 185].

- *Qubit costs without solving the Abelian Gauss law.*—During the onset of scientific quantum computing, each and every qubit is important to count. This framework would have direct benefit on qubit costs for the 1+1-dimensional theory and the 2+1-dimensional pure gauge theory, and those are important to study on their own. Beyond pure gauge theory in two dimensions, qubit requirements of directly simulating the multidimensional LSH formulation outpace those of simulating the Kogut-Susskind formulation. However, it is possible to push the LSH framework further by actually solving the Abelian Gauss law. If this is done, then simulating the gluons will cost fewer qubits in any number of dimensions.

These drawbacks are resource oriented, rather than theoretical. Given that the LSH framework is just being introduced, we can hope that novel algorithmic solutions will alleviate the practical issues.

5.5 Conclusion

In this chapter we have provided a complete Hamiltonian for $SU(2)$ gauge theory coupled to staggered fermions in $1 + 1$, $2 + 1$, and $3 + 1$ dimensions. Dynamics is described in terms of physical and local observables: hadrons and segments of flux loops and meson strings. By using a staggered fermion prescription, the matter field carried only a color (no spinor) index, allowing the LSH dynamics to be formulated without unnecessary complications. Studying adaptations of the LSH framework to other fermion discretizations or to more flavors will be of future interest.

We also point out that, while the focus of this chapter was limited to $SU(2)$ for concreteness, the geometric approach makes no explicit use of the $SU(2)$ angular momentum characterization of states or of $SU(2)$ Clebsch-Gordon coefficients. The prepotential formulation from which this LSH formulation was derived has already been generalized to $SU(3)$ [59] and even $SU(N)$ [51,180]. Generalization to $SU(3)$ preserves the local loop Hilbert space construction, this time with two Abelian Gauss laws for every link and each of the AGLs of the

same form as in $SU(2)$. However, finding a suitable point splitting scheme to describe the dynamics using only physical degrees of freedom is not done yet and is of significant interest to work out in the future.

We have illustrated in this chapter how the present scheme translates the dynamics of all possible irreps of the gauge group into the dynamics of many local towers of states characterized by single integers. This is a major gain of this formalism over the Kogut-Susskind one. The LSH framework makes non-Abelian gauge theory dynamics more similar to that of Schwinger model by completely solving the non-Abelian Gauss law constraint. This particular formalism, which is structurally closer to $U(1)$ gauge theories, stands to directly benefit from algorithms developed for Abelian theories.

The major price paid is the introduction of more lattice links and a new AGL on each virtual link. It turns out, however, that half or more of the bosonic degrees of freedom can be removed by solving the Abelian Gauss law. Solving the Abelian Gauss law would render the qubit cost of LSH simulation less than that of the Kogut-Susskind formulation in any dimension and will be the subject of future work. Nonetheless, even before solving the AGL, the truncated LSH framework costs fewer qubits than the truncated Kogut-Susskind formulation would for theories that will be important milestones along the way to three-dimensional simulations.

Combining all the above benefits, the LSH framework may take us one step closer to quantum-simulating theories that model fundamental interactions of Nature.

Chapter acknowledgments

IR thanks Z. Davoudi for many useful discussions and comments during the preparation of this work. JRS thanks D. B. Kaplan and S. Caspar for helpful discussions, and Z. Davoudi and the Maryland Center for Fundamental Physics (MCFP) at the University of Maryland at College Park for hosting him while part of this research was carried out. IR was supported by the U.S. Department of Energy (DOE), Office of Science, Office of Advanced Scientific Computing Research (ASCR) Quantum Computing Application Teams program,

under fieldwork proposal number ERKJ347, and by the MCFP. JRS was supported by DOE Grant No. DE-FG02-00ER41132 and by the National Science Foundation Graduate Research Fellowship under Grant No. 1256082. Part of this research was carried out with support from a Thomas L. and Margo G. Wyckoff Endowed Faculty Fellowship.

Chapter 6

**SOLVING GAUSS'S LAW ON DIGITAL QUANTUM
COMPUTERS
WITH LOOP-STRING-HADRON DIGITIZATION**

From the viewpoint of digital quantum simulation, the loop-string-hadron formulation of lattice gauge theory introduced in chapter 5 offers potential advantages as a digitization scheme. The Hilbert space is characterized in terms of discrete flux and quark excitations, which is to say the states are naturally parametrized in terms of binary fermionic occupation numbers and unbounded bosonic occupation numbers. In addition, the elementary excitations are intrinsically $SU(2)$ -invariant; non-Abelian gauge redundancy is therefore completely eradicated. The problem of unphysical sectors does still persist in the form of Abelian Gauss law constraints requiring flux conservation along links, but the LSH constraints are all simultaneously diagonalized, so basis states are each definitely allowed or definitely unallowed. The Hamiltonian then mixes states among each other via raising and lowering operations on all the occupation numbers.

In this chapter,¹ we first apply the loop-string-hadron formulation to digital quantum simulations of non-Abelian gauge theories. In section 6.1 we review the elements of the LSH framework for $SU(2)$ gauge fields coupled to one staggered fermion flavor in $d = (1, 2, 3)$ spatial dimensions and give a digitization scheme for this basis. In section 6.1, we give a digitization scheme for the LSH framework of $SU(2)$ gauge fields coupled to one staggered fermion flavor in $d = (1, 2, 3)$ spatial dimensions. Then, in section 6.2, we take advantage of the digitized LSH basis to present the first decompositions of $SU(2)$ physicality oracles, i.e., quantum algorithms that probe charge conservation of an $SU(2)$ lattice gauge theory

¹This chapter is drawn from *Physical Review Research* 2, 033039 (2020), done in collaboration with I. Raychowdhury.

wave function. Finally, in section 6.3 we discuss the resources involved with implementation on digital hardware and the known advantages and disadvantages compared to group representation bases.

6.1 LSH digitization

For the purposes of this chapter, we are primarily interested in the LSH Hilbert space structure derived from one quark flavor interacting with SU(2) gauge bosons. The full suite of LSH operators available depends on the topology of the lattice. As in chapter 5, we consider Cartesian lattices in d spatial dimensions, equipped with the appropriate scheme of point splitting.

Regardless of the spational dimensionality, the virtual topology is such that there are only two possible elementary structures—the quark sites and gluonic sites introduced in chapter 5. The two types of site are associated with their own local Hilbert space structures (cf. section 5.1 and section 5.2).

The ingredient of the Hilbert space most important to this chapter is the Abelian Gauss law constraints. The Abelian Gauss law is the same physical requirement across all links of the lattice, in any dimension: the total flux magnitudes at each end of a link must be equal.

A given link end within the point-split lattice attaches to either a quark site or a gluonic site. If that link end attaches to a quark site, the relevant flux number operator is denoted by \mathcal{N}_L (\mathcal{N}_R) if the link end is “outgoing” (“incoming”) relative to the site. In particular,

$$\mathcal{N}_L |n_l, n_i, n_o\rangle = [n_l + n_o(1 - n_i)] |n_l, n_i, n_o\rangle \ , \quad (6.1a)$$

$$\mathcal{N}_R |n_l, n_i, n_o\rangle = [n_l + n_i(1 - n_o)] |n_l, n_i, n_o\rangle \ . \quad (6.1b)$$

If instead the link end attaches to a gluonic site, say, along direction $i(= p, q, r)$ relative to

the site, the relevant flux number operator is denoted by \mathcal{N}_i . In this case,

$$\mathcal{N}_p |\ell_{pq}, \ell_{qr}, \ell_{rp}\rangle = (\ell_{rp} + \ell_{pq}) |\ell_{pq}, \ell_{qr}, \ell_{rp}\rangle , \quad (6.2a)$$

$$\mathcal{N}_q |\ell_{pq}, \ell_{qr}, \ell_{rp}\rangle = (\ell_{pq} + \ell_{qr}) |\ell_{pq}, \ell_{qr}, \ell_{rp}\rangle , \quad (6.2b)$$

$$\mathcal{N}_r |\ell_{pq}, \ell_{qr}, \ell_{rp}\rangle = (\ell_{qr} + \ell_{rp}) |\ell_{pq}, \ell_{qr}, \ell_{rp}\rangle . \quad (6.2c)$$

Using these, the Abelian Gauss law is the requirement that, for any link of the lattice, the number operators at each end agree. For brevity, we refer to links joining two gluonic sites as ‘ gg ’ links, a quark site and a gluon site as ‘ qg ’ links, and two quark sites (for $d = 1$) as ‘ qq ’ links.

In one spatial dimension every link joins two quark sites, and the Abelian Gauss laws read

$$[\mathcal{N}_L(x) - \mathcal{N}_R(x+1)] |\text{phys}\rangle = 0 , \quad (6.3)$$

for every site x . Meanwhile, the 2D Abelian Gauss laws along the three directions of the hexagonal lattice are

$$[\mathcal{N}_j(x') - \mathcal{N}_{\bar{j}}(\overline{x + e_j'})] |\text{phys}\rangle = 0 \quad (j = 1, 2) , \quad (6.4a)$$

$$[\mathcal{N}_3(x') - \mathcal{N}_R(x)] |\text{phys}\rangle = 0 , \quad (6.4b)$$

$$[\mathcal{N}_{\bar{3}}(\bar{x}') - \mathcal{N}_L(x)] |\text{phys}\rangle = 0 . \quad (6.4c)$$

And in 3D space, using the labeling from Figure 5.8, the Abelian Gauss laws read

$$[\mathcal{N}_j(x') - \mathcal{N}_{\bar{j}}(\overline{x + e_j'})] |\text{phys}\rangle = 0 \quad (j = 1, 2) , \quad (6.5a)$$

$$[\mathcal{N}_3(x'') - \mathcal{N}_{\bar{3}}(\overline{x + e_3''})] |\text{phys}\rangle = 0 , \quad (6.5b)$$

$$[\mathcal{N}_5(x') - \mathcal{N}_{\bar{5}}(\bar{x}'')] |\text{phys}\rangle = 0 , \quad (6.5c)$$

$$[\mathcal{N}_6(x'') - \mathcal{N}_{\bar{6}}(\bar{x}')] |\text{phys}\rangle = 0 , \quad (6.5d)$$

$$[\mathcal{N}_4(x'') - \mathcal{N}_i(x)(1 - \mathcal{N}_o(x))] |\text{phys}\rangle = 0 , \quad (6.5e)$$

$$[\mathcal{N}_{\bar{4}}(\bar{x}'') - \mathcal{N}_o(x)(1 - \mathcal{N}_i(x))] |\text{phys}\rangle = 0 . \quad (6.5f)$$

The Abelian constraints above stand in contrast to the ordinary situation in Hamiltonian lattice gauge theory. The chosen degrees of freedom do not automate flux conservation along links, which is why the constraint is Abelian flux conservation. Ordinarily flux conservation along links is automatic, and color charge conservation must be imposed at vertices.

Naïvely, checking non-Abelian gauge invariance would pose a significant practical challenge on a quantum computer. SU(2) Gauss law operators take the form

$$\hat{\mathcal{G}}_\alpha(x) = \sum_{i=1}^d \left[\hat{L}_{\alpha,i}(x) + \hat{R}_{\alpha,i}(x) \right] + \hat{\rho}_\alpha(x) ,$$

$$\hat{\rho}_\alpha(x) = \hat{\psi}^\dagger(x) \frac{\sigma_\alpha}{2} \hat{\psi}(x) ,$$

where $\alpha = (1, 2, 3)$ for SU(2) and ψ is a two-component staggered fermion field for this example. To confirm $\hat{\mathcal{G}}_\alpha(x)\hat{\mathcal{G}}_\alpha(x) = 0$, it would be sufficient to confirm two of the three color components annihilate a given wavefunction. The most conventional basis choice would be one that diagonalizes the 3-components [i.e., all the $\hat{L}_3(x)$, $\hat{R}_3(x)$, and $\hat{\rho}_3(x)$] and the Casimirs [\hat{L}_i^2 and \hat{R}_i^2 for each i individually]. One could then directly evaluate $\mathcal{G}_3(x)$ using diagonal operations, in direct analogy to what was done for U(1) theories in chapter 2. To check another component, say $\mathcal{G}_1(x)$, one could simulate an internal color rotation about the 2-axis on every electric link register $|j, m\rangle$ and on the fermion doublet—requiring $2d+1$ basis transformations. Such rotations would have to isolate every j sector and mix them in just the right way. At that point, $\mathcal{G}_1(x)$ could be checked like $\mathcal{G}_3(x)$ was, and the bases could be rotated back.

Better protocols than the above could exist, but digital quantum algorithms have yet to be furnished to validate states subjected to non-Abelian constraints. This technical endeavor would likely suffer from sensitivity to the chosen digitization. We instead pursue the problem in the LSH basis with Abelian constraints.

A convenient feature of the Abelian Gauss law constraints, from the viewpoint of quantum simulation, is that they all commute. The LSH framework simultaneously diagonalizes these constraints so that basis states are definitely allowed or definitely unallowed. In contrast, in

the conventional Kogut-Susskind framework, the only basis state that is gauge invariant is that with vanishing electric fields.

By the same token, since the LSH basis simultaneously diagonalizes all the constraints, projective measurements in this basis do not spoil gauge invariance. With basis states mapped to the computational basis of a quantum computer, (noiseless) readout of the qubit registers will therefore conserve charge. This could also have benefits for preparing entangled states that satisfy gauge constraints.

To represent the theory on a quantum computer we first truncate the Hilbert space on irreducible representations of the gauge group. The representations are labeled by angular momenta j , related to the flux number operators by $j = \mathcal{N}/2$. To simulate all states with SU(2) representations up to and including spin \bar{j} , it is sufficient to use the following qubit resources:

1. $N + 1$ qubits per quark site loop number n_ℓ ,
2. N qubits per gluonic site loop number ℓ_{ij} ,

where

$$N = \lceil \log_2(\bar{j} + 1) \rceil . \quad (6.6)$$

The quark occupancy numbers require no truncation.

The loop quantum numbers can then be represented by a computational basis of binary integers. For example, with the loop numbers expressed in binary form by

$$n_\ell = \sum_{m=0}^N 2^m n_{\ell,m} \quad (n_{\ell,m} = 0, 1) , \quad (6.7)$$

$$\ell_{ij} = \sum_{m=0}^{N-1} 2^m \ell_{ij,m} \quad (\ell_{ij,m} = 0, 1) , \quad (6.8)$$

their associated kets are

$$|n_\ell\rangle = \bigotimes_{m=0}^N |n_{\ell,m}\rangle , \quad (6.9)$$

$$|\ell_{ij}\rangle = \bigotimes_{m=0}^{N-1} |\ell_{ij,m}\rangle . \quad (6.10)$$

Here and below the quantum computing-related conventions follow Ref. [35].

Note how straightforward it is to truncate the above mapping – we simply choose a maximum flux saturation strength and require links to have matching flux on either side. Were we to keep the color-projection quantum numbers (J_i^3), a choice would have to be made regarding how to represent the $\sum_{n=1}^{2\bar{j}+1} n^2$ states on a qubit register and how to exclude some “extra” states in the register from dynamics. That is all in addition to having to satisfy the non-Abelian constraints within the mapped representations.

The lattice Hilbert space can be regarded as a tensor product space of all the site-local Hilbert spaces (provided a simulation accounts for the fermionic nature of the quark numbers). In practice a volume truncation and choice of boundary conditions are implicit, but we are concerned with only the local structure in the bulk.

6.2 Implementing gauge invariance

Having access to “Gauss law oracles” within a simulation opens the door to designing error detection and mitigation protocols that help to preserve gauge invariance. Such oracles seems especially crucial to making noisy simulations robust against unphysical errors. Thanks to the diagonalization of the gauge constraints, the space of allowed states is akin to a computational “code space,” and validating wavefunctions is likened to measurement of the appropriate “stabilizers”; Gauss’s law itself defines a code space within a larger Hilbert space that is stabilized by any charge-conserving Hamiltonian. The associated parity can be thought of as +1 for the Abelian-Gauss-law-satisfying subspace and –1 for the rest of the states. Detection of a large class of bit-flip errors can therefore be achieved without any additional encoding of the qubits.

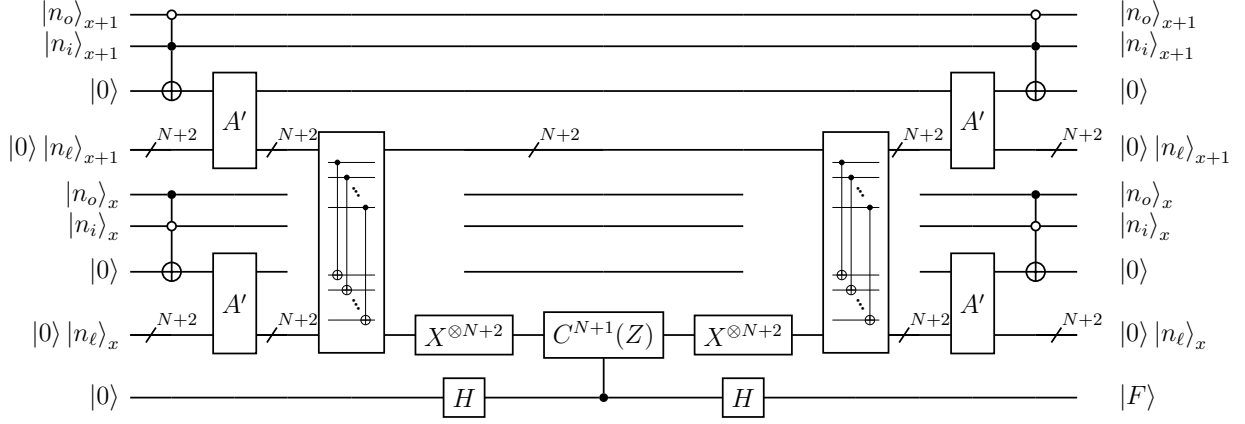


Figure 6.1: A routine for checking the Abelian Gauss law along a link joining two quark sites. The registers here are specific to a 1D link, with the constraint $[n_\ell + n_o(1 - n_i)]_x = [n_\ell + n_i(1 - n_o)]_{x+1}$.

In terms of quantum numbers in the LSH basis, the constraints on states take the following forms:

- For $d = 1$

$$[n_\ell + n_o(1 - n_i)]_x = [n_\ell + n_i(1 - n_o)]_{x+1} . \quad (6.11)$$

- For $d = 2$

$$n_j(x') = n_{\bar{j}}(\overline{x + e_j'}) \quad (j = 1, 2), \quad (6.12a)$$

$$n_3(x') = n_l(x) + n_i(x)[1 - n_o(x)], \quad (6.12b)$$

$$n_{\bar{3}}(\bar{x}') = n_l(x) + n_o(x)[1 - n_i(x)], \quad (6.12c)$$

where $n_1 = l_{31} + l_{12}$, $n_2 = l_{12} + l_{23}$, and $n_3 = l_{23} + l_{31}$ are the eigenvalues from (6.2).

- For $d = 3$

$$n_i(x') = n_{\bar{j}}(\overline{x + e_j'}) \quad (j = 1, 2), \quad (6.13a)$$

$$n_3(x'') = n_{\bar{3}}(\overline{x + e_3''}) , \quad (6.13b)$$

$$n_5(x') = n_{\bar{5}}(\overline{x'}) , \quad (6.13c)$$

$$n_6(x'') = n_{\bar{6}}(\overline{x''}) , \quad (6.13d)$$

$$n_4(x'') = n_i(x)[1 - n_o(x)] , \quad (6.13e)$$

$$n_{\bar{4}}(\overline{x''}) = n_o(x)[1 - n_i(x)] . \quad (6.13f)$$

In Fig. 6.1 we give a quantum circuit for checking the Abelian Gauss law along a ($d = 1$) qq link. The non-standard circuit notations used are the bit-adder gates A' , which add one bit to an M -bit integer via

$$|y\rangle |0\rangle^{\otimes M} |c_0\rangle \rightarrow |y + c_0\rangle |c_{M-1}c_{M-2} \dots c_1\rangle |c_0\rangle$$

(see Fig. 6.2), and the string of controlled NOTs (CNOTs), used to compute the *bitwise sum* of two integers, i.e.,

$$\begin{aligned} & |x_{r-1}\rangle |x_{r-2}\rangle \dots |x_0\rangle \otimes |y_{r-1}\rangle |y_{r-2}\rangle \dots |y_0\rangle \\ \rightarrow & |x_{r-1}\rangle |x_{r-2}\rangle \dots |x_0\rangle \otimes \\ & \otimes |y_{r-1} \oplus x_{r-1}\rangle |y_{r-2} \oplus x_{r-2}\rangle \dots |y_0 \oplus x_0\rangle . \end{aligned}$$

The constraint (6.11) is equivalent to saying that the $(N + 2)$ -bit integers $n_L(x) = [n_\ell + n_o(1 - n_i)]_x$ and $n_R(x + 1) = [n_\ell + n_i(1 - n_o)]_{x+1}$ are identical bit by bit. So the constraint is checked by (i) computing the sums $n_L(x)$ and $n_R(x + 1)$, (ii) computing the bit-wise sum of $n_L(x)$ and $n_R(x + 1)$, and (iii) flagging the query qubit if and only if that bit-wise sum is all zeros. The subsequent gates just uncompute the nonquery registers back to their original configurations. The query output $F = 1$ ($F = 0$) if the link does (does not) satisfy the Abelian Gauss law.

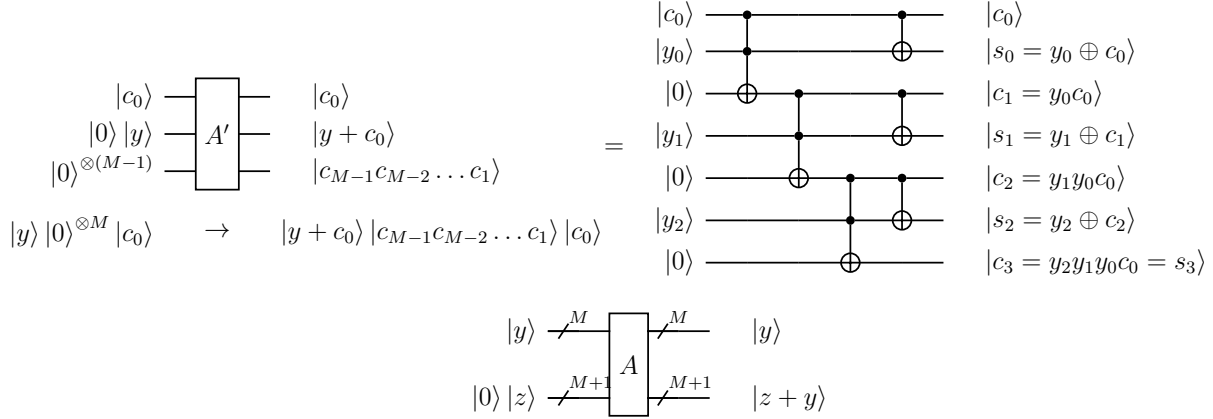


Figure 6.2: Top: A reduced adder A' for adding one bit to an M -bit integer (shown for $M = 3$). Here c_0 is added to the M -bit integer y , with the $(M + 1)$ -bit result $s = y + c_0$. This uses M ancillae, M Toffoli gates, and M CNOTs. Bottom: A generic adder circuit A for in-place addition of two M -bit integers, $(y, z) \rightarrow (y, z + y)$. One ancilla is introduced to express the $(M + 1)$ -bit output.

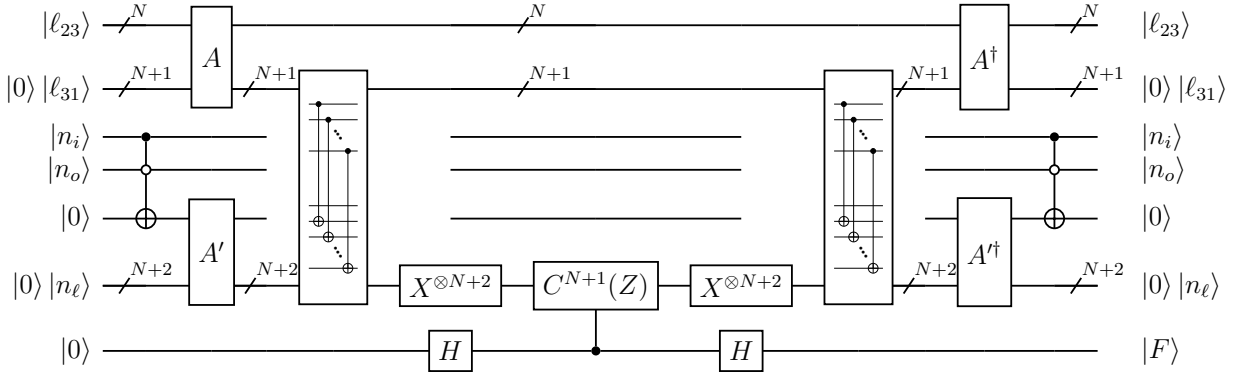


Figure 6.3: A routine for checking the Abelian Gauss law along a link joining a quark site and a gluonic site. The registers here are specific to a 3- i (virtual) link in two dimensions, with the constraint $\ell_{23} + \ell_{31} = n_\ell + n_i(1 - n_o)$. The adders A and string of CNOTs are detailed in Fig. 6.2 and in the text, respectively.

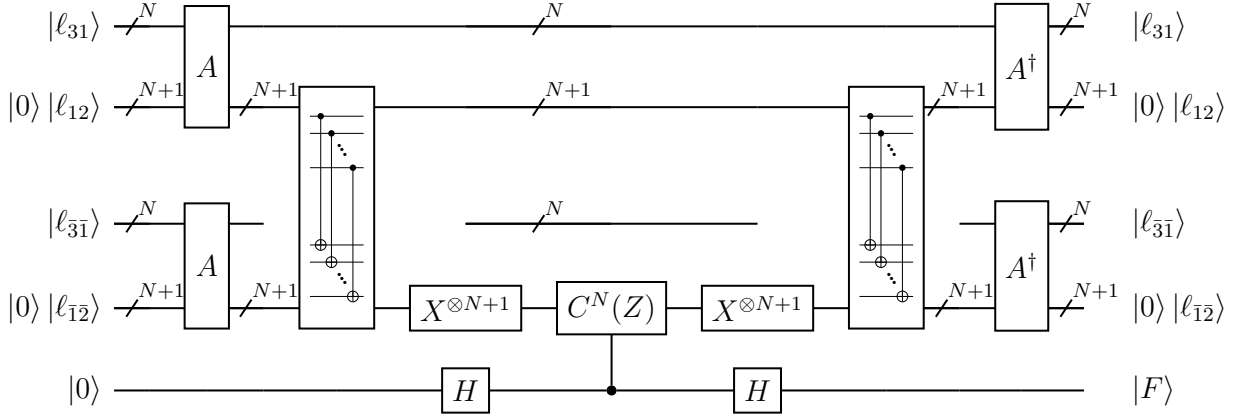


Figure 6.4: A routine for checking the Abelian Gauss law along a link joining two gluonic sites. The registers here are specific to a $1-\bar{1}$ (physical direction) link in 2D space, with the constraint $\ell_{23}(x) + \ell_{31}(x) = \ell_{\bar{2}\bar{3}}(x + e_1) + \ell_{\bar{3}\bar{1}}(x + e_1)$. The adder circuits A are detailed in Fig. 6.2, and the CNOTstring is detailed in the text.

In Fig. 6.3 we give a quantum circuit for checking the Abelian Gauss law along a qg link in $d \geq 2$. The additional non-standard circuit notation introduced is the N -bit addition gate A , detailed in Fig. 6.2. The input and output registers specifically consider (6.12b), i.e., the Abelian Gauss law across a $3-i$ link of the 2D lattice. This constraint is checked by (i) computing the sums $n_3 = \ell_{23} + \ell_{31}$ and $n_R = n_\ell + n_i(1 - n_o)$, (ii) computing the bit-wise sum of n_3 and n_R , and (iii) flagging the query qubit if and only if that bitwise sum is all zeros.

In Fig. 6.4, we give a quantum circuit for checking the Abelian Gauss law along a gg link in $d \geq 2$. The input and output registers in Fig. 6.4 specifically apply to (6.12a), namely, the Abelian Gauss law across a $1-\bar{1}$ gg link of the 2D lattice. The circuit (i) separately computes $n_1 = \ell_{31}(x) + \ell_{12}(x)$ and $n_{\bar{1}} = \ell_{\bar{3}\bar{1}}(x + e_1) + \ell_{\bar{1}\bar{2}}(x + e_1)$, (ii) computes the bitwise sum of n_1 and $n_{\bar{1}}$, and (iii) flags the query output qubit if and only if that bitwise sum is all zeros.

In Table 6.1, we give resource costs for the oracles using simple algorithms from the literature. The main measure of complexity considered is the number of Toffoli gates, broken

Circuit	Explicit components			A gate adders (with A using ripple-carry [2])			A' gate adder (A' as in Fig. 6.2)			Multicontrolled Z [3] (using LSH workspace)
	Anc.	CNOT	$C^2(X)$ cong.	Anc.	CNOT	$C^2(X)$ cong.	Anc.	CNOT	$C^2(X)$ cong.	exact $C^2(X)$
<i>qq</i>	4	$2(N+2)$	4	-	-	-	$2(N+1)$	$4(N+1)$	$4(N+1)$	$4N$
<i>qg</i>	3	$2(N+1)$	2	1	$2(5N-3)$	$2(2N-1)$	$N+1$	$2(N+1)$	$2(N+1)$	$4N$
<i>gg</i>	2	$2(N+1)$	0	2	$4(5N-3)$	$4(2N-1)$	-	-	-	$4(N-1)$

Table 6.1: Resource counts for implementing the oracles using simple subroutines from the literature. $N \geq 3$ refers to the gluonic loop number register size; the quark site loop number register size is $N + 1$. The counted resources are numbers of ancillary qubits (Anc.), CNOTgates, and Toffoli-congruent [$C^2(X)$ cong.] or exact Toffoli [$C^2(X)$] gates.

down into “Toffoli-congruent” gates and exact Toffolis. By Toffoli-congruent gates we mean three-qubit gates that map computational basis states like a Toffoli but with possible phase shifts. The freedom of phase shifts means Toffoli-congruent gates can be implemented more efficiently than exact Toffolis [3]. Toffoli-congruent gates are acceptable in the oracles’ adders since the undesired phases get removed during the uncomputation cycle. However, these phases cannot be introduced in the multi-controlled Z operation.

To give complete gate counts we had to choose algorithms for the subroutines. We have already chosen to implement the bit adders A' in the tailored way given earlier. For the adder gates A , we considered the ripple-carry addition algorithm (in place and with no incoming carry bit) from [2]. And for the multicontrolled Z operations, we apply Lemma 7.2 of [3] by using some of the nonparticipating LSH registers as work space; in the *gg* circuit the N -qubit work space could be the $|\ell_{\bar{3}1}\rangle$ register, while in the *qg* circuit the $(N + 1)$ -qubit workspace could be the $|0\rangle |\ell_{31}\rangle$ register. In applying the algorithms of Refs. [2, 3], $N \geq 3$ is assumed.

By taking advantage of Toffoli congruence and using Corollary 6.2 of [3] for the exact Toffolis, we can consolidate the multiqubit gate counts into equivalent CNOTcounts. These are reported in Table 6.2.

Circuit	Equivalent CNOTs
qq	$42N + 32$
qg	$56N + 4$
gg	$70N - 46$

Table 6.2: CNOTcounts for the circuits assuming $N \geq 3$, the use of Toffoli-congruent gates, and Corollary 6.2 of [3].

6.3 Discussion

The tradeoff of the LSH approach may be an increase in qubits needed for simulation. For the truncation level \bar{j} defined above, the total number of logical qubits required for simulating the LSH basis is

$$V (\{ 6(d-1) \lceil \log_2(\bar{j} + 1) \rceil \} + \{ \lceil \log_2(\bar{j} + 1) \rceil + 3 \}) ,$$

where V is the Cartesian volume and the curly brackets separate the costs of gluonic sites and quark sites. The per-site count stems from the ℓ_{ij} 's at $2(d-1)$ gluonic vertices, the quantum numbers of the quark vertex, and the definition of N from (6.6). For the Kogut-Susskind representation basis as conventionally formulated [83], the best-case cost is

$$V (\{ d \lceil \log_2[\frac{8}{3}(\bar{j} + \frac{1}{2})(\bar{j} + \frac{3}{4})(\bar{j} + 1)] \rceil \} + 2) .$$

In this case the per-site count arises from counting up all irreducible representation states $|j, m, m'\rangle$ on d links and the quark occupancies. These costs are displayed in Figs. 6.5 and 6.6. However, as pointed out earlier, the $|j, m, m'\rangle$ basis seems ill suited to digitization, so a better comparison to make could be with a variation of Kogut-Susskind gauge theory in which the link ends are treated separately: $|j, m, m'\rangle \rightarrow |j, m\rangle \otimes |j', m'\rangle$ with the physical requirement $j = j'$ along links. In this case, each site would be associated with $2d$ link ends plus the quark doublet, and the logical qubit costs would be

$$V(\{2d \lceil \log_2[(\bar{j} + 1)(2\bar{j} + 1)] \rceil \} + 2) .$$

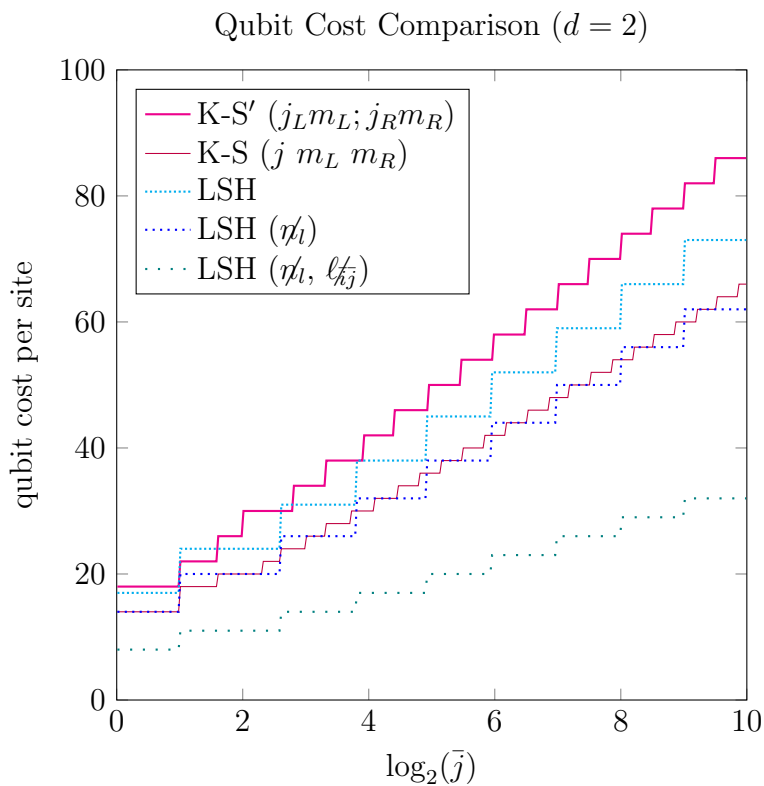


Figure 6.5: The qubit costs per (unsplit) 2D lattice site as a function of the Casimir cutoff \bar{j} . The bases considered are the conventional Kogut-Susskind (K-S, thin solid line), loop-string-hadron (LSH), and modifications of these as described in the text.

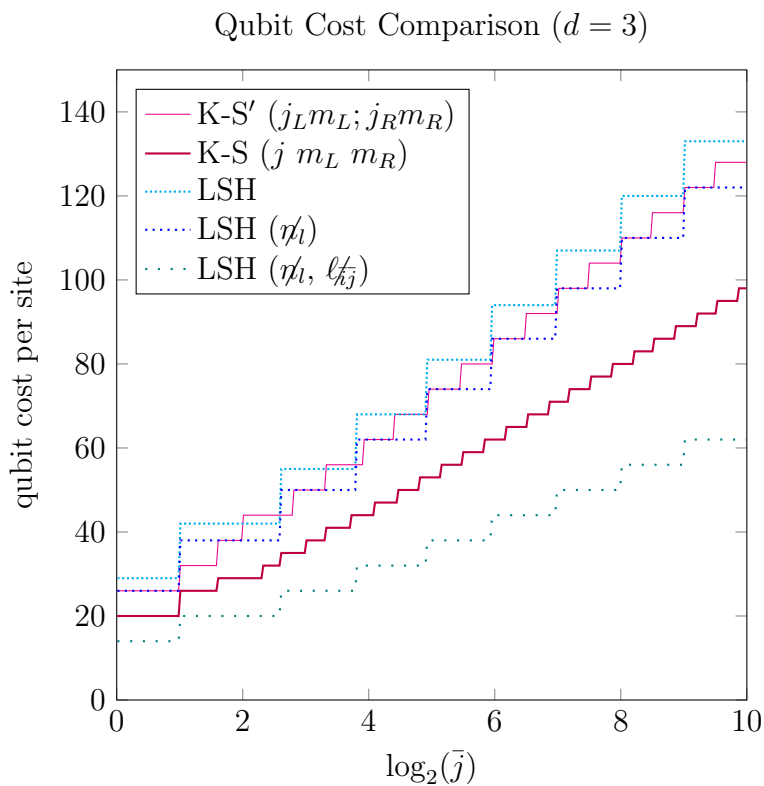


Figure 6.6: The qubit costs per (unsplit) 3D lattice site as a function of \bar{j} . The bases considered are the conventional Kogut-Susskind (K-S, thick solid line), loop-string-hadron (LSH), and modifications of these as described in the text.

We see from Figs. 6.5 and 6.6 that in 2D space with matter, or in 3D space, the LSH basis indeed calls for more qubits to reach a fixed cutoff than does the conventional representation basis (labeled K-S); the asymptotic logical qubit cost of LSH with one staggered quark flavor is 16.7% higher in $d = 2$ and 44.4% higher in $d = 3$. The persistent redundancy of the Hilbert space is apparently the price paid for trading non-Abelian constraints for Abelian ones. However, it is a common situation in both quantum computation and in gauge theories where expanding a Hilbert space with extra degrees of freedom can yield a more convenient theoretical description. Digitization of the conventional representation basis could even benefit from a treatment with separate Hilbert spaces at the link ends (labeled K-S'), in which case LSH asymptotically saves 12.5% of qubits in $d = 2$ and costs only 8.33% more in $d = 3$.

Another possibility is to solve the LSH constraints and cut the number of bosonic degrees of freedom in half, but this may increase the range of the interactions between registers and also complicate the interactions in the Hamiltonian. Additionally, triangle inequalities involving the dynamical quantum numbers would surface, so some unphysical states would still persist. Although it is not known yet whether this complete reduction has a net advantage, we display the associated qubit counts in Figs. 6.5 and 6.6 [indicated by $(\mathcal{N}_l, \ell_{\bar{j}})$].

One could instead settle for a smaller reduction, eliminating the quark-site bosonic variables n_l , without running into the aforementioned complications. This slightly reduced LSH variant costs about the same qubits as standard K-S in $d = 2$, and the same as or fewer than K-S with separated link ends in $d = 3$. This LSH reduction is similarly shown in Figs. 6.5 and 6.6 [indicated by (\mathcal{N}_l)].

The essential benefit that was exploited above was the trading of non-commuting Gauss law constraints for commuting Abelian Gauss law constraints. Thus, no change of basis is necessary to check the constraints, and one can immediately proceed with computation. For this reason we could easily furnish the first explicit algorithms to validate wave functions of a non-Abelian lattice gauge theory. The algorithms call for common subroutines and are easily adapted to different qubit mappings or even to qudits. For illustrative purposes we

focused on the most straightforward binary integer representation.

6.4 Conclusion

The loop-string-hadron formulation as a basis for digital quantum simulation offers important theoretical advantages. While the exact same physics as Kogut-Susskind gauge theory is being described, this treatment has expedited the process of turning lattice gauge theory formalism into input for quantum algorithm research. The physicality diagnostics are likely to be useful in digital simulations because non-gauge invariant errors can easily arise from the Trotter approximation to $\exp(-it\hat{H})$ or from quantum noise (cf. chapter 2). Previously, Gauss law oracles had only been decomposed for $U(1)$ and $Z(N)$ gauge theories. Because the LSH framework has cast all constraints into an Abelian form, those techniques could be ported over for use with $SU(2)$.

The LSH framework also endows $SU(2)$ lattice gauge theory with another similarity to $U(1)$ theories: the plaquette operators in $d \geq 2$ manifestly decompose into a sum of one-sparse ladder operators. This commonality presents the opportunity for $SU(2)$ simulations to potentially benefit from algorithms designed for $U(1)$ simulations. A key distinguishing feature of $SU(2)$ to overcome will be that the nonzero matrix elements of the $SU(2)$ ladder operator are functions of the electric flux, whereas the nonzero matrix elements of the $U(1)$ plaquette operator are all identical.

The approach to decomposing physicality oracles presented should generalize to $SU(3)$ just as well. In the prepotential formulation of $SU(3)$, one obtains two Abelian constraints along each link, so all the benefits of commuting constraints may carry over. There are still details to be worked out regarding the point splitting procedure and incorporation of matter before circuits can be furnished.

Much remains to be understood about the quantum simulation of lattice gauge theories. Even for the simplest gauge groups approaches to Gauss's law are still being researched [186]. New studies are also underway into the consequences of breaking gauge invariance [187, 188]. In this chapter we have made the argument that a more physically-motivated basis can be

used to enforce all gauge constraints and that there is reason to believe it will help advance simulation protocols.

Chapter acknowledgments

IR and JRS thank D.B. Kaplan, N. Klco, and M.J. Savage for helpful discussions and feedback during the course of this work. IR was supported by the U.S. Department of Energy (DOE), Office of Science, Office of Advanced Scientific Computing Research (ASCR) Quantum Computing Application Teams program, under Fieldwork Proposal No. ERKJ347, and by the Maryland Center for Fundamental Physics. IR was also supported in part by the Thomas L. and Margo G. Wyckoff Endowed Faculty Fellowship. JRS was supported by DOE Grant No. DE-FG02-00ER41132 and by the National Science Foundation Graduate Research Fellowship under Grant No. DGE-1762114.

Chapter 7

CONCLUSION

This dissertation has examined the problem of formulating gauge theories for simulation by quantum computers as well as the unique challenges they will present as compared to other many-body quantum theories. Local gauge symmetry of a theory is married to redundancy in its degrees of freedom, which presents one salient issue for quantum simulations. In addition, the theories of greatest interest for understanding our universe have non-Abelian gauge groups, which add further challenges to the problem of simulation.

The work presented in this dissertation began with the simple task of validating wave functions that are permitted by Gauss's law in Abelian gauge theories. These circuits, which could be "oracles" within larger algorithmic routines, were presented for a variety of possible Abelian gauge theories and the underlying task was essentially the evaluation of constraint functions. Whether or not these are ever implemented on hardware, these algorithms have provided the starting point for establishing what it means to have verifiably valid wavefunctions without destroying their correlations.

We then investigated the important question of what it means to work with Abelian $[U(1)]$ gauge theories if we insist on having Gauss's law locally built in. This naturally led us to a magnetic dual representation, which may come with its own constraints that are effectively magnetic Gauss laws. The variable transformation appears to be advantageous in $d < 3$ spatial dimensions, but its merits for $d = 3$ are less apparent due to the electric-magnetic duality.

Similar problems to the above were then taken up for the non-Abelian gauge group, $SU(2)$. For reasons explained in chapter 6, going straight into brute force algorithms for verifying gauge invariance is far less practical or straightforward in such theories. Therefore,

we first began by doing (scalable) analytic reductions at sites of a plaquette ladder, which also helped to reduced the system’s Hilbert space redundancy. At this point, simulating a small version of the theory was within reach of existing hardware, and a simulation was done using IBM’s Tokyo device. We used post-selection on allowed states (those satisfying appropriate triangle inequalities) to mitigate some of the errors that violate gauge constraints, and were able to reproduce expected results at low enough circuit depths.

To scale $SU(2)$ investigations up for future use, we extended the existing loop formulations of pure $SU(2)$ gauge theory to include matter and solve all pertinent constraints, resulting in what we call a loop-string-hadron or LSH formulation. Like what was pursued in chapter 3, charge conservation at sites was built in from the start by choosing more physically motivated UV degrees of freedom. In the process, however, a separation of links into halves was made, requiring that new conservation laws be introduced to compensate for this formal convenience. These Abelian Gauss laws are nothing but the requirement that flux be conserved as it flows across a link, and with the constraints being strictly Abelian, they seem preferable to work with.

As a first example of the LSH framework’s utility, we returned to the problem of establishing gauge invariant wave functions in $SU(2)$ gauge theories, with the task now essentially cast into the form of its $U(1)$ counterpart, save for the fact that the circuits operate on links instead of sites. Algorithms are now known that validate wave functions in $SU(2)$ gauge theories, in addition to $U(1)$ and $Z(N)$, with many structural similarities.

One of the most prominent issues not addressed by this dissertation would be actual time evolution. This is briefly discussed in the context of the Schwinger model in Appendix A, while a recent work was dedicated to a scaling analysis of Schwinger model Trotterization when the requirement of exact charge conservation is relaxed [189].

Time evolution algorithms will be a real test of the usefulness of the LSH framework. What is contained here is essentially the most pre-processing that we saw could be done before actually discussing qubit mappings or particular time evolution protocols. Our hope is that the derivations and intuition make the framework adaptable to the particular needs

that will inevitably arise in the process of developing such algorithms.

BIBLIOGRAPHY

- [1] N. Klco and M. J. Savage, “Minimally-entangled state preparation of localized wavefunctions on quantum computers,” 2019.
- [2] S. A. Cuccaro, T. G. Draper, S. A. Kutin, and D. P. Moulton, “A new quantum ripple-carry addition circuit.” Oct. 2004.
- [3] A. Barenco, C. H. Bennett, R. Cleve, D. P. DiVincenzo, N. Margolus, P. Shor, T. Sleator, J. Smolin, and H. Weinfurter, “Elementary gates for quantum computation,” *Physical Review A*, vol. 52, pp. 3457–3467, Nov. 1995.
- [4] K. G. Wilson, “Confinement of quarks,” *Phys. Rev. D*, vol. 10, pp. 2445–2459, Oct. 1974.
- [5] K. C. Bowler, R. D. Kenway, O. Oliveira, D. G. Richards, P. Ueberholz, UKQCD Collaboration, L. Lellouch, J. Nieves, C. T. Sachrajda, N. Stella, and H. Wittig, “Heavy baryon spectroscopy from the lattice,” *Phys. Rev. D*, vol. 54, pp. 3619–3633, Sept. 1996.
- [6] PACS-CS Collaboration, S. Aoki, K.-I. Ishikawa, N. Ishizuka, T. Izubuchi, D. Kadoh, K. Kanaya, Y. Kuramashi, Y. Namekawa, M. Okawa, Y. Taniguchi, A. Ukawa, N. Ukita, and T. Yoshié, “2+1 flavor lattice QCD toward the physical point,” *Phys. Rev. D*, vol. 79, p. 034503, Feb. 2009.
- [7] A. Bazavov, T. Bhattacharya, M. Cheng, N. H. Christ, C. DeTar, S. Ejiri, S. Gottlieb, R. Gupta, U. M. Heller, K. Huebner, C. Jung, F. Karsch, E. Laermann, L. Levkova, C. Miao, R. D. Mawhinney, P. Petreczky, C. Schmidt, R. A. Soltz, W. Soeldner, R. Sugar, D. Toussaint, and P. Vranas, “Equation of state and QCD transition at finite temperature,” *Phys. Rev. D*, vol. 80, p. 014504, July 2009.
- [8] Y. Aoki, S. Borsányi, S. Dürr, Z. Fodor, S. D. Katz, S. Krieg, and K. Szabo, “The QCD transition temperature: Results with physical masses in the continuum limit II,” *J. High Energy Phys.*, vol. 2009, pp. 088–088, June 2009.
- [9] S. Borsányi, Z. Fodor, S. D. Katz, S. Krieg, C. Ratti, and K. K. Szabó, “Freeze-Out Parameters: Lattice Meets Experiment,” *Phys. Rev. Lett.*, vol. 111, p. 062005, Aug. 2013.

- [10] NPLQCD Collaboration, B. C. Tiburzi, M. L. Wagman, F. Winter, E. Chang, Z. Davoudi, W. Detmold, K. Orginos, M. J. Savage, and P. E. Shanahan, “Double- β decay matrix elements from lattice quantum chromodynamics,” *Phys. Rev. D*, vol. 96, p. 054505, Sept. 2017.
- [11] NPLQCD Collaboration, M. J. Savage, P. E. Shanahan, B. C. Tiburzi, M. L. Wagman, F. Winter, S. R. Beane, E. Chang, Z. Davoudi, W. Detmold, and K. Orginos, “Proton-Proton Fusion and Tritium β Decay from Lattice Quantum Chromodynamics,” *Phys. Rev. Lett.*, vol. 119, p. 062002, Aug. 2017.
- [12] A. S. Kronfeld, “Twenty-first century lattice gauge theory: Results from the quantum chromodynamics Lagrangian,” *Annu. Rev. Nucl. Part. Sci.*, vol. 62, no. 1, pp. 265–284, 2012.
- [13] R. P. Feynman, “Simulating physics with computers,” *Int. J. Theor. Phys.*, vol. 21, pp. 467–488, June 1982.
- [14] F. Arute, K. Arya, R. Babbush, D. Bacon, J. C. Bardin, R. Barends, R. Biswas, S. Boixo, F. G. S. L. Brandao, D. A. Buell, B. Burkett, Y. Chen, Z. Chen, B. Chiaro, R. Collins, W. Courtney, A. Dunsworth, E. Farhi, B. Foxen, A. Fowler, C. Gidney, M. Giustina, R. Graff, K. Guerin, S. Habegger, M. P. Harrigan, M. J. Hartmann, A. Ho, M. Hoffmann, T. Huang, T. S. Humble, S. V. Isakov, E. Jeffrey, Z. Jiang, D. Kafri, K. Kechedzhi, J. Kelly, P. V. Klimov, S. Knysh, A. Korotkov, F. Kostritsa, D. Landhuis, M. Lindmark, E. Lucero, D. Lyakh, S. Mandrà, J. R. McClean, M. McEwen, A. Megrant, X. Mi, K. Michielsen, M. Mohseni, J. Mutus, O. Naaman, M. Neeley, C. Neill, M. Y. Niu, E. Ostby, A. Petukhov, J. C. Platt, C. Quintana, E. G. Rieffel, P. Roushan, N. C. Rubin, D. Sank, K. J. Satzinger, V. Smelyanskiy, K. J. Sung, M. D. Trevithick, A. Vainsencher, B. Villalonga, T. White, Z. J. Yao, P. Yeh, A. Zalcman, H. Neven, and J. M. Martinis, “Quantum supremacy using a programmable superconducting processor,” *Nature*, vol. 574, pp. 505–510, Oct. 2019.
- [15] D. Banerjee, M. Dalmonte, M. Müller, E. Rico, P. Stebler, U.-J. Wiese, and P. Zoller, “Atomic Quantum Simulation of Dynamical Gauge Fields Coupled to Fermionic Matter: From String Breaking to Evolution after a Quench,” *Phys. Rev. Lett.*, vol. 109, p. 175302, Oct. 2012.
- [16] M. C. Bañuls and K. Cichy, “Review on novel methods for lattice gauge theories,” *Rep. Prog. Phys.*, vol. 83, p. 024401, Jan. 2020.
- [17] M. C. Bañuls, R. Blatt, J. Catani, A. Celi, J. I. Cirac, M. Dalmonte, L. Fallani, K. Jansen, M. Lewenstein, S. Montangero, C. A. Muschik, B. Reznik, E. Rico,

- L. Tagliacozzo, K. Van Acoleyen, F. Verstraete, U.-J. Wiese, M. Wingate, J. Zakrzewski, and P. Zoller, “Simulating lattice gauge theories within quantum technologies,” *arXiv:1911.00003 [cond-mat, physics:hep-lat, physics:hep-th, physics:quant-ph]*, Oct. 2019.
- [18] E. Zohar, A. Farace, B. Reznik, and J. I. Cirac, “Digital Quantum Simulation of \mathbb{Z}_2 Lattice Gauge Theories with Dynamical Fermionic Matter,” *Phys. Rev. Lett.*, vol. 118, p. 070501, Feb. 2017.
- [19] C. Schweizer, F. Grusdt, M. Berngruber, L. Barbiero, E. Demler, N. Goldman, I. Bloch, and M. Aidelsburger, “Floquet approach to \mathbb{Z}_2 lattice gauge theories with ultracold atoms in optical lattices,” *Nat. Phys.*, vol. 15, pp. 1168–1173, Nov. 2019.
- [20] E. Rico, T. Pichler, M. Dalmonte, P. Zoller, and S. Montangero, “Tensor Networks for Lattice Gauge Theories and Atomic Quantum Simulation,” *Phys. Rev. Lett.*, vol. 112, p. 201601, May 2014.
- [21] C. Muschik, M. Heyl, E. Martinez, T. Monz, P. Schindler, B. Vogell, M. Dalmonte, P. Hauke, R. Blatt, and P. Zoller, “U(1) Wilson lattice gauge theories in digital quantum simulators,” *New J. Phys.*, vol. 19, no. 10, p. 103020, 2017.
- [22] N. Klco, E. F. Dumitrescu, A. J. McCaskey, T. D. Morris, R. C. Pooser, M. Sanz, E. Solano, P. Lougovski, and M. J. Savage, “Quantum-classical computation of Schwinger model dynamics using quantum computers,” *Phys. Rev. A*, vol. 98, p. 032331, Sept. 2018.
- [23] Z. Davoudi, M. Hafezi, C. Monroe, G. Pagano, A. Seif, and A. Shaw, “Towards analog quantum simulations of lattice gauge theories with trapped ions,” *Phys. Rev. Research*, vol. 2, p. 023015, Apr. 2020.
- [24] E. A. Martinez, C. A. Muschik, P. Schindler, D. Nigg, A. Erhard, M. Heyl, P. Hauke, M. Dalmonte, T. Monz, P. Zoller, and R. Blatt, “Real-time dynamics of lattice gauge theories with a few-qubit quantum computer,” *Nature*, vol. 534, pp. 516–519, June 2016.
- [25] T. Byrnes and Y. Yamamoto, “Simulating lattice gauge theories on a quantum computer,” *Phys. Rev. A*, vol. 73, p. 022328, Feb. 2006.
- [26] E. Zohar, J. I. Cirac, and B. Reznik, “Cold-Atom Quantum Simulator for SU(2) Yang-Mills Lattice Gauge Theory,” *Phys. Rev. Lett.*, vol. 110, p. 125304, Mar. 2013.

- [27] L. Tagliacozzo, A. Celi, P. Orland, M. W. Mitchell, and M. Lewenstein, “Simulation of non-Abelian gauge theories with optical lattices,” *Nat. Commun.*, vol. 4, p. 2615, Oct. 2013.
- [28] D. Banerjee, M. Bögli, M. Dalmonte, E. Rico, P. Stebler, U.-J. Wiese, and P. Zoller, “Atomic Quantum Simulation of U(N) and SU(N) Non-Abelian Lattice Gauge Theories,” *Phys. Rev. Lett.*, vol. 110, p. 125303, Mar. 2013.
- [29] U.-J. Wiese, “Ultracold quantum gases and lattice systems: Quantum simulation of lattice gauge theories,” *Ann. Phys.*, vol. 525, no. 10-11, pp. 777–796, 2013.
- [30] U.-J. Wiese, “Towards quantum simulating QCD,” *Nucl. Phys. A*, vol. 931, pp. 246–256, Nov. 2014.
- [31] A. Mezzacapo, E. Rico, C. Sabín, I. L. Egusquiza, L. Lamata, and E. Solano, “Non-Abelian SU(2) Lattice Gauge Theories in Superconducting Circuits,” *Phys. Rev. Lett.*, vol. 115, p. 240502, Dec. 2015.
- [32] NuQS Collaboration, H. Lamm, S. Lawrence, and Y. Yamauchi, “General methods for digital quantum simulation of gauge theories,” *Phys. Rev. D*, vol. 100, p. 034518, Aug. 2019.
- [33] NuQS Collaboration, A. Alexandru, P. F. Bedaque, S. Harmalkar, H. Lamm, S. Lawrence, and N. C. Warrington, “Gluon field digitization for quantum computers,” *Phys. Rev. D*, vol. 100, p. 114501, Dec. 2019.
- [34] N. Klco, M. J. Savage, and J. R. Stryker, “SU(2) non-Abelian gauge field theory in one dimension on digital quantum computers,” *Phys. Rev. D*, vol. 101, p. 074512, Apr. 2020.
- [35] M. A. Nielsen and I. L. Chuang, *Quantum Computation and Quantum Information: 10th Anniversary Edition*. New York, NY, USA: Cambridge University Press, tenth ed., 2011.
- [36] S. Weinberg, *The Quantum Theory of Fields: Modern Applications*, vol. 2. Cambridge: Cambridge University Press, 1996.
- [37] J. Smit, *Introduction to Quantum Fields on a Lattice*. Cambridge University Press, Sept. 2002.
- [38] C. Gatttringer and C. B. Lang, *Quantum Chromodynamics on the Lattice: An Introductory Presentation*. Heidelberg; New York: Springer, 2010.

- [39] J. Kogut and L. Susskind, “Hamiltonian formulation of Wilson’s lattice gauge theories,” *Phys. Rev. D*, vol. 11, pp. 395–408, Jan. 1975.
- [40] B. Sheikholeslami and R. Wohlert, “Improved continuum limit lattice action for QCD with wilson fermions,” *Nuclear Physics B*, vol. 259, pp. 572–596, Sept. 1985.
- [41] D. B. Kaplan, “A method for simulating chiral fermions on the lattice,” *Physics Letters B*, vol. 288, pp. 342–347, Aug. 1992.
- [42] Y. Shamir, “Chiral fermions from lattice boundaries,” *Nuclear Physics B*, vol. 406, pp. 90–106, Sept. 1993.
- [43] Y. Shamir, “Constraints on the existence of chiral fermions in interacting lattice theories,” *Phys. Rev. Lett.*, vol. 71, pp. 2691–2694, Oct. 1993.
- [44] V. Furman and Y. Shamir, “Axial symmetries in lattice QCD with Kaplan fermions,” *Nuclear Physics B*, vol. 439, pp. 54–78, Apr. 1995.
- [45] R. Narayanan and H. Neuberger, “Chiral fermions on the lattice,” *Phys. Rev. Lett.*, vol. 71, pp. 3251–3254, Nov. 1993.
- [46] P. H. Ginsparg and K. G. Wilson, “A remnant of chiral symmetry on the lattice,” *Phys. Rev. D*, vol. 25, pp. 2649–2657, May 1982.
- [47] P. Hasenfratz, “Analytic results — Selected non-stochastic developments on the Lattice,” *Nuclear Physics B - Proceedings Supplements*, vol. 34, pp. 3–14, Apr. 1994.
- [48] P. Hasenfratz, “Prospects for perfect actions,” *Nuclear Physics B - Proceedings Supplements*, vol. 63, pp. 53–58, Apr. 1998.
- [49] E. Zohar and M. Burrello, “Formulation of lattice gauge theories for quantum simulations,” *Phys. Rev.*, vol. D91, no. 5, p. 054506, 2015.
- [50] H. S. Sharatchandra, “Local observables in non-abelian gauge theories,” *Nuclear Physics B*, vol. 196, pp. 62–82, Mar. 1982.
- [51] I. Raychowdhury, *Prepotential Formulation of Lattice Gauge Theories*. PhD thesis, Calcutta U., 2013.
- [52] S. Mandelstam, “Charge-monopole duality and the phases of non-Abelian gauge theories,” *Phys. Rev. D*, vol. 19, pp. 2391–2409, Apr. 1979.

- [53] R. Loll, “Yang-Mills theory without Mandelstam constraints,” *Nucl. Phys. B*, vol. 400, pp. 126–144, July 1993.
- [54] N. J. Watson, “Solution of the SU(2) Mandelstam constraints,” *Phys. Lett. B*, vol. 323, pp. 385–392, Mar. 1994.
- [55] M. Mathur, “Harmonic oscillator pre-potentials in SU (2) lattice gauge theory,” *J. Phys. A: Math. Gen.*, vol. 38, no. 46, p. 10015, 2005.
- [56] J. Schwinger, “On angular momentum,” Tech. Rep. NYO-3071, U.S. Atomic Energy Commission, Oak Ridge, Tennessee, Jan. 1952.
- [57] M. Mathur, “Loop states in lattice gauge theory,” *Physics Letters B*, vol. 640, pp. 292–296, Sept. 2006.
- [58] M. Mathur, “Loop approach to lattice gauge theories,” *Nucl. Phys. B*, vol. 779, pp. 32–62, Sept. 2007.
- [59] R. Anishetty, M. Mathur, and I. Raychowdhury, “Prepotential formulation of SU (3) lattice gauge theory,” *J. Phys. A: Math. Theor.*, vol. 43, no. 3, p. 035403, 2010.
- [60] S. McArdle, X. Yuan, and S. Benjamin, “Error mitigated digital quantum simulation.” July 2018.
- [61] X. Bonet-Monroig, R. Sagastizabal, M. Singh, and T. E. O’Brien, “Low-cost error mitigation by symmetry verification,” *Phys. Rev. A*, vol. 98, p. 062339, Dec. 2018.
- [62] L. K. Grover, “Quantum Mechanics Helps in Searching for a Needle in a Haystack,” *Phys. Rev. Lett.*, vol. 79, pp. 325–328, July 1997.
- [63] V. Vedral, A. Barenco, and A. Ekert, “Quantum networks for elementary arithmetic operations,” *Phys. Rev. A*, vol. 54, pp. 147–153, July 1996.
- [64] T. G. Draper, “Addition on a Quantum Computer.” Aug. 2000.
- [65] T. G. Draper, S. A. Kutin, E. M. Rains, and K. M. Svore, “A logarithmic-depth quantum carry-lookahead adder,” *Quantum Inf. Comput.*, vol. 6, pp. 351–369, Nov. 2005.
- [66] P. Gossett, “Quantum Carry-Save Arithmetic.” Aug. 1998.

- [67] M. K. Thomsen and H. B. Axelsen, “Parallel optimization of a reversible (quantum) ripple-carry adder,” in *Unconventional Computing* (C. S. Calude, J. F. Costa, R. Freund, M. Oswald, and G. Rozenberg, eds.), Lecture Notes in Computer Science, pp. 228–241, Springer Berlin Heidelberg, 2008.
- [68] F. Wang, M. Luo, H. Li, Z. Qu, and X. Wang, “Improved quantum ripple-carry addition circuit,” *Sci. China Inf. Sci.*, vol. 59, p. 042406, Feb. 2016.
- [69] Y. Takahashi, S. Tani, and N. Kunihiro, “Quantum addition circuits and unbounded fan-out,” *Quantum Inf. Comput.*, vol. 10, no. 9-10, pp. 0872–0890, 2010.
- [70] C. Gidney, “Halving the cost of quantum addition,” *Quantum*, vol. 2, p. 74, June 2018.
- [71] K. Stannigel, P. Hauke, D. Marcos, M. Hafezi, S. Diehl, M. Dalmonte, and P. Zoller, “Constrained Dynamics via the Zeno Effect in Quantum Simulation: Implementing Non-Abelian Lattice Gauge Theories with Cold Atoms,” *Phys. Rev. Lett.*, vol. 112, p. 120406, Mar. 2014.
- [72] D. W. Berry, A. M. Childs, R. Cleve, R. Kothari, and R. D. Somma, “Simulating Hamiltonian Dynamics with a Truncated Taylor Series,” *Phys. Rev. Lett.*, vol. 114, p. 090502, Mar. 2015.
- [73] D. W. Berry, A. M. Childs, and R. Kothari, “Hamiltonian Simulation with Nearly Optimal Dependence on all Parameters,” in *2015 IEEE 56th Annual Symposium on Foundations of Computer Science*, pp. 792–809, Oct. 2015.
- [74] D. B. Kaplan and J. R. Stryker, “Gauss’s Law, Duality, and the Hamiltonian Formulation of U(1) Lattice Gauge Theory.” June 2018.
- [75] D. Horn, “Finite matrix models with continuous local gauge invariance,” *Phys. Lett. B*, vol. 100, pp. 149–151, Mar. 1981.
- [76] P. Orland and D. Rohrlich, “Lattice gauge magnets: Local isospin from spin,” *Nucl. Phys. B*, vol. 338, pp. 647–672, July 1990.
- [77] S. Chandrasekharan and U.-J. Wiese, “Quantum link models: A discrete approach to gauge theories,” *Nucl. Phys. B*, vol. 492, pp. 455–471, May 1997.
- [78] R. Brower, S. Chandrasekharan, and U.-J. Wiese, “QCD as a quantum link model,” *Phys. Rev. D*, vol. 60, p. 094502, Sept. 1999.

- [79] L. Tagliacozzo, A. Celi, A. Zamora, and M. Lewenstein, “Optical Abelian lattice gauge theories,” *Ann. Phys. (N. Y.)*, vol. 330, pp. 160–191, Mar. 2013.
- [80] T. Pichler, M. Dalmonte, E. Rico, P. Zoller, and S. Montangero, “Real-Time Dynamics in U(1) Lattice Gauge Theories with Tensor Networks,” *Phys. Rev. X*, vol. 6, p. 011023, Mar. 2016.
- [81] I. Raychowdhury, “Low Energy Spectrum of SU(2) Lattice Gauge Theory: An Alternate Proposal via Loop Formulation.” Apr. 2018.
- [82] M. Dalmonte and S. Montangero, “Lattice gauge theory simulations in the quantum information era,” *Contemporary Physics*, vol. 57, pp. 388–412, July 2016.
- [83] E. Zohar and M. Burrello, “Formulation of lattice gauge theories for quantum simulations,” *Phys. Rev. D*, vol. 91, p. 054506, Mar. 2015.
- [84] M. Creutz, *Quarks, Gluons and Lattices*. New York, NY, USA: Cambridge University Press, 1984.
- [85] D. Horn, M. Weinstein, and S. Yankielowicz, “Hamiltonian approach to $SU(N)$ lattice gauge theories,” *Phys. Rev. D*, vol. 19, pp. 3715–3731, June 1979.
- [86] G. H. Low and I. L. Chuang, “Hamiltonian Simulation by Qubitization,” *arXiv:1610.06546 [quant-ph]*, Oct. 2016.
- [87] R. Anishetty and H. S. Sharatchandra, “Duality transformation for non-Abelian lattice gauge theories,” *Phys. Rev. Lett.*, vol. 65, pp. 813–815, Aug. 1990.
- [88] I. Raychowdhury, “Low energy spectrum of SU(2) lattice gauge theory,” *Eur. Phys. J. C*, vol. 79, p. 235, Mar. 2019.
- [89] J. F. Haase, L. Dellantonio, A. Celi, D. Paulson, A. Kan, K. Jansen, and C. A. Muschik, “A resource efficient approach for quantum and classical simulations of gauge theories in particle physics,” *arXiv:2006.14160 [hep-lat, physics:quant-ph]*, July 2020.
- [90] K. G. Wilson, “Confinement of quarks,” *Phys. Rev.*, vol. D10, pp. 2445–2459, 1974.
- [91] M. Creutz, “Monte carlo study of quantized SU(2) gauge theory,” *Phys. Rev.*, vol. D21, pp. 2308–2315, 1980.
- [92] S. P. Jordan, K. S. M. Lee, and J. Preskill, “Quantum algorithms for quantum field theories,” *Science*, vol. 336, pp. 1130–1133, 2012.

- [93] S. P. Jordan, K. S. M. Lee, and J. Preskill, “Quantum computation of scattering in scalar quantum field theories,” 2011.
- [94] U.-J. Wiese, “Ultracold quantum gases and lattice systems: Quantum simulation of lattice gauge theories,” *Annalen Phys.*, vol. 525, pp. 777–796, 2013.
- [95] U.-J. Wiese, “Towards quantum simulating QCD,” in *Proceedings, 24th International Conference on Ultra-Relativistic Nucleus-Nucleus Collisions (Quark Matter 2014): Darmstadt, Germany, May 19-24, 2014*, vol. A931 of *Nuclear Physics*, pp. 246–256, 2014.
- [96] S. P. Jordan, K. S. M. Lee, and J. Preskill, “Quantum algorithms for fermionic quantum field theories,” 2014.
- [97] T. Pichler, M. Dalmonte, E. Rico, P. Zoller, and S. Montangero, “Real-time dynamics in U(1) lattice gauge theories with tensor networks,” *Phys. Rev.*, vol. X6, no. 1, p. 011023, 2016.
- [98] M. Dalmonte and S. Montangero, “Lattice gauge theory simulations in the quantum information era,” *Contemp. Phys.*, vol. 57, no. 3, pp. 388–412, 2016.
- [99] R. D. Somma, “Quantum simulations of one dimensional quantum systems,” *Quantum Info. Comput.*, vol. 16, pp. 1125–1168, Oct. 2016.
- [100] M. C. Bañuls, K. Cichy, J. I. Cirac, K. Jansen, and S. Kühn, “Efficient basis formulation for 1+1 dimensional SU(2) lattice gauge theory: Spectral calculations with matrix product states,” *Phys. Rev.*, vol. X7, no. 4, p. 041046, 2017.
- [101] E. Ercolessi, P. Facchi, G. Magnifico, S. Pascazio, and F. V. Pepe, “Phase transitions in Z_n gauge models: Towards quantum simulations of the schwinger-weyl QED,” *Phys. Rev.*, vol. D98, no. 7, p. 074503, 2018.
- [102] P. Sala, T. Shi, S. Kühn, M. C. Bañuls, E. Demler, and J. I. Cirac, “Variational study of U(1) and SU(2) lattice gauge theories with Gaussian states in 1+1 dimensions,” *Phys. Rev.*, vol. D98, no. 3, p. 034505, 2018.
- [103] A. Macridin, P. Spentzouris, J. Amundson, and R. Harnik, “Electron-phonon systems on a universal quantum computer,” *Phys. Rev. Lett.*, vol. 121, no. 11, p. 110504, 2018.
- [104] J. Preskill, “Simulating quantum field theory with a quantum computer,” in *Proceedings, 36th International Symposium on Lattice Field Theory (Lattice 2018): East Lansing, MI, United States, July 22-28, 2018*, vol. LATTICE2018 of *PoS*, p. 024, 2018.

- [105] D. B. Kaplan and J. R. Stryker, “Gauss’s law, duality, and the hamiltonian formulation of U(1) lattice gauge theory,” 2018.
- [106] N. Klco and M. J. Savage, “Digitization of scalar fields for quantum computing,” *Phys. Rev.*, vol. A99, no. 5, p. 052335, 2019.
- [107] D. C. Hackett, K. Howe, C. Hughes, W. Jay, E. T. Neil, and J. N. Simone, “Digitizing gauge fields: Lattice monte carlo results for future quantum computers,” *Phys. Rev.*, vol. A99, no. 6, p. 062341, 2019.
- [108] I. Raychowdhury and J. R. Stryker, “Tailoring non-Abelian lattice gauge theory for quantum simulation,” 2018.
- [109] A. Bazavov, S. Catterall, R. G. Jha, and J. Unmuth-Yockey, “Tensor renormalization group study of the non-Abelian Higgs model in two dimensions,” *Phys. Rev.*, vol. D99, no. 11, p. 114507, 2019.
- [110] A. Alexandru, P. F. Bedaque, S. Harmalkar, H. Lamm, S. Lawrence, and N. C. Warrington, “Gluon field digitization for quantum computers,” *Phys. Rev.*, vol. D100, no. 11, p. 114501, 2019.
- [111] E. Zohar, J. I. Cirac, and B. Reznik, “Simulating Compact Quantum Electrodynamics with ultracold atoms: Probing confinement and nonperturbative effects,” *Phys. Rev. Lett.*, vol. 109, p. 125302, 2012.
- [112] E. Zohar, J. I. Cirac, and B. Reznik, “Cold-atom quantum simulator for SU(2) yang-mills lattice gauge theory,” *Phys. Rev. Lett.*, vol. 110, no. 12, p. 125304, 2013.
- [113] D. Banerjee, M. Dalmonte, M. Muller, E. Rico, P. Stebler, U. J. Wiese, and P. Zoller, “Atomic quantum simulation of dynamical gauge fields coupled to fermionic matter: From string breaking to evolution after a quench,” *Phys. Rev. Lett.*, vol. 109, p. 175302, 2012.
- [114] D. Banerjee, M. Bögli, M. Dalmonte, E. Rico, P. Stebler, U. J. Wiese, and P. Zoller, “Atomic quantum simulation of U(N) and SU(N) non-abelian lattice gauge theories,” *Phys. Rev. Lett.*, vol. 110, no. 12, p. 125303, 2013.
- [115] D. Marcos, P. Widmer, E. Rico, M. Hafezi, P. Rabl, U. J. Wiese, and P. Zoller, “Two-dimensional lattice gauge theories with superconducting quantum circuits,” *Annals Phys.*, vol. 351, pp. 634–654, 2014.

- [116] L. García-Álvarez, J. Casanova, A. Mezzacapo, I. L. Egusquiza, L. Lamata, G. Romero, and E. Solano, “Fermion-fermion scattering in quantum field theory with superconducting circuits,” *Phys. Rev. Lett.*, vol. 114, no. 7, p. 070502, 2015.
- [117] A. Mezzacapo, E. Rico, C. Sabín, I. L. Egusquiza, L. Lamata, and E. Solano, “Non-abelian SU(2) lattice gauge theories in superconducting circuits,” *Phys. Rev. Lett.*, vol. 115, no. 24, p. 240502, 2015.
- [118] A. Bazavov, Y. Meurice, S.-W. Tsai, J. Unmuth-Yockey, and J. Zhang, “Gauge-invariant implementation of the Abelian Higgs model on optical lattices,” *Phys. Rev.*, vol. D92, no. 7, p. 076003, 2015.
- [119] E. Zohar, J. I. Cirac, and B. Reznik, “Quantum simulations of lattice gauge theories using ultracold atoms in optical lattices,” *Rept. Prog. Phys.*, vol. 79, no. 1, p. 014401, 2016.
- [120] K. Marshall, R. Pooser, G. Siopsis, and C. Weedbrook, “Quantum simulation of quantum field theory using continuous variables,” *Phys. Rev.*, vol. A92, no. 6, p. 063825, 2015.
- [121] E. Zohar, A. Farace, B. Reznik, and J. I. Cirac, “Digital lattice gauge theories,” *Phys. Rev.*, vol. A95, no. 2, p. 023604, 2017.
- [122] A. Bermudez, G. Aarts, and M. Müller, “Quantum sensors for the generating functional of interacting quantum field theories,” *Phys. Rev.*, vol. X7, no. 4, p. 041012, 2017.
- [123] T. V. Zache, F. Hebenstreit, F. Jendrzejewski, M. K. Oberthaler, J. Berges, and P. Hauke, “Quantum simulation of lattice gauge theories using Wilson fermions,” *Sci. Technol.*, vol. 3, p. 034010, 2018.
- [124] J. Zhang, J. Unmuth-Yockey, J. Zeiher, A. Bazavov, S. W. Tsai, and Y. Meurice, “Quantum simulation of the universal features of the Polyakov loop,” *Phys. Rev. Lett.*, vol. 121, no. 22, p. 223201, 2018.
- [125] E. Gustafson, Y. Meurice, and J. Unmuth-Yockey, “Quantum simulation of scattering in the quantum Ising model,” *Phys. Rev.*, vol. D99, no. 9, p. 094503, 2019.
- [126] Z. Davoudi, M. Hafezi, C. Monroe, G. Pagano, A. Seif, and A. Shaw, “Towards analog quantum simulations of lattice gauge theories with trapped ions,” 2019.

- [127] E. A. Martinez, C. A. Muschik, P. Schindler, D. Nigg, A. Erhard, M. Heyl, P. Hauke, M. Dalmonte, T. Monz, P. Zoller, and R. Blatt, “Real-time dynamics of lattice gauge theories with a few-qubit quantum computer,” *Nature*, vol. 534, pp. 516 EP –, June 2016.
- [128] N. Klco, E. F. Dumitrescu, A. J. McCaskey, T. D. Morris, R. C. Pooser, M. Sanz, E. Solano, P. Lougovski, and M. J. Savage, “Quantum-classical computation of Schwinger model dynamics using quantum computers,” *Phys. Rev.*, vol. A98, no. 3, p. 032331, 2018.
- [129] H.-H. Lu, N. Klco, J. M. Lukens, T. D. Morris, A. Bansal, A. Ekström, G. Hagen, T. Papenbrock, A. M. Weiner, M. J. Savage, and P. Lougovski, “Simulations of subatomic many-body physics on a quantum frequency processor,” *Phys. Rev.*, vol. A100, no. 1, p. 012320, 2019.
- [130] K. Yeter-Aydeniz, E. F. Dumitrescu, A. J. McCaskey, R. S. Bennink, R. C. Pooser, and G. Siopsis, “Scalar quantum field theories as a benchmark for near-term quantum computers,” *Phys. Rev.*, vol. A99, no. 3, p. 032306, 2019.
- [131] C. Kokail *et al.*, “Self-verifying variational quantum simulation of lattice models,” *Nature*, vol. 569, no. 7756, pp. 355–360, 2019.
- [132] J. Kogut and L. Susskind, “Hamiltonian formulation of Wilson’s lattice gauge theories,” *Phys. Rev. D*, vol. 11, pp. 395–408, Jan. 1975.
- [133] J. Preskill, “Quantum Computing in the NISQ era and beyond,” *Quantum*, vol. 2, p. 79, Aug. 2018.
- [134] C. Muschik, M. Heyl, E. Martinez, T. Monz, P. Schindler, B. Vogell, M. Dalmonte, P. Hauke, R. Blatt, and P. Zoller, “U(1) Wilson lattice gauge theories in digital quantum simulators,” *New J. Phys.*, vol. 19, no. 10, p. 103020, 2017.
- [135] S. A. Chin, O. S. van Roosmalen, E. A. Umland, and S. E. Koonin, “Exact ground-state properties of the SU(2) Hamiltonian lattice gauge theory,” *Phys. Rev. D*, vol. 31, pp. 3201–3212, June 1985.
- [136] G. Burgio, R. De Pietri, H. A. Morales-Tecotl, L. F. Urrutia, and J. D. Vergara, “The Basis of the physical Hilbert space of lattice gauge theories,” *Nucl. Phys.*, vol. B566, pp. 547–561, 2000.
- [137] M. Mathur, “Harmonic oscillator pre-potentials in SU(2) lattice gauge theory,” *Journal of Physics A: Mathematical and General*, vol. 38, pp. 10015–10025, Nov. 2005.

- [138] M. Mathur, “The loop states in lattice gauge theories,” *Phys. Lett.*, vol. B640, pp. 292–296, 2006.
- [139] T. Byrnes and Y. Yamamoto, “Simulating lattice gauge theories on a quantum computer,” *Phys. Rev. A*, vol. 73, p. 022328, Feb. 2006.
- [140] R. Anishetty, M. Mathur, and I. Raychowdhury, “Prepotential formulation of SU(3) lattice gauge theory,” *Journal of Physics A: Mathematical and Theoretical*, vol. 43, p. 035403, Dec. 2009.
- [141] P. Orland, “Subtleties of non-abelian gauge theories in cold-atomic lattices,” in *Proceedings, 31st International Symposium on Lattice Field Theory (Lattice 2013): Mainz, Germany, July 29-August 3, 2013*, vol. LATTICE2013 of *PoS*, p. 330, 2014.
- [142] K. Stannigel, P. Hauke, D. Marcos, M. Hafezi, S. Diehl, M. Dalmonte, and P. Zoller, “Constrained dynamics via the Zeno effect in quantum simulation: Implementing non-Abelian lattice gauge theories with cold atoms,” *Phys. Rev. Lett.*, vol. 112, no. 12, p. 120406, 2014.
- [143] M. Rizzi, “Quantum simulation of gauge potentials with cold atoms in optical lattices: A tunable platform for relativistic fermions and axions,” in *Proceedings, QCD-TNT-III, from Quarks and Gluons to Hadronic Matter: A Bridge Too Far?: Trento, Italy, September 2-6, 2013*, vol. QCD-TNT-III of *PoS*, p. 036, 2013.
- [144] R. Anishetty and I. Raychowdhury, “SU(2) lattice gauge theory: Local dynamics on nonintersecting electric flux loops,” *Phys. Rev.*, vol. D90, no. 11, p. 114503, 2014.
- [145] Y. Kuno, K. Kasamatsu, Y. Takahashi, I. Ichinose, and T. Matsui, “Real-time dynamics and proposal for feasible experiments of lattice gauge?Higgs model simulated by cold atoms,” *New J. Phys.*, vol. 17, no. 6, p. 063005, 2015.
- [146] Y. Liu and R. Liu, “Optical quantum simulation of Abelian gauge field using cold atomic ensembles coupled with arrays of optical cavities,” *Sci. China Phys. Mech. Astron.*, vol. 57, no. 12, pp. 2259–, 2014.
- [147] Y.-X. Hu, C. Miniatura, D. Wilkowski, and B. Gremaud, “U(3) artificial gauge fields for cold atoms,” *Phys. Rev.*, vol. A90, no. 2, p. 023601, 2014.
- [148] L. Tagliacozzo, A. Celi, and M. Lewenstein, “Tensor networks for lattice gauge theories with continuous groups,” *Phys. Rev.*, vol. X4, no. 4, p. 041024, 2014.

- [149] Y. Kuno, S. Sakane, K. Kasamatsu, I. Ichinose, and T. Matsui, “Quantum simulation of (1+1)-dimensional U(1) gauge-Higgs model on a lattice by cold Bose gases,” *Phys. Rev.*, vol. D95, no. 9, p. 094507, 2017.
- [150] E. Zohar and J. I. Cirac, “Eliminating fermionic matter fields in lattice gauge theories,” *Phys. Rev.*, vol. B98, no. 7, p. 075119, 2018.
- [151] J. Bender, E. Zohar, A. Farace, and J. I. Cirac, “Digital quantum simulation of lattice gauge theories in three spatial dimensions,” *New J. Phys.*, vol. 20, no. 9, p. 093001, 2018.
- [152] P. Dreher, “Challenges implementing non-Abelian SU(2) quantum chromodynamics gauge links on a universal quantum computer,” in *Proceedings, 36th International Symposium on Lattice Field Theory (Lattice 2018): East Lansing, MI, United States, July 22-28, 2018*, vol. LATTICE2018 of *PoS*, p. 036, 2018.
- [153] J. R. Stryker, “Oracles for Gauss’s law on digital quantum computers,” *Phys. Rev.*, vol. A99, no. 4, p. 042301, 2019.
- [154] D.-S. Li, C.-W. Wu, M. Zhong, W. Wu, and P.-X. Chen, “Digital quantum simulation of yang-mills theory and hadronization,” 2018.
- [155] E. Zohar, “Gauss law, minimal coupling and fermionic PEPS for lattice gauge theories,” in *Tensor Network and Entanglement Florence, Italy, June 18-22, 2018*, 2018.
- [156] H. Lamm, S. Lawrence, and Y. Yamauchi, “Quantum simulation of gauge theories,” 2019.
- [157] E. Zohar and J. I. Cirac, “Removing staggered fermionic matter in U(N) and SU(N) lattice gauge theories,” *Phys. Rev.*, vol. D99, no. 11, p. 114511, 2019.
- [158] A. M. Polyakov, “String representations and hidden symmetries for gauge fields,” *Phys. Lett.*, vol. 82B, pp. 247–250, 1979.
- [159] S. Mandelstam, “Charge - monopole duality and the phases of nonabelian gauge theories,” *Phys. Rev.*, vol. D19, p. 2391, 1979.
- [160] Y. Nambu, “QCD and the string model,” *Phys. Lett.*, vol. 80B, pp. 372–376, 1979.
- [161] A. M. Polyakov, “Gauge fields as rings of glue,” *Nucl. Phys.*, vol. B164, pp. 171–188, 1980.

- [162] W. Furmanski and A. Kolawa, “Yang-Mills vacuum: An attempt of lattice loop calculus,” *Nucl. Phys.*, vol. B291, pp. 594–628, 1987.
- [163] R. Gambini, L. Leal, and A. Trias, “Loop calculus for lattice gauge theories,” *Phys. Rev.*, vol. D39, p. 3127, 1989.
- [164] C. Di Bartolo, R. Gambini, and L. Leal, “Hamiltonian lattice gauge theories in a loop-dependent magnetic representation,” *Phys. Rev. D*, vol. 39, pp. 1756–1760, Mar. 1989.
- [165] R. Anishetty and H. S. Sharatchandra, “Duality transformation for nonAbelian lattice gauge theories,” *Phys. Rev. Lett.*, vol. 65, pp. 813–815, 1990.
- [166] B. Bruegmann, “Method of loops applied to lattice gauge theory,” *Phys. Rev.*, vol. D43, pp. 566–579, 1991.
- [167] N. J. Watson, “Solution of the SU(2) mandelstam constraints,” *Phys. Lett.*, vol. B323, pp. 385–392, 1994.
- [168] I. Raychowdhury, “Low energy spectrum of SU(2) lattice gauge theory,” *Eur. Phys. J.*, vol. C79, no. 3, p. 235, 2019.
- [169] D. Horn, “Finite matrix models with continuous local gauge invariance,” *Physics Letters B*, vol. 100, no. 2, pp. 149–151, 1981.
- [170] P. Orland and D. Rohrlich, “Lattice gauge magnets: Local isospin from spin,” *Nuclear Physics B*, vol. 338, no. 3, pp. 647–672, 1990.
- [171] S. Chandrasekharan and U. J. Wiese, “Quantum link models: A Discrete approach to gauge theories,” *Nucl. Phys.*, vol. B492, pp. 455–474, 1997.
- [172] R. Brower, S. Chandrasekharan, and U. J. Wiese, “QCD as a quantum link model,” *Phys. Rev.*, vol. D60, p. 094502, 1999.
- [173] L. Tagliacozzo, A. Celi, P. Orland, and M. Lewenstein, “Simulations of non-Abelian gauge theories with optical lattices,” *Nature Commun.*, vol. 4, p. 2615, 2013.
- [174] Y. Meurice, A. Bazavov, S.-W. Tsai, J. Unmuth-Yockey, L.-P. Yang, and J. Zhang, “Tensor RG calculations and quantum simulations near criticality,” in *Proceedings, 34th International Symposium on Lattice Field Theory (Lattice 2016): Southampton, UK, July 24-30, 2016*, vol. LATTICE2016 of *PoS*, p. 325, 2016.

- [175] R. Brower, “Formulating lattice field theory for a quantum computer,” May 2019.
- [176] Y. Meurice, “Quantum field theory with cold atoms,” May 2019.
- [177] 20-qubit backend: IBM Q team, IBM Q 20 Tokyo backend specification V1.2.5 with qiskit V0.11.0, 2019.
- [178] E. Zohar, J. I. Cirac, and B. Reznik, “Quantum simulations of gauge theories with ultracold atoms: Local gauge invariance from angular momentum conservation,” *Phys. Rev.*, vol. A88, p. 023617, 2013.
- [179] I. Raychowdhury and J. R. Stryker, “Solving Gauss’s law on digital quantum computers with loop-string-hadron digitization,” *Phys. Rev. Research*, vol. 2, p. 033039, July 2020.
- [180] M. Mathur, I. Raychowdhury, and R. Anishetty, “SU(N) irreducible Schwinger bosons,” *Journal of Mathematical Physics*, vol. 51, p. 093504, Sept. 2010.
- [181] R. Anishetty and I. Raychowdhury, “SU(2) lattice gauge theory: Local dynamics on nonintersecting electric flux loops,” *Phys. Rev. D*, vol. 90, p. 114503, Dec. 2014.
- [182] R. Anishetty and T. P. Sreeraj, “Mass gap in the weak coupling limit of (2+1)-dimensional SU(2) lattice gauge theory,” *Phys. Rev. D*, vol. 97, p. 074511, Apr. 2018.
- [183] R. Anishetty, M. Mathur, and I. Raychowdhury, “Irreducible SU(3) Schwinger bosons,” *Journal of Mathematical Physics*, vol. 50, p. 053503, May 2009.
- [184] H. F. Trotter, “On the product of semi-groups of operators,” *Proc. Amer. Math. Soc.*, vol. 10, no. 4, pp. 545–551, 1959.
- [185] M. Suzuki, “Generalized Trotter’s formula and systematic approximants of exponential operators and inner derivations with applications to many-body problems,” *Commun. Math. Phys.*, vol. 51, pp. 183–190, June 1976.
- [186] Y. Meurice, “Discrete aspects of continuous symmetries in the tensorial formulation of Abelian gauge theories,” *arXiv:2003.10986 [hep-lat, physics:hep-th, physics:quant-ph]*, Mar. 2020.
- [187] J. C. Halimeh and P. Hauke, “Staircase prethermalization and constrained dynamics in lattice gauge theories,” *arXiv:2004.07248 [cond-mat, physics:hep-th, physics:quant-ph]*, Apr. 2020.

- [188] J. C. Halimeh and P. Hauke, “Origin of staircase prethermalization in lattice gauge theories,” *arXiv:2004.07254* [*cond-mat*, *physics:hep-th*, *physics:quant-ph*], Apr. 2020.
- [189] A. F. Shaw, P. Lougovski, J. R. Stryker, and N. Wiebe, “Quantum Algorithms for Simulating the Lattice Schwinger Model,” *arXiv:2002.11146* [*hep-lat*, *physics:nucl-th*, *physics:quant-ph*], Feb. 2020.
- [190] J. Schwinger, “Gauge Invariance and Mass. II,” *Phys. Rev.*, vol. 128, pp. 2425–2429, Dec. 1962.
- [191] P. Jordan and E. Wigner, “über das Paulische Äquivalenzverbot,” *Z. Physik*, vol. 47, pp. 631–651, Sept. 1928.
- [192] D. W. Berry and A. M. Childs, “Black-box Hamiltonian simulation and unitary implementation,” *Quantum Inf. Comput.*, vol. 12, no. 1-2, pp. 29–62, 2012.
- [193] A. M. Childs and N. Wiebe, “Hamiltonian simulation using linear combinations of unitary operations,” *Quantum Inf. Comput.*, vol. 12, no. 11-12, pp. 901–924, 2012.
- [194] I. Márquez-Martín, P. Arnault, G. Di Molfetta, and A. Pérez, “Electromagnetic lattice gauge invariance in two-dimensional discrete-time quantum walks,” *Phys. Rev. A*, vol. 98, p. 032333, Sept. 2018.

Appendix A

TROTTER APPROXIMATION ERRORS IN THE SCHWINGER MODEL

As an example of non-gauge invariant errors, consider a Trotter step in the Schwinger model (a U(1) gauge theory in 1D) [190]. Discretizing space with staggered fermions [39], employing periodic boundary conditions, and using a Jordan-Wigner transformation [191], a rescaled Hamiltonian for this theory is [22, 24]

$$\hat{H} = x \sum_{s=0}^{2N_{\text{ph}}-1} [\sigma^-(s)\hat{U}(s)\sigma^+(s+1) + \text{H.c.}] + \sum_{s=0}^{2N_{\text{ph}}-1} [\hat{E}(s)^2 + \frac{\mu}{2}(-)^s \hat{Z}(s)] . \quad (\text{A.1})$$

Here, N_{ph} is the number of physical sites, x, μ are parameters, $\hat{E}(s), \hat{U}(s)$ are the operators introduced in section 2.1, and σ_n^\pm change fermionic occupation numbers (which follow a different map than the one assumed after (2.19)). Trotter errors induced by decomposing the electric energy or the mass term into separate steps by individual Pauli operators (if there are any such errors) will not affect Gauss's law. The troublesome part of the Hamiltonian is the hopping term,

$$\hat{H}_{\text{h}} = \sum_{s=0}^{2N_{\text{ph}}-1} \hat{H}_{\text{h}}(s) , \quad (\text{A.2})$$

$$\hat{H}_{\text{h}}(s) = \left[\sigma^-(s)\hat{U}(s)\sigma^+(s+1) + \sigma^+(s)\hat{U}^\dagger(s)\sigma^-(s+1) \right] . \quad (\text{A.3})$$

If the links are given a cutoff $n = 1$, then $\hat{H}_{\text{h}}(s)$ decomposes into four Pauli operators,

$$\hat{H}_{\text{h}}(s)|_{n=1} = \frac{1}{4}(XXX + XYY - YYX + YXY) . \quad (\text{A.4})$$

The notation here uses implicit tensor products where the first (last) operator acts on site s ($s + 1$), and operators in the middle act on the link. It turns out that all the operators

in (A.4) mutually commute, so for this special case elementary methods can be used to implement $\exp(-i \Delta t x H_h(s))$. When the cutoff is $n = 2$, however, $H_h(s)$ is the sum of 12 Pauli operators,

$$\begin{aligned} \hat{H}_h(s)|_{n=2} = & \frac{1}{4} [XIXX + XIYY - YIYX + YIXY] \\ & + \frac{1}{8} [XXXX + XY YX - XXYY + XYXY \\ & + YXYX - YYXX + YXXY + YYYY] . \end{aligned} \quad (\text{A.5})$$

These operators do not all commute with each other, and the Trotter step obtained by compounding 12 elementary rotations generally differs from $\exp(-i \Delta t x H_h(s))$ by errors that break Gauss's law. The situation worsens with increasing n , so naïve Trotterization is destined to create unphysical components in a state vector. Alternatives to Trotterization such as quantum walks [192, 193] could also face the same problems with gauge invariance, but whether the situation is better or worse was not investigated (see also [194]).

Appendix B

TWO PLAQUETTE SU(2) HAMILTONIAN AND DATA TABLES

For the two-plaquette lattice with periodic boundary conditions and truncation $\Lambda_j = 1/2$, the Hamiltonian implemented in the full 16-dimensional Hilbert space with the gauge variant completion (GVC) discussed in the main text is

$$\hat{H}^{(1/2)} = \frac{1}{2g^2} \begin{pmatrix} 0 & 0 & 0 & 0 & 0 & 0 & 0 & -2 & 0 & 0 & 0 & 0 & 0 & -2 & 0 & 0 \\ 0 & \frac{3g^4}{4} & 0 & 0 & 0 & 0 & -2 & 0 & 0 & 0 & 0 & 0 & -2 & 0 & 0 & 0 \\ 0 & 0 & \frac{3g^4}{2} & 0 & 0 & -2 & 0 & 0 & 0 & 0 & 0 & 0 & 0 & 0 & 0 & -\frac{1}{2} \\ 0 & 0 & 0 & \frac{9g^4}{4} & -2 & 0 & 0 & 0 & 0 & 0 & 0 & 0 & 0 & 0 & -\frac{1}{2} & 0 \\ 0 & 0 & 0 & -2 & \frac{3g^4}{4} & 0 & 0 & 0 & 0 & -2 & 0 & 0 & 0 & 0 & 0 & 0 \\ 0 & 0 & -2 & 0 & 0 & \frac{3g^4}{2} & 0 & 0 & -2 & 0 & 0 & 0 & 0 & 0 & 0 & 0 \\ 0 & -2 & 0 & 0 & 0 & 0 & \frac{9g^4}{4} & 0 & 0 & 0 & 0 & -\frac{1}{2} & 0 & 0 & 0 & 0 \\ -2 & 0 & 0 & 0 & 0 & 0 & 0 & 3g^4 & 0 & 0 & -\frac{1}{2} & 0 & 0 & 0 & 0 & 0 \\ 0 & 0 & 0 & 0 & 0 & -2 & 0 & 0 & \frac{3g^4}{2} & 0 & 0 & 0 & 0 & 0 & 0 & -\frac{1}{2} \\ 0 & 0 & 0 & 0 & -2 & 0 & 0 & 0 & 0 & \frac{9g^4}{4} & 0 & 0 & 0 & 0 & 0 & -\frac{1}{2} \\ 0 & 0 & 0 & 0 & 0 & 0 & 0 & -\frac{1}{2} & 0 & 0 & 3g^4 & 0 & 0 & -\frac{1}{2} & 0 & 0 \\ 0 & 0 & 0 & 0 & 0 & 0 & -\frac{1}{2} & 0 & 0 & 0 & 0 & \frac{15g^4}{4} & -\frac{1}{2} & 0 & 0 & 0 \\ 0 & -2 & 0 & 0 & 0 & 0 & 0 & 0 & 0 & 0 & 0 & -\frac{1}{2} & \frac{9g^4}{4} & 0 & 0 & 0 \\ -2 & 0 & 0 & 0 & 0 & 0 & 0 & 0 & 0 & 0 & -\frac{1}{2} & 0 & 0 & 3g^4 & 0 & 0 \\ 0 & 0 & 0 & -\frac{1}{2} & 0 & 0 & 0 & 0 & 0 & -\frac{1}{2} & 0 & 0 & 0 & 0 & \frac{15g^4}{4} & 0 \\ 0 & 0 & -\frac{1}{2} & 0 & 0 & 0 & 0 & 0 & -\frac{1}{2} & 0 & 0 & 0 & 0 & 0 & 0 & \frac{9g^4}{2} \end{pmatrix}, \quad (\text{B.1})$$

with matrix elements of the four-dimensional physical subspace highlighted. For the chosen coupling of $g^2 = 0.2$, the ground state energy density per plaquette, through exact (classical) diagonalization, is calculated to be -3.5658 and the lowest energy gap (the observable associ-

ated with the ‘‘SU(2)-glueball’’ mass in the infinite volume limit) is calculated to be 7.4139. Numerical values for these low-energy observables with increasing Λ_j truncation are provided in Table B.1 where percent-level convergence is achieved with three qubits per SU(2) gauge link.

For the quantum simulated system of two plaquettes with $\Lambda_j = 1/2$, the structure of the ground state wavefunction is

$$|\psi_{gs}\rangle = 0.6943|\begin{array}{|c|c|} \hline \square & \square \\ \hline \end{array}\rangle + 0.1666|\begin{array}{|c|c|} \hline \square & \square \\ \hline \square & \square \\ \hline \end{array}\rangle + 0.4951\left(|\begin{array}{|c|c|} \hline \square & \square \\ \hline \square & \square \\ \hline \end{array}\rangle + |\begin{array}{|c|c|} \hline \square & \square \\ \hline \square & \square \\ \hline \end{array}\rangle\right) . \quad (\text{B.2})$$

On each link, a single line corresponds to $j = 0$ and a double line corresponds to $j = 1/2$. The first electric, single plaquette operator in the full 16-dimensional space is diagonal

$$E_{\square_1}^2 = \frac{g^2}{2} \text{diag} \left(0, \frac{3}{4}, 0, \frac{3}{4}, \frac{3}{4}, \frac{3}{2}, \frac{3}{4}, \frac{3}{2}, \frac{3}{2}, \frac{3}{4}, \frac{3}{2}, \frac{3}{4}, \frac{3}{4}, 3, \frac{9}{4}, 3 \right) , \quad (\text{B.3})$$

with matrix elements serving as weights of the measured probabilities in the measurement of the electric energy expectation value as shown in Fig. 4.3. The the data appearing in Fig. 4.3 are presented in Tables B.2 and B.3.

B.1 Plaquette operator for $\Lambda_j = 1/2$ lattices of arbitrary plaquette number in one dimension

While the circuit implementation of the plaquette operator has been shown in Fig. 4.2 for the two-plaquette truncated lattice with periodic boundary conditions and $\Lambda_j = 1/2$, the operator for lattices of larger size may be implemented with 14 nearest-neighbor CNOT entangling gates as shown in Fig. B.1. This circuit is a massaged version of the circuit of four two-qubit-controlled $X \otimes X \otimes X$ operators with coefficients $\{1, 1/2, 1/2, 1/4\}$ for control states $|0\rangle, |1\rangle, |2\rangle, |3\rangle$ in the combined Hilbert space of j_ℓ and j_r . Just as in the main text, rotations are defined by linear combinations of $\hat{\square}^{(1/2)}$ matrix elements, as established

Electric Cutoff ($2\Lambda_j$)	Physical Dimension	Plaquette Matrix Elements	Ground State Energy Density	Gap ΔE
1	4	2	-3.5658	7.4139
2	27	31	-5.6437	2.0970
3	95	192	-6.8020	0.9285
4	304	790	-7.4258	0.5024
5	769	2494	-7.7527	0.3096
6	1784	6537	-7.9159	0.2220
7	3664	15028	-7.9921	0.1929
8	7081	31200	-8.0241	0.1885
9	12704	59894	-8.0355	0.1893
10	21823	107823	-8.0388	0.1900
11	35659	184268	-8.0396	0.1902
12	56420	301326	-8.0398	0.1902

Table B.1: Convergence of the ground state energy density and the energy gap to the first excited state, ΔE , of a two-plaquette $SU(2)$ lattice with periodic boundary conditions as the truncation in the maximum excitation on any single link, Λ_j , is increased. Columns two and three show the number of states included in the basis of physical states below truncation and the number of non-zero matrix elements in the single plaquette operator.

$N_{\text{Trot}} = 1$		$N_{\text{Trot}} = 2$	
time	$\langle H_{E,\square_1} \rangle$	time	$\langle H_{E,\square_1} \rangle$
0.02	0.009(9)	0.02	0.027(14)
0.07	0.052(6)	0.07	0.074(14)
0.12	0.127(7)	0.12	0.124(14)
0.17	0.201(12)	0.17	0.159(10)
0.22	0.261(10)	0.22	0.186(15)
0.27	0.282(7)	0.27	0.177(12)
0.32	0.278(8)	0.32	0.144(20)
0.37	0.254(6)	0.37	0.093(18)

Table B.2: Numerical values of the expectation value of the single electric plaquette energy contribution for time evolutions implemented with 1,2 Trotter steps as measured on IBM's quantum device Tokyo shown in the top panel of Fig. 4.3. Uncertainties represent statistical variation, as well as a systematic uncertainty estimated from reproducibility measurements.

Time	(N_{Trot}, r) Survival Probability Series				Linear Extrapolation
	(1,1)	(1,2)	(2,1)	(2,2)	
0.02	0.47(1)	0.29(2)	0.23(1)	0.27(1)	0.630(14)
0.07	0.49(2)	0.31(3)	0.24(2)	0.27(1)	0.640(16)
0.12	0.48(2)	0.28(2)	0.26(2)	0.24(1)	0.659(25)
0.17	0.47(2)	0.27(1)	0.24(1)	0.26(1)	0.647(33)
0.22	0.43(1)	0.25(1)	0.25(2)	0.25(2)	0.572(17)
0.27	0.41(2)	0.25(2)	0.23(2)	0.26(1)	0.554(14)
0.32	0.39(1)	0.23(1)	0.22(1)	0.28(1)	0.535(17)
0.37	0.37(1)	0.21(1)	0.22(1)	0.26(1)	0.527(17)

Table B.3: Survival probabilities in the physical subspace as measured on IBM’s quantum device *Tokyo* shown in the bottom panel of Fig. 4.3. The label indicates (N_{Trot}, r) values. The linear extrapolation is determined by extrapolation of computational basis state probabilities in r for $N_{\text{Trot}} = 1$. Uncertainties represent statistical variation, as well as a systematic uncertainty estimated from reproducibility measurements.

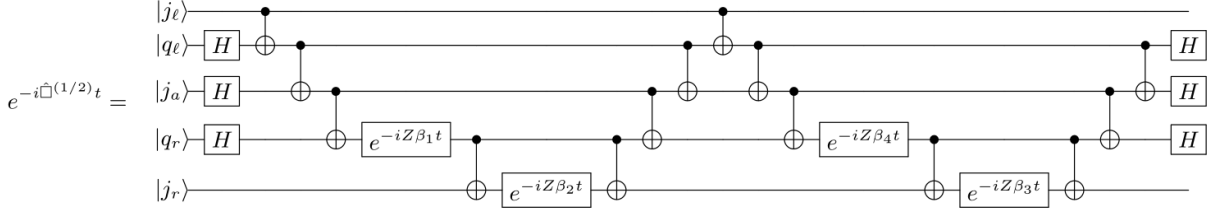


Figure B.1: Digital circuit implementation of the plaquette operator centered on j_a for a truncated lattice with $\Lambda_j = 1/2$. The circuit elements appearing in this circuit are the Hadamard, CNOT, and Z-axis single-qubit rotation implementing a Z-to-X basis change, a controlled bit flip, and a relative phase, respectively.

in Ref. [1], described by the following matrix structure:

$$\vec{\beta} = \begin{pmatrix} 1 & 1 & 1 & 1 \\ 1 & -1 & -1 & 1 \\ -1 & -1 & 1 & 1 \\ -1 & 1 & -1 & 1 \end{pmatrix}^{-1} \begin{pmatrix} 1 \\ 1/2 \\ 1/2 \\ 1/4 \end{pmatrix}, \quad \tilde{\beta} = \begin{pmatrix} 1 & 1 \\ -1 & 1 \end{pmatrix}^{-1} \begin{pmatrix} 1 \\ 1/4 \end{pmatrix}, \quad (\text{B.4})$$

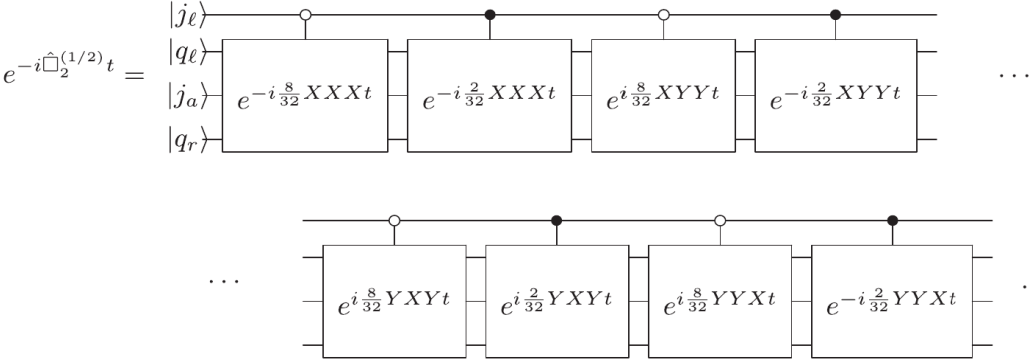
such that $\vec{\beta} = (3/16, 1/16, 3/16, 9/16)$ and $\tilde{\beta} = (3/8, 5/8)$.

B.2 Alternate plaquette gauge variant completion

The optimality of the operator decomposition in the physical subspace is hardware-specific. For simple comparison to the GVC used on superconducting hardware in this work, a more naïve implementation of the plaquette operator for the two-plaquette lattice would be to use the operator exactly as defined by the matrix elements in Eq. (4.6) with no modifications in the unphysical space (i.e., different charge superselection sectors). In this case, the Pauli decomposition contains eight operators

$$\hat{\square} = \left(\frac{5}{32}\mathbb{I} + \frac{3}{32}Z \right) \otimes X \otimes X \otimes X + \left(-\frac{3}{32}\mathbb{I} - \frac{5}{32}Z \right) \otimes X \otimes Y \otimes Y \\ + \left(-\frac{5}{32}\mathbb{I} - \frac{3}{32}Z \right) \otimes Y \otimes X \otimes Y + \left(-\frac{3}{32}\mathbb{I} - \frac{5}{32}Z \right) \otimes Y \otimes Y \otimes X, \quad (\text{B.5})$$

and it remains convenient for the Trotterization that these eight operators commute. However, the number of CNOT gates required to implement this operator increases by a factor of four compared to the operator structure of Fig. 4.2, implemented now in four different bases



This makes clear that the quantum resources for operator implementation depends even on the unphysical details of the calculation design—the choice of gauge invariant completion allows hardware-specific optimization leveraging this sensitivity.

Appendix C

SIMPLE HARMONIC OSCILLATOR

Below, we recall facts about the simple (bosonic) harmonic oscillator and the occupation number basis. These are included for reference because the construction of LSH states is a generalization of the same ideas.

The pertinent operator algebra involves an operator a and its Hermitian adjoint:

$$[\hat{a}, \hat{a}^\dagger] = 1 .$$

The Hamiltonian \hat{H} is a linear function of the “number operator” $\hat{N} = \hat{a}^\dagger \hat{a}$.

We call \hat{a} (\hat{a}^\dagger) an “annihilation” (“creation”) operator because it changes the eigenvalue of \hat{N} by -1 (+1):

$$[\hat{N}, \hat{a}] = -\hat{a} , \tag{C.1}$$

$$[\hat{N}, \hat{a}^\dagger] = \hat{a}^\dagger , \tag{C.2}$$

Given any eigenstate $|\lambda\rangle$ ($\hat{N}|\lambda\rangle = \lambda|\lambda\rangle$), we can apply \hat{a} arbitrarily many times to get the eigenvalue of \hat{N} as low as we wish; the Hilbert space for any physical system (on which \hat{H} has a ground state) must include a state $|\Omega\rangle$ that terminates this lowering:

$$\hat{a}|\Omega\rangle = 0 .$$

This is a state with “zero excitations” since $\hat{N}|\Omega\rangle = 0$. It is safe to assume this state is non-degenerate.

Now working toward the conventional $|n\rangle$ basis, we define a normalized vacuum state $|0\rangle$ by

$$|0\rangle = \frac{1}{\sqrt{\langle\Omega|\Omega\rangle}} |\Omega\rangle ,$$

$$\hat{a}|0\rangle = 0 .$$

The n^{th} level eigenspace of \hat{N} ($\hat{N} |\lambda_n\rangle = n |\lambda_n\rangle$) can be reached by acting on $|0\rangle$ with n powers of \hat{a}^\dagger . The commutation relations show us how \hat{a}^\dagger rescales magnitude at each application:

$$\begin{aligned} \langle 0 | \hat{a}^n \hat{a}^{\dagger n} | 0 \rangle &= \langle 0 | \hat{a}^{n-1} \hat{a} \hat{a}^\dagger \hat{a}^{\dagger n-1} | 0 \rangle \\ &= \langle 0 | \hat{a}^{n-1} (1 + \hat{a}^\dagger \hat{a}) \hat{a}^{\dagger n-1} | 0 \rangle \\ &= n \langle 0 | \hat{a}^{n-1} \hat{a}^{\dagger n-1} | 0 \rangle . \end{aligned}$$

By recursion, we learn that

$$\langle 0 | \hat{a}^n \hat{a}^{\dagger n} | 0 \rangle = n! .$$

The simplest definition of an orthonormal basis is then

$$|n\rangle = \frac{\hat{a}^{\dagger n}}{\sqrt{n!}} |0\rangle .$$

In this basis, we have the familiar properties

$$\begin{aligned} \hat{a} |n\rangle &= \sqrt{n} |n-1\rangle , \\ \hat{a}^\dagger |n\rangle &= \sqrt{n+1} |n+1\rangle . \end{aligned}$$

The simple harmonic oscillator has a U(1) symmetry:

$$\begin{aligned} \hat{a} &\rightarrow e^{i\theta} \hat{a}, \\ \hat{a}^\dagger &\rightarrow e^{-i\theta} \hat{a}^\dagger \end{aligned}$$

for real θ . The symmetry transformation is generated by \hat{N} , in accordance with Equation C.1 and Equation C.2. The fact that \hat{H} commutes with \hat{N} (number is conserved) is trivial in a system this simple.

Appendix D

GLUONIC SITE STATE NORMALIZATION

Below we shall see that the following states are normalized:

$$|\ell_{12}, \ell_{23}, \ell_{31}\rangle \equiv \frac{1}{\sqrt{\ell_{12}!\ell_{23}!\ell_{31}!(\ell_{12} + \ell_{23} + \ell_{31} + 1)!}} \mathcal{L}_{12}^{++\ell_{12}} \mathcal{L}_{23}^{++\ell_{23}} \mathcal{L}_{31}^{++\ell_{31}} |0\rangle \quad (\text{D.1})$$

To do this, we will first calculate the norm of $\mathcal{L}_{31}^{++\ell_{31}} |0\rangle$, then $\mathcal{L}_{23}^{++\ell_{23}} \mathcal{L}_{31}^{++\ell_{31}} |0\rangle$, and finally $\mathcal{L}_{12}^{++\ell_{12}} \mathcal{L}_{23}^{++\ell_{23}} \mathcal{L}_{31}^{++\ell_{31}} |0\rangle$. The calculations generalize the normalization of simple harmonic oscillator states, which is reviewed in Appendix C.

To begin one should first derive some commutators that will frequently arise:

$$\begin{aligned} [\mathcal{L}_{ij}^{--}, \mathcal{L}_{ij}^{++}] &= a^\dagger(i) \cdot a(i) + a(j) \cdot a^\dagger(j) \\ &= a^\dagger(i) \cdot a(i) + a^\dagger(j) \cdot a(j) + N , \\ [\mathcal{L}_{ij}^{--}, \mathcal{L}_{ij}^{++k}] &= k(\mathcal{L}_{ij}^{++})^{k-1} (a(i)^\dagger a(i) + a(j) a^\dagger(j) + (k-1)) \\ &= k(a(i)^\dagger a(i) + a(j) a^\dagger(j) - (k-1)) (\mathcal{L}_{ij}^{++})^{k-1} . \end{aligned}$$

Also, we clearly have

$$\begin{aligned} \mathcal{L}_{ij}^{--} |0\rangle &= 0 , \\ \mathcal{L}_{12}^{--} \mathcal{L}_{23}^{++\ell_{23}} |0\rangle &= 0 \text{ (and cyclic permutations)} . \end{aligned}$$

Using these, for any $\ell_{31} \geq 1$ we find

$$\begin{aligned} \langle 0 | \mathcal{L}_{31}^{--\ell_{31}} \mathcal{L}_{31}^{++\ell_{31}} |0\rangle &= \langle 0 | \mathcal{L}_{31}^{--\ell_{31}-1} [\mathcal{L}_{31}^{--}, \mathcal{L}_{31}^{++\ell_{31}}] |0\rangle \\ &= \ell_{31}(\ell_{31} + N - 1) \langle 0 | \mathcal{L}_{31}^{--\ell_{31}-1} \mathcal{L}_{31}^{++\ell_{31}-1} |0\rangle . \end{aligned}$$

The norm of $\mathcal{L}_{31}^{++\ell_{31}} |0\rangle$ has been expressed in terms of $\mathcal{L}_{31}^{++(\ell_{31}-1)} |0\rangle$. The evaluation is

therefore recursive, and repeating the same steps eventually leads to

$$\begin{aligned} \langle 0 | \mathcal{L}_{31}^{-\ell_{31}} \mathcal{L}_{31}^{+\ell_{31}} | 0 \rangle &= \frac{\ell_{31}!(\ell_{31} + N - 1)!}{(N - 1)!} \langle 0 | 0 \rangle \\ &= \frac{\ell_{31}!(\ell_{31} + 1)!}{1!} . \end{aligned}$$

This formula also works for $\ell_{31} = 0$.

The next step goes through similarly. One first shows that

$$\begin{aligned} &\langle 0 | \mathcal{L}_{31}^{-\ell_{31}} \mathcal{L}_{23}^{-\ell_{23}} \mathcal{L}_{23}^{+\ell_{23}} \mathcal{L}_{31}^{+\ell_{31}} | 0 \rangle \\ &= \langle 0 | \mathcal{L}_{31}^{-\ell_{31}} \mathcal{L}_{23}^{-\ell_{23}-1} [\mathcal{L}_{23}^{-}, \mathcal{L}_{23}^{+\ell_{23}}] \mathcal{L}_{31}^{+\ell_{31}} | 0 \rangle \\ &= \ell_{23}(\ell_{23} + \ell_{31} + N - 1) \langle 0 | \mathcal{L}_{31}^{-\ell_{31}} \mathcal{L}_{23}^{-\ell_{23}-1} \mathcal{L}_{23}^{+\ell_{23}-1} \mathcal{L}_{31}^{+\ell_{31}} | 0 \rangle . \end{aligned}$$

Recursion of this process leads to

$$\begin{aligned} \langle 0 | \mathcal{L}_{31}^{-\ell_{31}} \mathcal{L}_{23}^{-\ell_{23}} \mathcal{L}_{23}^{+\ell_{23}} \mathcal{L}_{31}^{+\ell_{31}} | 0 \rangle &= \frac{\ell_{23}!(\ell_{23} + \ell_{31} + N - 1)!}{(\ell_{31} + N - 1)!} \langle 0 | \mathcal{L}_{31}^{-\ell_{31}} \mathcal{L}_{31}^{+\ell_{31}} | 0 \rangle \\ &= \frac{\ell_{23}!(\ell_{23} + \ell_{31} + N - 1)! \ell_{31}!(\ell_{31} + N - 1)!}{(\ell_{31} + N - 1)! (N - 1)!} \\ &= \frac{\ell_{23}! \ell_{31}! (\ell_{23} + \ell_{31} + N - 1)!}{(N - 1)!} \end{aligned}$$

The third and final step can be tricky. The facts that $\mathcal{L}_{31}^{-} | 0 \rangle = 0$ and $\mathcal{L}_{23}^{-} \mathcal{L}_{31}^{+\ell_{31}} | 0 \rangle = 0$ were very useful for turning products of \mathcal{L}_{ij} s into functions of number operators. But the naïve arguments for them are not any good here: at a mathematical level, \mathcal{L}_{12}^{-} does not obviously annihilate $\mathcal{L}_{23}^{+\ell_{23}} \mathcal{L}_{31}^{+\ell_{31}} | 0 \rangle$ because the state can have modes excited along both directions 1 and 2. Nonetheless, by beginning with

$$\mathcal{L}_{12}^{-} \mathcal{L}_{23}^{+\ell_{23}} \mathcal{L}_{31}^{+\ell_{31}} | 0 \rangle = [\mathcal{L}_{12}^{-}, \mathcal{L}_{23}^{+\ell_{23}}] \mathcal{L}_{31}^{+\ell_{31}} | 0 \rangle ,$$

it is not too difficult to show that we do in fact have

$$\mathcal{L}_{12}^{-} \mathcal{L}_{23}^{+\ell_{23}} \mathcal{L}_{31}^{+\ell_{31}} | 0 \rangle = 0 .$$

(Intermediate results I used were $[\mathcal{L}_{12}^{-}, \mathcal{L}_{23}^{+}] = -\mathcal{L}_{31}^{+}$, $[\mathcal{L}_{12}^{-}, \mathcal{L}_{23}^{+k}] = -k \mathcal{L}_{23}^{+k-1} \mathcal{L}_{31}^{+}$, and $[\mathcal{L}_{31}^{+}, \mathcal{L}_{31}^{+}] = [\mathcal{L}_{31}^{+}, \mathcal{L}_{31}^{+\ell}] = 0$.)

Equipped with this, it is easy to calculate the norm of $\mathcal{L}_{12}^{++\ell_{12}} \mathcal{L}_{23}^{++\ell_{23}} \mathcal{L}_{31}^{++\ell_{31}} |0\rangle$ by following similar steps to the earlier two calculations. The end result is

$$\begin{aligned}
& \langle 0 | \mathcal{L}_{31}^{--\ell} \mathcal{L}_{23}^{--\ell_{23}} \mathcal{L}_{12}^{--\ell_{12}} \mathcal{L}_{12}^{++\ell_{12}} \mathcal{L}_{23}^{++\ell_{23}} \mathcal{L}_{31}^{++\ell} | 0 \rangle \\
&= \frac{\ell_{12}! (\ell_{12} + \ell_{23} + \ell_{31} + N - 1)!}{(\ell_{23} + \ell_{31} + N - 1)!} \langle 0 | \mathcal{L}_{31}^{--\ell_{31}} \mathcal{L}_{23}^{--\ell_{23}} \mathcal{L}_{23}^{++\ell_{23}} \mathcal{L}_{31}^{++\ell_{31}} | 0 \rangle \\
&= \frac{\ell_{12}! (\ell_{12} + \ell_{23} + \ell_{31} + N - 1)! \ell_{23}! \ell_{31}! (\ell_{23} + \ell_{31} + N - 1)!}{(\ell_{23} + \ell_{31} + N - 1)! (N - 1)!} \\
&= \frac{\ell_{12}! \ell_{23}! \ell_{31}! (\ell_{12} + \ell_{23} + \ell_{31} + N - 1)!}{(N - 1)!} .
\end{aligned}$$

With $N - 1 = 1$ for SU(2), this confirms (D.1).

VITA

Jesse Stryker was born in San Diego, California in 1992. As a boy, some of his favorite hobbies were drawing, playing video games, and solving jigsaw or other kinds of puzzles. His family relocated to Palm Springs, California in 2000. Through his classes in the new school's Gifted and Talented Education program, he got interested in earth and planetary science. He was inspired to take up rock collecting as another hobby. A field trip to NASA's Jet Propulsion Laboratory especially stands out in his memory of these years, for that marked the day he learned the finiteness of light speed. In middle school, Jesse became intimately familiar with gravity as he got interested in skateboarding.

Jesse's middle school had an 'accelerated math' program that allowed him to work on math at his own pace, which resulted in him testing into algebra a year early. His math assignments filled the role of puzzles for him to work on when he was not outside skateboarding. As a high school freshman, Jesse first learned what physics really was as a scientific discipline of its own. A book about black holes and general relativity bent his imagination in a deeply satisfying way and he was introduced to astrophysics as a career that aligned with his interests.

What seemed like a steady progression toward that astrophysics destiny was interrupted when he moved to Arizona mid-sophomore year. His new pre-calculus teacher could not care less about helping him through the work he would need to do to synchronize with the class. Jesse struggled to teach himself trigonometry and conic sections, as well as the topics that were being taught while he was busy catching up. He ultimately passed the class by the skin of his teeth. Angered by the experience, he dedicated himself to acing calculus and the rest of his high school classes. The experience turned out to be good preparation though, as he would tap into those self-teaching skills again and again in the years to come.

Jesse went on to Arizona State University as a Physics major. He soon added a Mathematics major and joined Barrett, the Honors College. While he was always eager to learn more from his physics courses, the experimental research experience he was acquiring never quite felt like the right fit. He applied to physics graduate programs as an aspiring theorist and was thrilled by his acceptance to University of Washington. He graduated *summa cum laude* from Arizona State University in summer 2014.

Jesse's time at the Institute for Nuclear Theory and University of Washington Physics has been nothing short of transformative, and he had the fortune of meeting so many incredible individuals there. David Kaplan and Martin Savage, as well as their former students, Dorota Grabowska and Michael Wagman, constantly inspired him to become a better physicist and to strive to produce research of the highest quality. Jesse will remember his time at the University of Washington fondly as he starts his first postdoc at the University of Maryland, where he looks forward to working at the interface of nuclear physics and quantum information.